From the field of Medical Biochemistry and Molecular Biology

Theoretical Medicine and Biosciences

Of the Medical Faculty

Of the Saarland University, Homburg/Saar

Characterization of the transmembrane protein 109 in SRP-independent protein targeting to the human endoplasmic reticulum and its involvement in the cellular calcium homeostasis

Dissertation for the Degree of Doctor of Natural Sciences of the Faculty of Medicine

SAARLAND UNIVERSITY

2022

Submitted by: Andrea Tirincsi

Born on: 25.03.1991 in Debrecen (Hungary)

Day of the oral examination: 09. December 2022

Dean of the Faculty: Univ. Professor Dr. med. Michael D. Menger

Examinants: Professor Dr. Richard Zimmermann
Professor Dr. Adolfo Cavalié
PD Dr. Elmar Krause

1 TABLE OF CONTENTS

2 TABLE OF FIGURES

3 TABLE OF TABLES

4 ABBREVIATIONS

ATF6: activating transcription factor 6

ATP: adenosine-5'-triphosphate

ATP2A: ATPase sarcoplasmic/endoplasmic reticulum calcium transporting protein (SERCA)

BiP: binding immunoglobulin protein (also known as Hsp70, GRP78)

bp: base pair

BP: biological process

°C: degree Celsius

CAML: calcium modulating cyclophilin ligand

CAMLG: calcium modulating cyclophilin ligand gene

CC: cellular components

CRAC: Ca^{2+} release-activated Ca^{2+} channels

e.g.: for example

eIF: eukaryotic initiation factor

EMC: ER membrane complex

ER: endoplasmic reticulum

ERAD: ER-associated degradation

GPI-APs: glycophosphatidylinositol anchored proteins

GPIAS: GPI attachment signal sequence

GTP: guanosine-5'-triphosphate

HDR: homology-directed repair

HSPA5: heat shock protein family A member 5 gene (encodes BiP)

IRE1: inositol-requiring enzyme 1

ITPR1: inositol 1,4,5-trisphosphate receptor type 1

KO: knockout

M: molar concentration

MF: molecular function

µl: microliter

µM: micromolar concentration

ml: milliliter

mM: millimolar concentration

NCKX: Na^{+}/Ca^{2+}-K^{+} exchanger

NCX: Na^{+}/Ca^{2+} exchanger

NHEJ: non-homologous end-joining

nM: nanomolar concentration

ORAI: calcium release-activated calcium channel protein

OST: oligosaccharyltransferase complex

PAM: protospacer adjacent motif

PANX: pannexin

PAT10: protein associated with the ER translocon of 10 kDa (also known as Asterix)

PDI: protein disulfide isomerase

% : percent

PERK: protein kinase RNA-like endoplasmic reticulum kinase

PMCA: plasma membrane calcium ATPase

RM extract: rough microsome extract

rpm: rotation per minute

RT-qPCR: real-time quantitative PCR

RyR: ryanodine receptor

SDS-PAGE: sodium dodecyl sulfate-polyacrylamide gel electrophoresis

SEC61A: protein transport protein Sec61 subunit alpha

SERCA: Sarco/endoplasmic reticulum calcium ATPase

SND: SRP- independent

SOCE: store-operated calcium entry

SP: signal peptide

SPC: signal peptidase complex

SR: signal recognition particle receptor

SRP: signal recognition particle

SRPRA: SRP receptor subunit alpha gene (encodes SRα)

SRPRB: SRP receptor subunit beta gene (encodes SRβ)

STIM: stromal interaction molecule

TMH: transmembrane helix

TMD: transmembrane domain

TMEM109: transmembrane protein 109

TMEM208: transmembrane protein 208 (also known as human Snd2)

TMCO1: transmembrane and coiled-coil domain 1

TRAP: translocon-associated protein complex

TRC: transmembrane recognition complex

TRP: transient receptor potential channel

TSS: transcription start site

U/ml: unit per milliliter

UTR: untranslated region

UVC: ultraviolet C radiation

% (v/v): volume concentration (volume per volume)

WRB: tryptophan-rich basic protein (also known as guided entry of tail-anchored proteins factor 1)

% (w/v): mass concentration (weight per volume)

One and three-letter codes for amino acids

Nonpolar, hydrophobic amino acids
A (Ala) alanine
V (Val) valine
L (Leu) leucine
I (Ile) isoleucine
P (Pro) proline
F (Phe) phenylalanine
M (Met) methionine
W (Trp) tryptophan
G (Gly) glycine
C (Cys) cysteine

Uncharged polar, hydrophilic amino acids
N (Asn) asparagine
Q (Gln) glutamine
S (Ser) serine
T (Thr) threonine
Y (Tyr) tyrosine

Positively charged polar, hydrophilic amino acids
K (Lys) lysine
R (Arg) arginine
H (His) histidine

Negatively charged polar, hydrophilic amino acids
D (Asp) aspartic acid
E (Glu) glutamic acid

5 ABSTRACT

Protein transport to the endoplasmic reticulum mainly relies on the signal recognition particle pathway. However, in the past decades, novel pathways and modes of protein transport have been identified to complement known transport routes for specific protein substrates to reach the endoplasmic reticulum. The signal recognition particle-independent (SND) pathway was identified in yeast cells as a tripartite system (Snd1-3). It presumably conducts protein clients to the endoplasmic reticulum due to a targeting signal located downstream of the N-terminus. However, the entire pathway has not been identified in human cells, so far. Only one component, the ER membrane protein hSnd2, is known in mammalian cells. This work aimed to identify the missing ER membrane protein, the hSnd3 of the pathway.

Previous co-immunoprecipitation and subsequent mass spectrometry results revealed the interacting proteins with the hSnd2. Amongst these proteins, the transmembrane protein 109 (TMEM109) was enlisted, and it also showed simultaneous lower abundance when hSnd2 was knocked down. TMEM109 is a three-transmembrane domain protein resident in the endoplasmic reticulum membrane. A luminescence reporter assay described in this work also confirmed the interaction between the two proteins in living cells.

TMEM109 knockdown resulted in the compensatory elevated abundance of the translocon Sec61α subunit and known targeting receptors, such as the signal recognition particle receptor. Accordingly, an improved transport efficiency of signal recognition particle-dependent substrates was observed. These results were consistent and congruent with data obtained when hSnd2 was knocked down. The model protein, cytochrome b5, a tail-anchored membrane protein showed partial dependence on the SND pathway based on *in vitro* translation assay results; however, re-expressing *TMEM109* after its silencing did not rescue its transport efficiency to the endoplasmic reticulum.

Using the CRISPR-Cas9 gene-editing system, a *TMEM109* knockout cell line was generated. In TMEM109 knockout cells, similar but much more pronounced compensatory effects as in the knockdown cells were observed. Conversely, the partial SND dependence of the tail-anchored membrane protein, cytochrome b5 was not observed in TMEM109 knockout cells, likely due to the activated compensatory mechanisms.

TMEM109 has been described as a calcium channel in the endoplasmic reticulum membrane. Live-cell calcium imaging shed light on the fact that lower TMEM109 abundance can disturb the calcium homeostasis; however, it was not observed in the cells completely lacking TMEM109.

Based on the obtained results, TMEM109 is possibly implemented in protein targeting to the endoplasmic reticulum as an SND pathway element in human cells. However, no *bona fide* human SND pathway substrate has been identified so far. Further research would address the subset of proteins that require the SND pathway to transport to the endoplasmic reticulum. It is also possible that the SND

pathway complements already known transport pathways, or it is activated under specific cellular circumstances.

6 ZUSAMMENFASSUNG

Der Proteintransport zum endoplasmatischen Retikulum beruht hauptsächlich auf dem Signalerkennungspartikelweg. In den letzten Jahrzehnten wurden jedoch neue Wege und Arten des Proteintransports identifiziert, die zum endoplasmatischen Retikulum bekannte Transportwege für bestimmte Proteinsubstrate ergänzen oder ersetzen.

Der Signalerkennungspartikel-unabhängige (SND) Weg wurde in Hefezellen als Dreikoponentensystem (Snd1-3) identifiziert und leitet aufgrund eines Zielsignals Proteine zu dem endoplasmatischen Retikulum, welches sich vermutlich abseits des N-Terminus befindet. In menschlichen Zellen wurde bisher nicht der gesamte Signalweg identifiziert. Nur eine Komponente, das ER-Membranprotein hSnd2, ist in Säugetierzellen bekannt. Das Ziel dieser Arbeit war das fehlende ER-Membranprotein, hSnd3 des Weges zu identifizieren.

Frühere Co-Immunopräzipitation und anschließende Massenspektrometrie-Ergebnisse zeigten die mit hSnd2 interagierenden Proteine. Es wurde unter anderem das Transmembranprotein 109 (TMEM109) identifiziert, welches zudem eine verringerte Abundanz nach siRNA-vermittelter hSnd2 Depletion aufwies. TMEM109 ist ein Membranprotein des endoplasmatischen Retikulums mit drei Transmembrandomänen. Ein Lumineszenz-Reporter-Assay, der in dieser Arbeit beschrieben wurde, bestätigte ebenfalls die Interaktion zwischen den beiden Proteinen in lebenden Zellen.

Der Knockdown von TMEM109 führte zu einer kompensatorisch erhöhten Abundanz der zentralen Translokon-Untereinheit Sec61α und bekannter Targeting-Rezeptoren, wie etwa der Signalerkennungspartikel-Rezeptor. Dementsprechend wurde eine verbesserte Transporteffizienz von Signalerkennungspartikel-abhängigen Substraten beobachtet. Diese Ergebnisse stimmten mit den Daten überein, die durch Silencing von hSnd2 gewonnen wurden. Das Modellprotein Cytochrom b5, ein C-terminal verankerte Membranprotein zeigte eine partielle Abhängigkeit vom SND-Weg, basierend auf In-vitro-Translationsassay-Ergebnissen. Die Reexpression von *TMEM109* nach Silencing rettete jedoch nicht seine Transporteffizienz zum endoplasmatischen Retikulum.

Mithilfe des CRISPR-Cas9-Gen-Editing-Systems wurde eine *TMEM109*-Knockout-Zelllinie erzeugt. In TMEM109-Knockout-Zellen wurden zu den Knockdown-Proben ähnliche, aber deutlich stärkere, kompensatorische Änderungen beobachtet. Auf Grund der starken kompensatorischen Anpassung konnte die partielle SND-Abhängigkeit des C-terminal verankerten Membranproteins Cytochrom b5 in TMEM109-Knockout-Zellen nicht beobachtet werden.

TMEM109 wurde als Kalziumkanal in der Membran des endoplasmatischen Retikulums beschrieben. Live-Cell-Calcium-Imaging hat gezeigt, dass eine geringere TMEM109-Abundanz die Kalzium-

Homöostase stören kann. Dies konnte jedoch in den Zellen in denen TMEM109 vollständig fehlt, nicht beobachtet werden.

Anhand dieser Ergebnisse nimmt TMEM109 in menschlichen Zellen möglicherweise als Element des SND-Wegs am Transport von Proteinen in das endoplasmatische Retikulum teil. Bisher wurde kein spezifisches Substrat des SND-Weges identifiziert. Weitere Forschungen würden sich mit solchen Proteine befassen, die den SND-Weg für ihren Transport zum endoplasmatischen Retikulum benötigen. Es ist auch möglich, dass der SND-Weg entweder bereits bekannte Transportwege ergänzt oder unter bestimmten zellulären Umständen aktiviert wird.

7 INTRODUCTION

7.1 THE ENDOPLASMIC RETICULUM

The endoplasmic reticulum (ER) is a cellular organelle with diverse functions. It is the site of protein synthesis, protein folding and modifications, lipid and steroid synthesis, and it is responsible for calcium ion storage and release (Schwarz and Blower, 2016; Voeltz *et al.*, 2002). The ER exists as nuclear and peripheral ER. The outer nuclear envelope represents the nuclear ER membrane, and the encapsulated lumen outlines the nucleus. The peripheral ER is continuous from the nuclear ER and stretches through the cytoplasm as interconnected smooth tubules or rough sheets (Voeltz *et al.*, 2002). ER sheets studded with ribosomes, known as rough ER, are responsible for the protein synthesis (Gray, 2013).
The ER takes up approximately 30 % of a cell's volume (Valm *et al.*, 2017). It shows connection with other cellular organelles, and it can also interact with the plasma membrane and the cytoskeleton. Electron microscopy and live-cell fluorescence microscopy revealed that these membrane contact sites could be formed between the ER- and the Golgi, mitochondria, endosomes, and other cellular organelles (Phillips and Voeltz, 2016).

7.1.1 ROUGH MICROSOMES

During cell homogenization, the ER breaks into small fragments; these fragments are resealed into small vesicles, known as microsomes. With ribosomes on its surface, the rough ER forms the rough microsomes. Smooth ER lacks ribosomes, and the corresponding vesicles are called smooth microsomes. Using ultracentrifugation, these vesicles can be obtained in one fraction. Subsequent sedimentation centrifugation can separate the rough and smooth microsomes from each other; the rough microsomes have a higher sedimentation rate, while the smooth microsomes have a lower density and lower sedimentation rate. Microsomes are frequently derived from canine pancreatic tissue. The rough microsomes are suitable to test in cell-free system protein translocation across the ER membrane, based on protein modifications in the ER, such as glycosylation (Palade and Siekevitz, 1956; Guth *et al.*, 2004; Sabatini, 2014).

7.2 THE CALCIUM HOMEOSTASIS OF THE ENDOPLASMIC RETICULUM

In general, cellular calcium concentration is lower in the cytosol (~100 nM), and the highest concentration of calcium ions is found extracellularly, approximately 1-2 mM. However, the ER is a major calcium storing organelle within the cells; it stores calcium ions at a concentration of 100-800 µM (Schwarz and Blower, 2016). Calcium can act as a second messenger and influence many cellular responses or signaling pathways. As a second messenger, it is essential for muscle contraction, cellular proliferation and metabolism, fertilization, activation of certain transcription factors, neurotransmitter release, stimulation of cytosolic and mitochondrial adenosine-5'-triphosphate (ATP)-synthesis, and apoptosis initiation (Berridge *et al.*, 2000). Calcium channels, exchangers, and calcium-sensing proteins influence the calcium content at a given time within a cell (Berridge *et al.*, 2000) (Figure 1). One of the most important and ubiquitous calcium-binding proteins is the intracellular calcium receptor protein called calmodulin. The binding of calcium initiates conformational changes in the calmodulin protein. The conformational change liberates the hydrophobic residues, which allows the interaction of calmodulin with target proteins, such as calcium/calmodulin-dependent kinase II (CaM-kinase II) or myosin light chain kinase/MLCK (Clapham, 2007). The CaM-kinase II can phosphorylate an array of proteins. For example, it has been established that it can activate the 5'-adenosine monophosphate-activated kinase/AMPK, which drives the glycolytic ATP production in the cytosol, and a subsequent increase in the ATP level was observed in the ER (Klein *et al.*, 2018; Vishnu *et al.*, 2014).

Calcium can also upregulate the mitochondrial ATP synthesis; a rise in the cytosolic calcium concentration allows the mitochondria to uptake calcium through specific channels, such as the voltage-dependent anion channel/VDAC and the mitochondrial Ca^{2+} uniporter/MCU. Citric acid cycle enzymes, namely pyruvate dehydrogenase, isocitrate dehydrogenase, and α-ketoglutarate dehydrogenase, proved to be calcium-sensitive. The presence of calcium can promote ATP and nicotinamide adenine dinucleotide/NADH production in the mitochondria (Rizzuto *et al.*, 2012).

The ER membrane contains different calcium channels and receptors. Two important calcium release channels of the ER are the ryanodine receptors (RyRs) and inositol 1,4,5-trisphosphate (IP_3) receptors (IP_3Rs). These receptors help to regulate the calcium release out of the ER. IP_3 production happens when the membrane phosphoinositides, such as phosphatidylinositol 4,5-bisphosphate (PIP_2), are cleaved by phospholipase C-β (PLCβ). The cleavage produces diacylglycerol (DAG) and IP_3. IP_3 diffuses into the cytosol and binds and opens the IP_3-gated channels in the ER membrane, and Ca^{2+} is released into the cytosol transiently. The other second messenger, the DAG that is produced by the PIP2 cleavage, remains in the plasma membrane and activates in cooperation with Ca^{2+} the protein kinase C (PKC). PKC can phosphorylate other target proteins depending on the cell type (Clapham, 2007). IP_3Rs can be activated by Ca^{2+} or IP_3 or other proteins via phosphorylation/dephosphorylation. IP_3Rs can form heterotetrameric calcium release channels; alternative splicing can also produce multiple isoforms of the IP_3Rs (Mekahli *et al.*, 2011).

RyRs are also tetrameric complexes, and they open in response to the Ca^{2+} signal, and as positive feedback, more RyRs open; this process is the so called Ca^{2+}-induced Ca^{2+}-release (CICR). The increase in the cytosolic Ca^{2+} concentration leads to the inhibition of RyRs. The removal of the Ca^{2+} from the cytosol by Ca^{2+} pumps causes a decline in the cytosolic Ca^{2+} concentration as delayed negative feedback, which again opens RyRs and allows the rise of the cytosolic Ca^{2+} concentration repeatedly. This phenomenon results in a Ca^{2+} oscillation (Berridge *et al.*, 2000).

Another Ca^{2+} channel in the ER membrane is the Sec61 translocon channel (Lang *et al.*, 2011). Given that the channel allows the passive flux of Ca^{2+} out of the ER without ligand-stimulation, it is described as a Ca^{2+} leak channel (Lang *et al.*, 2011). The Sec61-mediated Ca^{2+} leakage is regulated by the soluble ER chaperone BiP, the ER membrane protein Sec62, and the cytosolic protein calmodulin. Passive Ca^{2+} diffusion can happen right after protein translocation when the translocon is not engaged by a polypeptide (Erdmann *et al.*, 2011; Woolhead *et al.*, 2004). Ca^{2+} bound calmodulin can bind to the IQ motif found in the cytosolic N-terminal end of the Sec61α protein. Sec61α represents the central, pore-forming subunit of the heterotrimeric Sec61 complex. The binding of calmodulin can inhibit passive Ca^{2+} leakage, and at the same time, it does not disturb co-translational protein transport. Also, Sec62 can associate with the Sec61α and inhibit the Ca^{2+} efflux (Linxweiler *et al.*, 2017). BiP is known to seal the Sec61 channel from the luminal side in order to inhibit passive Ca^{2+} outflow from the ER (Woolhead *et al.*, 2004). The functionality and structure of the Sec61 channel are discussed in more detail in a following paragraph.

The transmembrane and coiled-coil domain 1 (TMCO1), a two-transmembrane domain protein in the ER membrane, can homotetramerize in response to high ER calcium concentrations and can initiate calcium release from the ER by forming a channel (Wang *et al.*, 2016) so that it can prevent calcium overloading in the ER. (The additional function of the TMCO1 as a subunit of a specialized ER protein translocon is described in Paragraph 7.9.)

A subset of transient receptor potential (TRP) proteins also localize to the ER membrane; however, most TRP calcium channels are found on the plasma membrane. They represent high variability in the mode of activation and ion selectivity. Six subfamilies represent the six-transmembrane TRP family TRPC, TRPV, TRPM, TRPA, TRPP, and TRPML. TRPP2 is a non-selective cation channel in the ER membrane, and it can also modulate the activity of the IP_3R and RyR (Venkatachalam and Montell, 2007). TRPC1 is expressed in the plasma membrane, where it regulates calcium entry, and it is also expressed in the SR of muscle cells and promotes muscle contraction by calcium release (Berbey *et al.*, 2009). TRPM8 is a non-selective cation channel in the mitochondria-associated ER membrane. It can be activated in response to low temperature and initiates ER calcium leak, promoting mitochondrial ATP synthesis. TRPV receptors are regulated mainly by heat and play an important role in signal transduction in the nervous system by ER calcium release (Venkatachalam and Montell, 2007).

Pannexins have also been described as calcium channels in the ER membrane. It has been demonstrated that pannexins can conduct calcium ions to neighboring cells through gap junction formation as well as

can initiate calcium efflux of the ER by forming calcium channels. Pannexin channels are also known to be permeable to ATP (Abeele Vanden *et al.*, 2006).

Anti- and proapoptotic proteins have also been described as they can regulate calcium homeostasis. Anti-apoptotic Bcl-2 has been linked to low ER calcium concentration. It has been described that it could possibly block the activity of the sarco/endoplasmic reticulum Ca^{2+} ATPase (SERCA), resulting in a lower ER calcium concentration (Dremina *et al.*, 2004). (The SERCA pump is described in detail later in this chapter). Bcl-2 might regulate the sensitivity of the IP_3R to IP_3. However, the results are mixed regarding the effect of Bcl-2 on IP_3R activity. Pro-apoptotic Bax that belongs to the Bcl-2 family can also be localized in the ER membrane, however, in low amounts. It has been described to be able to lower the ER calcium concentration when it is knocked out. However, both the Bcl-2 and Bax can form a pore *in vitro*; it is under debate whether they conduct ions and behave as ER calcium channels (Chami *et al.*, 2004; Pinton and Rizzuto, 2006).

Transmembrane protein 109 (TMEM109), also known as Mitsugumin 23 (MG23), has also been described as a calcium release channel in the ER membrane (Reilly-O'Donnell *et al.*, 2017; Takeshima *et al.*, 2015; Venturi *et al.*, 2011). TMEM109 is a three-transmembrane domain protein in the ER/SR and nuclear membranes. Chemical cross-linking experiments suggested that it forms a homo-oligomer, presumably a minimum of 2-6 subunits. It is assumed that the "crescent-shape" monomers form an oligomer resembling a "bowl" with a putative pore. X-ray crystallography results propose that this central pore of the oligomer is responsible for cation conductivity rather than single monomers; however, the gating of the channel remains elusive (Venturi *et al.*, 2011). It has also been proposed that TMEM109 might be important in diastolic functions in heart muscle cells, and dysregulated Zn^{2+} concentrations can alter the ER Ca^{2+} leakage leading to irregular muscle contraction in heart failure (Reilly-O'Donnell *et al.*, 2017). The role of the TMEM109 in calcium homeostasis is discussed in this work.

Excessive Ca^{2+} loss from the ER could result in unfolded protein response (UPR) and apoptosis initiation (Mekahli *et al.*, 2011). Ion exchangers and calcium pumps in the cell and the ER membrane maintain the resting Ca^{2+} concentration. The SERCA pumps Ca^{2+} into the ER; one Ca^{2+} is transported per ATP hydrolysis, and it lowers the cytosolic calcium concentration and refills the ER calcium content. Different tissues express different SERCA pumps, SERCA1-3 (encoded by *ATP2A1-3*). The plasma membrane calcium ATPase (PMCA) (encoded by *ATP2AB1-4*) pumps one Ca^{2+} out of the cytosol per ATP hydrolysis. Another way of removing cytosolic Ca^{2+} is the Na^+ /Ca^{2+} exchanger (NCX), three Na^+ are imported, and one Ca^{2+} is exported out of the cell. The Na^+ /Ca^{2+}-K^+ exchanger (NCKX) cotransports Ca^{2+} and K^+ out of the cell while four Na^+ are imported into the cell (Clapham, 2007). Extensive Ca^{2+} depletion in the ER could activate the store-operated calcium entry (SOCE) to refill the ER calcium content. Stromal interacting molecule (Stim1 and 2) ER membrane proteins sense the low calcium concentration in the ER, and subsequent conformational changes activate Ca^{2+} release-activated Ca^{2+} channels (CRAC), oligomers of Orai1, 2, and 3 calcium channels in the plasma membrane. The Orai1,

2, and 3 calcium channels conduct Ca^{2+} ions into the cytosol through Stim1 clusters at ER-plasma membrane junctions (Zheng *et al.*, 2018). Stim1 can also activate TRPC4, 5, and 6 in the plasma membrane, and they can act like store-operated calcium channels to mediate the calcium influx (Yuan *et al.*, 2007).

The exact calcium concentration within the ER is diverse and based on the cell type and the activity of the SERCA pumps. As well as, fluctuations occur due to calcium leak channels allowing passive diffusion of Ca^{2+} out of the ER (Lemos *et al.*, 2021; Lang *et al.*, 2011).

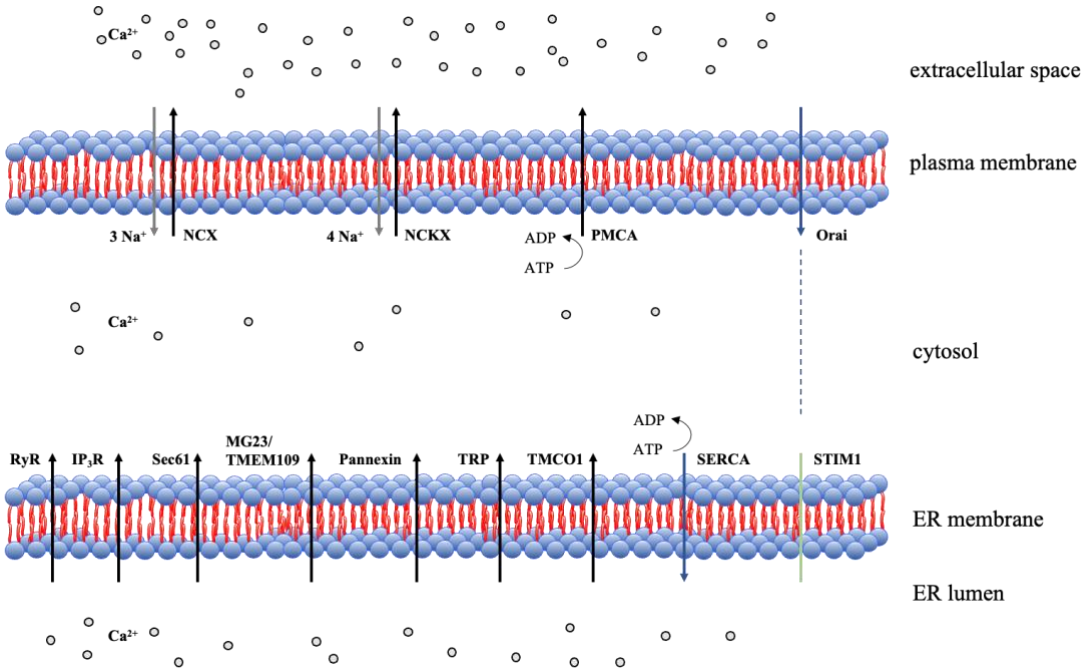

Figure 1. Simplified cartoon of the cellular calcium homeostasis

Black and blue arrows display the flow of the calcium ions, and grey arrows demonstrate the flow of the sodium ions. The SERCA pump allocates Ca^{2+} ions into the ER after ATP hydrolysis. The NCX transports one Ca^{2+} ion out of the cell and three Na^{+} into the cytoplasm. The NCKX transports one Ca^{2+} and one K^{+} ion out of the cell and four Na^{+} into the cytoplasm. The PMCA transports Ca^{2+} ions from the cell against the electrochemical gradient by ATP hydrolysis. In response to low ER calcium concentration, the STIM1 proteins initiate the conformational changes of Orai plasma membrane proteins and initiate the calcium flow into the cytosol via direct Orai-STIM1 connections. Note that there is an ER-plasma membrane junction between the STIM1 and Orai channels; they are in proximity, which is not depicted in the figure. RyR, IP_3R, Sec61, MG23/TMEM109, pannexin channels, TMCO1, and certain TRP channels result in Ca^{2+} release from the ER/SR.

Abbreviations: IP_3R: inositol 1,4,5-trisphosphate receptor type, NCKX: Na^{+}/Ca^{2+}-K^{+} exchanger, NCX: Na^{+}/Ca^{2+} exchanger, PMCA: plasma membrane calcium ATPase, RyR: ryanodine receptor, SERCA: sarco/endoplasmic reticulum Ca^{2+} ATPase, STIM: stromal interaction molecule. MG23: mitsugumin 23/TMEM109: transmembrane protein 109, TMCO1: transmembrane and coiled-coil domain 1, TRP: transient receptor potential.

7.3 PROTEIN BIOGENESIS

The primary function of the ER is protein synthesis, transport, and processing, such as folding and modification (Schwarz and Blower, 2016). Newly synthesized soluble proteins or membrane proteins can be targeted to various cellular organelles, such as peroxisomes, mitochondria, chloroplast (in plants), or the ER (Hasan *et al.*, 2013; Avendaño-Monsalve *et al.*, 2020; Shao *et al.*, 2011; Thomson *et al.*, 2020). The most significant number of protein clients are delivered to the ER, including secretory proteins, membrane proteins, or proteins destined for the endomembrane system can enter the ER equally for further processing after or during their synthesis (Hegde and Keenan, 2011).

The synthesis takes place on cytosolic ribosomes/polyribosomes attached to the ER membrane (Palade, 1975). Ribosomes are megadalton-sized ribonucleoproteins, and they are composed of two subunits: the 60S and the 40S subunit (in eukaryotes); their name is based on their sedimentation coefficients (Ben-Shem *et al.*, 2010). As the Central Dogma of Molecular Biology was formulated 60 years ago, we know that the genetic information is transferred from DNA to RNA and then to the protein (Crick, 1970). As the genetic material cannot leave the cell nucleus, it has to be transferred to a messenger molecule, the messenger RNA (mRNA) (Venters and Pugh, 2009). The mRNA leaves the nucleus and is translated into protein on cytosolic ribosomes. Amino acids are delivered as aminoacyl tRNAs by eukaryotic initiation factors (eIFs) (EF-Tu in prokaryotes). The start codon, methionine, is delivered by the eIF2. The peptide bond is formed between the incoming correct amino acids after GTP hydrolysis by eIFs after the codon-anticodon base pairing. The large ribosome subunit catalyzes the peptide bond formation between the incoming amino acids in the peptidyl transferase center (PTC) (Jackson *et al.*, 2010; Loveland *et al.*, 2020). The nascent chain leaves the ribosome through the ribosomal exit tunnel.

Based on cryo-EM and X-ray crystallography results, it was shown that the prokaryotic ribosome exit tunnel is generally larger than the eukaryotic one (Duc *et al.*, 2019). The geometry of the upper part of the tunnel is conserved across species, and the lower part shows more diversity in all three kingdoms of life (Yusupova and Yusupov, 2017; Duc *et al.*, 2019). In eukaryotes, proteins uL23, uL29, and eL39 shape the exit port of the exit tunnel (Duc *et al.*, 2019; Fedyukina and Cavagnero, 2011). Close to the PTC and near the mouth of the ribosome exit tunnel, most nascent polypeptide chains appear to form α-helical structures (Wruck *et al.*, 2021; Wilson and Beckmann, 2011). This suggests that the ribosome is more than a passive protein conducting element; it can help proteins fold into secondary structures (Fedyukina and Cavagnero, 2011; Lu and Deutsch, 2005). It was also observed that the distal end of the ribosome exit tunnel could assist in the formation of transient tertiary structures in prokaryotes (O'Brien *et al.*, 2010; Kosolapov and Deutsch, 2009). Membrane proteins are more likely to form secondary structures than soluble proteins in the ribosomal tunnel (Fedyukina and Cavagnero, 2011). The ribosomal exit tunnel's inner wall is predominantly lined with negatively charged amino acids, resulting in a negative electrostatic potential (Lu *et al.*, 2007; Lu and Deutsch, 2008). While in the exit port, positively charged amino acids are found (Duc *et al.*, 2019).

Cryo-EM microscopy results revealed that translational stalling could advance the secondary structure formation of the nascent chain due to more time allowance in the tunnel. Hence, the structure of the nascent chain is modified, and it can alter the recruitment of different chaperones or accessory proteins to the ribosome, for example, NAC or SPR (Tsai *et al.*, 2008; Wilson and Beckmann, 2011). However, excessive stalling can result in misfolding of proteins or frameshift mutations or degradation of the mRNA (Schuller and Green, 2018; Sitron and Brandman, 2020; Tsai *et al.*, 2008). The geometry of the tunnel itself can alter the translational speed and subsequent folding events (Duc *et al.*, 2019).

As the nascent polypeptide chain emerges from the exit tunnel, it becomes available to variable ribosome-associated protein biogenesis factors (RPBs). Usually, these RPBs dock near or at the exit tunnel, ready to associate with the nascent chain. How the RPBs recognize their specific nascent substrate is not well understood, especially in the eukaryotic cells (Hsieh *et al.*, 2020). The signal recognition particle (SRP) is indispensable for co-translational protein targeting to the ER. It directs the newly synthesized proteins, nascent proteins, together with the ribosome to the signal recognition particle receptors (SR) and then to the ER translocon. The SRP recognizes the ribosome-nascent chain complex (RNC) when the nascent chain carries a signal peptide (SP), or it has a transmembrane domain (TMD) (Wild *et al.*, 2019). The SRP specifically recognizes the proteins on the translating ribosome that are destined to the ER and not to other cellular organelles or cytosolic proteins. However, this selection is not well established (Hsieh *et al.*, 2020). Previous studies revealed that the SRP could bind to the ribosome before the SP leaves the exit tunnel, and it can also bind to ribosomes without RNC. The presence of a SRP near the ribosome can accelerate the SRP targeting to the SR (Lee *et al.*, 2018).

The nascent polypeptide-associated complex (NAC) is a chaperone protein in eukaryotic cells. NAC is a heterodimer of two subunits, the NACα and β; it forms a β-barrel structure. NAC regulates SRP association to the nascent chain and can contribute to co-translational folding as well (Gamerdinger *et al.*, 2019; Zhang *et al.*, 2012). It exists in equimolar concentration in comparison to ribosomes, while SRP is underrepresented in cells in contrast to NAC. The αNAC is associated with the outer ribosome surface, while a part of the βNAC is inserted deeply into the ribosomal exit tunnel. This insertion is critical for subsequent Sec61 translocon targeting; βNAC senses the actively translating ribosomes, preventing the delivery of empty ribosomes to the translocon (Gamerdinger *et al.*, 2019).

SGTA and Bag6 are other components that can be recruited to the ribosome before the nascent chain has emerged. The transmembrane domain recognition (TRC) pathway (GET pathway in yeast) is responsible for post-translational ER targeting of tail-anchored proteins. (Both the SRP and the TRC pathway are described in more detail later.) Mammalian Bag6, a member of the TRC pathway, has been shown to interact with the ribosome and assumably helps in early substrate recognition. SGTA is also associated with the ribosome before the nascent polypeptide is released from the exit tunnel. In addition, SGTA can bind to the hydrophobic TMD of the newly synthesized polypeptide chain and can relay it to further TRC pathway components or ER membrane complex (EMC) components for following membrane insertion (Leznicki and High, 2020). Get4/5 helps position the sgt2 (mammalian SGTA) at

the ribosomal exit tunnel in yeast. Get4/5 binds to the ribosomes substrate unspecifically; however, it shows a higher affinity to protein clients with C-terminal TMDs (Zhang *et al.*, 2021).
It has been uncovered that whether a nascent chain is part of a soluble or a membrane protein is early detected by the ribosome rather than the translocon. FRET, photocrosslinking, and fluorescence quenching data revealed that the translocon pore first is closed at the luminal side by the BiP chaperone then it is open to the cytosol when the C-terminal end of the TMD is 4-9 amino acids away from the tRNA (Liao *et al.*, 1997; Woolhead *et al.*, 2004). Photocrosslinking experiments shed light on the fact that at this stage of the targeting neither the Sec61α nor the TRAM is associated with the nascent chain rather ribosomal proteins are. Changes in the ribosome-translocon complex are mediated by the TMD of the newly synthesized polypeptide chain inside the ribosome (Liao *et al.*, 1997).

7.3.1 THE UNFOLDED PROTEIN RESPONSE

Protein folding in the ER involves the activation of specific enzymes and chaperones, such as BiP or protein disulfide isomerases (PDIs); the latter are responsible for disulfide bond formation or destruction. N-linked glycosylation and polypeptide oligomerization are also important modifications for proteins to reach a mature state. Unfolded proteins are retained in the ER with the help of ER chaperones, such as calnexin or calreticulin. These chaperones require calcium for their proper function. Through cycles of glucosylation and deglucosylation, unfolded proteins can reach their mature form. The glucosyltransferase has a high affinity to unfolded proteins. It keeps adding glucose to the deglucosylated unfolded proteins to retain them in the ER until they are correctly folded and ready to exit the ER. However, prolonged time spent in the ER activates the mannosidase enzyme and the PDI, and the unfolded proteins are destined for retrotranslocation to the cytosol for degradation (Tsai *et al.*, 2002). Many unfolded proteins undergo ATP-dependent ubiquitination and are degraded by the proteasome; the process is known as ER-associated degradation (ERAD). It was speculated that unfolded proteins presumably use the Sec61 channel for retro-translocation with accessory proteins, (Tsai *et al.*, 2002); however, this mechanism of the translocon channel was dismissed. The ER luminal Hrd3 and the ER membrane resident Hrd1-Der1 complex have been proposed to form a channel for the retro-translocation (Wu *et al.*, 2020; Schoebel *et al.*, 2017).
Cells evolved a systematic mechanism in response when unfolded proteins are accumulated to a large extent. To overcome the ER stress and restore ER function, cells initiate the unfolded protein response (UPR) (Lin *et al.*, 2008). Specific transmembrane proteins sense the large amount of unfolded or misfolded proteins and initiate downstream reactions to restore the physiological function of the ER. These specific ER transmembrane proteins are the inositol-requiring enzyme 1 (IRE1) kinase/endoribonuclease, protein kinase RNA-like endoplasmic reticulum kinase (PERK), and activating transcription factor 6 (ATF6).
Upon ER stress, ER membrane protein IRE1 undergoes conformational changes. After oligomerization becomes activated through autophosphorylation. Once autophosphorylated, it gains endoribonuclease

activity in its cytosolic domain and splices the x-box protein 1 mRNA (*XBP1*). The spliced *XBP1* mRNA is efficiently translated, and the corresponding Xbp1 protein initiates the transcription of specific genes, for example, genes that encode for chaperones. PERK, similarly to IRE1, becomes active in response to ER stress. The kinase function of the cytosolic domain becomes active and phosphorylates the eukaryotic initiation factor (eIF2) to slow down overall protein synthesis. Specific mRNAs that encode transcription regulators can still be translated to help the cells overcome the ER stress; for example, it initiates the synthesis of chaperone proteins. ATF6 is another ER transmembrane protein. When misfolded proteins accumulate in the ER, ATF6 is transported into the Golgi, and its cytosolic domain is cleaved off. After cleavage, the cytosolic ATF6 fragment can enter the nucleus and act as a transcription factor. It initiates the transcription of specific genes involved in ER stress, such as chaperone proteins, e.g., BiP (Lin *et al.*, 2008).

However, if the cells undergo ER stress for a prolonged period of time, UPR can initiate a pro-apoptotic outcome. (Guha *et al.*, 2017; Wu *et al.*, 2018; Lindner *et al.*, 2020)

7.4 THE SEC61 TRANSLOCON

The translocation of 30 % of the proteins encoded by the genome is carried out by the Sec61 protein conducting channel, a protein complex residing in the ER membrane of all nucleated cells (Chen, 2004). Proteins can reach the ER via co- and post-translational mechanisms (Figure 4), described in more detail in a following chapter.

Sec61 is a heterotrimeric membrane protein complex in the ER membrane of eukaryotes. The mammalian Sec61 translocon consists of 3 subunits, the α, β, and γ (Rapoport, 2007; Berg *et al.*, 2004) (Figure 2B). All subunits have a cytosolic N-terminus. The α subunit is indispensable for protein translocation. It comprises ten helices and two pseudo-symmetrical halves between transmembranes 1-5 and 6-10. Its shape resembles an hourglass forming the channel's pore and allowing the passage of polypeptides into the ER lumen (Rapoport, 2007). The constriction of the hourglass shape is the pore ring. A single Sec61α forms the pore region. The interior of the pore ring consists mainly of amino acids with hydrophobic side chains. SecY is the bacterial, and Sec61p is the yeast orthologue of the mammalian Sec61α subunit (Breyton *et al.*, 2002; Bostina *et al.*, 2005; Rapoport, 2007).

A plug domain closes the pore from the ER luminal side, and it is formed by the luminal loop 1 of the α subunit (Figure 2A). During protein translocation, the plug domain moves to allow the conduction of newly synthesized proteins into the ER (Itskanov *et al.*, 2021; Rapoport, 2007). The loop between transmembrane segments 5-6 functions as a "hinge," allowing the lateral opening of the gate at transmembrane helices 2/3 and 7/8 for the insertion of membrane proteins (Figure 2A). Accordingly, transmembrane segments are inserted into the lipid bilayer of the ER (Voorhees and Hegde, 2016).

The β and γ subunits are tail-anchored proteins. Sbh1 is the yeast, and SecG is the bacterial ortholog of the mammalian β subunit, while the mammalian γ subunit is known as Sss1p in yeast and SecE in bacteria. It has been established that in *Saccharomyces cerevisiae* and *Escherichia coli*, the corresponding α and γ subunits are essential for cell survival. In contrast, the β subunit did prove to be dispensable in all three kingdoms of life. The γ subunit connects the two pseudo-symmetrical halves of the α subunit near the previously described "hinge" region (Berg *et al.*, 2004).

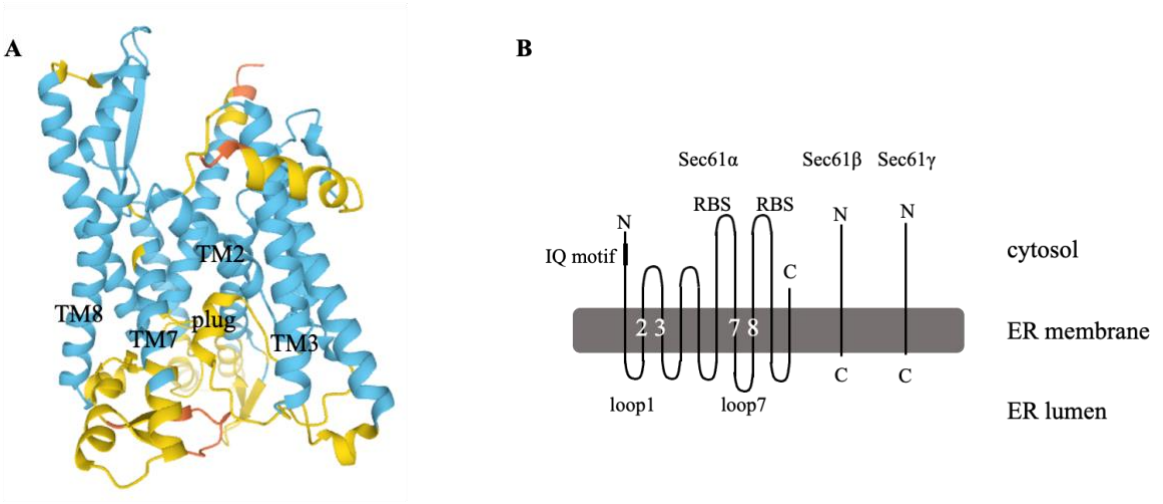

Figure 2. Structure and topology of the Sec61 translocon

Figure A depicts the structure of the Sec61α subunit, highlighting the plug domain (loop1) and the transmembrane helices (2/3, 7/8) that form the lateral gate of the translocation channel; for details, see the text above. TM stands for transmembrane helix. Figure A was created by the https://alphafold.ebi.ac.uk webpage. Figure B displays the topology of the Sec61 complex (Sec61α, β, and γ). Loop1 of the Sec61α forms the plug domain, and loop7 is responsible for BiP interaction. Loops 6 and 8 can bind the ribosome during co-translational protein translocation, labeled as RBS: ribosome binding sites. The N-terminal IQ motif is responsible for calmodulin binding.

The Sec61 complex with accessory proteins helps the conduction of precursor polypeptides and the modification of these polypeptides. Previously characterized accessory proteins are the Sec62, Sec63, signal peptidase complex (SPC), the oligosaccharyltransferase (OST) complex, translocon-associated protein (TRAP) complex, translocating chain-associating membrane protein (TRAM), and other chaperone proteins (Gemmer and Förster, 2020; Skach, 2007). Sec62 and Sec63 associated with Sec61 are important for post-translational protein translocation to the ER. Sec62 is a two-transmembrane domain protein, and both the N- and C-terminal ends are cytosolic. The C-terminal end of the Sec62 interacts with the N-terminal end of the Sec61α. Sec62 might be essential for the translocation of short presecretory proteins that due to their length transport post-translationally (Lang *et al.*, 2012; Lakkaraju *et al.*, 2012). It could be essential for stabilizing the Sec61α lateral gate for inserting less hydrophobic signal sequences post-translationally (Weng *et al.*, 2020). Sec63 is a three-transmembrane domain protein, and it has a luminal N-terminal and a cytosolic C-terminal end. The J domain of Sec63 is associated with the ER luminal chaperone BiP, which is important for translocating the polypeptides through the channel. BiP is also known to seal the Sec61 pore in order to prevent Ca^{2+} efflux (Schäuble *et al.*, 2012). The substrate-binding domain of the BiP is associated with loop 7 of the Sec61α (Hamman *et al.*, 1998). Sec62/Sec63 complex and BiP might be essential for short presecretory proteins with less hydrophobic signal sequences regarding the efficient targeting to the ER and insertion by the Sec61 (Haßdenteufel *et al.*, 2018).

The ER-resident signal peptidase complex (SPC) is a heterotetrameric serine protease that removes signal peptides (SP) after the translocation of proteins bearing an N-terminal SP. The cleavage happens

in the c-region of the SP. The SP is inserted into the lipid bilayer, where it is degraded rapidly by proteases in the ER membrane (Gemmer and Förster, 2020; Paetzel *et al.*, 2002; Liaci *et al.*, 2021).

The OST complex is indispensable for one of the most diverse post-translational modifications, the N-glycosylation (Schjoldager *et al.*, 2020). Glycosylation can be enzymatic or non-enzymatic. The majority of the proteins are glycosylated enzymatically in the ER and the Golgi system. We distinguish four major types of enzymatic glycosylations: the N-linked and the O-linked glycosylation, C-mannosylation, and glypiation; the latter is typical for GPI anchored proteins. The OST-complex catalyzes N-glycosylation in the ER by the addition of a preformed glycan consisting of N-acetylglucosamine ($GlcNAc_2$), mannose (Man_9), and glucose (Glc_3) to the asparagine amino acid residues. Two isoforms of the OST complex exist in mammalian cells that differ in the catalytic subunit, the STT3A or STT3B (Schjoldager *et al.*, 2020). STT3A is part of the OST-A complex and is believed to catalyze co-translational glycosylation, primarily. At the same time, STT3B is part of the OST-B complex and can contribute to post-translocational glycosylation. OST-A is a ribosome and translocon-associated oligosaccharyltransferase. Nevertheless, OST-B and the catalytic STT3B subunit depict little or no association with the ribosome or the translocon (Harada *et al.*, 2019; Ruiz-Canada *et al.*, 2009).

The TRAP complex is a heterotetrameric membrane complex, and it consists of α, β, δ, γ subunits (also known as SSR1-4), and it is responsible for the stimulation of protein translocation. The α, β, and δ subunits are single-pass transmembrane proteins, and the γ subunit is presumably a four-transmembrane domain protein (Pfeffer *et al.*, 2017). Protein clients bearing a SP rich in proline and glycine are proved to be TRAP-dependent for their ER translocation (Kriegler *et al.*, 2020). The TRAP complex assumably can affect the topology of membrane proteins (Pfeffer *et al.*, 2017). Furthermore, mutations in the δ subunit of TRAP have been shown to initiate reduced N-glycosylation of proteins (Ng *et al.*, 2015; Losfeld *et al.*, 2014), which suggests the role of the TRAP in glycoprotein biogenesis. It has been found that the α and β subunits can promote N-glycosylation of protein substrates in ER stress (Phoomak *et al.*, 2021). TRAM is an eight-transmembrane glycoprotein, transiently associated with the Sec61 complex, and it promotes the translocation of substrate proteins and the integration of membrane proteins (Tamborero *et al.*, 2011). TRAM has been described to support SRP-dependent protein transport into the ER (Voigt *et al.*, 1996).

During protein translocation, the integrity of the membrane is maintained by the ribosome bound to the translocon and luminally by the BiP chaperone, as well as certain residues in the Sec61α seal the pore surrounding the translocating polypeptide chain. The opening and the closing of the translocation channel are highly regulated to avoid passive ion leakage (Woolhead *et al.*, 2004). The interaction between the chaperone and Sec61α is promoted by the Sec63 protein to ensure the unidirectional transport (Linxweiler *et al.*, 2017; Zimmermann *et al.*, 2011).

7.5 TARGETING SIGNALS

The signal hypothesis was formulated 50 years ago by Günter Blobel and David Sabatini. They stated that a cleavable N-terminal signal sequence/signal peptide (SP) on the proteins directs them to the ER, and after translocation, the SP is cleaved off (Blobel and Sabatini, 1971). These targeting signals on proteins function as a molecular label to direct the proteins to the ER, and their amino acid sequence varies greatly (Martoglio and Dobberstein, 1998).

The N-terminal SP has specific features rather than a consensus sequence; it is a highly hydrophobic stretch of amino acids that engages with the SRP. The SP consists of the so called n-, h-, and c- regions and is typically 15-30 residues long (Janda *et al.*, 2010; Rapoport, 2007). The n-region comprises positively charged amino acids, while the h-region consists of 8-15 hydrophobic amino acids, and the c-region consists of polar amino acids. The h-region finds its specific interaction partner with the SRP ribonucleoprotein (Janda *et al.*, 2010). The ribosome nascent chain complex engaged with the SRP is targeted to the ER membrane with the help of the SR (Nagai *et al.*, 2003). The translocation is initiated into the ER through the Sec61 translocon, and the SP is cleaved off by the SPC. It has been shown in yeast cells that the SRP can fail to engage with the N-terminal SP if it is less hydrophobic (Ast *et al.*, 2013). A point mutation induced in the hydrophobic core of the SP reduced the translocation efficiency of a model protein (Arnold *et al.*, 1990). SRP-deficient yeast cells show impaired growth and translocation efficiency into the ER (Hann and Walter, 1991). The SPC has to distinguish SP selectively from transmembrane segments, which is likely due to the specific interaction of the SP with the Sec61α and the difference in their lengths (Gamerdinger *et al.*, 2019; Donnell *et al.*, 2020).

Approximately 26 % of the proteins in mammals are membrane proteins (Fagerberg *et al.*, 2010). A vast majority of membrane proteins are inserted into the ER membrane; the insertion is greatly influenced by the length and the hydrophobicity of the transmembrane segments (Hegde and Keenan, 2021). Also, chaperone binding and folding capacity can affect the membrane insertion potential (Janoschke *et al.*, 2021). The lateral gate of the Sec61α enables membrane protein insertion, as described in Paragraph 7.4. Positively charged amino acids influence the orientation of a membrane protein; their insertion occurs based on the positive inside rule; positively charged ends are facing the cytosol (Janoschke *et al.*, 2021).

Based on the orientation of a transmembrane segment, we distinguish type I, type II, type III, and tail-anchored membrane proteins. Type I transmembrane proteins' orientation is N_{exo}/C_{cyto}, and they carry a cleavable N-terminal SP, which is cleaved off after ER transfer. Type II proteins have N_{cyto}/C_{exo} orientation. Type III proteins are inserted into the ER membrane as the type I proteins (N_{exo}/C_{cyto}); however, they do not carry a cleavable SP. Tail-anchored membrane proteins are anchored to the lipid bilayer by their C-terminal end; their N-terminus is cytosolic, providing an N_{cyto}/C_{exo} orientation (Figure 3) (Hegde and Keenan, 2021; O'Keefe *et al.*, 2021).

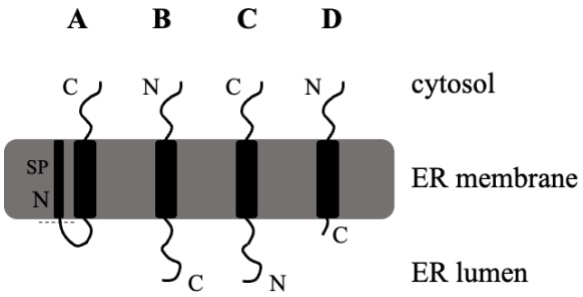

Figure 3. Membrane topology of single-pass transmembrane proteins

Topology of single-pass transmembrane proteins, the orientation of the N- or C-terminal end of the proteins flank the cytosol or the ER lumen, depending on the type of transmembrane protein.
A) type I membrane protein, B) type II membrane protein, C) type III membrane protein, and D) tail-anchored membrane protein. SP stands for signal peptide, which is cleaved off by the SPC in the case of type I transmembrane proteins after their insertion into the ER membrane.

The membrane-spanning segment of a TMD has, in general, an α-helical structure. These hydrophobic segments are usually 20 amino acid long residues and enriched in very hydrophobic amino acids, such as tyrosine or tryptophan, near the polar lipid heads in the bilayer. The final topology of a membrane protein is influenced by charges, hydrophobicity, folding of the TMD, and the charges preceding or following the TMD. Partially folded TMD segments and mutations that lowered the hydrophobicity resulted in a reduced integration threshold (Janoschke *et al.*, 2021). The orientation of the membrane proteins is also influenced by an N-terminally folded segment preceding the first TMD, which promotes the N-terminal cytosolic integration (Denzer *et al.*, 1995).

Type II membrane proteins are inserted "head-first" just like type I membrane proteins; however, in the final topology, their C-terminal end is ER luminal, so they must invert. This inversion is facilitated in the Sec61α channel. A tight ribosome-translocon junction ensures the proper sealing of the channel. The synthesized polypeptide regions (~30 aa) after the TMD are accumulated in the ribosome exit tunnel. After the nascent chain reached sufficient length (~125-133 aa), the inversion is facilitated, and the C-terminal end is released into the ER lumen, and the N-terminus is flipped to the cytosol. The inversion is mainly initiated by the charges in the TMD maintaining the positive inside rule (Devaraneni *et al.*, 2011).

In the case of transmembrane or multipass transmembrane proteins, their TMD serves as a stop-transfer sequence. As soon as a stop-transfer sequence reaches the Sec61 translocon, it allows the opening of the lateral gate, and the hydrophobic transmembrane segment or segments are inserted into the ER membrane. The process is repeated until all segments are membrane inserted, and a start transfer sequence initiates further translocation. Usually, the first inserted TMD influences the orientation of the downstream TMDs (Sato *et al.*, 1998). Interactions between TMDs have also been shown to influence the topology of multipass membrane proteins, as well as the inserted TMD's interaction with lipids in the bilayer. The lipid composition of the ER bilayer also impacts the topology of a membrane protein (Dowhan and Bogdanov, 2009). A hydrophobic mismatch can also occur if a TMD is too short in the

bilayer so that polar amino acids would be exposed to the hydrophobic lipid bilayer or it exceeds the thickness of the bilayer and hydrophobic amino acids would be exposed to an aqueous environment. In these scenarios, both the TMD (by dimerization, interhelical interactions) and the bilayer (by deformations) can adapt flexibly (Orzáez *et al.*, 2000; Sparr *et al.*, 2005; Killian, 1998).

7.6 CO- AND POST-TRANSLATIONAL PROTEIN TARGETING TO THE ENDOPLASMIC RETICULUM

Nearly 30 % of the proteome reaches the ER via the SRP-dependent protein transport pathway, the so called SRP-dependent co-translational protein targeting mode (Akopian *et al.*, 2013) (Figure 4A). The cytosolic SRP ribonucleoprotein associates with the, typically, N-terminally located SP on the proteins emerging from the translating ribosome. The SRP comprises the 7SL RNA and six protein subunits: SRP9, SRP14, SRP19, SRP54, SRP68, and SRP72. The 7SL RNA is folded into a Y-like shape secondary structure. The SRP has two functional domains: the Alu and the S domain. The SRP9-SRP14 heterodimer is connected to the "stem region" of the 7SL RNA, which forms the Alu domain. At the same time, the S domain comprises the rest of the protein subunits and the "fork region" of the 7SL RNA. SRP54 consists of an N-terminal domain, a GTPase G domain, and a C-terminal helical methionine-rich M domain. The M domain of the SRP54 builds the connection between the SRP and the nascent polypeptide chain as it emerges from the ribosome, forming the RNC. The SRP-RNC complex binds to the SR. SR is a heterodimer, and it has two subunits, the α, and the β. The α subunit is anchored to the β subunit, which is a single-pass transmembrane protein in the ER membrane (Fu *et al*., 2019; Lee *et al*., 2018; Nagai *et al*., 2003). The NG domain of the SRP54 interacts with the homologous NG domain on the SR. Their interaction is GTP dependent, as well as the transfer of the SP with the Sec61 translocon. After GTP hydrolysis, the SP can interact with the SRP, and in the presence of GMP, the SP can connect with the Sec61 translocon. This type of GTPase is regulated by nucleotide-dependent dimerization cycles (Akopian *et al.*, 2013). After GTP hydrolysis, the nascent polypeptide chain is directed to the Sec61 protein conducting channel (Voorhees and Hegde, 2016). SRP is retrieved and reused in another translocation cycle (Hsieh *et al.*, 2020). During protein transport through the Sec61 channel, the ribosome is recruited at the Sec61. The cytosolic loops 6 and 8 of the Sec61α subunit and the N terminal end of the Sec61γ subunit interact with the ribosome (Voorhees *et al.*, 2014; Rapoport, 2007) (Figure 2B). The translocon binds to the ribosome near the exit tunnel (uL23, eL29) (Voorhees *et al.*, 2014) close to where the S domain of the SRP binds to the ribosome (uL23, uL35) (Halic and Beckmann, 2005). Thus, the handover of the RNC to the Sec61 complex requires the release of the SRP from the nascent chain.

The two-step opening of the channel is due to the ribosomal association with the Sec61, which initiates the opening (priming) of the cytosolic side of the lateral gate at transmembrane helix 2. The hydrophobic h-region in the SP possibly interacts with the helix 2 in the lateral gate of Sec61α in the cytosolic side of the channel, which initiates its opening. In step two, the lateral gate of the channel further opens, allowing the SP insertion. Opening of the lateral gate of the channel results in the displacement of the plug domain in the interior of the tunnel, which allows the nascent chain translocation (Voorhees *et al.*, 2014).

The post-translational protein transport mechanism has some characteristic differences as opposed to the co-translational (Gemmer and Förster, 2020; Linxweiler *et al.*, 2017). After complete synthesis of

the protein, it dissociates from the ribosome, and chaperones, such as cytosolic Hsp40 and Hsp70, bind to the unfolded protein (Weng *et al.*, 2020; Itskanov *et al.*, 2021) (Figure 4B). N-terminal sequences that are less hydrophobic or polypeptides that are too short for efficient SRP-dependent targeting are directed post-translationally to the ER (Linxweiler *et al.*, 2017). Post-translational protein translocation requires the Sec61 channel to associate with auxiliary proteins like Sec62 and Sec63, as well as the luminal BiP chaperone ATPase (Itskanov *et al.*, 2021). When the fully synthesized polypeptide chain reaches the translocation channel, the cytosolic chaperones are displaced. The TM2 of the Sec62 could be essential for opening (priming) the lateral gate of the Sec61α, which could be further opened by the TMD1 of Sec62, helping to translocate less hydrophobic signal sequences post-translationally by the Sec61α. The movement of the lateral gate in the Sec61α initiates the plug domain movement for the polypeptide chain translocation (Weng *et al.*, 2020). The Sec62 N-terminal end carries predominantly positive charges and is associated with the negatively charged C-terminal end of the Sec63 (Weng *et al.*, 2020). The ER luminal chaperone BiP ensures the unidirectional transport of the precursor chain in transit. BiP association with the J domain of the Sec63 stimulates its binding nonspecifically to substrate proteins that are being translocated through the Sec61 channel. The substrate-binding pocket of the BiP associates with the emerging nascent polypeptide chain after ATP hydrolysis. As the nascent polypeptide moves into the ER, additional BiP proteins bind to it in response to ATP hydrolysis until the polypeptide chain is fully translocated (Tyedmers *et al.*, 2000). Nucleotide exchange factors (NEFs) stimulate the release of ADP in exchange for ATP in the nucleotide-binding pocket of the BiP. This initiates the substrate release from BiP, which can be recycled (Misselwitz *et al.*, 1998; Rapoport, 2007). The role of the Sec62 is most possibly to help the efficient translocation of short secretory proteins (Linxweiler *et al.*, 2017). It has been uncovered that Sec62 can also induce recovery from ER stress. The C-terminal LIR domain has been shown to interact with the LC3 on phagophores, which induces the formation of autophagosomes and targeted delivery to lysosomes. Sec62 proved to assist in selective lysosomal degradation of certain ER components (e.g., accumulated chaperones) after ER stress (Fumagalli *et al.*, 2016; Birgisdottir *et al.*, 2013). Sec62 can interact both with Sec61 and Sec63; the N-terminus of Sec62 interacts with the C-terminus of Sec61α.

Sec63 proved to be essential for sufficient translocation for a subset of proteins, while other proteins do not require Sec63 for this process (Linxweiler *et al.*, 2017). Proteomics data revealed that proteins with SP bearing a longer but less hydrophobic h-region and reduced polarity in the c-region than usual depend on the Sec62/63 and BiP to access the ER (Schorr *et al.*, 2020). This promotes the idea that the Sec62/63 is not only important for the post-translational transport of short presecretory proteins.

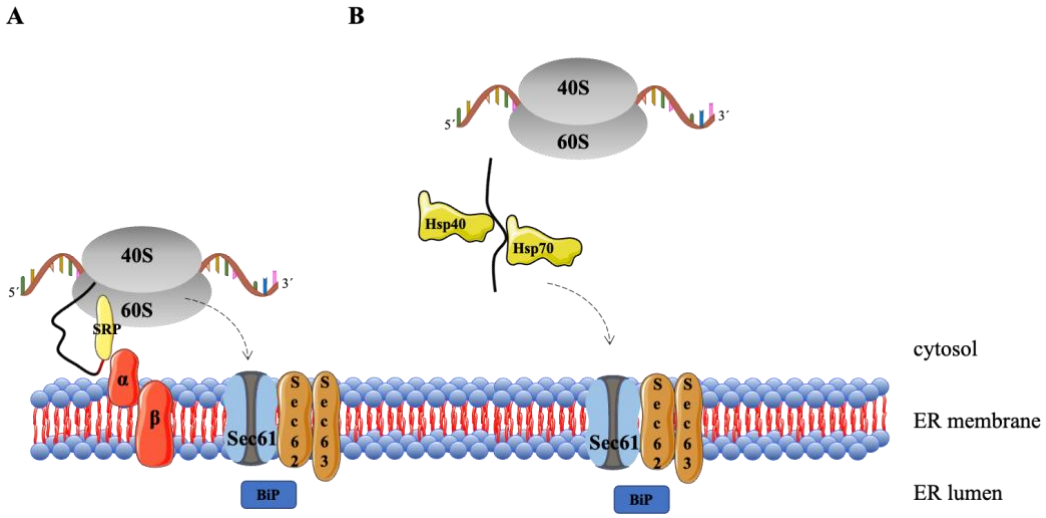

Figure 4. Co- and post-translational protein targeting to the endoplasmic reticulum

Abbreviations: SP: signal peptide, SRP: signal recognition particle, Hsp: heat shock protein

A: Co-translational protein targeting to the ER. During co-translational protein transport, the ribonucleoprotein SRP binds to the N-terminal hydrophobic SP on the emerging polypeptide and the ribosome as well. The SRP directs the nascent polypeptide chain to the SRP receptor (SRα and β). After GTP hydrolysis, SRP dissociates, and the nascent polypeptide chain is inserted into the Sec61 channel. BiP can help the protein translocation and seal the channel in the absence of protein translocation.

B: Post-translational protein targeting to the ER. After cytosolic polypeptide synthesis, Hsp40 and Hsp70 chaperones associate with the hydrophobic regions of the newly synthesized polypeptide. The protein is targeted to the Sec61 translocon, where the Sec61 associated Sec62 and Sec63 help the translocation of the protein. BiP helps the protein translocation by applying pulling force and ensures unidirectional transport. BiP can also seal the channel in the absence of protein translocation.

7.7 THE TRANSMEMBRANE DOMAIN RECOGNITION COMPLEX (TRC) PATHWAY

As opposed to proteins containing N-terminal SP, tail-anchored proteins use a different pathway for targeting and being inserted into the ER membrane (Stefanovic and Hegde, 2007). Tail-anchored proteins lack an N-terminal SP in their structure, and they carry a C-terminal hydrophobic region that anchors them into the membrane. As during protein synthesis, the N-terminus of the newly synthesized polypeptide chain emerges from the ribosome, co-translational SRP targeting of the C-terminus is not possible for tail-anchored proteins. Instead, tail-anchored proteins are inserted post-translationally into the ER membrane, targeted by their C-terminal TMD, using the transmembrane recognition complex (TRC) pathway (Borgese *et al.*, 2003; Stefanovic and Hegde, 2007; Favaloro *et al.*, 2008). However, certain tail-anchored proteins can be inserted into the ER membrane without the presence of the TRC pathway (Borgese *et al*., 2003; O'Keefe *et al*., 2021; Shurtleff *et al*., 2018). The TRC pathway is highly conserved throughout the domains of life. It is well established in mammalian, yeast, and plant cells. In yeast and plant cells, it is known as the guided entry of tail-anchored proteins (GET) pathway (Xing *et al.*, 2017; Chio *et al.*, 2017; Asseck *et al.*, 2021).

In yeast, the GET pathway has six components. First, the tail-anchored protein is recognized by the Sgt2 in association with Get4/5. Get4/5 has a high affinity to the ribosome, and upon the emergence of the C-terminal TMD, it helps Sgt2 interact with it. Then, the tail-anchored protein is transferred to the cytosolic component of the pathway to the Get3 ATPase. Get3 conducts the protein to the Get1/2 membrane receptor in the ER membrane for insertion (Hegde and Keenan, 2011; Mateja *et al.*, 2015; Simpson *et al.*, 2010).

In higher eukaryotic cells, the homologs of the pathway components are the SGTA (Sgt2), TRC35 (Get4), UBL4A (Get5), TRC40 (Get3), and WRB/Caml (Get1/2) (Figure 5B). In eukaryotes, there is an additional component of the pathway, which is the Bag6. Bag6 associates with the TRC35 and the UBL4A, and they form the Bag6 complex. Bag6 functions as quality control for tail-anchored proteins. It recognizes hydrophobic TMD segments on the proteins and can influence downstream reactions such as targeting to the ER membrane or proteasomal degradation by ubiquitination (Chio *et al.*, 2017).

3-5 % of the proteome are tail-anchored proteins (Hegde and Keenan, 2011). Tail-anchored proteins are represented in all membranes and participate in vesicular trafficking, apoptosis, or protein insertion. Representatives for tail-anchored proteins are, for example, SNARE proteins such as synaptobrevin, Sec61 component: Sec61β, or members of the Bcl2 family (Hegde and Keenan, 2011; Borgese *et al.*, 2003). First, it was found that synaptobrevin membrane insertion did not require SRP or Sec61, albeit its insertion depended on a protein component and ATP (Kutay *et al.*, 1995).

In contrast to the co-translational acting SRP and SR depending on GTP hydrolysis, the yeast Get3 and its mammalian counterpart, transmembrane domain recognition complex subunit of 40kDa (TRC40), are ATPases. The helical TMD of the tail-anchored protein binds to the hydrophobic groove of the Get3/TRC40. It was shown that by replacing the hydrophobic amino acids with more hydrophilic ones

in the substrate-binding domain of the Get3, the mammalian SGTA failed to passage the tail-anchored protein to the Get3 (Mateja *et al.*, 2015).

Get3 is a dimer, and the two subunits are held together by zink ions and cysteine bridges. The so called closed and open state is maintained by the rotation of the two subunits towards or away from each other, respectively. 13 α-helices and 7 β-strands form the secondary structure. α-helices from α4 to α9 are assumably associated with maintaining the closed and open state, while the remaining helices and strands form the nucleotide-binding domain (NBD). α-helices 7, 8, and 9 can be important for substrate binding, and it was observed that the closed state might be more favorable for substrate binding. Switch I and II domains are responsible for ATP binding, referred to as NBD. How ATP hydrolysis exactly happens is still not well established. After Get3 binds to the Get1/2 insertase, the closed form is stabilized. After ATP hydrolysis, the Get3 probably has an open conformation. The tail-anchored protein is released and is inserted into the ER membrane while Get3 dissociates into the cytosol (Mateja *et al.*, 2015; Simpson *et al.*, 2010).

TRC40 is also known as Asna1 (arsenical pump-driving ATPase protein) in mammals. The TRC40, like the Get3, conducts proteins to the WRB/Caml insertase. It transfers tail-anchored proteins with the help of the Bag6 complex, which comprises Bag6, TRC35, and UBL4. The structure of the TRC40 shows similarity to the bacterial and the yeast Get3 (Farkas *et al.*, 2019; Favaloro *et al.*, 2010). TRC40 loss by knockout resulted in embryonic lethality in mice, suggesting its importance in the embryonic development (Mukhopadhyay *et al.*, 2006).

The Get1/2 or the mammalian counterpart, the WRB/Caml, inserts tail-anchored proteins into the ER membrane. It has been shown that mutations induced in the TMD of the Get1/2 resulted in a decreased insertion into the bilayer of a yeast SNARE tail-anchored protein. It is assumed that the TMDs and the cytosolic domains of the Get1/2 cooperate to help substrate release from the Get3 for membrane insertion. The TMD of the tail-anchored protein presumably interacts with the hydrophilic pocket of the TMD of the Get1/2 insertase. This likely lowers the required activation energy for membrane insertion, which helps substrate release into the bilayer (Wang *et al.*, 2014).

Get1 and WRB share structure similarities, and both are predicted to have three-transmembrane domains. However, Get2 and Caml both have three-transmembrane domains; they show a lower sequence homology (Yamamoto and Sakisaka, 2012). In the Caml structure, a cytosolic helix probably interacts with the TRC40, which helps the tail-anchored protein to move towards the membrane (McDowell *et al.*, 2020). Get1/2, similarly to WRB/Caml insertase, undergoes conformational changes; heterotetramerization allows the insertion of the tail-anchored protein into the membrane. Assumably, the heterotetramerization is triggered by the changes from closed to open state in the TRC40 or Get3 so that the tail-anchored protein can be handed to the insertase (McDowell *et al.*, 2020).

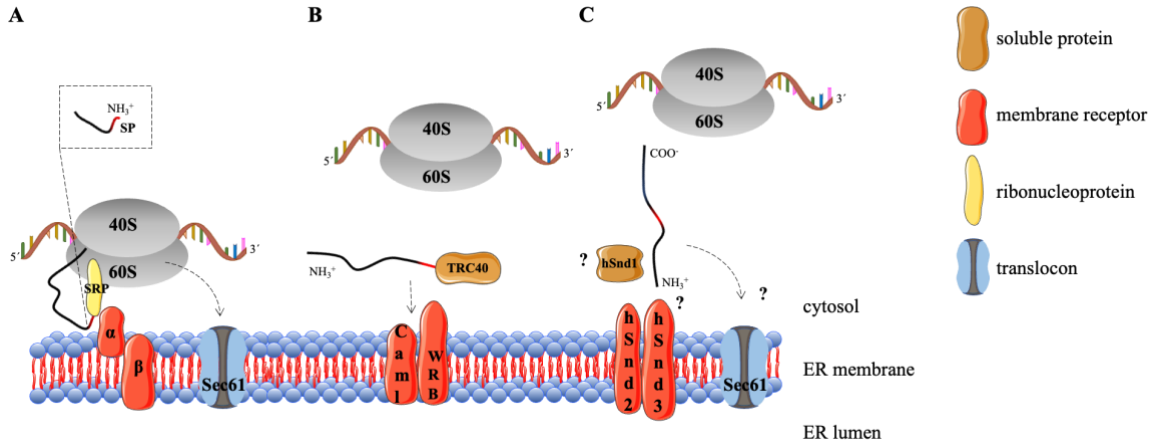

Figure 5. Major protein transport pathways to the human endoplasmic reticulum

Abbreviations: SP: signal peptide, SRP: signal recognition particle, SND: SRP-independent, TRC: transmembrane recognition complex.

Note: the associated proteins to the Sec61 are not visualized in this figure. The SP or transmembrane region of the nascent polypeptide chain is visible in red color.

A) Co-translational SRP-dependent protein targeting to the ER

During co-translational protein transport, the ribonucleoprotein SRP binds to the N-terminal hydrophobic SP on the emerging polypeptide and the ribosome. The SRP directs the nascent polypeptide chain to the SRP receptor (SRα and β). After GTP hydrolysis, SRP dissociates, and the nascent polypeptide chain is inserted into the Sec61 channel.

B) Post-translational TRC protein targeting pathway

Proteins with a C-terminally located transmembrane segment are targeted to the ER via the TRC pathway. The cytosolic TRC40 binds to the hydrophobic C-terminal end of the synthesized protein and guides them to the WRB and Caml transmembrane proteins for membrane insertion. (Ribosome-associated proteins of the pathway are not visualized here.)

C) SRP-independent (SND) protein targeting pathway

The SND pathway presumably delivers proteins with a hydrophobic signal sequence located downstream of the N-terminus. The first component of the pathway, hSnd1 is believed to be soluble, while hSnd2 and hSnd3 are believed to be transmembrane proteins. The hSnd1 and hSnd3 are not known in eukaryotic cells. How exactly the SND substrates are inserted into the ER and whether they use the Sec61 translocon or not is unknown.

7.8 THE SRP-INDEPENDENT (SND) PATHWAY

Many proteins can reach the ER independently from the previously described pathways due to lacking a cleavable SP, for example. The signal recognition particle-independent (SND) pathway has been characterized in yeast cells as an additional targeting route for proteins destined to the ER. A library was created generating mutations in every yeast gene in around 6000 strains. An unbiased high-content screening approach revealed the strains that were unable to transport or differentially transported the tested model protein into the ER than the wild type. A model protein, Gas1, was fused to RFP (Gas1-RFP). Its localization could be monitored visually using a fluorescence microscopy platform. Aggregation of Gas1-RFP in the cytosol indicated the transport defect (Aviram *et al.*, 2016). Gas1 is known to depend partially on the GET pathway and is completely SRP-independent (Ast *et al.*, 2013; Aviram *et al.*, 2016). Strains that carried the mutant translocon subunit Sec61, or a mutant auxiliary component of the translocon (Sec62, Sec63, Sec66, Sec72), or mutant GET pathway component (Get3), Gas1-RFP aggregated in the cytosol. Impaired localization of the model protein in three other mutants was similar to the Get3 mutant strain. These new elements were named SND, and as expected, these mutants did not hamper the localization of SPR-dependent substrates. Snd1 is believed to be a soluble, cytosolic protein, while Snd2 and Snd3 are transmembrane proteins in the ER membrane. Snd2 assumably is a four-transmembrane domain protein, while Snd3 is predicted as a single-pass transmembrane protein (Aviram *et al.*, 2016).

Snd2 and Snd3 immunoprecipitated together, which suggested that they work cooperatively in the SND pathway. Snd2 also co-immunoprecipitated with Snd3 and also Sec61. Subsequent mass spectrometry results confirmed that Snd2 and Snd3 physically interact with the targeting and translocation components in yeast. Native blue gel electrophoresis also confirmed that Snd2 and Snd3 form a complex with Sec61. Pull-down assays established Snd2 and Snd1 interaction. An epistatic link is also established between the SND genes, their depletion is phenotypically manifested in impaired colony growth and Gas1 aggregation (Aviram *et al.*, 2016).

Proximity-specific ribosome profiling identified that in all three Snd mutant samples, substrates with N-terminal TMD were not affected; however, mRNAs encoding for proteins with downstream, more centrally located TMD were depleted. Promoting the idea that the SND machinery has an impact on conducting such substrates to the ER membrane (Aviram *et al.*, 2016).

To verify this, a model protein that carries a central TMD, the Ynl181w, represented reduced ER transport efficiency when Snd1, 2, or 3 was depleted. Reduced SRP activity led to synthetic lethality in strains lacking *SND2* or *SND3*; however, overexpression of *SND2* and *SND3* rescued the complete loss of SRP function and reverted the growth defect. It was also found that the SND and the GET pathway could complement each other. Complete loss of SND became lethal if the GET pathway was not present. The SND pathway can likely compensate or serve as an alternative route to the ER for substrates of the SRP-dependent and the GET pathway (Aviram *et al.*, 2016).

So far, the entire SND pathway has not been described in human cells. The putative second component of the pathway, the hSnd2, also known as TMEM208, was identified based on *in vitro* experiments in the human HeLa cell line (Haßdenteufel *et al.*, 2017). HSnd2 has been shown to localize into the ER membrane (Zhao *et al.*, 2013), and it showed membrane topology similarities with its yeast homolog (Haßdenteufel *et al.*, 2017). It also has been reported that it might be necessary for the biosynthesis of several multipass transmembrane proteins (Talbot *et al.*, 2019). It has been recently described to mediate the ER targeting of proteins with low hydrophobicity GPI attachment signals (Yang *et al.*, 2021).

HSnd2 has been found to have an oxygen-sensitive prolyl hydroxylation motif and also HIF1α transcription factor binding sites in the promoter region (Lei *et al.*, 2020). Based on that, *HSND2* could be a target gene of the HIF1α transcription factor, and its expression could be hypoxia-regulated. HIF1α is a key element in response to hypoxia. It is an oxygen sensor, and it recruits an array of other factors to help the cells cope with low levels of oxygen (Lee *et al.*, 2019; Semenza, 2012).

Co-immunoprecipitation assays confirmed that hSnd2 interacts with various translocon components, such as subunits of the Sec61, the OST complex, or the TRAP complex. This suggests that its contribution to protein targeting to the ER is indeed possible (Haßdenteufel *et al.*, 2017).

Using small interfering RNA-mediated depletion of hSnd2 shed light on compensatory responses by affecting the expression of other targeting pathway receptors. With hSnd2 depletion, SRP receptor subunits (SRα, SRβ) became more abundant, and as a result, improved protein transport efficiency of SRP-dependent substrates occurred, such as preprolactin. Elevated SR protein abundance is likely a compensation mechanism in response to the lower hSnd2 abundance (Haßdenteufel *et al.*, 2017).

SRα and WRB (TRC pathway receptor subunit) simultaneous depletion resulted in elevated hSnd2 protein abundance. This suggests that hSnd2, WRB, and SRα might fulfill similar functions in cells and conduct proteins to the ER in human cells. Sec61β, which is a tail-anchored protein and known to depend on the TRC pathway in its ER transport, was not affected by hSnd2 nor by SRα or SRβ silencing (Haßdenteufel *et al.*, 2017).

HSnd2 silencing affected Qsox1 and cytochrome b5 transport efficiency to the ER. This means that the SND pathway can conduct proteins with less hydrophobic C-terminal TMD into the ER, such as cytochrome b5. Qsox1 carries an N-terminal SP besides the hydrophobic C-terminal TMD and accordingly could depend on the SRP-dependent pathway and might be recognized by the TRC and the SND pathway as well. Cytochrome b5 transport efficiency was further reduced when Sec61α was knocked down simultaneously with the WRB or the hSnd2. This could confirm the potential functional link between the SND and the TRC protein targeting pathways and the human ER translocon complex (Haßdenteufel *et al.*, 2017). The human SND pathway is believed to be composed of three components (Figure 5C); however, only one human SND pathway element is known so far (Haßdenteufel *et al.*, 2017).

Co-immunoprecipitated proteins with hSnd2 were determined by label-free mass spectrometry (Haßdenteufel *et al.*, 2017) (Table 1). As previously described, hSnd2 showed interaction with the oligosaccharyltransferase (OST), translocon-associated protein (TRAP) complex, and the Sec61 complex (Haßdenteufel *et al.*, 2017).

Table 1. List of proteins interacting with hSnd2

Nr.	Identified protein	Accession	MW	Sum
1	fatty aldehyde dehydrogenase	AL3A2_HUMAN	55 kDa	31
2	cytoskeleton-associated protein 4	CKAP4_HUMAN	66 kDa	29
3	receptor expression-enhancing protein 5	REEP5_HUMAN	21 kDa	25
4	minor histocompatibility antigen H13	HM13_HUMAN	41 kDa	24
5	PRA1 family protein 3	PRAF3_HUMAN	22 kDa	23
6	transmembrane emp24 domain-containing protein 10	TMEDA_HUMAN	25 kDa	14
7	leucine-rich repeat-containing protein 59	LRC59_HUMAN	35 kDa	14
8	very-long-chain enoyl-CoA reductase	TECR_HUMAN	36 kDa	13
9	reticulon-3	RTN3_HUMAN	113 kDa	12
10	sigma non-opioid intracellular receptor 1	SGMR1_HUMAN	25 kDa	10
11	transmembrane emp24 domain-containing protein 2	TMED2_HUMAN	23 kDa	8
12	transmembrane and coiled-coil domain-containing protein 1	TMCO1_HUMAN	21 kDa	7
13	transmembrane protein 109	TM109_HUMAN	26 kDa	6
14	proteolipid protein 2	PLP2_HUMAN	17 kDa	5
15	protein YIPF5 (enriched in ER exit sites)	YIPF5_HUMAN	28 kDa	4

Proteins that were co-immunoprecipitated with hSnd2 (TMEM208) were identified by label-free mass spectrometry. Oligosaccharyltransferase (OST) complex subunits and translocon complex subunits were excluded and not displayed in this table as well as components that show no ER localization. The table was adapted based on the data from Haßdenteufel *et al*., 2017.

Abbreviations: Nr: number; MW: molecular weight; Sum: summation, indicates the number of identified peptides.

In order to reveal additional cellular constituents of the SND pathway or putative substrates of the pathway, the same technique, label-free quantitative mass spectrometry, was performed after siRNA-mediated depletion of hSnd2. These unpublished data are displayed in Figure 6. A membrane protein of the ER, transmembrane protein 109 (TMEM109), was found in both analyses. TMEM109 showed interaction with hSnd2 (Table 1) and depicted a lower abundance when hSnd2 was depleted (Figure 6). Proteins that displayed a highly significant reduction in Figure 6 are mainly cytoskeletal proteins and not ER membrane proteins (PTGIS, MYO9A, CDK5RAP2, TRCN1, ZFX). In this work, the role of the TMEM109 in SND protein targeting to the human ER is described in detail in the following chapters.

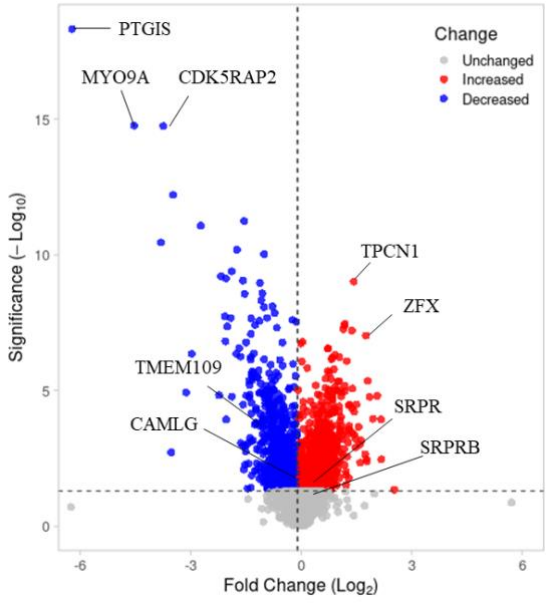

Figure 6. Mass spectrometry results after 96 hours of hSnd2 depletion

The volcano plot depicts proteins with significantly reduced or increased abundance after hSnd2 depletion. The plot highlights some of the proteins that showed highly significant enhancement or reduction, as well as important proteins that represent other targeting pathway receptors and the putative hSnd3 protein, the TMEM109. (Abbreviations: CDK5RAP2: CDK5 regulatory subunit-associated protein 2, MYO9A: unconventional myosin-IXa, PTGIS: prostacyclin synthase, TPCN1: two-pore calcium channel protein 1, ZFX: zinc finger X-chromosomal protein, **CAMLG**: calcium modulating cyclophilin ligand, **SRPR**: signal recognition particle receptor α, **SRPB**: signal recognition particle receptor β, **TMEM109**: transmembrane protein 109). Proteins highlighted in bold are targeting receptors or possible targeting receptors. The picture displays the average log2 fold change and significance from two different siRNA treatments (hsnd2-UTR-2 and hSnd2-UTR-3). Unpublished data. The figure was generated by the https://huygens.science.uva.nl/VolcaNoseR/ webpage.

7.9 OTHER TRANSPORT PATHWAYS AND PROTEIN TRANSPORT MACHINERIES

There is evidence that proteins can be delivered into the ER independently from the previously described pathways. One study has elucidated that short secretory proteins can be targeted to the Sec61 translocon by the TRC40 ATPase (Johnson *et al.*, 2012). Also, unassisted translocation of tail-anchored proteins with moderately hydrophobic TMD into protein-free liposomes has been defined (Brambillasca *et al.*, 2006). The term unassisted was given as the model proteins were integrated into the lipid bilayer without the assistance of any membrane protein. Cytochrome b5 and protein tyrosine phosphatase 1B were used as tail-anchored protein models. It was found that these tail-anchored proteins with moderate hydrophobicity were able to insert into protein-free liposomes. However, when the C-terminal end was elongated from 85 amino acid residues to 125 residues, post-translational insertion of the model proteins was severely impaired. When the TMD of the cytochrome b5 was replaced by the TMD of a more hydrophobic TA (the synaptobrevin), it failed to insert into protein-free liposomes. When the TMD of this construct was engineered to maintain a less hydrophobic character, it was inserted efficiently into liposomes. The other model protein, which TMD has a similar degree of hydrophobicity to cytochrome b5, performed correspondingly to the previous results. Unassisted membrane insertion of proteins appears to be an ATP-independent process. Hydrophobicity is a crucial element for predicting downstream targeting pathways to the ER. The hydrophobicity of a TMD can enormously impact the choice of targeting (Brambillasca *et al.*, 2005; Brambillasca *et al.*, 2006). However, considering the macromolecular crowding found inside living cells, the concept of unassisted membrane insertion found *in vitro* might not be effective or feasible.

Based on crosslinking experiments, calmodulin has been found to associate with short secretory proteins. ER targeting of these proteins can happen by the calmodulin interaction with the hydrophobic SP. As calmodulin can interact with the SP and the remaining of the polypeptide chain, it can protect it from ubiquitination and subsequent degradation. However, the activity of calmodulin could be influenced by the calcium concentration within a cell. Short secretory proteins showed improved ER transport efficiency at higher calcium concentration (Shao *et al.*, 2011).

It has been proposed that certain membrane proteins can be integrated into the ER by the ER membrane complex (EMC). The EMC was first characterized in yeast with six components, EMC1-6, and two accessory components, the Emc10 and Sop4 (Jonikas *et al.*, 2009) (Figure 8A). It has been proposed that the EMC contributes to the proper protein folding (Jonikas *et al.*, 2009). In yeast cells, affinity purification followed by SDS-PAGE and mass-spectrometry analysis revealed that EMC3 interacts with all the other core EMC components and various multipass transmembrane proteins (Shurtleff *et al.*, 2018).

In vertebrates, ten subunits of the complex are known (EMC1-10). The structure of the EMC3 shows homology to the bacterial YidC insertase, which inserts proteins into the bacterial cytoplasmic membrane. EMC proteins are highly conserved in yeast and mammalian cells with similar functions (Bai *et al.*, 2020).

The EMC interacting protein clients were mainly proteins with multipass TMDs. Observations indicated that tail-anchored proteins could also be inserted into the ER membrane by the EMC (Guna *et al.*, 2018). The EMC interacting domain on the substrate proteins was found to be enriched in moderately hydrophobic, polar, or charged amino acids (Alvira *et al.*, 2021; Shurtleff *et al.*, 2018). It was also found that the EMC can conduct proteins to the ER co-translationally and with the assistance of the Sec61 translocon (Bai *et al*., 2020; O'Keefe *et al.*, 2021; Shurtleff *et al.*, 2018). Type III transmembrane proteins can uniquely access the ER membrane by the EMC. Upon Sec61α depletion, *in vitro*, in a eukaryotic cell line, type III transmembrane protein integration was bypassed entirely. Substantially, reduced transport efficiency was observed when EMC5 and Sec61α were simultaneously knocked down, which indicates the importance of the EMC5 for co-translational ER membrane insertion of type III transmembrane proteins by the EMC (O'Keefe *et al*., 2021). In yeast cells, a reduced abundance was observed of EMC client proteins after EMC2 and 4 depletion (Shurtleff *et al.*, 2018).

In mammalian cells, the TMD of the substrate protein likely engages with cytosolic EMC subunits, such as the EMC2 and 8 (O'Donnell *et al.*, 2020). EMC substrate-binding pocket presumably comprises the EMC1, 3, 4, 5, and 6 (Bai *et al.*, 2020; Alvira *et al.*, 2021). Positive charges in the substrate-binding hydrophilic groove facilitate the interaction with the hydrophobic TMD and eliminate SP interaction. EMC3 and 6 can transiently bind the substrate and then conduct it into the bilayer (Alvira *et al.*, 2021).

The transmembrane and coiled-coil domain 1 (TMCO1) is a three-transmembrane domain protein in the ER that was found to associate with the Sec61 translocon and ribosomal proteins (Anghel *et al.*, 2017). The TMCO1 also formed a complex with the Sec61 without the ribosome (Anghel *et al.*, 2017). There is structural homology between the TMCO1 and the EMC3 insertase and the WRB/Get1 insertase, which belongs to the TRC/GET pathway (Anghel *et al.*, 2017; McDowell *et al.*, 2020) (Figure 7). They share topological homology based on 3D structural prediction; they are three-transmembrane domain proteins with ER luminal N-terminus and cytosolic C-terminus. The YidC, found in the inner bacterial membrane, the mitochondrial Oxa1 protein, and the ER-resident TMCO1, EMC3, and Get1/WRB membrane proteins show a similarly important role in membrane protein biogenesis. As part of the "Oxa1 superfamily", they share key topological features, such as having three or more TMD core, a coiled-coil structure between TMD1 and 2, as well as having an N-terminal luminal and C-terminal cytosolic orientation (Anghel *et al.*, 2017). As TMCO1 showed association with the ribosome and the Sec61, it strongly suggests that it helps to conduct transmembrane proteins co-translationally.

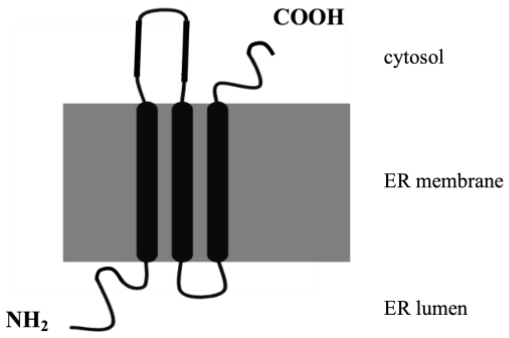

Figure 7. Topology of WRB/Get1, EMC3, and TMCO1

Part of the Oxa1 superfamily, WRB/Get1, EMC3, and TMCO1 features hydrophobic three-transmembrane domain core and ER luminal N-terminus and cytosolic C-terminus. However, mitochondrial Oxa1 and bacterial YidC are five-transmembrane domain proteins. Oxa1 superfamily proteins are linked to transmembrane protein biogenesis. There is a cytosolic coiled-coil domain between TMD1 and 2 (displayed in the figure), which possibly interacts with substrate polypeptides.

Another study identified that the ribosome-bound TMCO1 was co-immunoprecipitated with Sec61, Nicalin, TMEM147, NOMO, and CCDC47 (Calumin) (Figure 8B) (McGilvray *et al.*, 2020). Without the presence of the ribosome, the Nicalin-TMEM147-NOMO formed a complex, indicating that TMCO1-CCDC47 associates with them after they are attached to the ribosome. Affinity purification of ribosomes associated with Flag-tagged TMCO1 revealed the mRNAs on translating ribosomes. RNA sequencing results shed light on the fact that the TMCO1-linked transcripts encode proteins with four or more TMDs. Cryo-electron microscopy results revealed that TMCO1 and accessory proteins are arranged at the Sec61 at similar positions to certain OST complex proteins. It suggests that they compete for Sec61 association and might alternately interact with Sec61. TMCO1 proved to localize at the 'back' side of Sec61, where it might help the TMD insertion into the created lipid-filled cavity. The cytosolic part of the CCDC47 is localized close to the ribosomal exit tunnel, which suggests it might help regulate the Sec61 channel opening. TMEM147 showed association with the hinge region of the Sec61, which promotes the idea that it helps to open the lateral gate of the Sec61. The ER luminal domain of Nicalin possibly could aid the translocation of the loop segments (McGilvray *et al.*, 2020). As described earlier, TMCO1 can also prevent excessive calcium from accumulating in the ER. In response to high ER calcium concentration, reversible homotetramerization occurs in order to form an active calcium channel; the tetramers dissociate once the calcium concentration is physiological (Wang *et al.*, 2016).

The PAT complex, composed of the protein associated with the ER translocon of 10 kDa (PAT10 or Asterix) and CCDC47 forming an intramembrane heterodimer chaperone (Figure 8C), has also been described to be recruited at the Sec61 channel for aiding multipass transmembrane proteins' passage into the ER. First, it has been described that the PAT-10 was associated with the Sec61α and β and the first TMD of the seven-transmembrane domain protein, opsin (Ismail *et al.*, 2006; Meacock *et al.*, 2002).

These site-specific crosslinking results revealed that the PAT complex associates with multipass transmembrane proteins with hydrophilic TMDs. The PAT complex was associated at a higher rate with truncated versions of transmembrane proteins (mimicked translation intermediates) than the full-length, indicating its chaperone nature and helping the proper folding of multipass transmembrane proteins (Chitwood and Hegde, 2020).

In view of the fact that CCDC47 is a subunit of the PAT complex and the TMCO1 translocon, they might act cooperatively to fold and insert transmembrane proteins with less hydrophobic transmembrane segments (Culver and Mariappan, 2020). Cell lines lacking either the TMCO1 translocon or PAT complex subunits show impaired cellular fitness (Chitwood and Hegde, 2020; McGilvray *et al.*, 2020).

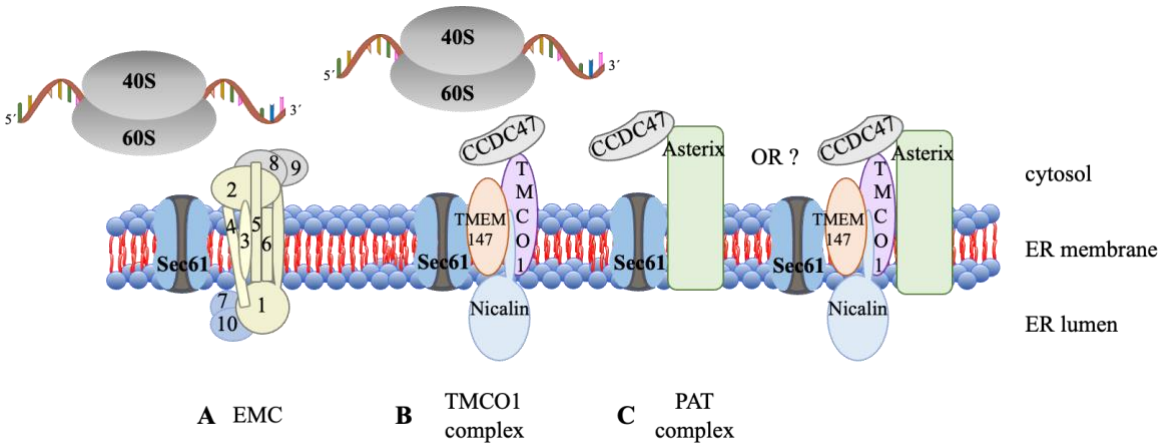

Figure 8. Alternative pathways for membrane protein insertion

Figure A depicts the EMC, which aids the insertion of type III transmembrane proteins and multipass transmembrane proteins in association with the Sec61; it can help transmembrane segment insertion into the ER membrane. EMC subunits are labeled numerically in the figure. Figures B and C depict the recently discovered TMCO1 and PAT complexes, respectively. In cooperation with Sec61, they assist in transmembrane protein insertion. Whether the two work together is not clarified yet.

8 OBJECTIVES

This work aimed to characterize the role of the transmembrane protein 109 (TMEM109) in protein targeting to the human endoplasmic reticulum (ER). As novel pathways have been characterized in the past years, the classical SRP-dependent protein targeting pathway does not stand its place alone in terms of protein targeting to the ER. The concept has been massively expanded in the last decade.

The SRP-independent (SND) pathway has been identified in yeast cells with three components and presumably conducts proteins with a transmembrane domain positioned other than N-terminally. The term SRP-independent was given because knockdown of the pathway components in yeast cells did not disturb the SRP-dependent substrate conduction into the ER. Substrates of the TRC pathway were not entirely independent of the SND pathway. However, no SND-specific substrate has been identified in mammalian cells so far. It is also possible that the SND pathway can help the enhancement the performance of known protein conducting pathways and is activated in response to disturbed protein homeostasis.

TMEM109 has been found as a putative SND pathway element as it showed interaction with the previously identified human SND pathway component, the transmembrane protein 208 (TMEM208/ hSnd2), and lower abundance in response to hSnd2 silencing.

This work aimed to further test the interaction between the hSnd2 and the TMEM109. The second goal of this project was to elucidate the relation of TMEM109 to protein transport to the endoplasmic reticulum and find possible protein clients that could be transported to the ER by the SND pathway. This was carried out in TMEM109 knockdown by small interfering RNA and TMEM109 knockout cells. As TMEM109 has been described as a calcium channel in the endoplasmic reticulum, this work also intended to better understand the role of the TMEM109 in the ER calcium homeostasis using live-cell calcium imaging.

9 MATERIALS AND METHODS

9.1 CHEMICALS

- Acetic acid 99.7 %, glacial, analytical grade (Fisher Chemical)
- 40 % (w/v) acrylamide solution (Serva)
- Agarose NEEO ultra quality (Carl Roth)
- Albumin Fraction V (Carl Roth)
- Ampicillin sodium salt (Sigma Aldrich)
- Amino acid mixture without methionine (Promega)
- Ammonium persulfate (Serva)
- Antipain (Sigma-Aldrich)
- BbsI-HF restriction enzyme (20 000 U/ml, NEB)
- Bgl II restriction enzyme (10 U/µl, Thermo Fisher Scientific)
- Bromphenol blue (Millipore)
- β-mercaptoethanol (Sigma-Aldrich)
- Calcium chloride (VWR)
- Calf Intestinal Alkaline Phosphatase (CIAP) Reaction Buffer (10x, Promega)
- Calf Intestinal Alkaline Phosphatase (CIAP) (Promega)
- CAP analog (m^7GpppG solution, Promega)
- Chemiluminescence substrate (West Pico PLUS, Thermo Scientific)
- Chymostatin (Sigma-Aldrich)
- Coomassie Brilliant Blue G-250 (Bio-Rad)
- Coomassie Brilliant Blue R-250 (Bio-Rad)
- CutSmart Buffer 10x (NEB)
- Digitonin (Calbiochem)
- Dimethyl sulfoxide (DMSO) (Sigma-Aldrich)
- Disodium-hydrogen-phosphate-dihydrate (Emsure)
- Dithiothreitol (Roche)
- DMEM (Dulbecco's Modified Eagle Medium, Gibco)
- DNA ladder 1 kb (SM0311, Thermo Scientific)
- DNA ladder 50 bp (SM0372, Thermo Scientific)
- DNase I (Roche)

- DNeasy Blood and Tissue Kit (Qiagen)
- Dodecyl sulfate-sodium salt pellet (Serva)
- Dpn I restriction enzyme (20 000 U/ml, NEB)
- EDTA (Uni SB, ZCHL)
- EGTA (Carl Roth)
- Elastatinal (Sigma-Aldrich)
- Ethanol absolute, undenatured (Serva)
- Ethanol (Uni SB, ZCHL)
- Fetal bovine serum (Sigma Aldrich)
- Fura-2-AM cell membrane-permeant calcium indicator (Invitrogen)
- 6x gel loading dye (Purple 6x, no SDS, B7025S, NEB)
- GelRed nucleic acid gel stain (Biotium)
- 86 % glycerol (Grüssing)
- Glycine (VWR)
- Glucose D+ (Carl Roth)
- Hydrochloric acid fuming 37 %, analytical grade (Emsure)
- Ionomycin (Invitrogen)
- LB medium (Carl Roth)
- LB medium for agar plates (Luria/Miller, Carl Roth)
- Leupeptin (Sigma-Aldrich)
- Magnesium acetate-tetrahydrate (Emsure)
- Magnesium chloride-hexahydrate (Serva)
- Methanol analytical grade (Fisher Chemicals)
- Methanol (Uni SB, ZCHL)
- Mounting media (Mount FluorCare DAPI, Carl Roth)
- Nano-Glo live cell substrate dilution buffer (Promega)
- Nano-Glo live cell substrate (Promega)
- N-(2-Hydroxyethyl)piperazine-N'-2-ethane sulfonic acid (HEPES) (Carl Roth)
- 2 % (w/v) N, N`-methylene bisacrylamide solution (Serva)
- N, N, N, N`-tetramethyl-ethylenediamine solution (Serva)
- Nuclease-free water (Qiagen)
- Opti-Minimal Essential Medium (MEM) reduced serum (Gibco)
- Opti- Minimal Essential Medium (MEM) without phenol red (Gibco)
- 10x PCR buffer with 20 mM $MgSO_4$ (Promega)
- Page ruler (prestained protein ladder, Thermo Scientific)
- 16 % (w/v) paraformaldehyde solution (Alfa Aesar)

- PCR purification kit (28106, Qiagen)
- Penicillin-streptomycin (Gibco)
- Pepstatin A (Sigma-Aldrich)
- Phusion Polymerase (Phu DNA Polymerase, 100 U, Promega)
- Plasmid Midi Kit (Qiagen)
- Propane-2-ol (Fisher Chemicals)
- Potassium acetate (Riedel de Häem)
- Potassium chloride (Merck)
- Powdered milk, blotting grade (Carl Roth)
- Pure Yield Miniprep system (Promega)
- PVDF membrane (Immobilion-P membrane, 0.45 µm, Millipore)
- QIAamp RNA Blood Mini Kit (Qiagen)
- QIAquick gel extraction kit (Qiagen)
- Radioactively labeled methionine (L-[^{35}S]-methionine, 5 mCi, Perkin Elmer)
- ReliaPrep DNA Clean-Up and Concentration System (Promega)
- Reticulocyte lysate (L416A and L483A, Promega)
- Ribonuclease inhibitor (RNasin, Promega)
- RNase A (Roche)
- Sac I restriction enzyme (10 U/µl, Thermo Fisher Scientific)
- Saponin (Sigma-Aldrich)
- Sodium chloride (Emsure)
- Sodium-dihydrogen-phosphate-monohydrate (Emsure)
- Superscript Vilo cDNA synthesis kit (Invitrogen)
- S6 polymerase (Promega)
- Tango Buffer 10x (Thermo Scientific)
- TaqMan gene expression master mix (Applied Biosystems)
- Terrific-Broth-Medium (Carl Roth)
- Thapsigargin (Invitrogen)
- TNT rabbit reticulocyte lysate (Promega)
- TNT reaction buffer (Promega)
- TNT T7 polymerase (Promega)
- Transfection reagent (Fugene, Promega)
- Transfection Reagent (HiPerFect, Qiagen)
- Trypan blue stain 0.4 % (Gibco)
- TRIS (Tris-(hydroxymethyl)-aminomethane, Millipore)
- Trypsin-EDTA 0.05 % (v/v) (Gibco)

- Trypsin inhibitor (MP Biomedicals)
- Tween 20 (Sigma-Aldrich)
- T4 DNA ligase (5 U/µl, Thermo Scientific)
- T4 DNA ligase buffer 10x (Thermo Scientific)
- T7 polymerase (Promega)
- T4 polynucleotide kinase (10 000 U/ml, NEB)
- Urea (Serva)
- Wizard SV Gel and PCR Clean-Up System (Promega)

9.2 TECHNICAL TOOLS

- Cell culture dishes (3.5 cm, 6 cm, 10 cm diameter, Greiner Bio-One)
- Centrifuge tubes (Sarstedt, 50 ml, 15ml)
- Coverslips (10 mm diameter, Karl Hecht)
- Coverslips (25 mm diameter, Neolab)
- Cryovials (Greiner Bio-One)
- Filter paper (BP002, Hahnemülle)
- Freezing container (Kemesser, CellHome-30)
- Glass beads (Sigma-Aldrich)
- Gloves (Carl Roth)
- Glass labware (Schott Duran, beakers with various volumes, graduated cylinders with various volumes, Erlenmeyer flasks with various volumes)
- Glasplates used for casting SDS gels (Wenzel Glasswork, custom made)
- Metal cell chamber (Invitrogen)
- Microscope slide (Menzel)
- Microtubes (Sarstedt, 1500 µl, 2000 µl)
- Microliter syringe 25 µl (Hamilton)
- Parafilm (Carl Roth)
- PCR reaction microtubes (Microply Pro cup, Sarstedt)
- Pipettes (Gilson, 0.2-2 µl, 2-20 µl, 20-200 µl, 100-1000 µl)
- Pipette tips (Sarstedt, 10µl, 200 µl, 1000µl)
- Polypropylene centrifuge tubes (Beckman Coulter)
- RTCA E-plates (300600900, Agilent)
- Rotor (TLA 100.3, Beckman Coulter)
- Storage phosphor screen (Kodak, SD230, GE Healthcare)

- 96 well assay plate (655 073, Greiner Bio-One)
- 96 well reaction plate (MicroAmp Optical Plate, N8010560, Applied Biosystems)
- 96 well sterile cell culture plate (82.1581.001, Sarstedt)

9.3 TECHNICAL DEVICES

- Analytical balance (BP61, Sartorius)
- Automatic vacuum system (Jet 1)
- Automated cell counter (C10227, Countess)
- Balance (model extend, Sartorius)
- Biosafety cabinet (82126, Gelaire)
- Biosafety cabinet (UV F 6.12 S, Froebel)
- Blotting chamber (transfer blot cell, 49BR, Bio-Rad)
- Centrifuge (GS-6KR, Beckmann)
- Cooling coil (LKB MultiTemp II, Pharmacia)
- Heat block (5320, Eppendorf)
- Humidified incubator (Hera Cell 150i, Heraeus Kendro)
- Incubator (B5042E, Heraeus)
- Incubator (AJ112/6, Infors)
- Incubator (Memmert)
- Milli-Q ultrapure water system (MilliQ Plus 185, Millipore)
- Orbital shaker (3015, GFL)
- PBS (Phosphate buffered saline solution 1x, Gibco)
- pH meter (pH537, WTW)
- Power supply (EPS3500, Pharmacia)
- Roller mixer (L209, Froebel)
- Tabletop centrifuge (5415D, Eppendorf)
- Tabletop centrifuge, refrigerated model (5415R, Eppendorf)
- Tilting shaker (Rocky)
- Thermal cycler (Primus 96, Peqlab)
- Typhoon Trio Variable Mode Image Scanner (GE Healthcare)
- Ultracentrifuge (Beckman Coulter, Optima Max-E)
- UV transilluminator (ECX-20-L, Peqlab)
- UV transilluminator (Image Master VDS, Pharmacia Biotech)
- UV-Vis Spectrophotometer (NanoDrop Technologies)

9.4 SOLUTIONS

- Blotting buffer: 12.8 mM TRIS (Tris-(hydroxymethyl)-aminomethane), 95 mM glycine dissolved in ultrapure water.
- 10x cell lysis buffer: 10 mM NaCl, 10 mM Tris-HCl (pH 8.1), 3 mM $MgCl_2$, 0.5 % NP40, 0.1 % (v/v) PLAC, 0.1 mM PMSF, 0.1 mg/ml DNase I in ultrapure water.
  - PLAC solution: 3 mg/ml pepstatin A, 3 mg/ml leupeptin, 3 mg/ml antipain, 3 mg/ml chymosatin in DMSO.
  - PMSF solution: 1 M PMSF solution dissolved in acetone and diluted to 0.1 M in ethanol.
- Coomassie dye: 0.2 % (w/v) Coomassie brilliant blue R250, 0.005 % (w/v) Coomassie brilliant blue G250, 40 % (v/v) methanol, 10 % (v/v) acetic acid in ultrapure water.
- Destaining solution I: 40 % methanol with 10 % acetic acid and 2 % glycerol in ultrapure water.
- Destaining solution II (neutralizing solution): 50 % methanol and 1 % glycerol in ultrapure water.
- External buffer solution: 140 mM NaCl solution, 5 mM KCl solution, 1 mM $MgCl_2$ solution, 10 mM glucose solution, 10 mM HEPES-KOH (pH 7.2) buffer, 0.5 mM EGTA solution in ultrapure water.
- HEPES buffer-KOH (pH 7.2): 90 mM HEPES-KOH (pH 7.2) and 50 mM potassium acetate diluted in ultrapure water.
- KHM buffer-KOH (pH 7.2): 20 mM HEPES-KOH (pH 7.2), 2 mM magnesium acetate, 110 mM potassium acetate diluted in ultrapure water.
- 5x Laemmli sample buffer: 300 mM Tris-HCl (pH 6.8), 50 % (v/v) glycerol, 10 % (w/v) SDS, 25 % (v/v) β-mercaptoethanol, 0.01 % (w/v) bromophenol blue in ultrapure water.
- 2x Laemmli sample buffer: 125 mM Tris-HCl (pH 6.8), 20 % (v/v) glycerol, 4 % (w/v) SDS, 10 % (v/v) β-mercaptoethanol, 0.01 % (w/v) bromophenol blue in ultrapure water.
- 1x Laemmli sample buffer: 60 mM Tris/HCl, 10 % (v/v) glycerin, 2 % (v/v) SDS, 5 % (v/v) β-mercaptoethanol, 0.01 % (w/v) bromophenol blue in ultrapure water.
- 10x PBS-HCl (pH 7.3): 22.9 mM sodium-dihydrogen-phosphate-monohydrate, 100 mM disodium-hydrogen-phosphate-dihydrate, and 1540 mM sodium chloride dissolved in ultrapure water.
- SDS-PAGE buffer: 50 mM TRIS, 384 mM glycine, and 0.1 % (w/v) SDS in ultrapure water.
- SDS-PAGE buffer for urea gels: 50 mM TRIS, 192 mM glycine, and 0.1 % (w/v) SDS in ultrapure water.
- 1x TAE buffer: 40 mM Tris-acetate (pH 8.0), 1 mM EDTA in ultrapure water.
- Urea SDS-PAGE buffer: 192 mM glycine, 50mM Tris, 0.1 % (w/v) SDS.

9.5 CELL CULTURE

HeLa, human cervical cancer cell line (CCL2, ATCC), and its derived TMEM109 knockout cell line were cultured in Dulbeccos Modified Eagle Medium (DMEM) supplemented with 10 % fetal bovine serum and 1 % penicillin-streptomycin. Cells were cultured at 5 % CO_2 and 37 °C in a humidified incubator. Adherent cells were washed with 1x PBS and trypsinized for 3 minutes at 37 °C when approximately 80 % confluency was reached. Trypsin was inactivated by the addition of standard culture medium (supplemented with fetal bovine serum and penicillin-streptomycin as described earlier). Cells were seeded at the desired density after cell number determination by automated cell counter using trypan blue staining at a 1:1 ratio using 10 µl cell suspension.

9.6 TRANSFECTION OF HELA CELLS FOR SIRNA-MEDIATED GENE SILENCING

Small interfering RNA (siRNA) or short interfering RNA is a double-stranded RNA that mediates transcriptional gene silencing. The long double-stranded RNA is cleaved within the cells by the Dicer endoribonuclease enzyme, creating the siRNA (approximately 23 bp long). Interaction of other proteins, such as Argonaute, with the siRNA, creates the RNA-induced silencing complex (RISC). In the RISC complex, the siRNA becomes single-stranded. The RISC can find its specific target by forming the siRNA-mRNA complex. The target mRNA is rapidly degraded after the cleavage (Alberts *et al.*, 2015).

For siRNA-mediated silencing, 660 000 HeLa cells were seeded in a 3.9 ml DMEM in 6 cm cell culture dishes. Floating cells were directly transfected with designated siRNAs at a desired final concentration (20, 25, 35, 40, or 45 nM). (Qiagen, custom siRNAs, 1027423, 20 µM each:

- TMEM109-UTR-1, 5'-GGUUUGAUGUGGAAUCACATT-3'
- TMEM109-UTR-2, 5'-CCGCCAGUGUCAUACCAAATT-3'
- TMEM109-UTR-3, 5'-GGCUUGGCACAUGAUGUGATT-3'
- TMEM109-UTR-4, 5'-CCAUACUGUAUGUAGGAAATT-3'
- WRB-UTR-3, 5'-ACACGUAUGUACUAGUGAATT-3'
- hSnd2-UTR-2, 5'-CUAUAGGGUCGUUGAAUAATT-3'
- hSnd2-UTR-3, 5'-GGGCAAAGUGGGCACGAGATT-3').

Each siRNA targets the 3' untranslated region (UTR). As control conditions, cells were transfected with scrambled siRNA at the desired final concentration (AllStars negative control siRNA, Qiagen, 1027281, 20 µM). The control siRNA does not show any sequence homology with any human mRNA. Transfection reagent (HiPerFect) was added based on the manufacturer's instructions, 20 µl. Transfection mixes containing transfection reagent and siRNAs were diluted in a 100 µl reduced serum

medium. After 10 minutes of incubation time, transfection mixes were added to the appropriate culture dishes. After 24 hours, the culture medium was renewed, and cells were transfected for a second time and cultivated for the desired time interval.

9.7 GENERATION OF NANOBIT CONSTRUCTS FOR LUMINESCENCE PROTEIN-PROTEIN INTERACTION ASSAY

The luminescence protein-protein interaction assay was performed to test the interaction between TMEM109 and hsnd2 and the homo-oligomerization capability of TMEM109. For this, pBiT1.1-C [TK/LgBiT] (N196) and pBiT2.1-C [TK/SmBiT] (N197) vectors were engineered to encode for C-terminally truncated TMEM109 protein. (These steps are described in the following paragraphs.)
pBiT2.1-N [TK/SmBiT] (N199) vector was engineered to encode for full-length hSnd2 (TMEM208, NM014187, OriGene). pBiT1.1-C [TK/LgBiT] (N196) and pBiT2.1-C [TK/SmBiT] (N197) vectors were engineered to encode for the full length TMEM109 protein. The last three constructs were generated by Dr. Mark Sicking and kindly provided to use for the protein-protein interaction assay.

9.7.1 TMEM109 TRUNCATION

TMEM109 C-terminal truncation after the third TMD was carried out by PCR amplifying the gene sequence of the *TMEM109* encoding for the 1st-205th amino acids. The forward (5'-TAATACGACTCACTATAGG-3', RZ 747) and reverse primers (5'-GCTAGAGCTCTCGGGGAGCCAGTGAGCC-3', RZ 813) were designed for the PCR reaction and purchased from Eurofins Genomics company as custom-designed oligonucleotides. The reverse primer contains the SacI restriction site for integrating it into the truncated *TMEM109* sequence. 100 µl PCR reaction contained: 1x PCR buffer with 20 mM $MgSO_4$, 200 µM dNTP, 0.1 µM forward primer (RZ747), 0.1 µM reverse primer (RZ 813), 50 ng/µl TMEM109 plasmid (OriGene, NM024092), 2.5 U Phusion Polymerase, and nuclease-free water.
The following heat profile was used on the thermal cycler: 95 °C for 2 minutes; 95 °C for 30 seconds, 53.1 °C for 30 seconds, 72 °C for 90 seconds (35 cycles); 72 °C for 2 minutes; and 8 °C for infinite time. The PCR product was purified using PCR purification kit.

9.7.2 AGAROSE GEL ELECTROPHORESIS

130 ng PCR product in 12 µl reaction, containing 1x gel loading dye was loaded into 2 % agarose gel made with 1x TAE buffer. 100 ng 50 bp DNA ladder was loaded as a molecular weight size marker. The gel ran at 200 V for 1.5 hours. The gel was stained overnight in ultrapure water containing 7.5 µl nucleic acid dye. UV illumination of the stained gel confirmed the correct size of the truncated PCR product (705 bp).

9.7.3 DOUBLE DIGESTION OF THE VECTORS AND INSERT FRAGMENTS

Restriction by Sac I enzyme (Sac I (10U/µl)

5'...G A G C T↓C...3'

3'...C↑T C G A G...5'

1 µg plasmid DNA or PCR product, 2µl 10x Tango Buffer 1 µl Sac I restriction enzyme was added to nuclease-free water up to 20 µl. The tubes were gently mixed and spun down for a few seconds. Mixtures were incubated at 37 °C for 1 hour.

Restriction by Bgl II enzyme (Bgl II (10U/µl)

5'...A↓G A T C T...3'

3'...T C T A G↑A...5'

To the previous mixtures, 2.5 µl 10x Tango Buffer (to get the final 2x concentration) and 1 µl Bgl II restriction enzyme were added. The tubes were gently mixed and spun down for a few seconds. Mixtures were incubated at 37 °C for 1 hour.

9.7.4 DEPHOSPHORYLATION OF THE 5' OVERHANGS ON THE DIGESTED VECTOR PLASMIDS

To the plasmid double digestion reactions, 1x CIAP Reaction Buffer, 1µl 0.01 u/µl CIAP, and nuclease-free water up to 50 µl were added. The mixtures were incubated at 37 °C for 30 minutes.

9.7.5 AGAROSE GEL ELECTROPHORESIS

Samples were diluted in gel loading dye and nuclease-free water to get a final 1x concentration of the loading dye. Samples were loaded into 2 % agarose gels made with 1x TAE. 100 ng uncut plasmids were loaded as negative controls for restriction digestions. 100 ng 50 bp DNA ladder and 100 ng 1 kb DNA ladder were loaded as molecular-weight size markers. Subsequent steps are identical as written in Paragraph 9.7.2. UV illumination of the stained gel confirmed the correct size of the products: C-terminally truncated TMEM109 after double digestion: 644bp, double digested LgBiT (N196) plasmid: 3835bp, double digested SmBiT (N197) plasmid: 3393 bp.

9.7.6 GEL EXTRACTION AND PURIFICATION OF THE CORRECT BANDS

ReliaPrep DNA Clean-Up and Concentration System was used to isolate DNAs from gel pieces based on the manufacturer's instructions.

9.7.7 LIGATION OF THE CORRECT PRODUCTS

Ligation was carried out by adding 20 ng of the digested vector, digested insert DNA (at 1:1 vector:insert ratio), 1x T4 DNA ligase buffer, 1 Weiss U T4 DNA ligase, and nuclease-free water up to 20 µl. The reaction mixtures were incubated for 1 hour at 22°C.

9.7.8 TRANSFORMATION OF COMPETENT CELLS WITH THE EXPERIMENTAL DNA

100 µl of XL1-Blue chemically competent cells (Agilent) were thawed on ice. Competent cells were incubated with 8 ng experimental DNA from the ligation reaction for 30 minutes on ice. The cells were heat-pulsed in a 42 °C water bath for 45 seconds and then incubated on ice for 2 minutes. 900 µl preheated SOC medium was added to the cells and incubated at 37 °C for 1 hour, applying rotation at 225-250 rpm. Cells were concentrated by centrifugation at 1000 rpm for 10 minutes. ≤ 200 µl of the transformation mixture was plated on LB agar plates containing the appropriate antibiotic, ampicillin sodium salt (100 mg/ml), at a 1:1000 ratio. Plates were incubated at 37 °C overnight. The following day single colonies were picked from LB plates with wooden sticks. 2 ml Terrific-Broth-Medium liquid culture containing 1:1000 ampicillin was inoculated with single colonies. Colonies were cultured at 37 °C for at least 12 hours.

9.7.9 PLASMID DNA EXTRACTION

Plasmid DNA was extracted using the Pure Yield Miniprep system based on the manufacturer's instructions. Plasmids were eluted in nuclease-free water, provided with the kit, for the sake of subsequent sequencing.

9.7.10 DNA SEQUENCING

Plasmids were sent for sequencing to the LGC Genomics company at a concentration of 100 ng/µl in 14 µl volume in ultrapure water, containing 4 µl of a 5 µM primer. Forward sequencing primer: 5'-GCATATTAAGGTGACGCGTG-3' (RZ 758), reverse sequencing primer: 5'-CCTCCCCCTGAACCTGAAAC-3' (RZ 759). Sequencing results were aligned using SeqMan software (Lasergene, DNASTAR) to the predicted sequence, which was created *in silico* using SeqBuilder software (Lasergene, DNASTAR).

9.7.11 AMPLIFICATION OF THE RIGHT PLASMID CONSTRUCTS (TRANSFORMATION OF COMPETENT CELLS WITH THE EXPERIMENTAL DNA)

100 µl of DH5α chemically competent cells were thawed on ice and incubated with 10 ng of experimental DNA for 30 minutes on ice. The cells were heat-pulsed in a 42 °C water bath for 90 seconds and then incubated on ice for 2 minutes. 900 µl preheated SOC medium was added to the cells and incubated at 37 °C for 1 hour, applying rotation at 225–250 rpm. The transformation mixture was added into an Erlenmeyer flask containing 100 ml LB medium containing the appropriate antibiotic, ampicillin sodium salt (100 mg/ml), at a 1:1000 ratio. The flask was incubated at 37 °C overnight, applying 120 rpm agitation.

9.7.12 PLASMID DNA ISOLATION

The following day plasmid DNA was extracted using Plasmid Midi Kit. Plasmid DNA was eluted in the provided elution buffer, and the DNA concentration was set to 1 µg/µl. DNA concentration was determined by UV-VIS spectrophotometer.

9.8 LUMINESCENCE PROTEIN-PROTEIN INTERACTION ASSAY

The NanoBit protein-protein interaction system is based on measuring the luminescence signal generated by an enzyme-substrate reaction. The enzyme, an optimized variant of the *Oplophorus gracilirostris* deep-sea shrimp luciferase, is split into two subunits called Small BiT and Large BiT. The two subunits are fused to the proteins of interest, usually to either the N- or the C-terminal end of the proteins (Paragraph 9.7). If the proteins of interest are interacting, the two subunits of the enzyme come in proximity and reconstitute a functional luciferase. After the addition of the substrate furimazine, the emitted luminescence signal is captured and analyzed. Whether the Small or the Large BiT is fused to the C- or the N-terminal end of the proteins that give the strongest signal is, to a certain extent, based on empirical results, as well as very much shaped by the topology of the interaction partners (Dixon *et al.*, 2016). The latter is important to consider for membrane proteins, as the Small BiT and Large BiT-tags found on the same side of a membrane are capable of interaction.

9.8.1 TRANSFECTION OF THE CELLS WITH THE APPROPRIATE PLASMIDS

20 000 HeLa cells were seeded per well in 100µl standard culture media in 96 well assay plates (655 073). The kit contained the necessary positive (PKA-LgB and PKA-SmB) and negative (Halo-Sm) controls. The following plasmids were diluted to 0.1 µg/µl concentration in reduced serum Opti-MEM:

Table 2. Plasmid constructs used for NanoBiT assay

Construct	Abbreviation
SmallBiT fused to the HaloTag	Halo-SmB (Nr.202)
LargeBiT fused to the protein kinase A regulatory subunit	PKA-LgB (LgBit Nr.203)
SmallBiT fused to the protein kinase A catalytic subunit	PKA-SmB (SmBit Nr.204)
C-terminal end of the TMEM109 fused to the LargeBiT	TMEM109-C-T-LgB (Nr.205)
C-terminal end of the TMEM109 fused to the SmallBit	TMEM109-C-T-SmB (Nr.206)
N-terminal end of the hSnd2 fused to the SmallBit	hSnd2-N-T-SmB (Nr.210)
C-terminal end of the C-terminally truncated TMEM109 fused to the LargeBiT	TMEM109-C-T'-LgB (Nr.240)
C-terminal end of the C-terminally truncated TMEM109 fused to the SmallBiT	TMEM109-C-T'-SmB (Nr.241)

Plasmid constructs that were used for protein-protein interaction assay are listed in the table, containing the necessary negative and positive controls. The N-terminal end of hSnd2 was fused to the SmallBiT plasmid. Either the full length or the C-terminally truncated version of the TMEM109 was fused to the LargeBiT or the SmallBiT C-terminally. " C-T' " with an apostrophe means C-terminally truncated.

Transfection solutions were prepared by adding plasmids (Table 3) at 6.25 ng/µl final concentration in a 30 µl reduced serum medium containing a 1.1 µl transfection reagent (Fugene). After the addition of the transfection reagent, the tubes were spun shortly to collect all liquid at the bottom of the tubes. After 10 minutes of incubation time, 8 µl was added off the transfection mixes to the appropriate wells in triplicates for each sample. As a result, 50 ng plasmid was added of each construct into one well. The control cells were supplemented only with the transfection reagent. The plate was mixed orbitally by hand. The plate was incubated for 24 hours at 37 °C, 5 % CO_2 in a humidified incubator.

Table 3. Cell transfection with the NanoBiT plasmid constructs

Test type	Plasmids
mock	-
positive control	PKA-LgB and PKA-SmB
negative control	TMEM109-C-T-LgB and Halo-SmB
negative control	TMEM109-C-T'-LgB and Halo-SmB
TMEM109 and hSnd2 interaction	TMEM109-C-T-LgB and hSnd2-N-t-SmB
C-terminally truncated TMEM109 and hSnd2 interaction	TMEM109-C-T'-LgB and hSnd2-N-t-SmB
TMEM109 homo-oligomerization	TMEM109-C-T-LgB and TMEM109-C-T-SmB
TMEM109 oligomerization between C-terminally truncated and full-length TMEM109	TMEM109-C-T'-LgB and TMEM109-C-T-SmB
TMEM109 oligomerization between full-length and C-terminally truncated TMEM109	TMEM109-C-T-LgB and TMEM109-C-T'-SmB
TMEM109 oligomerization when TMEM109 is C-terminally truncated	TMEM109-C-T'-LgB and TMEM109-C-T'-SmB

Table shows the plasmid constructs that were used in transfection mixes to test the interaction between TMEM109 and hSnd2, as well as concomitant disruption of the interaction furthermore to test the homo-oligomerization of the TMEM109.

9.8.2 PROTEIN-PROTEIN INTERACTION ASSAY

The reduced-serum medium without phenol red was warmed up to 37 °C. The Tecan reader (M200, Tecan iControl software, Tecan Infinite) was preheated 20 min before the experiment to 37 °C.
The cell culture medium was discarded and was replaced by a 100 µl prewarmed reduced-serum medium without phenol red in the 96 well plate. The plate was placed back into the incubator until the measurement to maintain 37 °C. Baseline luminescence was measured every minute for 10 minutes. Nano-Glo live cell assay reagent was prepared by combining 1 volume of Nano-Glo live cell substrate with 19 volumes of Nano-Glo live cell substrate dilution buffer. 20 µl of the Nano-Glo live cell assay reagent was added into each well and mixed by the plate reader. The luminescence signal was measured every minute for 10 minutes.

9.9 REAL-TIME QUANTITATIVE PCR (RT-qPCR)

For measuring the mRNA level, RT-qPCR was carried out. After the desired culturing time, cells were harvested and washed in 1x PBS, and cell pellets were stored at -80 °C after flash-freezing in liquid nitrogen. For isolating the total RNA content, QIAamp RNA Blood Mini Kit was used based on the manufacturer's instructions. The concentration of the isolated RNA was determined by spectrophotometer using NanoDrop 1000 software. The isolated RNA was reverse transcribed using Superscript Vilo cDNA synthesis kit. After purification of the PCR product, the concentration was determined by UV-VIS spectrophotometer. For real-time quantitative PCR analysis, a 10 µl reaction mixture was pipetted into 96 well reaction plate (N8010560). The reaction mixture is composed of a 5 µl TaqMan gene expression master mix, 0.5 µl of the TaqMan gene expression assay reagent, which contains the specific probes and primers recognizing the target sequence, and 25 ng cDNA. In the negative control wells, nuclease-free water was added instead of the cDNA. The following TaqMan gene expression assay reagents were used: beta-actin (Applied Biosystems, Hs00357333_g1), Caml (Hs00266143_m1), HSPA5 (BiP) (Hs99999174_m1), Sec61α (Hs00273698_m1), SRα (Hs01112418_g1), SRβ (Hs00253639_m1), TMEM109 (Hs00934376_m1), hSnd2 (TMEM208) (Hs00204388_m1). In order to collect all ingredients at the bottom of the wells, the plate was centrifuged at 1000 rpm for 1 minute (Eppendorf centrifuge 5430, FA45-30-11 rotor). StepOnePlus Real-Time PCR System (Applied Biosystem, 4376600) was used with StepOnePlus Software v2.3 (Applied Biosystems).
The following thermal cycle profile was used: heating the reaction to 95 °C to denature the DNA, then cooling the reaction to 60 °C; this was repeated through 40 cycles. As the reaction cools, the TaqMan probes bind to their target sequence, followed by the forward and reverse primers. As the polymerase synthesizes the opposite DNA strand, the quencher is digested away on the probe; then, the reporter can freely diffuse, and the fluorescence signal is detected.

The beta-actin housekeeping gene was used for normalization. For comparative analysis, $2^{-\Delta\Delta Ct}$ values were calculated to determine the relative fold change compared to the control sample.

9.10 REAL-TIME CELL ANALYSIS (RTCA)

To reveal the effect of the siRNA treatment on cell proliferation and viability, the cell index was measured by real-time cell analysis. During the measurement, the cells are in contact with a gold electrode, and a mild electrical current is applied, which does not influence the cell behavior. Throughout the culturing time, the viability and proliferation change and so does the impedance (Ke *et al.*, 2011).
As the first step, cells were transfected with designated siRNAs as described in Paragraph 9.6. After 30 hours of culture, the cells were washed with 1x PBS and incubated with 500 µl trypsin for 5 minutes at 37 °C. Samples were harvested in standard culture medium. Cell numbers were determined by an automated cell counter. 96 well plates (RTCA E-plates) were used for the measurement, designed explicitly for RTCA measurement, with gold electrodes on the bottom. The E-plate containing 100 µl of standard culture medium was used to measure the background signal. After measuring the background signal, 5000 cells were added per well. The measurement was carried out based on the manufacturer's instructions, provided with the real-time cell analyzer (xCELLigence real-time cell analyzer SP, ACEA, 003800601030). Data collection and analysis were carried out by the RTCA 2.0 software (Agilent).

9.11 RNA SEQUENCING

Whether TMEM109 silencing could cause any changes in the gene expression pattern was tested by RNA sequencing.
HeLa cells were transfected with the designated siRNAs as it was described in Chapter 9.6. At the end of the culturing time point, cells were harvested by trypsinization and the quality of the isolated RNA (Qiagen, RNeasy Kit, 74104) was determined by their RNA integrity number (RIN) (Agilent, Bioanalyzer 2100, and 2100 expert software) based on the manufacturer's instructions. The isolated RNAs were sent to the Novogene Company for RNA sequencing.
After sample arrival, the quality determination was carried out by the company as well. The sample preparation for sequencing includes the reverse transcription of the RNA samples to cDNA. After that, the samples were fragmented, and adaptors and bar codes were attached to the fragments. Due to the addition of such bar codes, each fragment could be identified during the sequencing procedure. The sequencing took place on the surface of a glass plate, the so called flow cell. The flow cell contained multiple lanes; two types of oligonucleotides were tethered in these lanes. Each fragment has adhered to one type of oligonucleotide from the two on the glass surface; the sequence of these oligonucleotides was complementary to the adaptors on the end of the fragments. After the addition of a polymerase, the

complementary strand was synthesized, and the original strand was washed away. The fragments were clonally amplified by bridge amplification, generating clusters of the fragments. Due to the application of two different capture oligonucleotides on the glass surface, both the reverse and the forward strands were amplified. The reverse strands were cleaved and washed away at this step, leaving only the forward strands. The first read was generated after the addition of the first sequencing primer. Fluorescently labeled oligonucleotides were added, and by laser excitation, the fluorescence signal was captured by the camera when a base was incorporated. This technique is called sequencing by synthesis (SBS). After the first read, the sequencing products were washed away, and the index primer was hybridized to identify the unique fragments. When the index read was completed, the index reads were washed away. The 3' of the fragments were deprotected, and the fragments folded over to the second oligonucleotide on the flow cell. After the addition of the index 2 primers, index reads were performed. Then by the addition of a polymerase, the generation of the reverse strands was completed. The forward strands were cleaved and washed away. Read two primers were hybridized, and the sequence was read as previously described. The Illumina machine performs millions of reads simultaneously. The read counts were then converted into FPKM values (Illumina Inc., 2017; Fuller *et al.*, 2009). "FPKM is short for the number of Fragments Per Kilobase of transcript sequence per Millions of base pairs sequenced. This is the most common method of determining gene expression levels. This method takes into consideration both the sequencing depth and gene length, and the values are normalized based on that (Illumina Inc., 2017)." The FPKM values were generated by the company, and the log2 fold changes were used in most analyses. The forward and reverse reads were pared and aligned to reference sequences giving a contiguous sequence (Illumina Inc., 2017; Fuller *et al.*, 2009).

9.12 WESTERN BLOT ANALYSIS OF WHOLE-CELL PROTEIN EXTRACT

Western blot analysis has been a widely used technique to analyze proteins for over 40 years. The method is based on the separation of native proteins by sodium dodecyl sulfate-polyacrylamide gel electrophoresis (SDS-PAGE) and transferred to a porous membrane and detected by antibody staining (Burnette, 1981; Towbin *et al.*, 1979; Renart *et al.*, 1979).

After the desired culturing time point, cells were washed with 1x PBS and incubated with 500 µl trypsin for 5 minutes at 37 °C, and harvested in standard culture medium. Cell numbers were determined by automated cell counter. After washing in 1x PBS, cells were pelleted by centrifugation for 5 minutes at 2500 rpm.

Cells were resuspended in 1x cell lysis buffer and 5x Laemmli buffer to set the cell density to 10 000 cells/µl. For this, cells were first incubated with 1x lysis buffer at 4 °C with agitation for 10 minutes. After the addition of 5x Laemmli buffer to get 1x final concentration and some glass beads, the samples

were heated at 56 °C for 10 minutes. 200 000 cells (20 µl) per sample, as well as 5 µl page ruler, were loaded into SDS gels into separate wells.

Table 4. Composition of SDS-PAGE gels containing different concentrations of acrylamide

	Separating gel					Stacking gel	Urea stacking gel
Gel type (% (v/v) acrylamide) / Reagent	10	12	15	17.5	urea	5.0	
Urea (g)	-				5.88	-	1.80
60 % acrylamide/ 0.8 % bisacrylamide (ml)	-				5.25	-	0.42
40 % (w/v) acrylamide (ml)	3.8	4.7	5.6	6.6	-	0.9	-
2 % (w/v) bisacrylamide (ml)	1.0	1.3	1.5	1.8	-	0.2	-
Ultrapure water (ml)	4.0	2.9	1.7	0.4		5.0	2.60
1.875 M Tris- HCl (pH 8.8) (ml)	6.0					-	-
1.875 M Tris- NaCl- HCl (pH 8.8) (ml)	-				6.5	-	-
1 M Tris- HCl (pH 6.8) (ml)	-				-	0.9	0.63
10 % (w/v) SDS (µl)	150				160	72	50
20 % (w/v) AMPS (µl)	45				55	65.5	25
TEMED (µl)	5				6	10.5	5
Total volume (ml)	15				17.8	7.2	20

SDS gels with different acrylamide concentrations were used to separate different proteins. The higher the acrylamide concentration, the better the resolving power, suitable for separating smaller proteins. After the addition of SDS, AMPS, and TEMED, the liquid was mixed thoroughly; after the separating gel was polymerized, the stacking gel was mixed and poured on top of the separating gel. A gel comb was inserted to create wells into which the samples could be loaded. After polymerization, the gels were stored refrigerated for up to two weeks; in the case of urea gels, the storage happened at room temperature.

Proteins were separated according to molecular weight by SDS-PAGE. Gels ran overnight at 5 mA electrical current using normal or urea electrophoresis buffer. PVDF membrane was activated in methanol for 1 minute, applying agitation. The separated proteins were blotted onto the activated PVDF membrane at 10 °C for 3 hours at 400 mA in blotting buffer. During blotting, the temperature was regulated to prevent the degradation of proteins. Unspecific binding sites on the membrane were blocked in 5 % (w/v) BSA solution, dissolved in 1x PBS, for 60 minutes at room temperature, applying light agitation. Polyclonal or monoclonal antibodies were raised against peptides of the indicated target protein, which are summarized in Table 5.

Table 5. Primary and secondary antibodies used in Western blot analysis

External/internal ID	Species	Target protein (kDa)	Dilution	Monoclonal/ Polyclonal
primary antibodies				
Sigma-Aldrich, A5441	mouse	actin beta subunit (40)	1:10 000	monoclonal
1448 S10	rabbit	Caml (35)	1:250	polyclonal
N950 S1	rabbit	Bip (N-terminus) (70)	1:250	polyclonal
ABP-150 S5	rabbit	GRP170 (170)	1:1000	polyclonal
1402 S7	rabbit	hSnd2 (N-terminus) (19)	1:250	polyclonal
1636 S12	rabbit	Sec61(α-subunit, C-terminus) (36)	1:300	polyclonal
262b S8	rabbit	Sec62 (C-terminus) (45)	1:250	polyclonal
N178a S13	rabbit	SRα (N-terminus) (70)	1:300	polyclonal
310 S9	rabbit	SRβ (N-terminus) (28)	1:1000	polyclonal
1620 S7	rabbit	TMEM109 (C-terminus) (23)	1:500	polyclonal
secondary antibodies				
Cytiva, PA45011	goat	rabbit IgG antibodies	1:1000	polyclonal
Sigma-Aldrich, C2181	sheep	mouse IgG antibodies	1:2000	polyclonal

The table summarizes the antibodies that were used for Western blot analysis. Antibodies with internal ID were generated in the Medical Biochemistry and Molecular Biology Department of the Saarland University by Professor Dr. Martin Jung and Sabine Pelvay.

If needed, the membrane was cut into pieces horizontally after the blocking step. Antibodies were diluted at the specified ratios in 5 % (w/v) milk solution, dissolved in 1x PBS. Primary antibody incubation was carried out overnight at 4 °C or room temperature for 90 minutes, applying light agitation. The membrane was incubated with fluorescently labeled secondary antibodies (anti-rabbit or anti-mouse) for 120 minutes at room temperature. Membranes were washed in 1x PBS containing 0.05 % Tween 20 three times and in 1x PBS one time after each antibody incubation step. After thoroughly drying the

membrane, the membrane pieces were scanned using Typhoon Trio Variable Mode Image Scanner (GE Healthcare). Analysis was carried out by the ImageQuant TL 7.0 image analysis software (GE Healthcare).

9.13 COOMASSIE GEL STAINING

Coomassie dye staining is a sensitive and straightforward way to stain proteins in SDS-PAGE gels so that it is suitable to determine the overall protein content in samples. Coomassie brilliant blue is best soluble in polar molecules such as water, acetic acid, or methanol. The dye binds to proteins via weaker secondary bond formation. After washing steps, the proteins appear as blue bands on transparent background in the gels (Neuhoff *et al.*, 1985).
After sample preparation for Western blot analysis, 10 µl (100 000 cells) samples were loaded into 10 % SDS-PAGE gel. After the running was completed, the gel was stained in Coomassie dye for 40 minutes. The gel was incubated in the destaining solution I for 5 minutes on an orbital shaker. After that, the gel was incubated with destaining solution II overnight or for days until the gel background was transparent. The gel was scanned by ImageScanner III (GE Healthcare) and LabScan 6.0 software. The analysis was carried out by the ImageQuant TL 7.0 image analysis software (GE Healthcare).

9.14 IN VITRO TRANSCRIPTION OF DNA SUBSTRATES

Plasmid DNA or PCR products can serve as a template for transcription to produce mRNA products *in vitro*, which can be used as a template for downstream experiments, such as *in vitro* translation assay (9.15) (Ling *et al.*, 1989).

The reaction mixture contained the following ingredients: 30 µl premix A solution, 1.5 µl CAP analog (m^7GpppG) solution, 2.5 µl RNasin, 1 µl S6 or T7 polymerase, 1 µg plasmid, and nuclease-free water up to 50 µl. The reaction mixture was incubated at 40 °C for 3 hours. The mRNA products were stored at -80 °C.
Composition of premix A solution: 10 % (v/v) salt solution, 0.1 mg/ml BSA, 10 mM dithiothreitol, 0.5 mM nucleotide mixture, 0.1 mM GTP.
Composition of the salt solution: 400 mM HEPES (pH 7.4 KOH), 60 mM magnesium acetate, 20 mM spermidin.
Composition of the m^7GpppG solution: 5 U m^7GpppG, 10 mM HEPES (pH 7.9 KOH).
The following DNA substrates were transcribed to mRNA: preprolactin, invariant chain, cytochrome b5, prestatherin, Sec61β (Table 6).

Table 6. List of plasmid DNAs used for *in vitro* transcription assay

Recombinant DNA	Vector	Promoter	Species
preprolactin	pB4	SP6	bovine
invariant chain	pSPutK	SP6	human
cytochrome b5-OPG3	pGEM4	SP6	human
prestatherin-OPG2	pTNT	T7	human
Sec61β-OPG3	pcDNA3	T7	human

The table summarizes the plasmids that were used for *in vitro* transcription assay to generate mRNA transcripts.

9.15 IN VITRO TRANSLATION ASSAY OF mRNA SUBSTRATES

Efficient ER targeting of proteins involves the cleavage of the signal peptide and/or the N-linked glycosylation. Both processes are indicated by a change in the molecular weight, which can be detected by visualization of the translation products after SDS-PAGE.

In vitro translation reaction is carried out in the presence of reticulocyte lysate with the addition of amino acid mixture without methionine; semi-permeabilized cells and radioactively labeled methionine were also added to the reaction. As methionine is the start codon for mRNA translation, the radioactivity is guaranteed to be built in the growing nascent chain. Reticulocyte lysate is widely used in *in vitro* translation reactions. These immature red blood cells have intact translation machinery, and the endogenous mRNAs can be eliminated by nuclease treatment. Further nuclease activity is inhibited by EGTA to chelate the nuclease activator Ca^{2+} present in the system. Exogenous mRNAs can efficiently be translated in this system displaying minimal background signal.

After separating the ER processed translation products by SDS-PAGE and exposing the radiolabeled proteins to phosphor plates, one can gain information on the transport efficiency of specific substrates. *In vitro* translation means when mRNA substrate is used as a precursor molecule for protein synthesis (9.15.3). Coupled *in vitro* transcription and translation means when DNA substrate is used (9.26.2). The transport experiments were carried out in *in vitro* co-translational mode. As model proteins, preprolactin, invariant chain, cytochrome b5, prestatherin, and Sec61β mRNA were tested.

9.15.1 SAMPLE PREPARATION

After the desired culturing time point, cells were washed with 1x PBS and incubated with 500 µl trypsin for 5 minutes at 37 °C. Cells were resuspended in 3 ml 1x PBS containing 125 mg/ml trypsin inhibitor, and the cell numbers were determined by an automated cell counter as described in Paragraph 9.5. Cells were pelleted by centrifugation for 5 minutes at 2500 rpm. The cell pellet was resuspended in 6 ml KHM buffer. The plasma membrane was semi-permeabilized with 1 µl 40 mg/ml digitonin per 1x 10^6 cells for 5 minutes on ice. Before pelleting the cells, the volume was adjusted to 14 ml by adding KHM buffer. Cells were resuspended in 14 ml HEPES buffer and incubated on ice for 10 minutes. After pelleting the cells by centrifugation, 300 µl KHM buffer was added, and the cell pellet was mixed by pipetting. DNase I was added at 26.7 U/ml concentration and 0.6 mM calcium chloride to activate the DNAse I. After 12 minutes of incubation at room temperature, 0.6 mM EGTA was added to inhibit the DNAse I activity. After the addition of 3 ml KHM, cells were pelleted by centrifugation. Cell numbers were determined by an automated cell counter. After centrifugation, the cell density was set to 40 000 cells/µl in each sample with KHM buffer.

9.15.2 WESTERN BLOT ANALYSIS OF SEMI-PERMEABILIZED CELL EXTRACT

25 µl of the previously prepared semi-permeabilized cells were collected for subsequent Western blot analysis. 25 µl 2x Laemmli buffer was added, and samples were heated at 56 °C for 10 minutes. 800 000 cells (20 µl) per sample, as well as 5 µl page ruler, were loaded into SDS-PAGE gels (see Table 4) into separate wells. Proteins were separated according to molecular weight by SDS-PAGE as described in Paragraph 9.12.

9.15.3 IN VITRO TRANSLATION ASSAY

In vitro translation of mRNA substrates was carried out by the addition of ribonuclease inhibitor, amino acid mixture without methionine, reticulocyte lysate, radioactively labeled methionine, and nuclease-free water in the presence of semi-permeabilized cells (from steps described in Paragraph 9.15.1).
Composition of 16.5 µl master mix: 12.5 µl reticulocyte lysate (L416A), 0.5 µl amino acid mixture without methionine, 1.0 µl RNasin, 1 µl L-[^{35}S]-methionine, 2 µl nuclease-free water.
1 µl mRNA products from the *in vitro* transcription reactions (from steps described in Paragraph 9.14) were added to 16.5 µl master mix, in separate tubes for each different mRNA. [25 µl reaction: 16.5 µl master mix + 7.5 µl semi-permeabilized cells + 1 µl mRNA].
One sample was prepared for each mRNA substrate per silencing condition. 5 µl sample contained a 3.5 µl master mix with a designated mRNA substrate and 1.5 µl semi-permeabilized cells (from steps described in Paragraph 9.15.1). KHM buffer was added to the control samples at the same ratio as semi-permeabilized cells. The reaction mixtures were incubated at 30 °C for 1 hour, applying 800 rpm shaking. Cytochrome b5, prestatherin, and Sec61β translation products were centrifuged at 13 000 rpm

for 15 minutes; the lysate was removed by pipetting, not disturbing the pellet, in order to reduce possible background signal resulting from the accumulated heme. 20 µl 1x Laemmli sample buffer was added to the pellets, and 15 µl to the non-centrifuged samples. Samples were heated at 95 °C for 5 minutes. Samples were collected at the bottom of the tubes by short centrifugation. The translation products were separated by SDS-PAGE. Preprolactin and invariant chain were separated in a 15 % SDS-PAGE gel, while prestatherin and Sec61β were separated in a urea gel; a 17.5 % SDS-PAGE gel was used to separate cytochrome b5. Gels ran overnight at 5 mA electrical current in standard or urea electrophoresis buffer. After the running was completed, the gels were fixed in destaining solution I for 15 minutes and in neutralizing solution for 30 minutes on an orbital shaker. After fixation, the gels were dried on vacuum heat plates onto filter papers. The radioactive signals were captured on storage phosphor screens. Signal detection was carried out by Typhoon Trio Variable Mode Image Scanner (GE Healthcare). Analysis was done by the ImageQuant TL 7.0 image analysis software (GE Healthcare).

9.16 QUICK-CHANGE SITE-DIRECTED MUTAGENESIS PCR

Site-directed mutagenesis is a PCR-based technique to induce mutation in plasmid vectors. The designed complementary primers contain the mutation, which is inserted into the sequence of the replicated plasmid DNA through the amplification cycles. At the end of the amplification, the template DNA is digested by the addition of the Dpn I restriction enzyme. Dpn I cleaves only the methylated DNA so that the newly synthesized unmethylated PCR product stays intact. The amplified mutated PCR product is linear and will be sealed by the appropriate enzymes once it is transformed into *Escherichia coli* cells (Liu and Naismith, 2008).

The original *TMEM109* expression plasmid (NM024092, OriGene) was altered by quick-change site-directed mutagenesis PCR to remove the FLAG-tag by inserting a stop codon between the *TMEM109* and the downstream *Myc-DDK-Tag* of the encoded fusion protein. The forward (5'-GTGGAGGAGGAGTAACGTACGCGGCCG-3', RZ 764) and reverse primers (5'-CGGCCGCGTACGTTACTCCTCCTCCAC-3', RZ 765) were designed for the PCR reaction and purchased from Eurofins Genomics company as custom-designed oligonucleotides. 25 µl PCR reaction contained: 1x PCR buffer with 20 mM $MgSO_4$, 200 µM dNTP, 5 µM forward primer (RZ764), 5 µM rev primer (RZ 765), 100 ng/µl *TMEM109* plasmid (OriGene, NM024092), 2 U Phusion Polymerase, and nuclease-free water up to 25µl. The following heat profile was used on the thermal cycler: 95 °C for 2 minutes; 95 °C for 30 seconds, ramp for 30 seconds, 72 °C for 7 minutes (35 cycles); 72 °C for 2 minutes, and 8 °C for infinite time. For the digestion of the template DNA, 0.5 µl Dpn I enzyme was added to the PCR reaction and was incubated at 37 °C for 1 hour. Dpn I restriction enzyme cleaves the methylated DNA so that the template DNA.

9.16.1 TRANSFORMATION OF COMPETENT CELLS WITH THE EXPERIMENTAL DNA

The steps are identical as written in Paragraph 9.7.8. DNA extraction and sequencing steps are identical, as written in Paragraphs 9.7.9 and 9.7.10. For sequencing, forward sequencing primer 5'-TAATACGACTCACTATAGG-3' (T7 promoter primer, RZ 747) was used.

9.16.2 AMPLIFICATION OF THE RIGHT PLASMID CONSTRUCTS (TRANSFORMATION OF COMPETENT CELLS WITH THE EXPERIMENTAL DNA)

100 µl of JM101 chemically competent cells were thawed on ice; for subsequent steps, see Paragraphs 9.7.11 and 9.7.12.

9.17 TMEM109 COMPLEMENTATION ASSAY

To test the effect of TMEM109 complementation, HeLa cells were transfected with TMEM109-UTR-1 siRNA, or control siRNA at a final concentration of 25 nM, as described in Paragraph 9.6.
After 40 hours of TMEM109 silencing, the culture medium was renewed (3.8 ml), and cells were transfected with control plasmid (pCMV6-Entry Mammalian Expression Vector, PS 100001, OriGene) or TMEM109 expression plasmid (altered, not expressing Myc-DDK-Tag (from steps described in 9.16)) (NM024092, OriGene). Transfection mixes were prepared in a 200 µl Opti-MEM reduced serum medium containing 4 µg plasmid and 16 µl transfection reagent (Fugene). After 10 minutes of incubation time, transfection mixes were added to the appropriate culture dishes. After 60 hours of culturing, samples were prepared for Western blot analysis and *in vitro* translation assay as described in Paragraphs 9.15.1, 9.15.2, and 9.15.3.

9.18 TMEM109 AND WRB SIMULTANEOUS SILENCING

For testing the effect of simultaneous silencing of the SND pathway and the TRC pathway, HeLa cells were transfected with designated siRNAs (TMEM109-UTR-1 and WRB-UTR-3), as described in Paragraph 9.6 at 20 nM final concentration in the case of single siRNA silencing. Under simultaneous silencing conditions, each siRNA was added at 20 nM concentration to get a 40 nM final siRNA concentration. As control conditions, cells were transfected with scrambled siRNA at a final 40 nM final concentration. After 72 hours of culturing, samples were prepared for Western blot analysis and *in vitro* translation assay as described in Paragraphs 9.15.1, 9.15.2, and 9.15.3.

9.19 GENERATION OF CRISPR-CAS9-MEDIATED TMEM109 KNOCKOUT CELL LINE

The CRISPR-Cas9 technique is based on the fact that the RNA-guided Cas9 finds its target sequence within the cells. Then the Cas9 nuclease cleaves the target DNA upstream from the so called protospacer adjacent motif (PAM). The DNA double-strand break nick can be repaired by the non-homologous end joining (NHEJ) or the homology-directed repair (HDR). In the absence of a repair template, the NHEJ re-ligates the broken strands leaving an insertion/deletion (indel) mutation (Ran *et al.*, 2013).

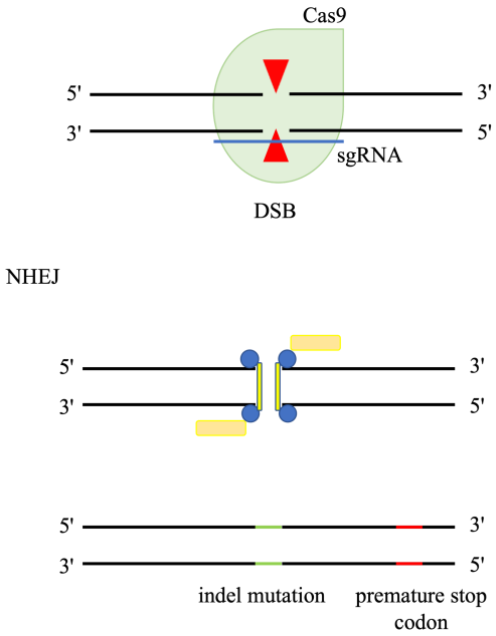

Figure 9. Double strand repair induced by Cas9

The figure depicts the possible outcomes of repairing a double-strand break (DSB). Homology-directed repair (HDR) uses a template to seal the nick (not visualized here), while the non-homologous end joining (NHEJ) is much error-prone to seal the incision as soon as possible, leaving an insertion/deletion mutation (Ran *et al.*, 2013). The figure was edited based on the figure generated by Ran *et al.*, 2013.

9.19.1 DESIGNING SGRNA INSERTS FOR THE GENERATION OF TMEM109 CRISPR-CAS9 PLASMID

Insert oligonucleotides (single guide RNA (sgRNA) pair) were designed on the https://chopchop.cbu.uib.no web page against the *TMEM109* as the target sequence: 5'-TCGATCTGTGCGAGGGACACTGG-3'. The inserts were ordered from Eurofins Genomics company as custom-designed oligonucleotides; the sequence of the forward insert was the following: 5'-CACCGTCGATCTGTGCGAGGGACAC-3' (RZ756) (5'-CACCG…-3' in the beginning is fixed), the sequence of the reverse insert was the following 5'-AAACGTGTCCCTCGCACAGATCGA-3' (RZ 757) (5'-AAAC…-3' in the beginning is fixed).

9.19.2 5' PHOSPHORYLATION OF THE DESIGNED OLIGONUCLEOTIDES

100 µl reaction contained: 1x T4 DNA ligase buffer, 5 µM forward insert (RZ756), 5 µM reverse insert (RZ 757), 10 U T4 polynucleotide kinase, and nuclease-free water. In the reaction, T4 DNA ligase buffer was used instead of the T4 polynucleotide kinase buffer because it is supplemented with ATP. The following heat profile was used on the thermal cycler: 37 °C for 30 minutes; 70 °C for 50minutes, 25 °C ramping down 1 °C/ minute, and 8 °C for infinite time. At the end of the incubation, 40 µl of nuclease-free water was added to the reaction to dilute the oligonucleotide concentration to 25 ng/µl.

9.19.3 RESTRICTION DIGESTION OF THE VECTOR

Plasmid pSpCas9n(BB)-2A-GFP (PX458, Addgene) was digested with the BbsI restriction enzyme. The enzyme cuts in the following consensus motif, excising 22 bp out of the 9229 bp vector. BbsI restriction site is encoded in the multiple cloning site (MCS) of the vector twice in the opposite orientation.

5'...G A A G A C (N) 2 ↓ …3'

3'...C T T C T G (N) 6 ↑....5'

1 µg plasmid DNA, 1x CutSmart Buffer, and 1 µl restriction enzyme were added to nuclease-free water up to 50 µl. The tubes were gently mixed and spun down for a few seconds. The reaction mixtures were incubated at 37 °C for 60 minutes. The restriction enzyme was inactivated at 80 °C for 20 minutes.

9.19.4 AGAROSE GEL ELECTROPHORESIS AND GEL EXTRACTION

Agarose gel electrophoresis and gel extraction were performed as written in Paragraphs 9.7.5 and 9.7.6. UV illumination of the stained gel confirmed the correct size of the products (uncut plasmid: 9229 bp and cut plasmid: 9207 bp). Gel extraction and purification of the correct band were carried out as written in Paragraph 9.7.6.

9.19.5 LIGATION REACTION AND TRANSFORMATION OF COMPETENT CELLS

Ligation reaction using the digested and purified vector DNA and the 5'-phosphorylated sgRNA inserts were carried out as written in Paragraph 9.7.7. Steps for the transformation of competent cells are identical as in Paragraph 9.7.8.

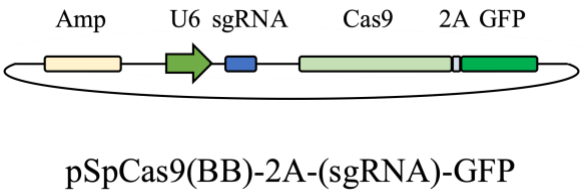

Figure 10. Simplified map of the plasmid expressing Cas9 and the sgRNA

The plasmid was digested with the BbsI restriction enzyme (restriction sites are not displayed) and ligated with the 5'-phosphorylated sgRNA pair. GFP served as a selection marker after plasmid transfection.

9.19.6 PLASMID DNA EXTRACTION AND DNA SEQUENCING

Plasmid DNA was extracted as described in Paragraph 9.7.9. The isolated plasmid DNA was sent for sequencing as described in section 9.7.10. Forward sequencing primer, 5'-GAGGGCCTATTTCCCATGATT-3' (hU6-F, RZ 785), was used.

9.19.7 AMPLIFICATION OF THE RIGHT PLASMID CONSTRUCTS AND DNA ISOLATION

The right clones were amplified in DH5α competent cells, and the plasmid DNA was extracted the following day as described in Paragraphs 9.7.11 and 9.7.12.

9.19.8 TRANSFECTION OF CELLS WITH TMEM109 CRISPR-CAS9 PLASMID

550 000 HeLa cells were seeded in 6 cm cell culture dishes. After a few hours, when the cells settled down, transfection mixes were prepared in 200 µl Opti-MEM reduced serum medium containing 1 µg plasmid and 4 µl transfection reagent (Fugene). After 10 minutes of incubation time, transfection mixes were added to the appropriate culture dishes. Control cells were cultured without the addition of any reagent as an untransfected control. After 40 hours of culturing, cells were harvested by trypsinization in 1x PBS.

9.19.9 FLUORESCENCE-ACTIVATED CELL SORTING (FACS)

A 96 well sterile cell culture plate was prepared with 300 µl previously collected, sterile filtered, conditioned DMEM. Transfected GFP positive cells were collected into 96 well plate by FACSAria III cell sorter (BD Biosciences) using BD FACS Diva software. Either 100, 50, 10, or 1 single cell was collected with each condition. FACS sorting was done with the help of PD Dr. Elmar Krause (Center for Integrative Physiology and Molecular Medicine).

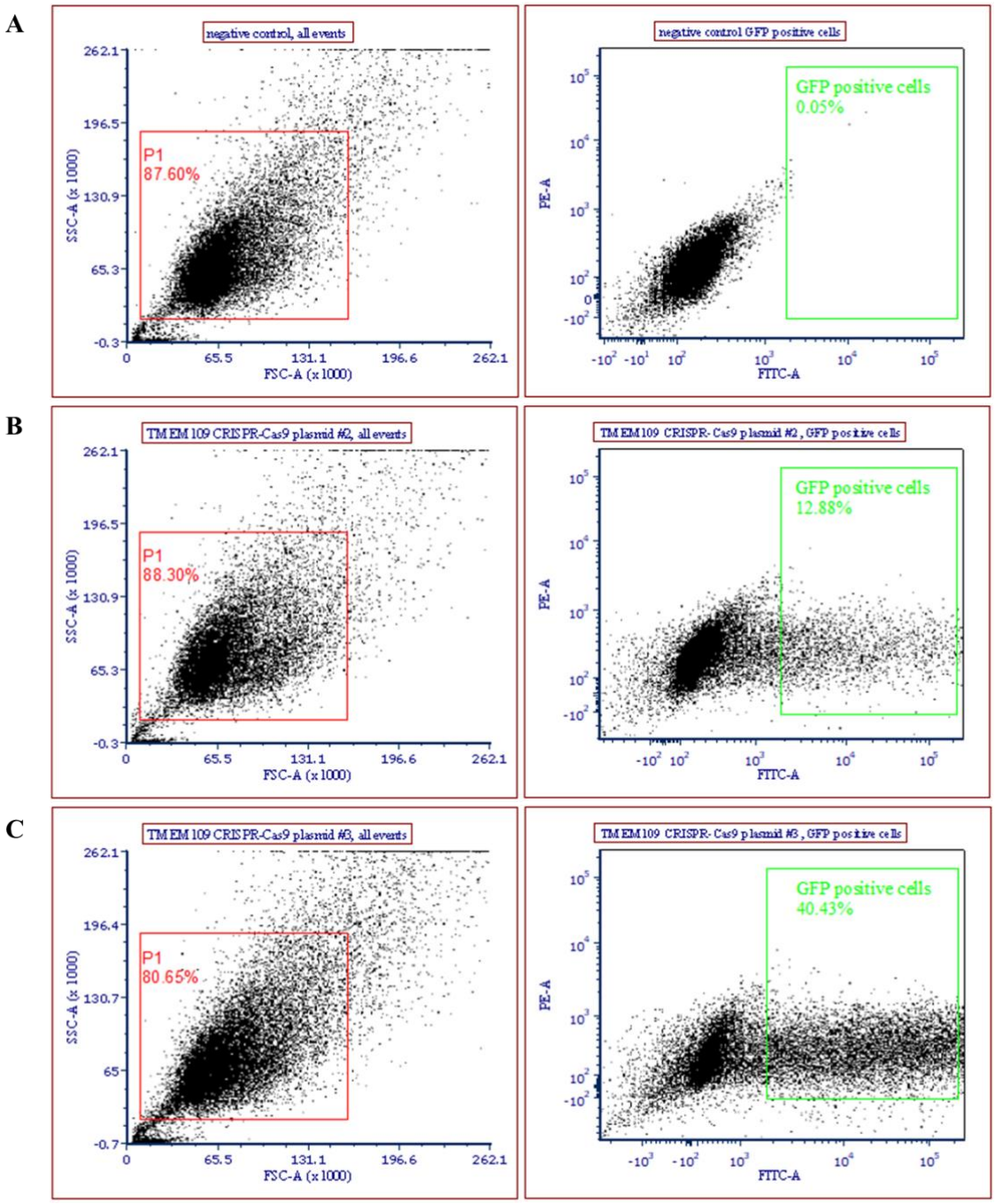

Figure 11. Fluorescence-activated cell sorting after transfecting HeLa cells with *TMEM109 CRISPR-Cas9* plasmid

Cells that were successfully transfected with the generated CRISPR-Cas9 plasmid could be distinguished based on GFP positivity. The figure displays debris exclusion in all samples in the first column and GFP positive cells in the second column. A) control cells, B) cells transfected with number 2 plasmid, C) cells transfected with number 3 plasmid. In the case of sample C, the transfection rate was higher, confirmed by FCS Express 7 software. As a negative control, cells were not treated with any reagent.

9.19.10 EXPANDING THE VIABLE CLONES

The culture medium was changed every 3 to 5 days based on need. Colonies appeared approximately 2 weeks after sorting. When cells reached 60 % confluency, clonal lines were passaged. During the expansion phase, when sufficient cells were growing, the clones were cryopreserved.
For cryopreservation of HeLa cells, 3x 10^6 cells were resuspended in 1500 µl DMEM containing a final concentration of 20 % FCS and 10 % DMSO and transferred to cryovials. The vials were kept in a freezing container at -80 °C for 24 hours and then transferred to -190 °C for long-term storage.

9.19.11 WESTERN BLOT ANALYSIS OF THE CLONES

To test the efficiency of the TMEM109 knockout in cells, Western blot analysis was performed based on the protocol written in 9.12. The two clones that are highlighted in the figure were expanded from single cells and were used in downstream experiments.

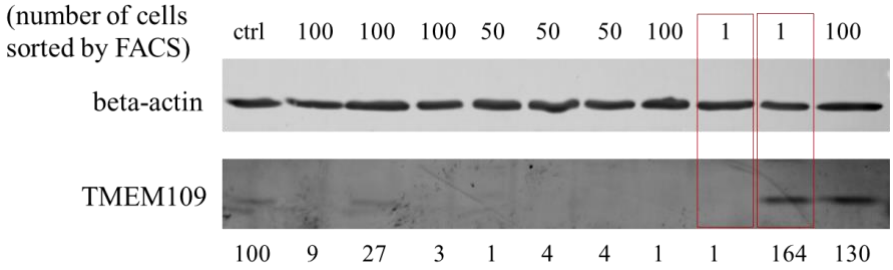

Figure 12. Western blot analysis of the expanded clones after *TMEM109* CRISPR-Cas9 plasmid transfection and fluorescence-activated cell sorting

Western blot results after *TMEM109* knockout. Numbers on the top of the figure indicate the number of cells that were collected during FACS analysis, meaning the clones were expanded from the defined number of cells. *TMEM109* knockout was not successful in each clone. The clones that still express *TMEM109* were used as controls. The two clones that are highlighted in the figure were expanded from single cells and were used in downstream experiments. The numbers at the bottom indicate the relative protein abundance compared to the control sample. Beta-actin served as a protein loading control due to its constitutive expression.

9.19.12 GENOMIC DNA ISOLATION

During cell passaging, some cell suspension was collected and washed in 1x PBS and stored at -80 °C for genotyping. For genomic DNA isolation, DNeasy Blood and Tissue Kit was used according to the manufacturer's instructions. The quality of the genomic DNA was verified by agarose gel electrophoresis in 0.5 % agarose gel (Figure 13). 100 ng of the DNA samples were diluted in 1x gel loading dye and nuclease-free water. Gel running and product visualization steps were identical as written in Paragraph 9.7.5.

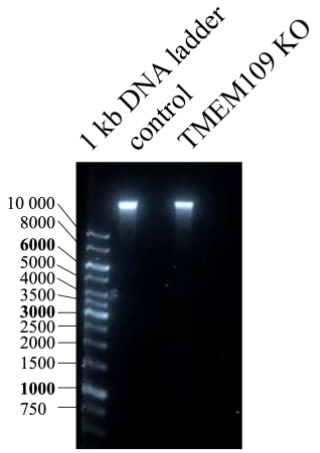

Figure 13. Visualization of genomic DNA in control and *TMEM109* knockout samples

Isolated genomic DNAs were loaded into a 0.5 % agarose gel. Genomic DNA has a high molecular weight, so it generally does not move far into the gel.

9.19.13 PCR AMPLIFICATION OF THE GENOME SEQUENCE THAT CONTAINED THE INITIATED MUTATION

The forward (5'-TTATCCTCCTCCACTCAGCATT-3', RZ 814) and reverse primers (5'-TCACACAGGGACTACCTTCCTT-3', RZ 815) were designed for the sequencing reaction on the https://chopchop.cbu.uib.no webpage and purchased from Eurofins Genomics company as custom-designed oligonucleotides. 100 µl PCR reaction contained: 1x PCR buffer with 20 mM $MgSO_4$, 200 µM dNTP solution, 0.1 µM forward primer (RZ814), 0.1 µM rev primer (RZ 815), 50 ng/µl genomic DNA, 2.5 U Phusion Polymerase, and nuclease-free water.

The following heat profile was used on the thermal cycler (Peqlab, Primus 96): 95 °C for 2 minutes; 95 °C for 30 seconds, 53.1 °C for 30 seconds, 72 °C for 90 seconds (35 cycles); 72 °C for 2 minutes; and 8 °C for infinite time.

Samples were supplemented with gel loading dye and loaded into 2 % agarose gels, cast with wide combs. 250 ng 50 bp DNA ladder was loaded as a molecular-weight size marker. Agarose gel electrophoresis steps are identical as described in Paragraph 9.7.5. UV illumination of the stained gel confirmed the correct size of the products: 188bp (Figure 14).

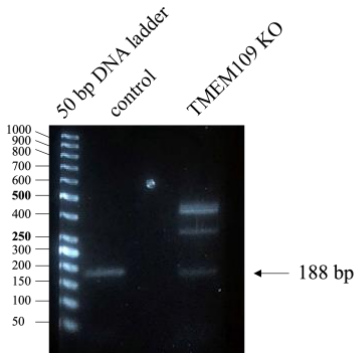

Figure 14. PCR amplified DNA fragment of the *TMEM109* gene that contained the recognition site by the *TMEM109* CRISPR-Cas9 plasmid

PCR amplification of the *TMEM109* gene containing the mutation site by CRISPR-Cas9 technique. Fragments show the correct 188 bp size. In the *TMEM109* knockout sample, additional DNA bands appear that are possibly genomic DNA fragment residuals from the PCR reaction.

9.19.14 DNA SEQUENCING

The correct bands (188 bp) were cut out from the gel, and PCR products were gel-purified using PCR- and gel cleanup system. Samples were eluted in 25 µl nuclease-free water provided with the kit.

PCR products at a concentration of 10 ng/µl in 14 µl volume (in ultrapure water) and 4 µl of a 5 µM primer were sent for sequencing to the LGC Genomics company. Forward sequencing primer: 5'-TTATCCTCCTCCACTCAGCATT-3' (RZ 814), reverse sequencing primer: 5'-TCACACAGGGACTACCTTCCTT-3' (RZ 815). For sequence alignment, SeqMan software (Lasergene, DNASTAR) was used (Figure 15).

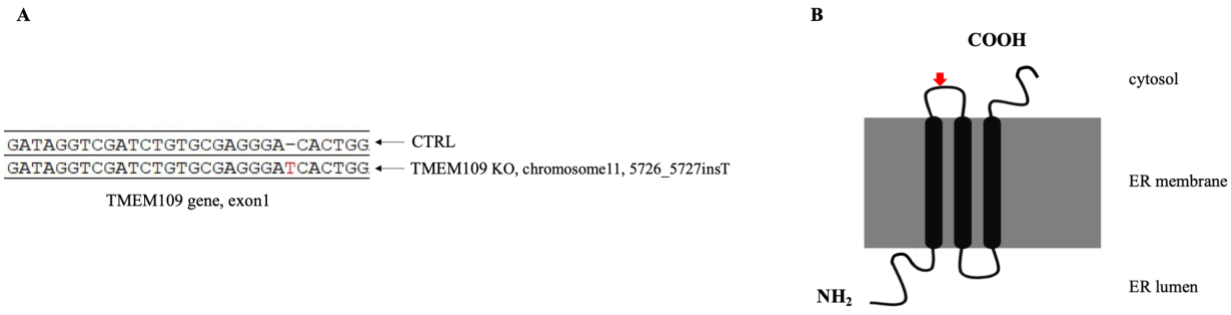

Figure 15. Frameshift mutation induced by CRISPR-Cas9 in the *TMEM109* gene

TMEM109 knockout cells carry the insertion mutation in their genome. These genotyping results are visualized in figure A. The frameshift mutation starts after Gly 63 (GGG), which results in a premature stop codon (aa114), generating a truncated protein product that is presumably degraded by the proteasome. Figure B displays the topology of the wild-type TMEM109; the arrowhead labels the premature stop codon in the *TMEM109* knockout samples.

9.20 LIVE-CELL CALCIUM IMAGING

As TMEM109 has been described as a calcium channel in the ER membrane, it was tested by live-cell calcium imaging whether its knockdown or knockout could disturb the cellular calcium homeostasis. Using calcium imaging, one can measure the calcium content of a living cell at a given time. The method used here is based on pre-loading cells with the calcium-sensitive fluorescent dye Fura-2, and the Ca^{2+} bound and Ca^{2+} free Fura-2 ratio can be measured. Fura-2-acetoxymethyl ester (Fura-2-AM) is a cell-permeable dye; the acetoxymethyl ester part is cleaved off by cytosolic esterases, thus losing its ability to cross organellar membranes. The Ca^{2+} bound Fura-2 is excitable best at 340 nm, while the Ca^{2+} free Fura-2 is excitable best at 380 nm wavelength. The Fura-2 emission peak is 510 nm wavelength and does not depend on the excitation wavelength. The calcium content in the cytosol can be determined based on the excitation wavelength, the 340/380 ratio (Roe *et al.*, 1990). The changes in the cytosolic calcium level can be monitored in response to different agents that can alter the calcium homeostasis within the cells, such as ionomycin and thapsigargin.

Ionomycin is a calcium-specific ionophore that releases calcium ions out of all cellular organelles so that it is suitable to determine the overall calcium content. In contrast, thapsigargin inhibits the SERCA pump, enabling measuring the ER-specific calcium leak.

9.20.1 MEASURING THE CALCIUM STATUS OF A CELL (LIVE-CELL CALCIUM IMAGING)

HeLa cells were cultured in 6 cm culture dishes as described in Paragraph 9.5, containing 2 coverslips (25 mm). After the desired culturing time, coverslips were transferred into 3.5 cm culture dishes containing standard culture medium, using sterilized forceps.

50 µg Fura-2-AM cell membrane-permeant calcium indicator was dissolved in 50 µl DMSO. The cells were stained in 1000 µl culture medium containing 4 µl Fura-2-AM at room temperature, protected from a direct light source. After 30 minutes of staining, the coverslip was transferred into a metal cell chamber and washed two times in 300 µl external solution.

For the measurement, the cells were kept in 300 µl external solution. IMIC microscope (Photonics) was used with DCLP410 and LP470 filters and Polychromator V (Photonics). The signal was captured by iXon EMCCD camera (model 885, Andor). Data collection and analysis were carried out by Live Acquisition software (Photonics) and Offline Analysis software (Photonics).

Ionomycin and thapsigargin were dissolved in DMSO to get the final concentration of stock solutions at 10 mM and 997 µM, respectively. Stock solutions were stored in aliquots at -80 °C. Before the measurement, ionomycin was diluted in 300 µl external solution to get 10 µM concentration per sample. Thapsigargin was diluted in 300 µl external solution to get 2 µM concentration per sample. After measuring the basal calcium content for one minute, 300 µl ionomycin or thapsigargin was added to the chamber during the measurement at 5 µM and 1 µM final concentration, respectively. Changes in the

calcium content were registered for 5 minutes in the case of ionomycin and 10 minutes in the case of thapsigargin.

9.21 CHEMICAL INDUCTION OF ER STRESS AND UPR

The effect of ER stress and UPR induction on the mRNA level and the abundance of ER protein targeting receptors were tested. For this, 560 000 HeLa cells were cultured in 6 cm cell culture dishes in DMEM. Cells were treated with 1 µM thapsigargin or 2.5 µg/ml tunicamycin after 24 hours of culturing. Since both agents are dissolved in DMSO, cells treated with DMSO at a final concentration of 0.1 % served as control conditions. After 20 hours of treatment, cells were harvested by trypsinization and the plasma membrane was semi-permeabilized, as written in Paragraph 9.15.1. Western blot analysis was performed according to the steps described in Paragraph 9.15.2.
Cells cultured in extra dishes were harvested for RT-qPCR analysis as written in Paragraph 9.9.

9.22 STATISTICAL ANALYSIS

Statistical analysis was carried out by Graphpad Prism 5.0 software. One-way ANOVA statistical analyses were performed, except in the case of the experiments with the TMEM109 knockout cells, where two-tailed t-tests were performed. Significant changes are indicated by * symbols: *** $P < 0.001$; ** $P < 0.01$; * $P < 0.05$, "ns" indicates non-significant results $P \geq 0.05$.

9.23 ADDITIONAL UNPUBLISHED EXPERIMENTS MENTIONED IN THE DISCUSSION SECTION

9.24 IMMUNOCYTOCHEMISTRY

To visualize the ER structure, immunocytochemistry was performed. 240 000 HeLa cells were seeded in 6 cm culture dishes as described in Paragraph 9.5, containing 8 coverslips (10 mm). After 6 hours, when the cells were settled down, transfection mixtures with designated siRNAs were added as described in Paragraph 9.6. After 65 hours of culturing, coverslips were transferred into 6 well culture plates. One well contained two coverslips per condition. The plates were placed on ice and washed in 1 ml cold 1x PBS. Cells were fixed in 1 ml 4 % paraformaldehyde solution (10 ml 16 % (w/v) paraformaldehyde, 8 ml 5x PBS, ultrapure water up to 40 ml) for 20 minutes on ice.
Cells were washed in 1 ml neutralization solution (1x PBS, 100 mM glycine, 4 mM $MgCl_2$) at room temperature four times for 5 minutes. Cells were incubated in saponin containing solution (1x PBS, 5 % (v/v) FBS, 0.1 % (w/v) saponin) containing 2 mg/ml RNase A. The plates were stored in a wet chamber.

Cells were incubated with primary antibodies (TMEM109 and hSnd2, Table 5) at a 1:50 ratio in saponin solution for 90 minutes at room temperature. Cells were washed in saponin solution four times for 5 minutes. Cells were incubated with anti-rabbit secondary antibodies (Table 5) at a 1:500 ratio in saponin solution for 90 minutes at room temperature in the dark. Cells were washed in saponin solution four times for 5 minutes. Coverslips were placed on a microscope slide and cured with mounting medium. (The mounting medium contained DAPI.) Microscopic examination was carried out by Nikon, Eclipse, TE-2000-S microscope, and imaging software NIS-Element F 4.60.00 (Nikon).

9.25 SPOT PEPTIDE ARRAY ANALYSIS TO IDENTIFY PROTEIN-PROTEIN INTERACTION SITES

The spot peptide array method allows researchers to perform easily replicable experiments with peptides. Peptides are synthesized on a porous membrane in the form of peptide spots that can be probed for protein-peptide interaction, whereas the interaction partner can be detected by immunostaining. After incubating the cellulose membrane with rough microsome (RM) extract, which contains all ER membrane proteins, including the solubilized hSnd2 and TMEM109 in digitonin micelles, it was suitable to identify the interaction between the two, as well as the homo-oligomerization capability of TMEM109.

9.25.1 PREPARATION OF ROUGH MICROSOMES AND ROUGH MICROSOME EXTRACTS

Dog pancreatic RM (rough microsomes) (ER membrane fragments) were prepared as described in Walter and Blobel's work from 1983 (Walter *et al.*, 1981).

After sedimentation by ultracentrifugation (Optima Max-E ultracentrifuge, TLA 100.3 rotor), the membranes were resuspended in 20 mM HEPES-KOH (pH 7.8), 5 mM magnesium acetate, 5 mM dithiothreitol, 10 µg/ml leupeptin, 5 µg/ml chymostatin, 15 % (w/v) glycerol, 0.4 % digitonin, containing 1 equivalents RMs per µl. ("1 equivalent (eq) is the amount of a fraction (supernatant fluid or membrane) that is derived from 1µl of a RM suspension at a concentration of 50 U/ml (A_{280})" (Walter *et al.*, 1981)). The mixture was centrifuged in an ultracentrifuge for 40 min at 100 000 rpm. The supernatant was named preextract.

The pellet was resuspended in extraction buffer (20 mM HEPES-KOH (pH 7.8), 12 mM magnesium acetate, 400 mM potassium acetate, 5 mM dithiothreitol, 10 µg/ml leupeptine, 5 µg/ml chymostatin, 15 % (w/v) glycerol, 4 % digitonin). After 10 minutes of incubation on ice, the mixture was centrifuged for 60 minutes at 100 000 rpm at 2 °C. The supernatant contained the RM extract and was used in downstream experiments.

9.25.2 CELLULOSE MEMBRANE PREPARATION

Peptide spots were synthesized by ResPep SL (Intavis) fully automated peptide synthesizer on derivatized cellulose membrane (32100, CEM) based on the manufacturer's instructions. The membrane was activated in methanol for 1 minute, applying agitation. Unspecific binding sites on the membrane were blocked in 1 % (w/v) BSA solution, dissolved in 1x PBS, for 60 minutes at room temperature, applying agitation. The extracted microsomes from step 9.25.1 were diluted at a ratio of 1:3 in 1x PBS and incubated with the membrane overnight at 4 °C, applying agitation. The membrane was washed in 1x PBS containing 0.05 % Tween 20 three times and in 1x PBS once.

9.25.3 IMMUNOSTAINING

Primary antibody incubation (TMEM109 and hSnd2, Table 5) was carried out at a 1:1000 ratio for 90 minutes at room temperature, applying agitation. The membrane was washed in 1x PBS containing 0.05 (v/v) % Tween 20 three times and in 1x PBS once. The membrane was incubated with POD labeled anti-rabbit antibodies for 120 minutes at room temperature at a 1:1000 ratio. The membrane was washed in 1x PBS containing 0.05 % Tween 20 three times and in 1x PBS once. Antibody detection was performed on Fusion SL (Peqlab) chemiluminescence imager and software after chemiluminescence substrate addition based on the manufacturer's instructions.

9.26 IN VITRO TRANSCRIPTION AND TRANSLATION ASSAY OF DNA SUBSTRATES

9.26.1 SAMPLE PREPARATION AND WESTERN BLOT ANALYSIS

Sample preparation and Western blot analysis steps are identical as described in Paragraphs 9.15.1 and 9.15.2, respectively.

9.26.2 IN VITRO TRANSCRIPTION AND TRANSLATION ASSAY

In vitro transcription and translation of the DNA substrate was carried out by the addition of ribonuclease inhibitor, amino acid mixture without methionine, TNT rabbit reticulocyte lysate, TNT T7 polymerase, TNT reaction buffer, radioactively labeled methionine, and nuclease-free water, in the presence of semi-permeabilized cells (the preparation of semi-permeabilized cells is described in Paragraph 9.15.1).
Composition of 16.5 µl master mix: 12.5 µl reticulocyte lysate (L483A), 0.5 µl amino acid mixture without methionine, 0.5 µl RNasin, 1.0 µl TNT reaction buffer, 0.5 µl T7 polymerase,1 µl L-[^{35}S]-methionine, 0.5 µl nuclease-free water.
1 µl experimental DNA (*TMEM109* plasmid, NM024092, OriGene) was added to 16.5 µl master mix. [25 µl reaction: 16.5 µl master mix + 7.5 µl semi-permeabilized cells + 1 µl experimental DNA].

One sample was prepared for each silencing condition. 5 µl sample contained a 3.5 µl master mix with the experimental DNA and 1.5 µl semi-permeabilized cells (from steps described in Paragraph 9.15.1). KHM buffer was added to the control sample at the same ratio as semi-permeabilized cells. The following steps are identical as described in Paragraphs 9.15.3. A 17.5 % SDS-PAGE gel was used to separate the translation products according to the molecular weight.

10 RESULTS

To test that TMEM109 is a possible component of the SND pathway in mammalian cells and its role in calcium homeostasis, research was performed with various techniques. These results are enlisted in the following paragraphs. All the experiments were carried out in HeLa cells, mammalian cervical cancer cells, which is the same cell model was used to describe the evolutionarily conserved function of its potential interaction partner, the hSnd2 protein (Haßdenteufel *et al.*, 2017). The immortal HeLa cell line was established over 70 years ago by culturing cells from a patient diagnosed with cervical adenocarcinoma. Since then, it has been widely used in scientific experiments due to its easy culturing, rapid growth, and easy transfection ability. However, the cell line represents aneuploidy and chromosomal rearrangements, which could make it challenging to translate the obtained results to normal human tissue cells (Landry *et al.*, 2013).

10.1 TMEM109 AND HSND2 INTERACTION BY LUMINESCENCE PROTEIN-PROTEIN INTERACTION SYSTEM

To confirm the interaction between the TMEM109 and the hSnd2 protein in intact cells, the NanoBiT assay system was used (see Paragraphs 9.7 and 9.8).

Based on structural predictions of TMEM109 and hSnd2 their topology is assumed as follows, see Figure 16.

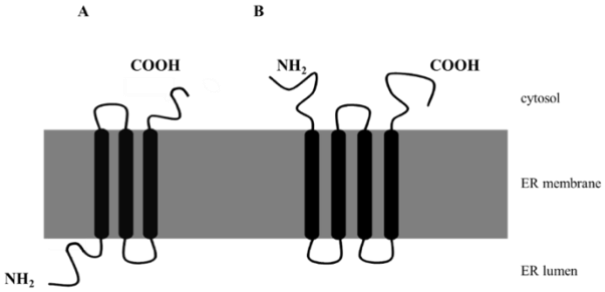

Figure 16. Predicted membrane topology of the TMEM109 and the hSnd2 protein

Predicted topology of the TMEM109 and the hSnd2 protein. A) TMEM109 is predicted as a three-transmembrane domain protein, the N-terminal end is flanking the ER lumen, and the C-terminal end is cytosolic. (The predicted position of the TMDs and the topological domains of the TMEM109 protein: signal sequence: 1-33, luminal domain: 34-83, TMD1: 84-104, cytoplasmic domain: 105-135, TMD2: 136-156, luminal domain: 157-185, TMD3: 186-205, cytoplasmic domain: 206-243. www.uniprot.org/uniprot/Q9BVC6, last accessed on 5 December 2021)

B) hSnd2 is believed to have four TMDs, both the N- and the C-terminus are cytosolic. (The predicted position of the TMDs and the topological domains of the hSnd2 (TMEM208) protein: cytoplasmic domain: 1-24, TMD1: 25-45, luminal domain: 46-50, TMD2: 51-68, cytoplasmic domain: 69-104, TMD3: 105-129, luminal domain: 130-134, TMD4: 135-154, cytoplasmic domain: 155-173. www.phobius.sbc.su.se, last accessed on 5 December 2021)

After testing the possible constructs of N- or C-terminal fusion of the Small or Large BiT, regarding the TMEM109 and hSnd2 protein; the following conformations gave the strongest signals during luminescence measurement: Large BiT fused to the C-terminal end of the TMEM109, and Small BiT fused to the N-terminal end of the hSnd2 (data is not shown here) (Figure 17).

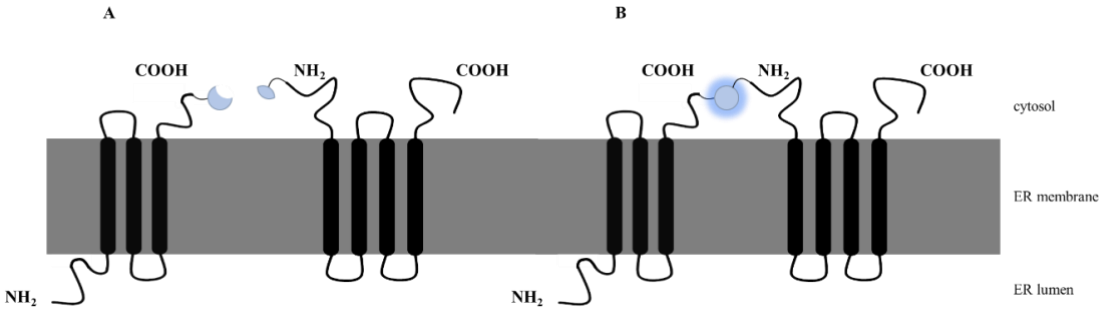

Figure 17. Schematic figure of TMEM109 and hSnd2 carrying the NanoBiT Large- and SmallBiT

Predicted topology of the TMEM109 and the hSnd2 protein carrying the NanoBiT Large and Small BiT. A) Plasmids, expressing the Large or the Small BiT were engineered to be expressed at the C-terminal end on the TMEM109 or the N-terminal end on the hSnd2, respectively. 24 hours post-transfection luminescence substrate was added and the luminescence signal was measured. B) If the proteins of interest are interacting the Large- and the Small BiTs form the functional luciferase enzyme and after substrate addition, the increase in the luminescence signal can be detected. (The assumed interaction between the two proteins is not depicted here for the sake of simplicity.)

The assay included a positive control, the protein kinase A, the catalytic subunit of the PKAα subunit is encoded by the *PRKACA* gene, while the *PRKAR2A* encodes the regulatory subunit. *PRKAR2A* was fused to the Large BiT (PKA-LgB), and *PRKACA* was fused to the Small BiT (PKA-SmB). As a negative control, the Small BiT protein was fused to the HaloTag protein, which should not interact with other fusion proteins of interest.

If the luminescence signal of a tested interaction is at least 10-fold higher than the respective negative control (interaction between the Large BiT fused to the protein of interest and the Small BiT-HaloTag) suggests that it is a specific protein-protein interaction (Sicking *et al.*, 2021). In addition, a C-terminally truncated TMEM109 construct was created to test whether deletion of this domain disrupts the TMEM109-hSnd2 interaction. The truncation affected the C-terminal end of the TMEM109 protein, the presumed cytosolic part of the protein was abolished after the 205th amino acid following shortly after the third TMD (Figure 18). The LargeBit was fused to the C-terminally truncated TMEM109.

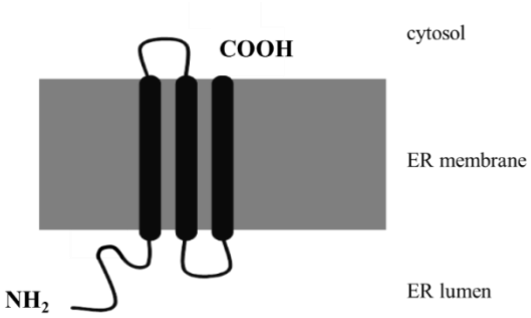

Figure 18. Topology of TMEM09 after C-terminal truncation

The figure depicts the C-terminally truncated TMEM109. The protein was truncated to 205 amino acids long. The predicted C-terminal cytosolic domain was abolished. The truncated product was fused to the Large BiT (not shown in this figure).

Figure 19 confirms the interaction between the TMEM109 and the hSnd2 proteins in live cells. As previously described, the Large BiT was fused to the C-terminal end of the TMEM109 and the Small BiT to the N-terminal end of the hSnd2. At first glance, these sites (C-terminus of the TMEM109 and N-terminus of the hSnd2) appeared to be responsible for the interaction between the two proteins. However, creating a C-terminally truncated TMEM109 and fusing it to the Large BiT did not disrupt the interaction between TMEM109 and hSnd2; the interaction was even slightly improved. Based on these results, it appears that the C-terminal end of TMEM109 is dispensable for the interaction with hSnd2, and further research is required to determine the exact site of the interaction between the two. (This will be discussed in more detail with the peptide spot array data in the Discussion section (Figure 52 and Figure 53).)

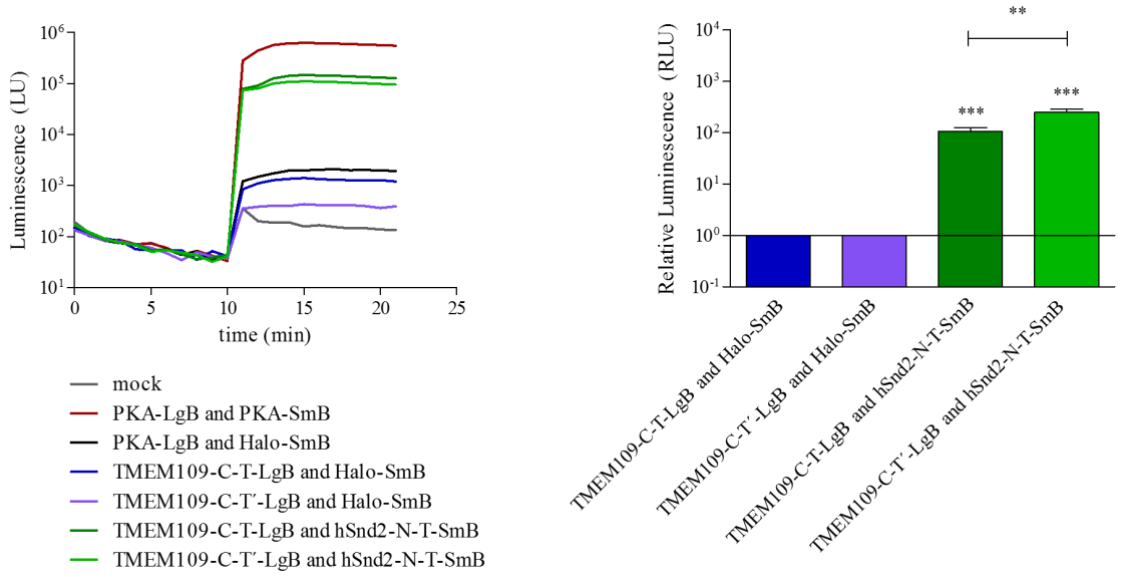

Figure 19. Protein-protein interaction between the TMEM109 and the hSnd2 protein

The figure displays the luminescence signal determined by the NanoBiT protein-protein interaction assay. Plasmids encoding the Large BiT or the Small BiT proteins were fused to the TMEM109 or the hSnd2 protein, respectively. Additionally, the Large BiT plasmid fused to the C-terminally truncated TMEM109 was tested. As a positive control, the subunits of the protein kinase A were fused to the Large or the Small BiT. As a negative control, HaloTag was fused to the Small BiT. After 24 hours post-transfection with the respective plasmids, the luminescence signal was measured by a plate reader. After furimazine substrate addition, a > 10-fold increase in the signal indicated a specific protein-protein interaction. The maximum values from the curves are displayed on the bar graph in comparison to the respective control. One representative measurement is displayed out of three independent repeats carried out in triplicates. One-way ANOVA statistical analysis was performed. Significant changes are indicated by * symbol: *** $P < 0.001$; ** $P < 0.01$; * $P < 0.05$.

10.2 OPTIMIZATION OF TMEM109 SILENCING

To reveal the contribution of TMEM109 to protein transport to the ER, an efficient depletion strategy was required to understand whether it can cause any change in the efficiency of protein transport. For this, the small interfering RNA (siRNA)-mediated gene silencing approach was used. A kinetic assay was performed to find the optimal silencing duration and dose. Three different siRNA concentrations were tested (25, 35, and 45 nM), and cells were harvested after 48 and 96 hours of silencing (Figure 20). TMEM109 depletion was more enhanced when cells were treated longer than 48 hours. The different siRNA concentrations did not have a pronounced different effect; similar silencing efficiency was observed for each concentration.

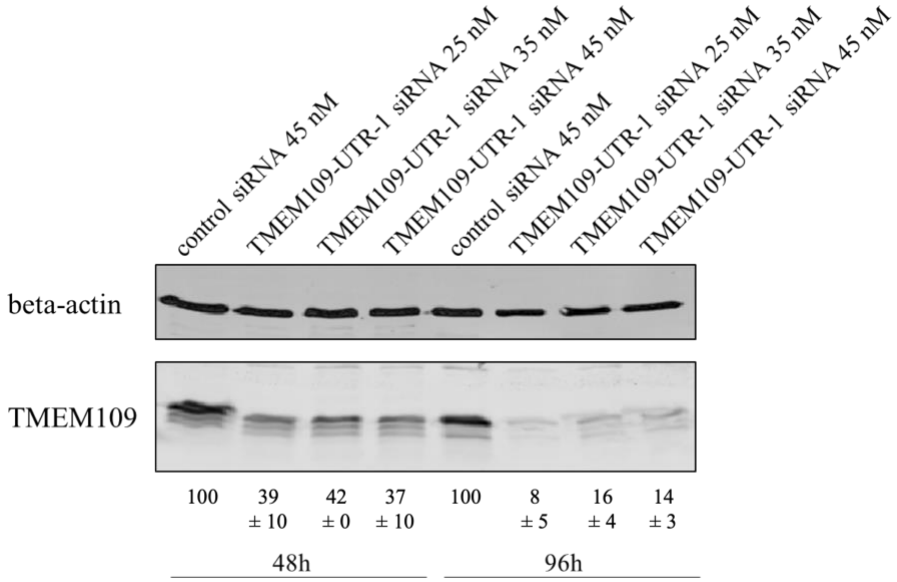

Figure 20. Time and concentration-dependent silencing of TMEM109

Western blot results after treating HeLa cells with siRNAs targeting the *TMEM109* mRNA at a final concentration of 25, 35, and 45 nM. Cells were harvested after 48 and 96 hours and prepared for Western blot analysis. One representative of at least two independent repeats is shown here. Numbers indicate the relative protein abundance in comparison to the respective control. Beta-actin served as a protein loading control due to its constitutive expression.

Confirming the efficiency of *TMEM109* silencing, real-time quantitative PCR (RT-qPCR) was performed to measure the changes in the mRNA level in response to siRNA-mediated silencing (Figure 21). Here, two different time points were tested, 48 and 72 hours, with a siRNA concentration of 25 nM. The mRNA depletion occurs much faster and is subsequently followed by a reduction of the target protein. This difference in the depletion kinetics between mRNA and the encoded protein is based on the protein's half-life. Both silencing time intervals proved to be efficient in terms of mRNA depletion, with an approximate 0.9-fold depletion of the *TMEM109* mRNA. Other targeting factors in ER protein transport pathways showed elevated mRNA levels. *HSND2* displayed an approximately 0.5-fold increase, and *SRβ* showed a 1-fold elevation. BiP, an abundant and multi-purpose chaperone protein of the ER, did not show elevated mRNA levels when *TMEM109* was knocked down. This indicates that silencing of TMEM109 for 48 or 72 hours did not induce ER stress.

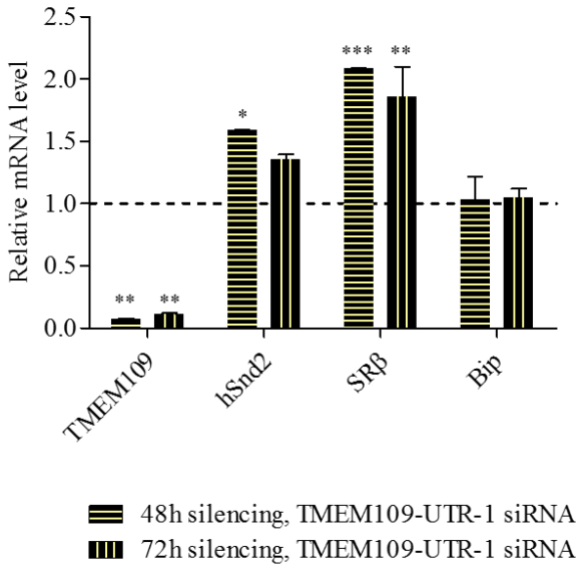

Figure 21. Real-time quantitative PCR results after 48 and 72hours of *TMEM109* depletion

The RT-qPCR result shows the relative mRNA level of *TMEM109* and different targeting receptors in comparison to the control, normalized to the endogenous control, beta-actin. After siRNA treatment at a final concentration of 25 nM, cells were harvested, and the total RNA was isolated and prepared for analysis. Numbers indicate the average of two repeated experiments carried out in triplicates. One-way ANOVA statistical analysis was performed. Significant changes are indicated by * symbol: *** $P < 0.001$; ** $P < 0.01$; * $P < 0.05$.

10.3 CHANGES IN CELL VIABILITY AND PROLIFERATION AFTER SIRNA-MEDIATED SILENCING OF TMEM109

To test the changes in cell viability upon depletion of *TMEM109*, the percent of viable cells was measured over the course of 72 hours by automated cell counter using trypan blue staining. Cells were harvested after 48, 60, and 72 hours. Two different siRNAs were tested against the 3' untranslated region (UTR) on the *TMEM109* mRNA. The cell viability showed a decline after 48 hours; it was reduced by more than 10 % in comparison to the control and dropped down further until 72 hours.

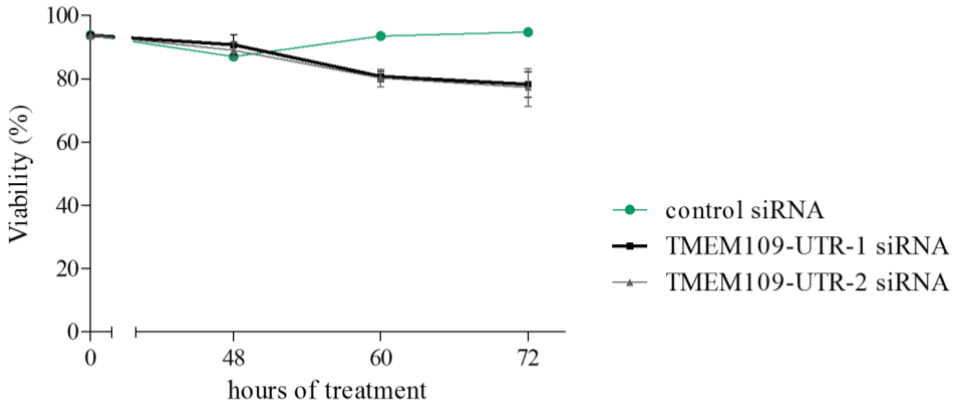

Figure 22. Viability of HeLa cells in response to siRNA treatment

The figure displays the cell viability after siRNA treatment. Cells were harvested after 48, 60, and 72 hours; the viability of cells was determined by an automated cell counter. Trypan blue negative cells indicated the viable cells. The average of five independent measurements is shown. One-way ANOVA statistical analysis was performed.
control siRNA vs TMEM109-UTR-1 siRNA; 60h:** P<0.01; 72h: *** P<0.001
control siRNA vs TMEM109-UTR-2 siRNA; 60h:** P<0.01; 72h: *** P<0.001

To further test the effect of *TMEM109* knockdown on the cellular viability and proliferation, the so called cell index was measured by the xCELLigence real-time cell analysis (RTCA) system (Figure 23). This system creates a cell index based on the measured impedance. Providing label-free monitoring of cell viability and proliferation, as both factors influence the impedance of a cell so that the cell index. Cell indices showed that siRNA-mediated silencing of *TMEM109* by each siRNA reduced cell proliferation and viability. Based on these results, TMEM109 proved to be important for cells to be viable. As in a study, cultured cells showed more susceptibility against UVC radiation when TMEM109 was knocked down (Yamashita *et al.*, 2013).

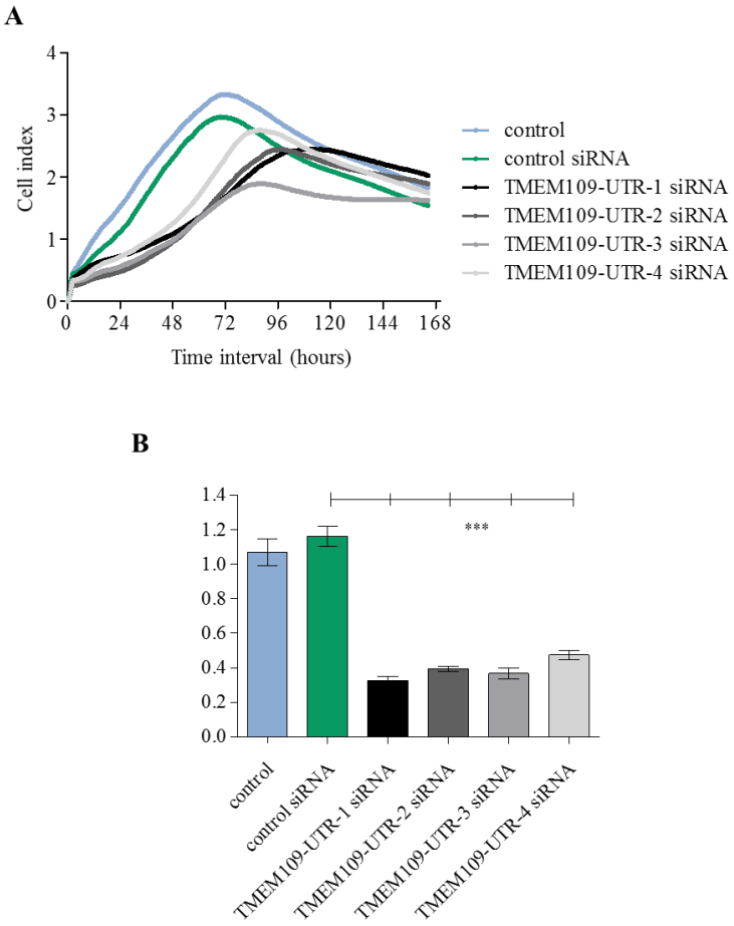

Figure 23. Real-time cell analysis system (RTCA) measurement

The figure shows A) Cell indices in response to siRNA-mediated silencing of TMEM109 and B) Maximum slope values determined from the cell index curve of the respective siRNA treatment.
Cells were treated with siRNAs at a final concentration of 25 nM. After 24 hours, cells were transfected for a second time. Control cells were not treated with any reagent and used as absolute control. After trypsinization, cells were analyzed with real-time cell analyzer.
Average results are displayed from octuplicates. One-way ANOVA statistical analysis was performed. Significant changes are indicated by * symbol: *** $P < 0.001$; ** $P < 0.01$; * $P < 0.05$ in comparison to the control siRNA treatment.

10.4 FINDING THE OPTIMAL TIME INTERVAL FOR TMEM109 SILENCING

Figure 24 depicts the silencing efficiency after 48, 60, and 72 hours of TMEM109 silencing showing the protein abundance levels determined by Western blot technique. Initially, two different siRNAs were used against TMEM109, both targeting the 3' UTR on the *TMEM109* mRNA. After 60 hours of depletion, the silencing was more pronounced (> 70 %) than after 48 hours duration. The eukaryotic SND pathway component, the hSnd2, showed elevated abundance, as well as the SR subunit β. The simultaneous elevation with TMEM109 silencing could be a compensatory mechanism. As TMEM109 protein abundance was reduced, and it might be involved in protein transport mechanisms to the ER, the cells likely compensated by enhancing the expression of other pathway receptors or other SND receptors.

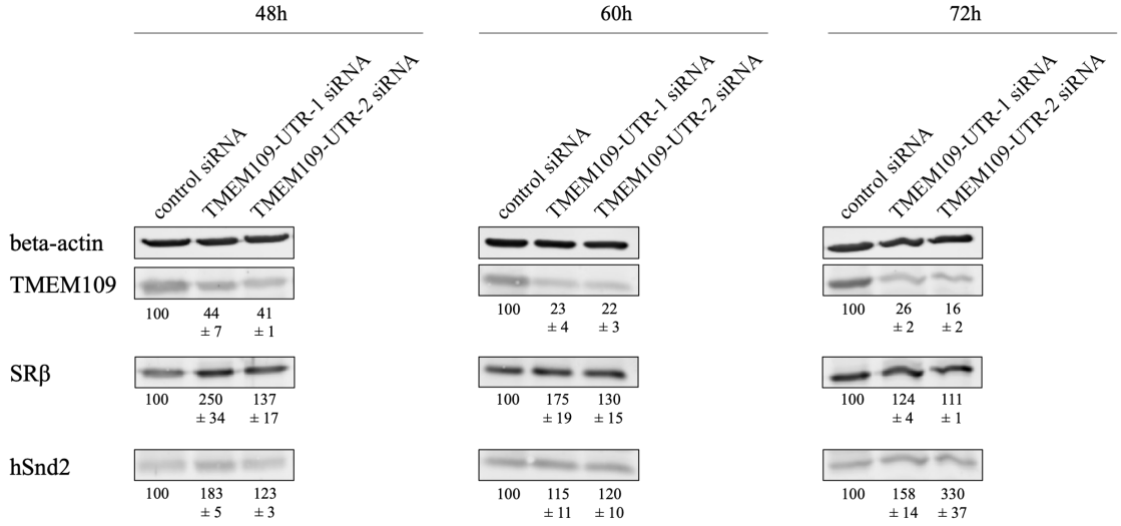

Figure 24. Western blot results of time-dependent siRNA-mediated silencing of TMEM109

Western blot results after 48, 60, and 72 hours of TMEM109 silencing. siRNAs were used at 25 nM final concentration. Samples were harvested and prepared for Western blot analysis at the end of the indicated culturing time points. Numbers indicate the average of three independent repeats. Numbers represent the relative protein abundance in comparison to the control sample. Beta-actin served as a protein loading control due to its constitutive expression.

60 hours of TMEM109 silencing proved to be optimal when the depletion was efficient and the cell viability was reduced less significantly (Figure 22). Based on these findings, for downstream experiments, preferentially, for functional assays, 60 hours of silencing condition was used.

10.5 RNA SEQUENCING

In order to gain a broader picture of the downstream events after *TMEM109* silencing, RNA sequencing was performed. With RNA sequencing, one can gain information on the influenced transcriptomic events, as well as the down- or upregulation of certain genes in response to a specific treatment. These genes can be annotated to pathways to draw a direct link between genes and the influenced biological pathway.

The total RNA was isolated after 60 hours of TMEM109 silencing, using TMEM109-UTR-1, TMEM109-UTR-3, and TMEM109-UTR-4 siRNAs, as well as control siRNA at a final concentration of 25 nM. An additional sample was prepared, and after hSnd2-UTR-2 siRNA treatment (25 nM) for 96 hours the total RNA was isolated. After quality determination, the RNA samples were sent to the Novogene company for RNA sequencing.

Figure 25 displays the differential gene expression pattern upon *TMEM109* silencing using three different siRNAs. The three siRNA treatment resulted in different expressions of various genes.

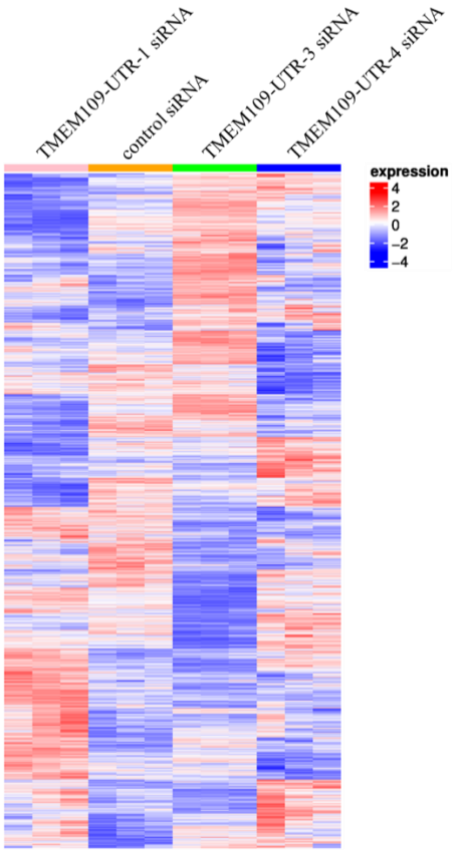

Figure 25. Heatmap after siRNA-mediated silencing of *TMEM109*

The heatmap displays the differentially expressed genes in response to siRNA silencing by the indicated siRNAs in comparison to the control siRNA. (Note that control conditions are displayed in the second column.) The blue color indicates the downregulation of a gene, and the red color indicates the overexpression of a gene. Down- or upregulation of a gene is determined based on the Log2(fpkm+1) value, evaluated by the Novogene Company. Fpkm stands for Fragments Per Kilobase of transcript sequence per Millions of base pairs sequenced. For definition see Paragraph 9.11.

Figure 26 depicts the relative expression of the *TMEM109* gene in response to siRNA-mediated silencing. The silencing efficiency was over 90 %, corresponding to the previous RT-qPCR results (Figure 21).

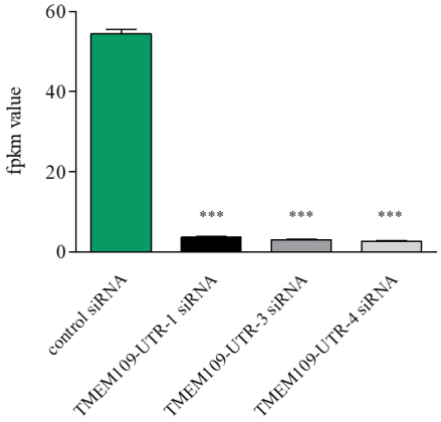

Figure 26. Relative expression of the *TMEM109* gene after 60 hours of silencing

Relative gene expression of *TMEM109* after silencing for 60 hours by the indicated siRNAs in comparison to control. Numbers referred to fpkm values stand for Fragments Per Kilobase of transcript sequence per Millions of base pairs sequenced. For definition see Paragraph 9.11. Fpkm values were evaluated by the Novogene Company. One-way ANOVA statistical analysis was performed. Significant changes are indicated by * symbol: *** $P < 0.001$; ** $P < 0.01$; * $P < 0.05$.

The overlap of differentially expressed genes for the three siRNA treatments in comparison to the control is displayed in Figure 27. In total, the same 1465 genes are differentially expressed in all samples in comparison to the control. The set of shared differentially expressed genes (DEG) was bigger for UTR-1 and UTR-3 siRNA treatment than between UTR-1 and UTR-4 or UTR-3 and UTR-4.

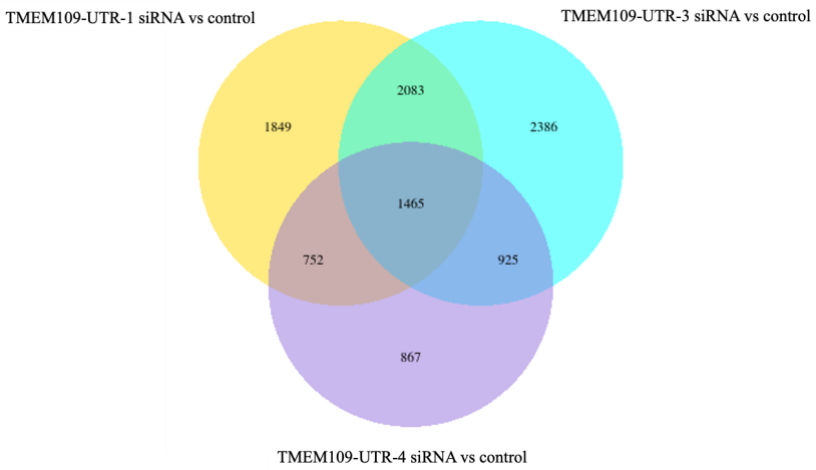

Figure 27. Venn diagram of differentially expressed genes (DEG) after *TMEM109* silencing in comparison to control siRNA treatment

The number of genes that are differentially expressed after 60 hours of *TMEM109* silencing by UTR-1, UTR-2, and UTR-3 siRNAs in comparison to control siRNA treatment. Gene expression values were calculated from fpkm values (Log2(fpkm+1)). Fpkm stands for Fragments Per Kilobase of transcript sequence per Millions of base pairs sequenced. For definition see Paragraph 9.11. Fpkm values were evaluated by the Novogene Company.

Volcano plots in Figure 28 display the significantly downregulated and upregulated genes after TMEM109-UTR-1 and hSnd2-UTR-2 siRNA treatments.

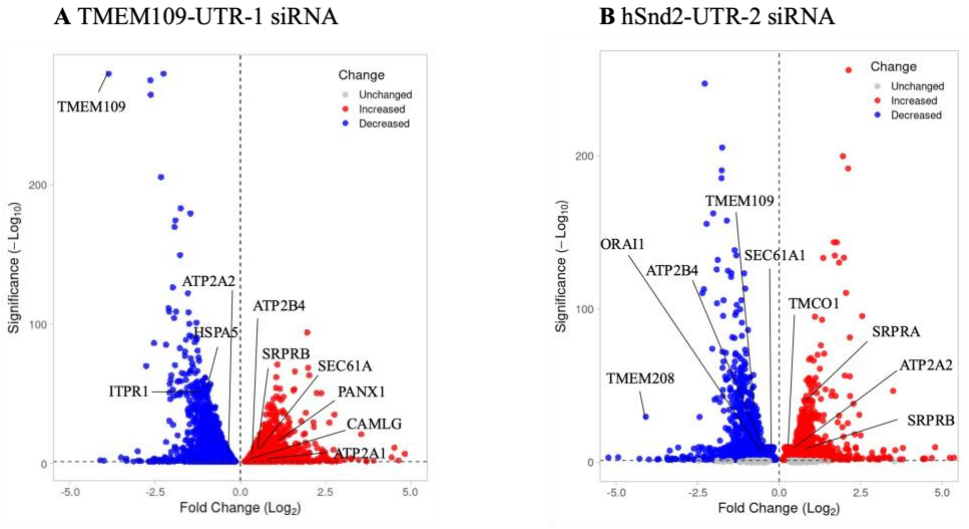

Figure 28. Volcano blots depict the differentially expressed genes in response to *TMEM109* and *HSND2* knockdown

Differentially expressed genes (DEG) after A) 60 hours of *TMEM109* silencing by UTR-1 siRNA in comparison to control siRNA treatment and B) 96 hours of *HSND2* silencing by UTR-2 siRNA in comparison to control siRNA treatment. Gene expression values were calculated from the fpkm values (Log2(fpkm+1)). Fpkm stands for Fragments Per Kilobase of transcript sequence per Millions of base pairs sequenced. For definition see Paragraph 9.11. Fpkm values were evaluated by the Novogene Company. Genes that play an important role in protein transport to the ER or calcium homeostasis are highlighted in the plots. Total DEG after TMEM109-UTR-1 siRNA treatment, downregulated: 2986, upregulated: 3163. Total DEG after hSnd2-UTR-2 siRNA treatment, downregulated: 3358, upregulated: 3465. The figure was generated by the https://huygens.science.uva.nl/VolcaNoseR/ webpage.

Abbreviations: ATP2A2 (SERCA2): sarcoplasmic/endoplasmic reticulum ATPase 1/2/3.CAMLG: calcium modulating cyclophilin ligand, HSPA5 (BiP, Hsp70): heat shock protein family A member 5, ITPR1: inositol 1,4,5-trisphosphate receptor type 1, ORAI: calcium release-activated calcium channel protein, PANX1: pannexin1, SEC61A: protein transport protein Sec61 subunit alpha, SRPRA: SRα subunit, SRPRB: SRβ subunit, STIM: stromal interaction molecule, TMCO1: transmembrane and coiled-coil domains 1, TMEM208 (hSnd2): transmembrane protein 208.

The genes whose expression was significantly reduced or increased and play an important role in protein transport to the ER or calcium homeostasis are highlighted in the plots. [The highly significantly down- or upregulated genes (that are not highlighted in the figure) fulfill various functions within eukaryotic cells. Some of these genes have little or no contribution to protein targeting to the ER. For example, to mention a few, *WARS1* was highly significantly increased by TMEM109-UTR-1 siRNA treatment, and it has a possible angiostatic activity (Wakasugi *et al.*, 2002). Amongst the highly significantly downregulated genes was found the *SMPD1*, which contributes to the ceramide biogenesis (Schuchman *et al.*, 1991); *TMED9*, *TMED10* are involved in the vesicular protein trafficking (Bremser *et al.*, 1999); and *METTL9* is responsible for the methylation of target proteins (Davydova *et al.*, 2021). While highly significantly downregulated genes by hSnd2-UTR-2 siRNA were, for example, *TMEM123*, which induces oncotic cell death or *VIM*, which encodes for cytoskeletal adhesion molecules; and *TXNIP*, an oxidative stress mediator was highly significantly expressed.]

Previously, it was observed that *TMEM109* silencing resulted in a 1.5-fold enhanced mRNA level in the case of the *SRβ* (Figure 21). However, with RNA sequencing, an approximately 0.3-fold increase in gene expression was observed for each of the three siRNA treatments (only TMEM-UTR-1 siRNA treatment is displayed here, Figure 28A). On the protein level, SRβ also showed elevation (Figure 24). The mRNA level of the *HSND2* was found to increase in the RT-qPCR results with *TMEM109* silencing (Figure 21); in RNA sequencing results, it was only enlisted with the TMEM109-UTR-3 siRNA, displaying a 0.8-fold decreased gene expression (data is not shown here), and it showed significantly increased protein abundance after 60 hours of TMEM109 silencing (Figure 24). The gene expression of the *CAMLG* and *SEC61A1* was significantly enhanced by TMEM109-UTR-1 treatment (Figure 28A).

Genes that are involved in calcium homeostasis, encoding for ER calcium leak or release channels, such as *SEC61A, PANX, ITPR,* as well as genes that encode for plasma membrane calcium channels (*ORAI, ATP2B)* or the ER calcium channel (*ATP2A*) that remove cytosolic calcium ions, displayed various expressions in response to siRNA treatments. In the case of TMEM109-UTR-1 siRNA treatment, the *PANX1, ATP2B4,* and *ATP2A1 s*howed significantly increased expression. Gene expression of *ATP2A2* and *ITRP1* was significantly decreased.
RNA sequencing results showed reduced gene expression of *TMEM109* after *HSND2* silencing (Figure 28B). Genes encode for calcium channels, receptors that play a role in cytosolic calcium removal, such as *ATP2B4* and *ORA1*, showed a significant decrease. *SEC61A1* ER calcium leak channel showed decreased expression. *ATP2A2* (encodes for SERCA2) and *TMCO1* were found to be expressed in significantly high amounts after *HSND2* silencing.

Gene ontology (GO) analysis annotates genes to biological processes (BP), molecular functions (MF), and cellular components (CC). Table 7 in the Appendix chapter summarizes the number of these significantly down- or upregulated genes linked to diverse functions. These gene ontology deductions could correlate with the previous results; for example, no ER stress was observed after *TMEM109* silencing (Figure 21). As in previous experiments, TMEM109 silencing induced enhancement of the SR subunits (Figure 24) could correlate to the RNA sequencing results, which suggest that the expression of certain genes that participate in protein targeting to the ER are significantly enhanced. This might be a consequent compensation mechanism for the reduced TMEM109 abundance.

Kyoto Encyclopedia of Genes and Genome (KEEG) annotates genes to pathway levels. Genes that showed downregulated or upregulated expression were annotated to pathway levels after *TMEM109* knockdown (Figure 29). For simplicity, results are only shown with TMEM109-UTR-1 siRNA (Figure 29) because this siRNA was used in most of the downstream experiments.
Pathway associated with "ribosome biogenesis in eukaryotes" showed enhancement with UTR-1 siRNA treatment. Amongst the significantly upregulated pathways was the "protein processing in the ER" enlisted after *TMEM109* silencing with UTR-3 and UTR-4 siRNA. Significantly downregulated pathways were, for example, "lysosome" and "protein processing in the ER" after TMEM109-UTR-1 siRNA. TMEM109-UTR-3 siRNA treatment caused, for example, the downregulation of "lysosome" or "carbon metabolism" pathways.

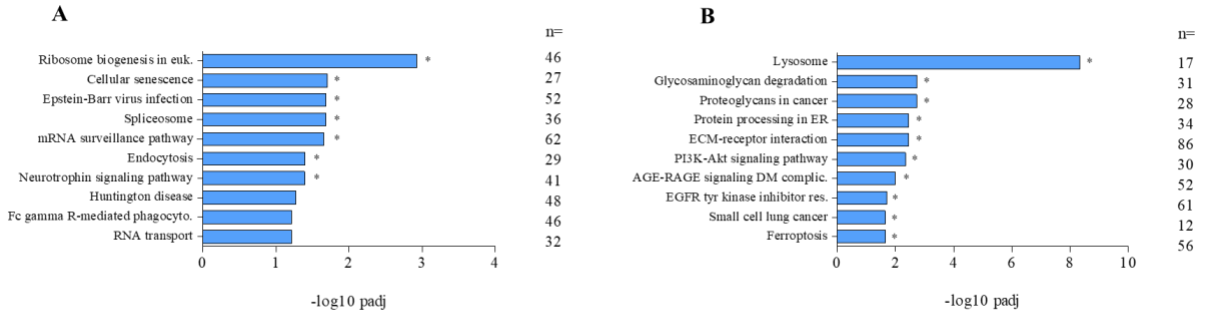

Figure 29. Genes annotated to biological pathways that are upregulated or downregulated after *TMEM109* silencing

Genes annotated to biological pathway levels in response to *TMEM109* silencing after UTR-1 siRNA treatment. Figure A) shows upregulated and Figure B) shows downregulated pathways. N labels the number of affected genes.
Gene expression values were calculated from the fpkm values (Log2(fpkm+1)). Fpkm stands for Fragments Per Kilobase of transcript sequence per Millions of base pairs sequenced. For definition see Paragraph 9.11. Fpkm values were evaluated by the Novogene Company. Padj values are adjusted p-values from statistical analyses, calculated by the Novogene Company. For simplicity, results only with the TMEM109-UTR-1 siRNA treatment are shown here.

10.6 Testing the effect of 60 hours of TMEM109 silencing with four different types of siRNAs

10.6.1 Western blot analysis

Western blot analysis revealed the changes regarding the abundance of proteins that are involved in protein transport to the endoplasmic reticulum. Four different siRNAs were tested; they target different parts of the untranslated region of the *TMEM109* mRNA. For simplicity, they were labeled numerically from 1 to 4. By each siRNA, the TMEM109 protein abundance was reduced by ≥ 80 % (Figure 30, Figure 31). However, its putative partner protein, hSnd2, depicted a significant reduction (TMEM109-UTR-3, UTR-4) or increase (TMEM109-UTR-2) and no significant change (TMEM109-UTR-1). Both SR subunits, SRα and SRβ, showed elevated protein abundance, except in the case of UTR-2 siRNA regarding SRα. Assumably the cells tried to compensate for less TMEM109 protein being present. The Caml protein, a TRC pathway receptor/translocase subunit, displayed enhanced abundance by TMEM109-UTR-2 and UTR-3 siRNA treatment; and showed reduced levels after the addition of TMEM109-UTR-1 and UTR-4 siRNA. The translocon subunit, Sec61α, was slightly elevated (UTR-1 and 2 siRNA) or significantly more abundant (UTR-3 and 4) upon TMEM109 silencing. While Sec62 abundance was reduced or not majorly influenced and was significantly increased only with TMEM109-UTR-2 siRNA. GRP170 and BiP did not show a significant change, suggesting that changes in the abundance of TMEM109 did not contribute to ER stress.

An even protein loading was determined by Coomassie gel staining beside probing the Western blot membrane for beta-actin (Supplementary materials, Figure 61).

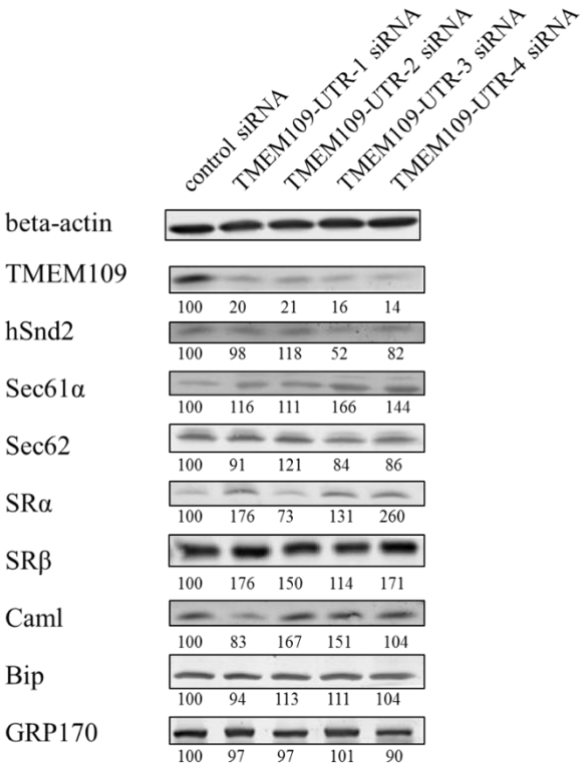

Figure 30. Western blot results after 60 hours of TMEM109 silencing

Western blot results depict the changes regarding the protein abundance of different targeting receptors, translocon components, or chaperones involved in ER protein targeting in response to TMEM109 silencing by four different types of siRNAs. After 60 hours of silencing with siRNAs at 25 nM final concentration, cells were harvested and prepared for Western blot analysis. Numbers indicate the relative protein abundance in comparison to control. Numbers display the average abundance of a specific protein for each condition. One representative blot of at least three independent repeats is shown. Beta-actin served as a protein loading control due to its constitutive expression.

Statistical analyses of these results are displayed in Figure 31.

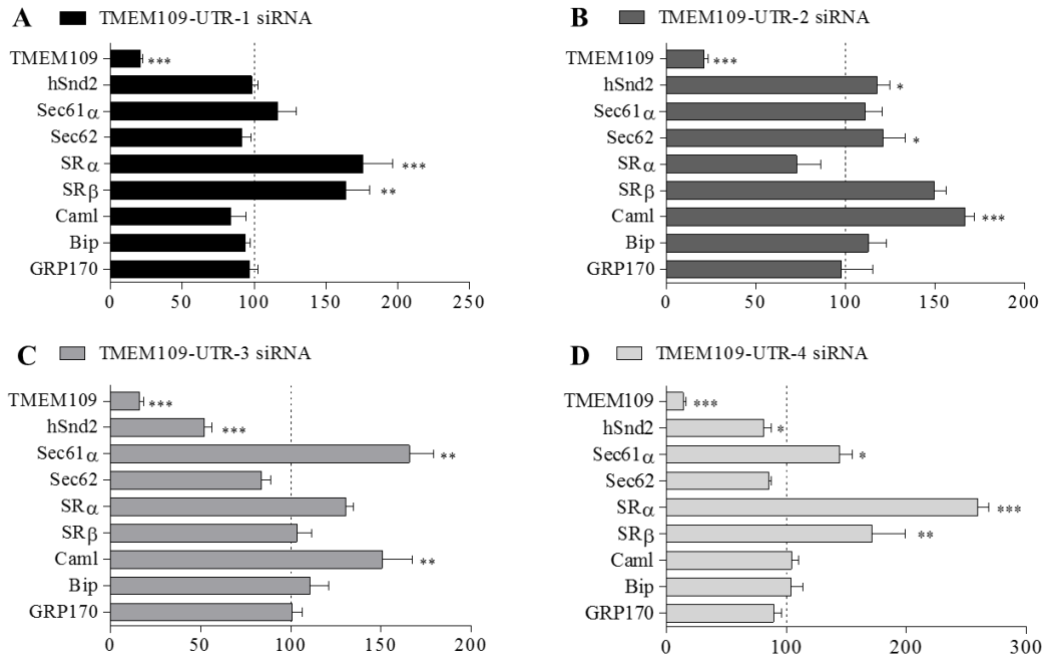

Figure 31. Statistical analysis of Western blot results after 60 hours of TMEM109 silencing

Bar graphs depict the protein abundance after 60 hours of TMEM109 silencing after the addition of four different types of siRNAs (Figure 30). A) TMEM109-UTR-1 siRNA B) TMEM109-UTR-2 siRNA C) TMEM109-UTR-3 siRNA D) TMEM109-UTR-4 siRNA treatment.

Numbers indicate the average of at least three independent repeats. One-way ANOVA statistical analysis was performed. Significant changes are indicated by * symbol: *** $P < 0.001$; ** $P < 0.01$; * $P < 0.05$.

10.6.2 IN VITRO TRANSLATION AND TRANSPORT ASSAY

Next, to test the idea of TMEM109 being involved in the transport of protein substrates into the ER more directly, an established assay was used that reconstitutes the ER protein import *in vitro* (see description in Paragraph 9.15). Different substrates were used to test the transport efficiency to the ER after TMEM109 knockdown.

Preprolactin is a classic example of proteins with a cleavable signal peptide and uses the classical SRP-dependent pathway to transport to the ER. Similarly, the invariant chain uses the SRP-dependent pathway; however, it does not have a cleavable N-terminal signal peptide. Its single transmembrane helix serves as an N-terminal hydrophobic stretch engaged with the SRP (Figure 32).

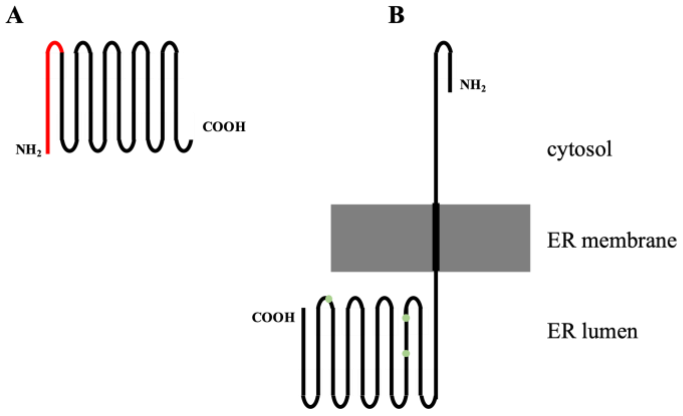

Figure 32. Topology of model protein substrates for classical SRP-dependent protein transportation to the ER

Schematic topology of classical SRP-dependent substrates depicting A) preprolactin B) invariant chain. The red color indicates the presence of a cleavable signal peptide. Green dots label the asparagine amino acids that are involved in N-glycosylation post-translational modification.

In their ER transport, the SRP ribonucleoprotein directs the proteins to the SR and then to the Sec61 translocon for subsequent ER translocation. After ER transport, the preprolactin's molecular weight becomes smaller due to the SP cleavage giving the product prolactin. The invariant chain's molecular weight becomes higher after N-glycosylation in the ER.

Sec61β is a tail-anchored protein that uses the TRC pathway to be delivered to and integrated into the ER membrane. Cytochrome b5, also a tail-anchored protein, has been shown to be partially dependent on the TRC pathway and SND pathway (Haßdenteufel *et al.*, 2017), and the partial SND dependence has been shown after depletion of hSnd2. This raises the question of whether it could be a substrate for the SND pathway and be dependent on TMEM109. Prestatherin, a short secretory protein, was also tested as a substrate (Figure 33).

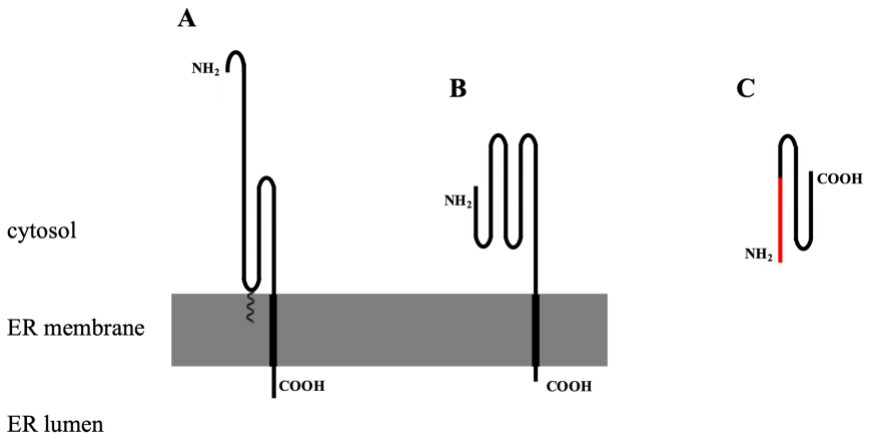

Figure 33. Topology of A) Sec61β B) cytochrome b5 C) prestatherin protein

Schematic topology of A) Sec61β B) cytochrome b5. C) prestatherin The red color indicates the presence of a cleavable signal peptide.
Sec61β is a classic example of tail-anchored proteins and can be transported to the ER via the TRC pathway. The thioester linkage results from the post-translational modification; S-palmitoylation of the cytoplasmic cysteine residue with a fatty acid chain. After its ER transport, certain serine and threonine amino acid residues become phosphorylated, resulting in a higher molecular weight of the processed protein. Cytochrome b5 is a tail-anchored protein and can be inserted into the ER membrane through the TRC pathway and possibly the SND pathway. The ER-processed cytochrome b5 contains acetylated alanine and lysine residues resulting in a higher molecular weight. Prestatherin is a short secretory protein and has a cleavable signal sequence. Its transport dependence on the SND pathway remains under debate. Prestatherin is processed in the ER by gaining phosphoserine residues, which is indicated by an increase in molecular weight.

As expected, the transport efficiency of Sec61β was not influenced by TMEM109 silencing. (Figure 34, Figure 35). As Sec61β is a classic example for TRC pathway substrates (Borgese *et al.*, 2019), and the level of the Caml receptor did not reduce majorly by TMEM109 silencing; it was even elevated with certain siRNAs. Based on these, it was not expected that the Sec61β would show SND dependence. The transport efficiency of preprolactin and the invariant chain was improved with TMEM109 knockdown. This phenomenon is likely due to the elevated SR subunits. Significantly enhanced protein transport efficiency was observed with each siRNA regarding the preprolactin and in the case of the invariant chain. Prestatherin transport was enhanced in comparison to control, which suggests that it is potentially not an SND substrate, or the SND dependence is obscured by the compensatory changes seen for the alternative targeting routes TRC and SRP. Cytochrome b5, which is only partially dependent on the TRC pathway, depicted decreased transport efficiency by TMEM109-UTR-1 and UTR-4 siRNA treatment (Figure 34, Figure 35). Based on the previously shown dependence of the cytochrome b5 substrate from the hSnd2 (Haßdenteufel *et al.*, 2017) and its dependence on TMEM109 (Figure 34; Figure 35A, D) indicates that TMEM109 could be involved in the transport of SND-dependent substrates.

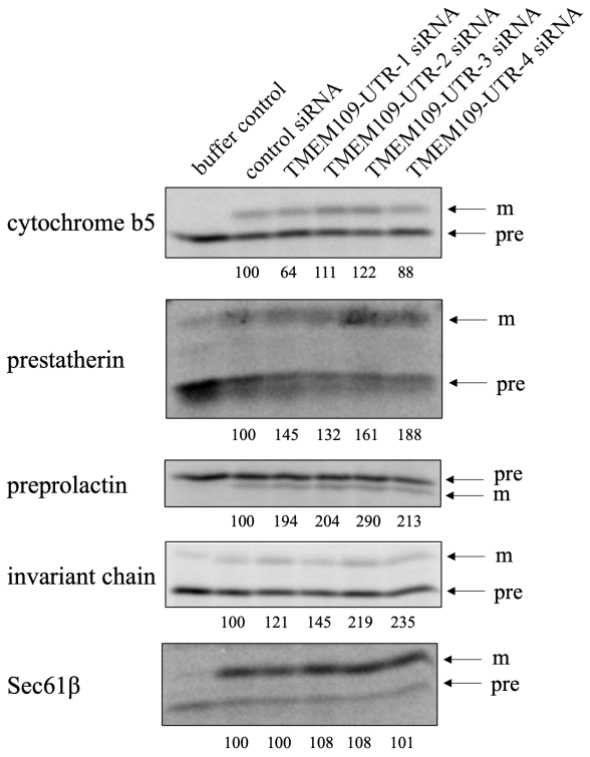

Figure 34. *In vitro* translation reaction after 60 hours of TMEM109 silencing

Changes in *in vitro* transport efficiency of proteins in response to TMEM109 silencing by four different types of siRNAs. After 60 hours of silencing with siRNAs at 25 nM final concentration, cells were harvested and prepared for *in vitro* translation analysis. After SDS-PAGE, radioactive signals were captured on phosphor plates and scanned. KHM buffer control served as cell-free so that ER membrane-free condition. Numbers indicate the relative protein transport efficiency in comparison to control. Numbers display the average transport efficiency of a specific protein for each condition. One representative autoradiograph of at least three independent repeats is shown. Pre means premature polypeptide, and m means mature protein.

Statistical analyses of these results are displayed in Figure 35.

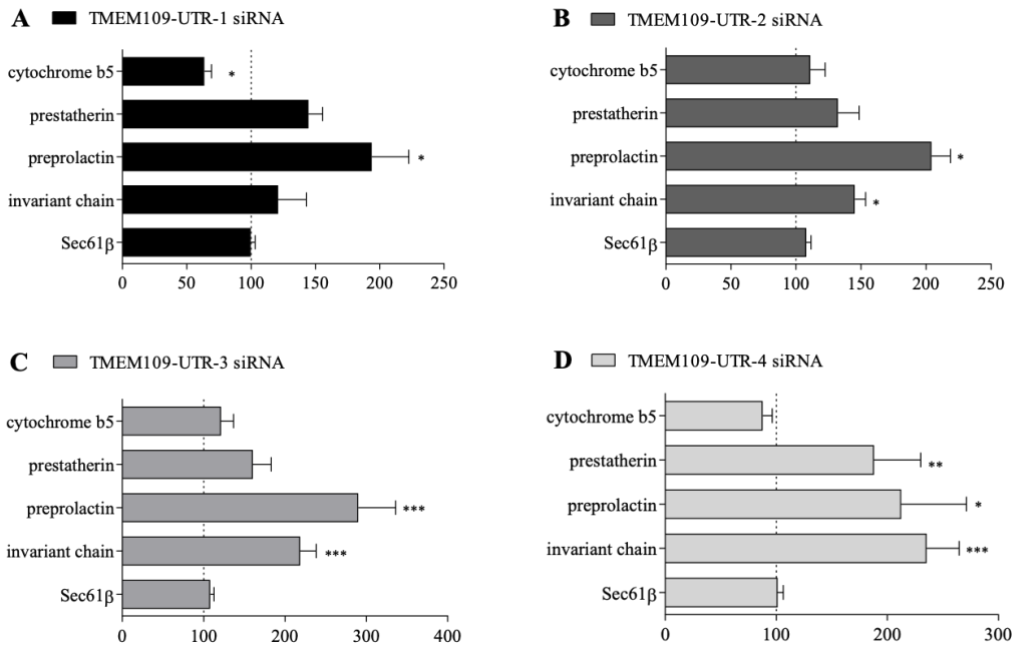

Figure 35. Bar graphs of *in vitro* translation reaction results after 60 hours of TMEM109 siRNA-mediated silencing

Bar graphs depict the *in vitro* translation results after 60 hours of TMEM109 silencing after the addition of four different types of siRNAs (Figure 34). A) TMEM109-UTR-1 siRNA B) TMEM109-UTR-2 siRNA C) TMEM109-UTR-3 siRNA D) TMEM109-UTR-4 siRNA

Numbers indicate the average of at least three independent repeats. One-way ANOVA statistical analysis was performed. Significant changes are indicated by * symbol: *** $P < 0.001$; ** $P < 0.01$; * $P < 0.05$.

10.7 TMEM109 COMPLEMENTATION ASSAY

10.7.1 WESTERN BLOT ANALYSIS

A complementation assay was performed to determine whether *TMEM109* re-expression after its silencing could rescue all or any of the observed phenotypes, including the compensatory changes in protein abundance of alternative targeting routes and the reduced transport efficiency in the case of cytochrome b5. After 40 hours of *TMEM109* silencing, cells were additionally transfected with an empty vector or a *TMEM109* encoding plasmid. For *TMEM109* knockdown, TMEM109-UTR-1 siRNA was chosen because it mimicked the phenotype the closest when hSnd2 was knocked down (Haßdenteufel *et al.*, 2017). Figure 36 highlights that, as previously shown, when less TMEM109 protein was present in the cells, it caused compensation and induced the expression of more SR. In this experiment, hSnd2 was also more abundant upon TMEM109 knockdown. When TMEM109 was present again, the elevated abundance of the SRα and hSnd2 proteins descended back. Such a phenomenon, the reversal of a phenotype by re-expression of a depleted target gene, substantiates the concept of a classic rescue experiment. As seen before, changes in TMEM109 abundance did not significantly affect the Sec61 translocon α subunit and the Sec62 protein abundance. ER chaperone BiP and GRP170 did not show major changes in the protein level, as previously observed.

An even protein loading was determined by Coomassie gel staining beside probing the Western blot membrane for beta-actin (Supplementary materials, Figure 62).

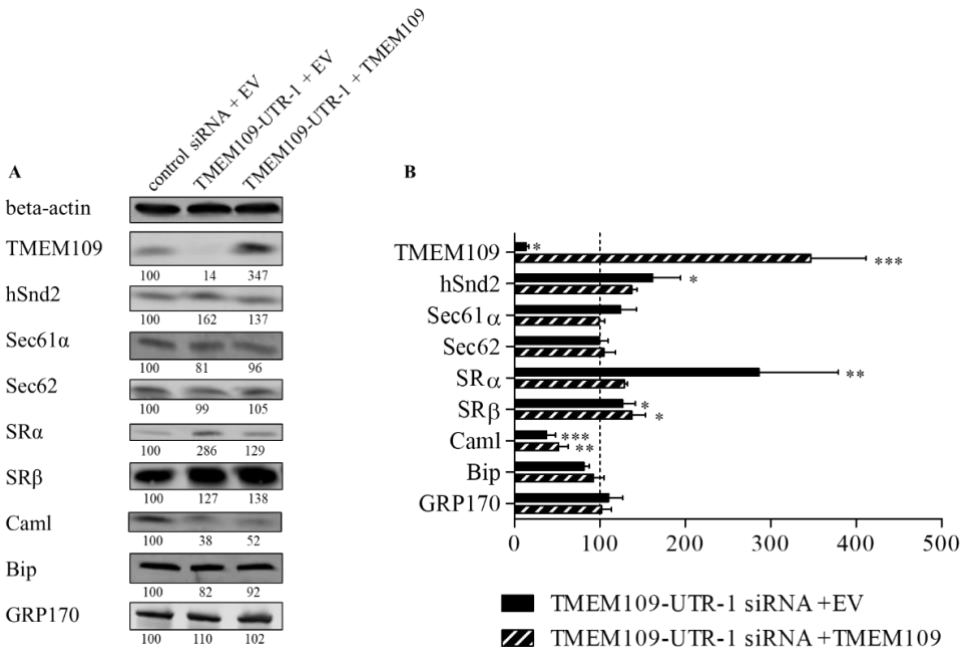

Figure 36. Protein abundance after *TMEM109* silencing and subsequent addition of empty vector or *TMEM109* plasmid

Changes in the protein levels in response to TMEM109 silencing (25 nM) and subsequent re-expression of TMEM109. After 40 hours of siRNA silencing, *TMEM109* encoding plasmid was added to the culture medium. After 60 hours of total culturing time, cells were harvested and prepared for Western blot analysis. A) Numbers indicate the relative protein abundance in comparison to control. Numbers display the average abundance minimum of three independent repeats. One representative blot is shown in the figure. Beta-actin served as a protein loading control due to its constitutive expression. B) One-way ANOVA statistical analysis was performed. Significant changes are indicated by * symbol: *** $P < 0.001$; ** $P < 0.01$; * $P < 0.05$.

10.7.2 IN VITRO TRANSLATION AND TRANSPORT ASSAY

After semi-permeabilization of the samples, *in vitro* translation of mRNA substrates happened in the presence of reticulocyte lysate with the addition of amino acid mixture without methionine, and radioactively labeled methionine (Paragraph 9.15). The following mRNA substrates were used: preprolactin, invariant chain, cytochrome b5, prestatherin, and Sec61β (Figure 32, Figure 33).

The transport efficiency of SRP-dependent substrates, preprolactin, and invariant chain, in *in vitro* transport assay was increased when TMEM109 was depleted (Figure 37). This correlates well with the Western blot results (higher expression of SR subunits). The acquired TMEM109 rescue normalized the abundance of the SRα protein, which in turn brought the elevated transport efficiency of the substrates preprolactin and invariant chain back to the level seen in control cells or nearly back to that level. The transport efficiency of the TRC-dependent substrate, Sec61β, remained unchanged. Prestatherin's transport rate descended back when more TMEM109 protein was present. This might suggest that its transport is not affected by the SND pathway and the TMEM109. The reduced cytochrome b5 transport was not rescued in its passage to the ER by the TMEM109 abundance. However, this might very well be correlated to the unanticipated impact of the mock and TMEM109 rescue procedure on the reduced protein level of Caml (Figure 36). As the efficient transport of cytochrome b5 partially depends on the WRB/Caml receptor, this might explain the missing rescue for this substrate upon the rescue of *TMEM109* expression.

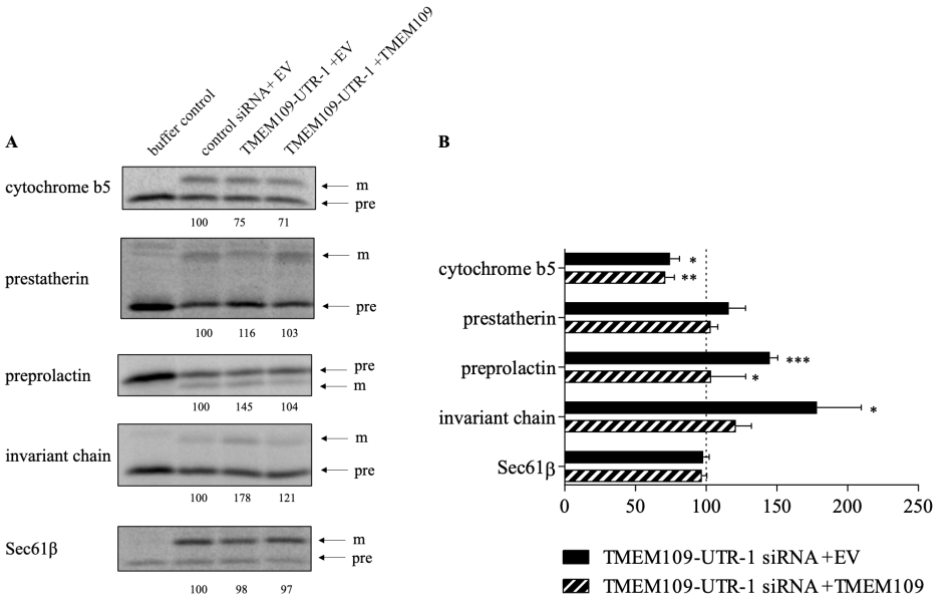

Figure 37. Relative transport of proteins after *TMEM109* silencing and subsequent addition of empty vector or *TMEM109* plasmid

Changes in *in vitro* transport efficiency of proteins in response to *TMEM109* silencing (25nM) and subsequent re-expression of *TMEM109*. After 40 hours of siRNA silencing, *TMEM109* encoding plasmid was added to the culture medium. After 60 hours of total culturing time, cells were harvested, and *in vitro* mRNA translation assay was performed. After SDS-PAGE, radioactive signals were captured on phosphor plates and scanned. KHM buffer control served as cell-free so that ER membrane-free conditions. A) Numbers indicate the relative transport efficiency in comparison to control. Numbers indicate the average of a minimum of three independent repeats. One representative autoradiograph is shown in the figure. Pre means premature polypeptide, and m means mature protein. B) One-way ANOVA statistical analysis was performed. Significant changes are indicated by * symbol: *** $P < 0.001$; ** $P < 0.01$; * $P < 0.05$.

10.8 SIMULTANEOUS SILENCING OF TMEM109 AND WRB

To better understand the role of the TMEM109 in protein targeting to the ER, experiments were done where TMEM109 and WRB were simultaneously silenced. As the protein level of the Caml was reduced with TMEM109 silencing (Figure 30, Figure 36), it was tested how changes occur in protein homeostasis when the TRC pathway was also knocked down.

The abundance of TMEM109 was significantly enhanced when WRB was silenced (Figure 38). Reduction of the Caml protein, the translocase receptor that works together with WRB for tail-anchored protein insertion, was decreased when TMEM109 was silenced individually, as also shown in previous experiments (Figure 30, Figure 36). It was further reduced when WRB was knocked down individually, as well as with simultaneous silencing (Figure 38). HSnd2 protein was slightly more abundant when WRB was knocked down individually or together with TMEM109 and significantly more abundant when TMEM109 was knocked down individually. The SR subunits (SRα and SRβ) were more abundant when TMEM109 was individually silenced compared to the conditions where WRB was knocked down individually or concurrently with TMEM109. Simultaneous or individual knockdowns did not significantly influence the Sec61α level.

An even protein loading was determined by Coomassie gel staining beside probing the Western blot membrane for beta-actin (Supplementary materials, Figure 63).

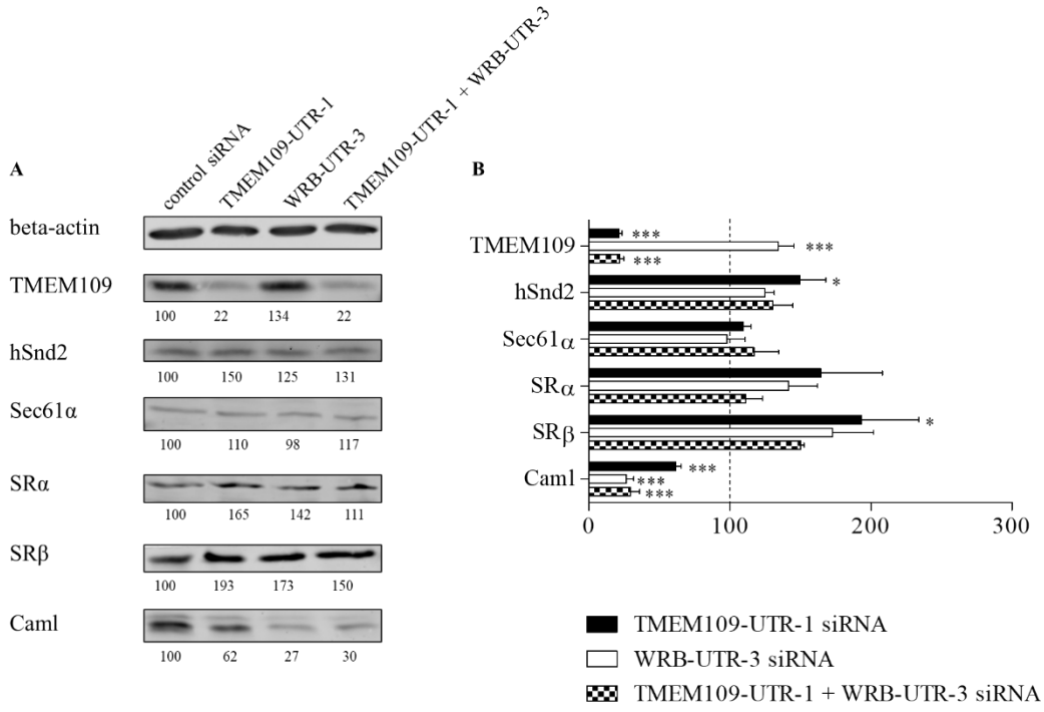

Figure 38. Relative protein abundance after 72 hours of TMEM109 and WRB and simultaneous silencing

Changes in the protein levels in response to TMEM109 silencing (20 nM) and WRB silencing (20 nM), as well as simultaneous silencing of the two. After 72 hours of siRNA-mediated silencing, cells were harvested and prepared for Western blot analysis. A) Numbers indicate the relative protein abundance in comparison to control. Numbers indicate the average of four independently repeated experiments; one representative blot is shown in the figure. Beta-actin served as a protein loading control due to its constitutive expression. B) One-way ANOVA statistical analysis was performed. Significant changes are indicated by * symbol: *** $P < 0.001$; ** $P < 0.01$; * $P < 0.05$.

In vitro translation assay results showed that the transport efficiency of Sec61β was marginally reduced with TMEM109 silencing, but not significantly (Figure 39). Yet, the depletion of WRB alone or in combination with TMEM109 caused a significant reduction in the transport of Sec61β. Sec61β is known to depend on the TRC pathway to be transported into the ER.

Transport of cytochrome b5 to the ER was significantly affected by TMEM109 knockdown (Figure 39) as observed beforehand (Figure 34, Figure 37). Silencing WRB did not significantly reduce the cytochrome b5 transport rate as well as the double silencing. One explanation could be that cytochrome b5 can access the ER by other transport pathways, and unassisted insertion can also happen (Paragraph 7.9). Cytochrome b5 might be a substrate for the SND pathway; however, it cannot only access the SND pathway to be conveyed to the ER.

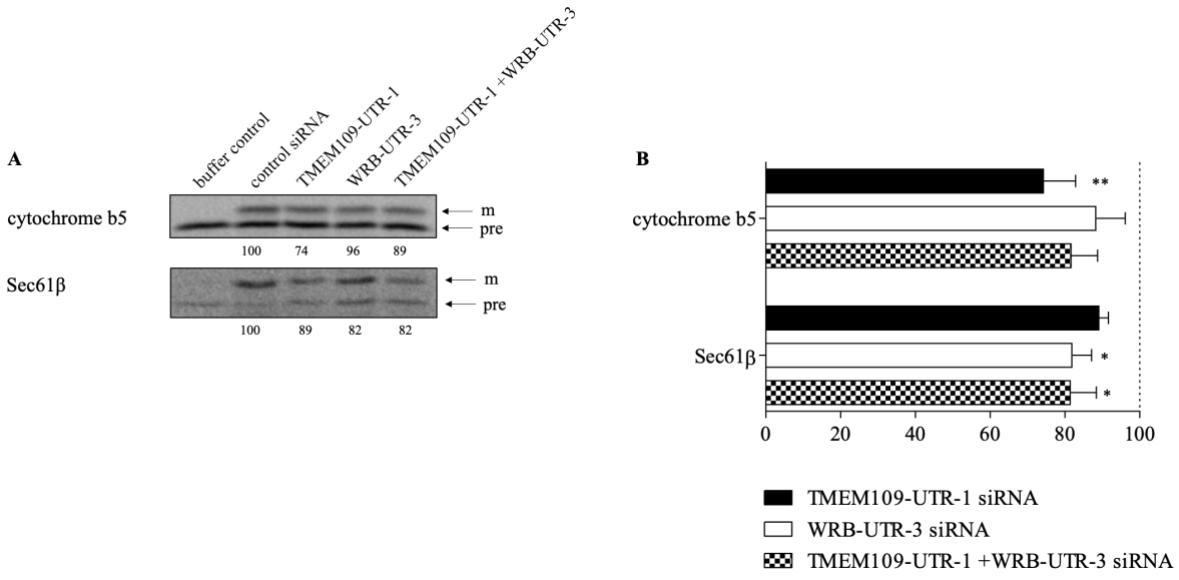

Figure 39. Relative transport of proteins after 72 hours of TMEM109 and WRB and simultaneous silencing

Changes in *in vitro* transport efficiency of proteins in response to TMEM109 silencing (20 nM) and WRB silencing (20 nM), as well as simultaneous silencing of the two. After 72 hours of siRNA silencing, cells were harvested, and *in vitro* mRNA translation assay was performed. After SDS-PAGE, radioactive signals were captured on phosphor plates and scanned. KHM buffer control served as cell-free so that ER membrane-free condition. A) Numbers indicate the relative transport efficiency in comparison to control. Numbers indicate the average of four independently repeated experiments; one representative autoradiograph is shown in the figure. Pre means premature polypeptide, and m means mature protein. B) One-way ANOVA statistical analysis was performed. Significant changes are indicated by * symbol: *** $P < 0.001$; ** $P < 0.01$; * $P < 0.05$.

10.9 THE EFFECT OF TMEM109 KNOCKOUT

The following experiments were carried out in the *TMEM109* knockout cell line. Instead of knocking down *TMEM109*, it was desired to test the effect of its complete loss in human cells. *TMEM109* knockout has been done in a mouse model and proved to be compatible with life (Yamazaki *et al.*, 2010). For the generation of a *TMEM109* knockout cell line, the CRISPR-Cas9 technique was used.

The base insertion in the *TMEM109* gene caused a frameshift mutation after Gly 63, generating a premature stop codon, resulting in a truncated translation product, which is likely degraded by the proteasome. The truncated product was 114 amino acids long, while the non-truncated TMEM109 protein is 243 amino acids long. After expanding the right cell clones that contained the insertion mutation in the *TMEM109* gene (chromosome 11, 5726_5727insT, see Paragraphs 9.19.11 and 9.19.14), downstream experiments were performed. Experiments were completed to test the changes regarding the abundance of different targeting receptors as well as the protein transport efficiency to the ER.

Albeit reduced by more than 70 %, a residual amount of the *TMEM109* mRNA was still detectable after its knockout (Figure 40A). Since a single nucleotide insertion mutation affects the DNA, the transcribed mRNA may still be detected by the primers and probes used for RT-qPCR. Nevertheless, an unfunctional, truncated protein is readily recognized and degraded by the proteasome within the cells. Western blot results verified that no TMEM109 protein could be detected in the TMEM109 knockout cell line (Figure 40B, C).

An even protein loading was determined by Coomassie gel staining beside probing the Western blot membrane for beta-actin (Supplementary materials, Figure 64).

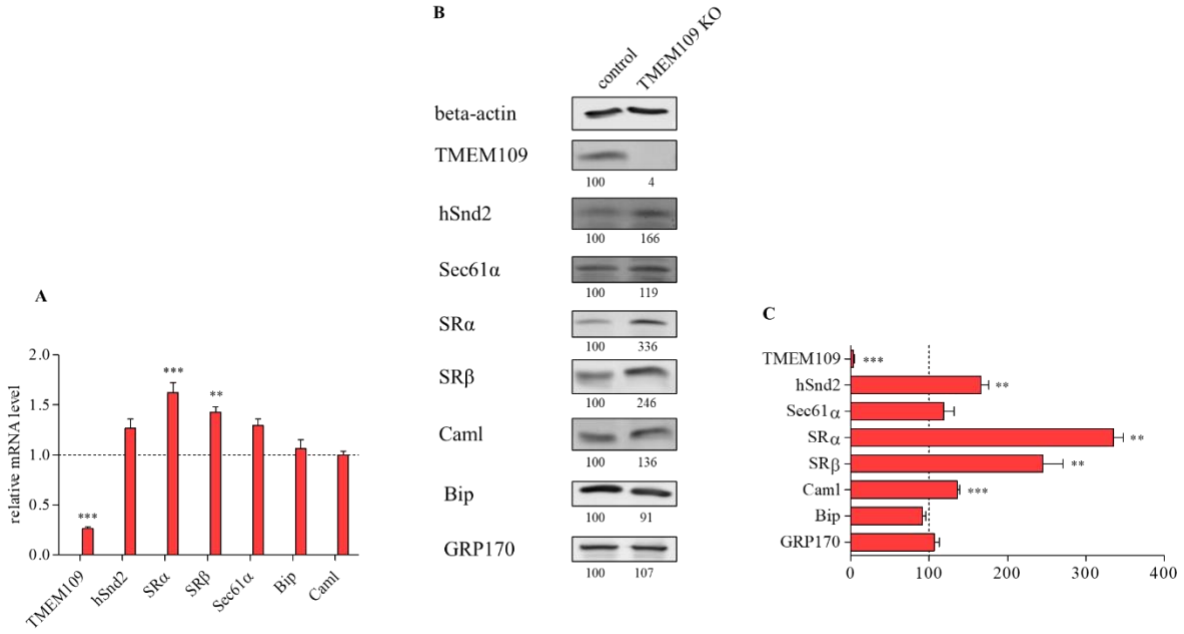

Figure 40. Relative mRNA level and protein abundance after *TMEM109* knockout

Figure A shows the relative mRNA level measured by RT-qPCR after TMEM109 knockout in comparison to control, normalized to the endogenous control, beta-actin. Figure B displays the relative protein level after TMEM109 knockout, generated by Western blot. One representative blot is shown. Numbers indicate the relative protein abundance in comparison to control. Numbers indicate the average of three independently repeated experiments. Beta-actin served as a protein loading control due to its constitutive expression. Figure C displays the Western blot results as a bar graph. A two-tailed t-test statistical analysis was performed. Significant changes are indicated by * symbol: *** $P < 0.001$; ** $P < 0.01$; * $P < 0.05$. KO means knockout.

The abundance of the TMEM109 protein was significantly reduced after its knockout, and the protein was basically undetectable. The trace amount of TMEM109 quantified in Figure 40B and C is presumably just a background signal.

The presence of the SR subunits and hSnd2 protein showed significant enhancement (Figure 40B, C). However, the Caml protein showed a significant increase in its abundance, the Sec61α increase was not significant. In response to lacking TMEM109 protein, the cells are likely to compensate and they increased the expression of other targeting receptors (Figure 40B, C).

The results are relatively correlated to the siRNA-mediated silencing approach. The increase in SR components was even more increased in TMEM109 knockout than knockdown cells (Figure 40B, C and Figure 31). The abundance of the Caml was significantly increased when TMEM109 was knocked out, which was not necessarily observed with each siRNA treatment. BiP and GRP170 were not present in higher amounts, which indicates that TMEM109 knockout similar to the knockdown did not induce ER stress (Figure 40B, C and Figure 31).

An even protein loading was tested by Coomassie gel staining beside probing the Western blot membrane for beta-actin (Supplementary materials, Figure 64).

The effect of TMEM109 knockout on the protein transport was tested by *in vitro* translation assay (Figure 41). Similar to the siRNA-induced silencing approach, the SRP-dependent substrates' transport efficiency was significantly enhanced, as the SR subunits were significantly more abundant. The transport efficiency of Sec61β was slightly improved; this could be due to the enhanced Caml abundance. Prestatherin showed slightly, however, not significantly reduced transport efficiency after TMEM109 knockout, which could suggest that TMEM109 might be involved in short secretory protein transport to the ER. Cytochrome b5, whose transport ratio was reduced with certain siRNAs, did not show a transport defect when TMEM109 was absent.

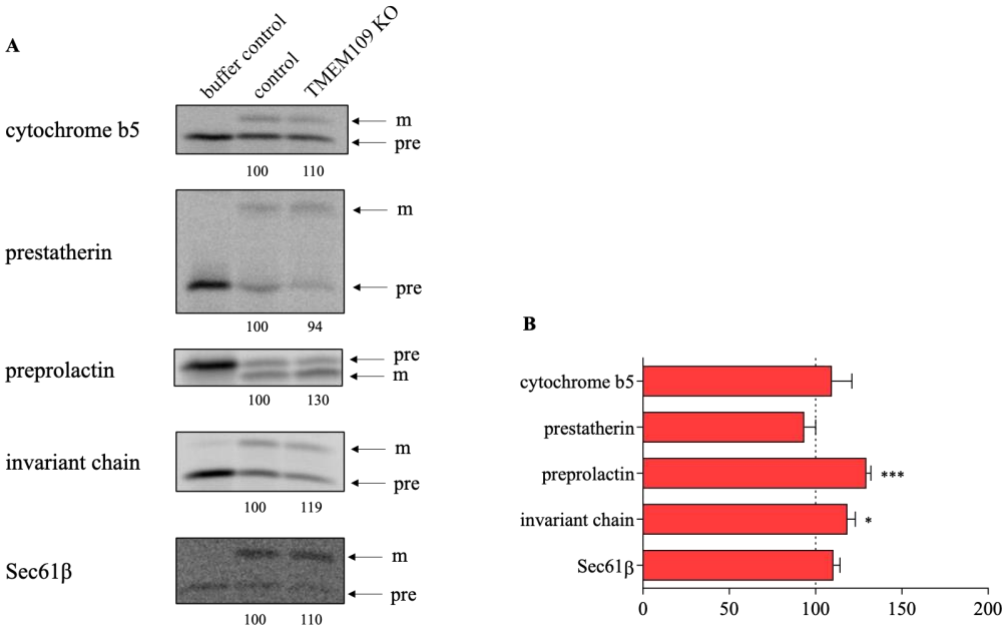

Figure 41. Relative transport of proteins after TMEM109 knockout

Changes in *in vitro* transport efficiency of proteins in response to TMEM109 knockout. After 60 hours of culturing, cells were harvested and prepared for *in vitro* translation analysis. After separating the translation products by SDS-PAGE, radioactive signals were captured on phosphor plates and scanned. KHM buffer control served as cell-free so that ER membrane-free condition. A) One representative autoradiograph is shown. Numbers indicate the relative protein transport efficiency in comparison to control. Numbers indicate the average of three independently repeated experiments. Pre means premature polypeptide, and m means mature protein. B) A two-tailed t-test statistical analysis was performed. Significant changes are indicated by * symbol: *** $P < 0.001$; ** $P < 0.01$; * $P < 0.05$. KO means knockout.

10.10 TMEM109 HOMO-OLIGOMERIZATION

There is evidence in the literature that TMEM109 is capable of homo-oligomerization, which might be essential for its ion-conducting property (Venturi *et al.*, 2011).

The previously described NanoBiT protein-protein interaction assay was used to address this point. Two additional constructs were created. One construct where the Small BiT was fused to the C-terminal end of TMEM109 (TMEM109-C-T-SmB) and a second one where the Small BiT was fused to the C-terminally truncated C-terminal end of the TMEM109 (TMEM109-C-T'-SmB) (Paragraph 9.7). The assay confirmed that the TMEM109 is capable of homo-oligomerization (Figure 42). However, C-terminal truncation did not disrupt the homo-oligomerization capability. Instead, the truncation increased the light output and, therefore, the TMEM109 homo-oligomerization. The homo-oligomerization feature of the TMEM109 did not depend on the C-terminal end of the protein but likely depends on its ER luminally located N-terminus. (This will be discussed in more detail with the peptide spot array data in the Discussion section (Figure 54).)

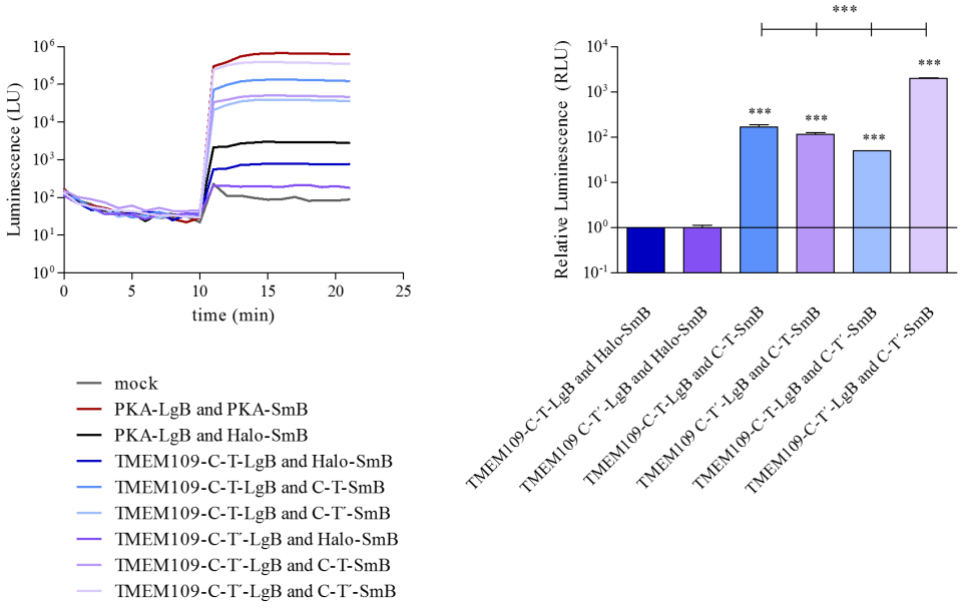

Figure 42. The homo-oligomerization feature of the TMEM109

Protein-protein interaction determined by NanoBiT assay. Plasmids encoding the Large BiT or the Small BiT proteins were fused to the TMEM109, or the C-terminally truncated TMEM109. As a positive control, the subunits of the protein kinase A were fused to the Large or the Small BiT. As a negative control, HaloTag was fused to the Small BiT. After 24 hours post-transfection with the respective plasmids, the luminescence signal was measured by a plate reader. After furimazine substrate addition, a > 10-fold increase in the signal indicated a specific protein-protein interaction. The maximum values from the curves are displayed on the bar graph in comparison to the respective control. One representative measurement of two repeats is displayed in the figure, carried out in triplicates. One-way ANOVA statistical analysis was performed. Significant changes are indicated by * symbol: *** $P < 0.001$; ** $P < 0.01$; * $P < 0.05$.

10.11 LIVE-CELL CALCIUM IMAGING

TMEM109 has been described as a cation channel in the ER membrane. It is assumed that the feature that it can homo-oligomerize can contribute to the formation of a pore within the ER membrane that can conduct cations (Venturi *et al.,* 2011; Lemos *et al.,* 2021). Therefore, the question was whether lower TMEM109 abundance could disturb the cellular calcium homeostasis.

Using calcium imaging, the cytosolic calcium concentration can be measured in living cells when the cells are prestained with the cell-permeable calcium-sensitive fluorescent dye Fura-2-acetoxymethyl ester (Fura-2-AM).

The changes in the cytosolic calcium level can be monitored in response to different agents that can alter the calcium homeostasis within the cells, such as ionomycin and thapsigargin (see details below).

A kinetic assay was performed, testing 48, 60, and 72 hours of TMEM109 silencing using two different siRNAs. After one-minute basal calcium content measurement, the cells were treated with ionomycin or thapsigargin, and the changes in the cytosolic calcium levels were measured for 5 and 10 minutes, respectively.

Ionomycin represents a calcium-specific ionophore that releases calcium ions out of all cellular organelles so that it is suitable to determine the overall calcium content within the cells (Hoth and Penner, 1992). Figure 43 shows these results after 48, 60, and 72 hours of TMEM109 silencing. After 48 hours of TMEM109 silencing, the calcium content was reduced; the reduction was significant only for the TMEM109-UTR-4 siRNA. After 60 hours of silencing, the calcium content compared to the control was not significantly but very moderately reduced. Silencing TMEM109 for 72 hours caused a significant reduction in the calcium content with both siRNA treatments.

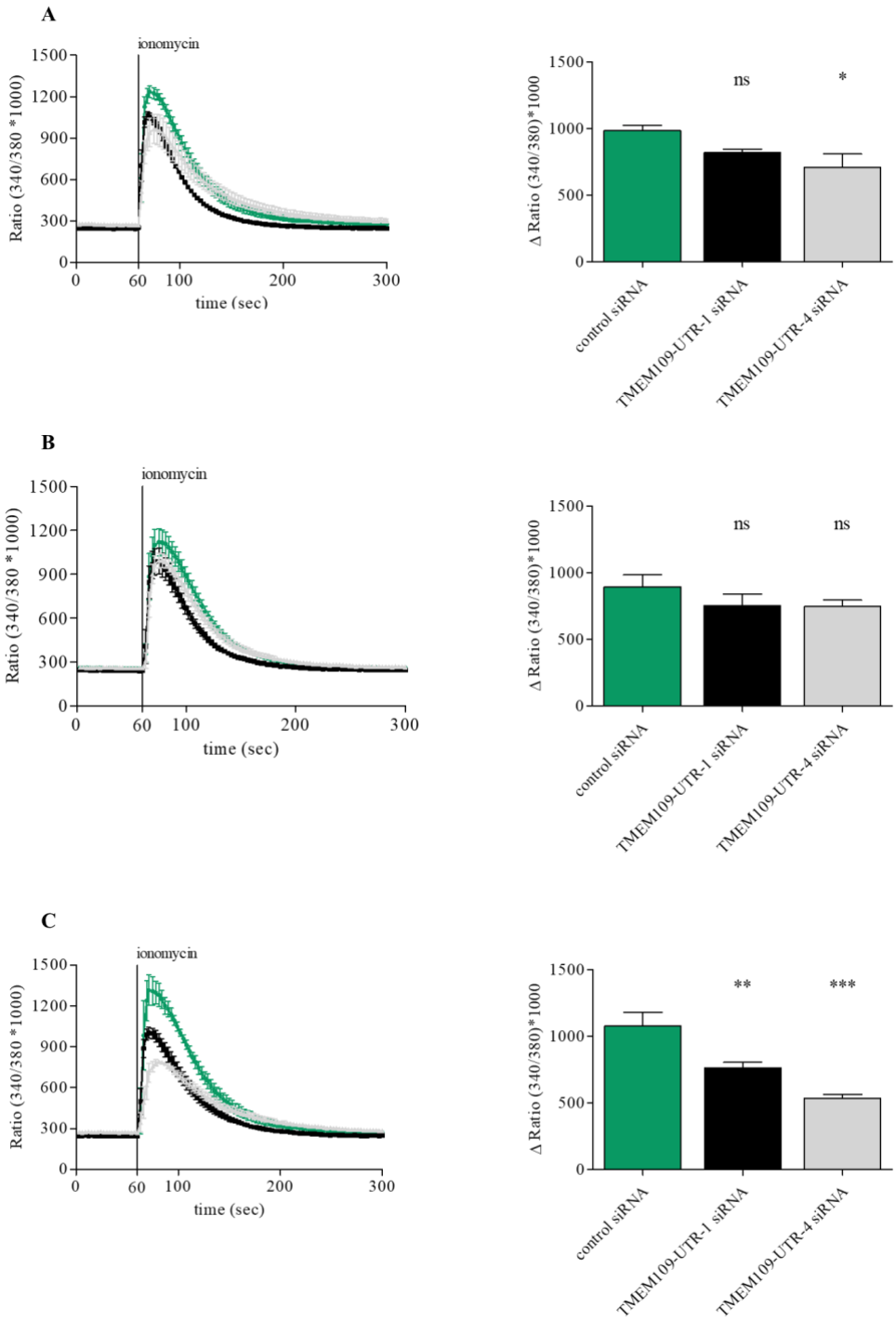

Figure 43. Changes in the cytosolic calcium content in response to ionomycin treatment after TMEM109 silencing

Changes in the calcium content in response to ionomycin treatment after TMEM109 silencing for A) 48 hours, B) 60 hours, and C) 72 hours. Cells were cultivated and silenced with the designated siRNAs on coverslips. After the determined culturing time points, the cells were stained with Fura-2-AM cell-permeant calcium-sensitive fluorescent dye. During the measurement, after 1 minute, ionomycin was added to the cells at a final concentration of 5 µM. Changes in the calcium content were registered every 3 seconds for 5 minutes (300 seconds). Bar graphs visualize the differences in the maximum height of each curve, excluding the basal signal level. The averages of a minimum of three independently repeated experiments are displayed. Per experiment, 50 cells were measured. One-way ANOVA statistical analysis was performed. Significant changes are indicated by * symbol: *** $P < 0.001$; ** $P < 0.01$; * $P < 0.05$, "ns" indicates non-significant results $P > 0.05$.

Since hSnd2 silencing caused a reduced abundance of the TMEM109 protein (Figure 6), it was tempting to speculate if knocking down hSnd2 could cause any difference in the overall calcium content. HSnd2 silencing by UTR-3 siRNA, but not UTR-2 siRNA, caused a significant reduction in the total cellular calcium content after 96 hours of silencing (Figure 44).

The efficiency of hSnd2 silencing was confirmed by Western blot analysis (Supplementary materials, Figure 65).

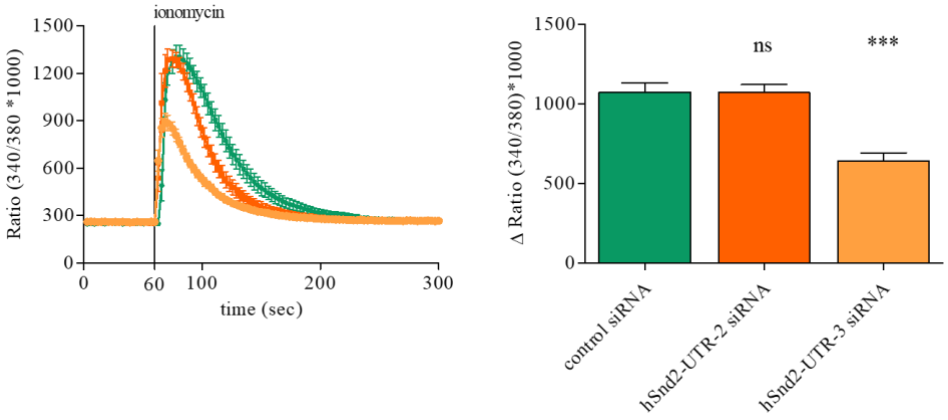

Figure 44. Changes in the cytosolic calcium content in response to ionomycin treatment after 96 hours of hSnd2 silencing

Changes in the calcium content in response to ionomycin treatment after hSnd2 silencing for 96 hours. Cells were cultivated and silenced with the designated siRNAs on coverslips. After the determined culturing time point, the cells were stained with Fura-2-AM cell-permeant calcium-sensitive fluorescent dye. During the measurement, after 1 minute, ionomycin was added to the cells at a final concentration of 5 µM. Changes in the calcium content were registered every 3 seconds for 5 minutes (300 seconds). Bar graphs visualize the differences in the maximum height of each curve, excluding the basal signal level. The averages of a minimum of three independently repeated experiments are displayed. Per experiment, 50 cells were measured. One-way ANOVA statistical analysis was performed. Significant changes are indicated by * symbol: *** $P < 0.001$; ** $P < 0.01$; * $P < 0.05$.

Thapsigargin is an agent that blocks the sarco-endoplasmic reticulum calcium ATPase (SERCA) in the ER and the SR membrane (Lindner *et al.*, 2020). The physiological role of the SERCA is to bring back calcium from the cytosol into the ER to maintain the steep calcium gradient between the cytosol and the ER. Thus, thapsigargin is used to measure the calcium content leaking out of the ER specifically, usually referred to as calcium leakage.

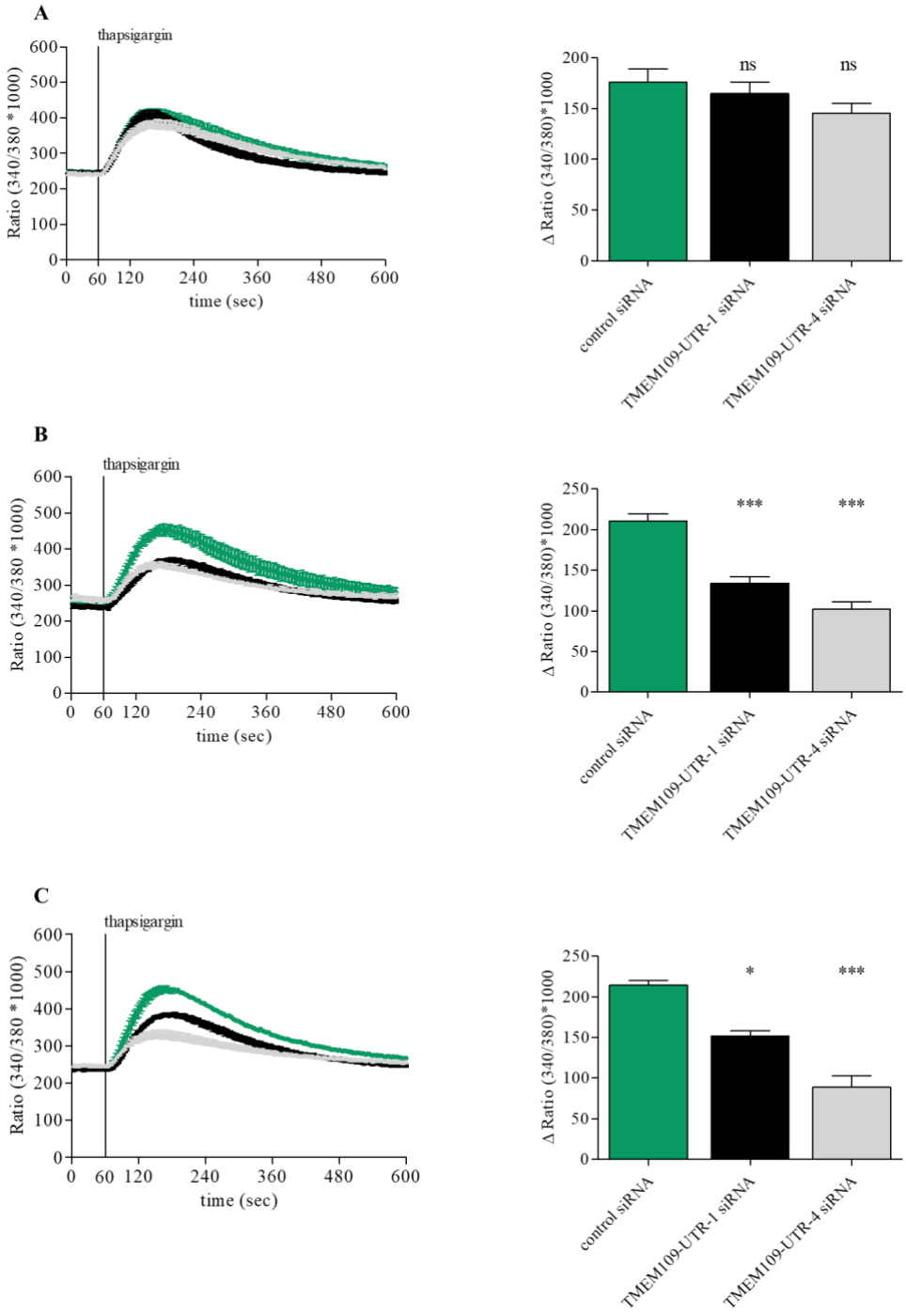

Figure 45. Changes in the cytosolic calcium content in response to thapsigargin treatment after TMEM109 silencing

Changes in the calcium content in response to thapsigargin treatment after TMEM109 silencing for A) 48 hours, B) 60 hours, and C) 72 hours. Cells were cultivated and silenced with the designated siRNAs on coverslips. After the determined culturing time points, the cells were stained with Fura-2-AM cell-permeant calcium-sensitive fluorescent dye. During the measurement, after 1 minute, thapsigargin was added to the cells at a final concentration of 1 μM. Changes in the calcium content were registered every 3 seconds for 10 minutes (600 seconds). Bar graphs visualize the differences in the maximum height of each curve, excluding the basal signal level. The averages of a minimum of three independently repeated experiments are displayed. Per experiment, 50 cells were measured. One-way ANOVA statistical analysis was performed.Significant changes are indicated by * symbol: *** $P < 0.001$; ** $P < 0.01$; * $P < 0.05$.

After 48 hours of TMEM109 silencing, no significant change was observed in the calcium leakage out of the ER in response to thapsigargin treatment (Figure 45). Calcium leakage out of the ER was significantly decreased after 60 hours of TMEM109 silencing as well as after 72 hours with both siRNAs (Figure 45). HSnd2 silencing by UTR-3 siRNA resulted in a significant reduction of calcium leakage out of the ER, but the significant change was not observed in the case of the UTR-2 siRNA (Figure 46). The efficiency of hSnd2 silencing was confirmed by Western blot analysis (Supplementary materials, Figure 65).

In this case, it is difficult to make a direct correlation whether hSnd2 silencing directly affected the TMEM109. Regarding that the silencing of either protein, TMEM109 or hSnd2, resulted in a similar change in the calcium homeostasis, suggests that the two proteins work together on some level. However, further research is required to determine whether the reduced calcium leakage is a direct effect of TMEM109 and hSnd2 silencing or not. It is also possible that the silencing of these proteins results in the change of the abundance of other calcium leak channels, which is, excluding the abundance of Sec61α, beyond the scope of this work, and further investigation would address the answer for that.

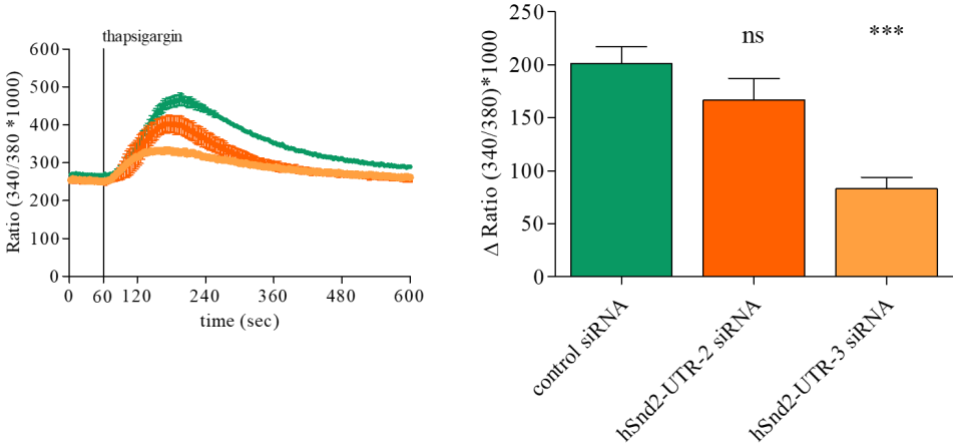

Figure 46. Changes in the cytosolic calcium content in response to thapsigargin treatment after 96 hours of hSnd2 silencing

Changes in the calcium content in response to thapsigargin treatment after hSnd2 silencing for 96 hours. Cells were cultivated and silenced with the designated siRNAs on coverslips. After the determined culturing time point, the cells were stained with Fura-2-AM cell-permeant calcium-sensitive fluorescent dye. During the measurement, after 1 minute, thapsigargin was added to the cells at a final concentration of 1 µM. Changes in the calcium content were registered every 3 seconds for 10 minutes (600 seconds). Bar graphs visualize the differences in maximum heights of each curve, excluding the basal signal level. The averages of a minimum of three independently repeated experiments are displayed. Per experiment, 50 cells were measured. One-way ANOVA statistical analysis was performed. Significant changes are indicated by * symbol: *** $P < 0.001$; ** $P < 0.01$; * $P < 0.05$.

The effect of TMEM109 as a calcium channel in the ER membrane was tested in *TMEM109* knockout HeLa cells. Correspondingly to the previously done calcium imaging approaches, ionomycin or thapsigargin was added during the measurement after one minute to reveal the changes regarding the calcium content or the calcium leakage out of the ER, respectively (Figure 47). The lack of TMEM109 resulted in a moderately enhanced cellular calcium content (Figure 47A). The calcium leakage out of the ER revealed by thapsigargin was significantly enhanced in the *TMEM109* knockout cells (Figure 47B). Such increased calcium leak out of the ER might be related to the increased abundance of the Sec61α protein (Figure 40B, C); as Sec61 translocon is a calcium leak channel in the ER membrane (Lang *et al.*, 2017; Linxweiler *et al.*, 2017). It is also likely that the cells try to compensate for the loss of TMEM109 by enhancing the abundance of other calcium leak channel or receptor proteins, which have not been tested in the TMEM109 knockout cells. Since TMEM109 has not been described as a major calcium channel in the ER membrane, its knockout is questionable to cause a defect in the calcium export out of the ER. It is also likely that the cells were well adapted to losing TMEM109 and compensated for its loss.

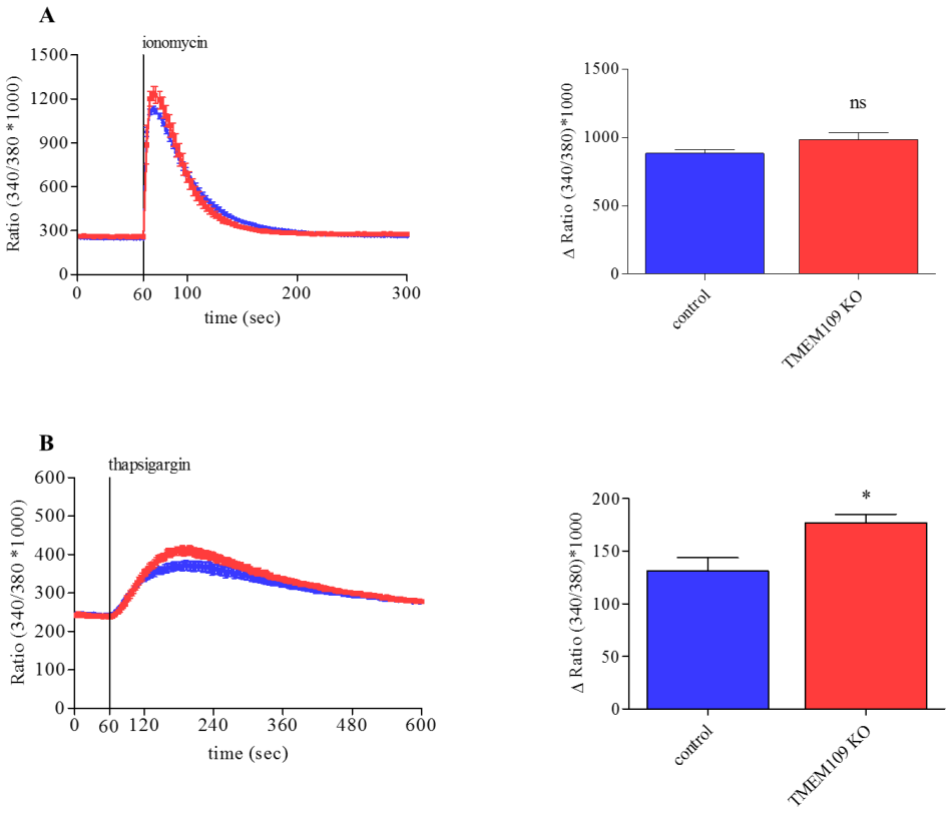

Figure 47. Changes in the cytosolic calcium content after TMEM109 knockout

Changes in the calcium content in response to A) ionomycin B) thapsigargin treatment after TMEM109 knockout. Cells were cultivated on coverslips. After 48 hours, the cells were stained with Fura-2-AM cell-permeant calcium-sensitive fluorescent dye. During the measurement after 1 minute, ionomycin or thapsigargin was added to the cells at a final concentration of 5 and 1 µM, respectively. Changes in the calcium content were registered every 3 seconds for 5 minutes (300 seconds) with ionomycin treatment and 10 minutes (600 seconds) with thapsigargin treatment. Bar graphs visualize the differences in the maximum height of each curve, excluding the basal signal level. The averages of a minimum of three independently repeated experiments are displayed. Per experiment, 50 cells were measured. A two-tailed t-test statistical analysis was performed. Significant changes are indicated by * symbol: *** $P < 0.001$; ** $P < 0.01$; * $P < 0.05$. KO means knockout.

10.12 The effect of ER stress induction on the TMEM109 *and other protein targeting receptors*

Previously it was tested whether *TMEM109* knockdown or knockout could induce ER stress, and the results could confirm that cells having less or no TMEM109 protein did not induce ER stress. In order to investigate the effect of ER stress induction on TMEM109 and other ER protein targeting receptors, cells were treated with ER stress inducers, 1 µM thapsigargin or 2.5 µg/ml tunicamycin. Since both agents were dissolved in DMSO, DMSO-treated cells were used as the control condition. After 20 hours, cells were harvested and prepared for Western blot analysis. Simultaneously, total RNA was isolated for subsequent RT-qPCR analysis.

Tunicamycin has been shown to inhibit the N-glycosylation step in the ER, initiating the formation of misfolded proteins (Guha *et al.*, 2017; Wu *et al.*, 2018). At the same time, thapsigargin induces ER stress by depleting the ER calcium content by blocking the SERCA. The scarcity in the ER calcium concentration results in the improper function of the calcium-dependent ER chaperones, such as calnexin or calreticulin (Kamiya *et al.*, 2013; Lindner *et al.*, 2020). Furthermore, it has also been observed that thapsigargin can initiate the activation of the extrinsic apoptotic pathway by the upregulation of the mRNA and protein level of DR1/2/4/5 and TRAIL-R1 (Lindner *et al.*, 2020).

Figure 48 depicts the changes in the relative mRNA level in response to UPR, induced by thapsigargin and tunicamycin. As expected, *BiP* showed ~70-fold enhancement by both agents. SR subunits were significantly elevated, the β subunit showed a 6-fold enhanced mRNA level by both agents, and the enhancement was slightly lower in the case of the α subunit, specifically by tunicamycin treatment. The *Caml* mRNA level doubled, while *hSnd2* showed 3-fold higher levels by both treatments. The abundance of the *TMEM109* transcript was significantly enhanced, a 1.2-fold change with thapsigargin, while tunicamycin treatment induced an approximate 1.8-fold elevation.

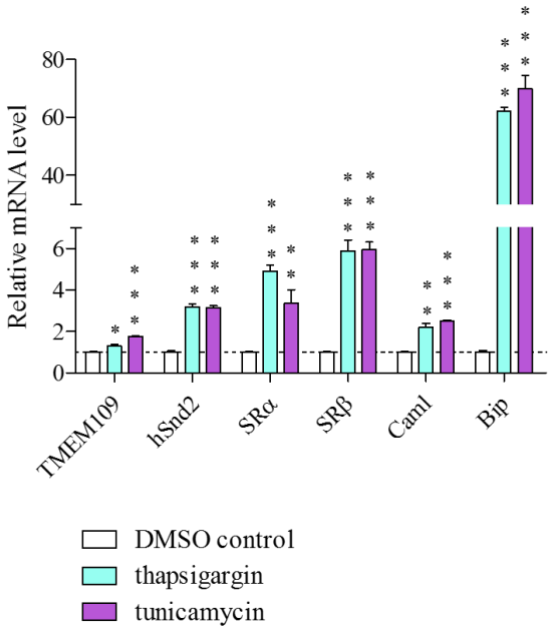

Figure 48. Relative mRNA level after the induction of ER stress

The RT-qPCR result shows the relative mRNA level of *TMEM109* and different targeting receptors in comparison to the control, normalized to the endogenous control, beta-actin. After 20 hours of ER stress and UPR induction cells were harvested, the total RNA was isolated and prepared for analysis. Numbers indicate the average of two independently repeated experiments carried out in triplicates. One-way ANOVA statistical analysis was performed. Significant changes are indicated by * symbol: *** $P < 0.001$; ** $P < 0.01$; * $P < 0.05$.

Next, changes of the same targets on the protein level were tested via Western blot analysis. There was no significant change observed in the protein level regarding the Caml and the TMEM109; however, Caml was slightly reduced by tunicamycin treatment (Figure 49). As it was anticipated, the ER chaperone, BiP, was significantly more abundant. SRα abundance was significantly enhanced by tunicamycin treatment and the β subunit by thapsigargin treatment. HSnd2 was more abundant; however, most possibly due to the variance of the results, the increase was not significant; as it could be the reason for SRα by thapsigargin treatment and SRβ by tunicamycin treatment.

The targeting receptors showed elevated mRNA levels, and their protein level was also increased, except for the Caml and the TMEM109. Hence, SR subunits are essential for SRP-dependent ER targeting, and one-third of the proteins carry an N-terminal signal peptide; and certain proteins are still synthesized even during UPR, the level of the SR subunits is highly upregulated in UPR. HSnd2 is known to be part of the ER protein targeting machinery, the SND pathway, and it showed elevation in response to UPR. We cannot rule out, based on these results, whether TMEM109 plays a role in protein targeting to the ER or in protein homeostasis in general or not. As Caml, a known key player in ER protein targeting, did not show any significant change in the protein level in response to UPR, TMEM109 could also be an element in protein targeting and not affected by the induction of ER stress and UPR.

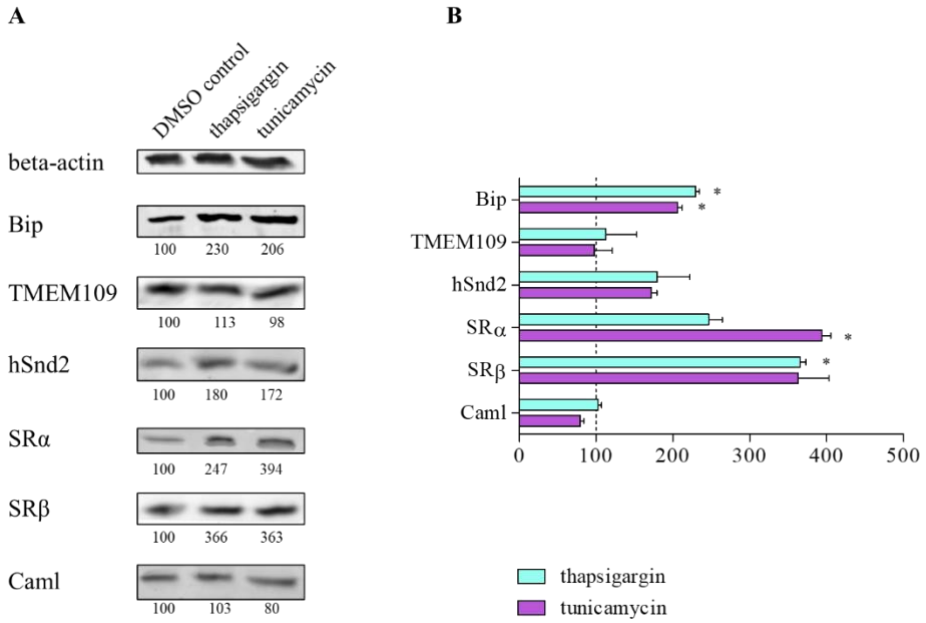

Figure 49. Relative abundance of proteins in response to ER stress

Western blot results after 20 hours of ER stress and UPR induction. Cells were harvested and prepared for Western blot analysis. A) Numbers indicate the relative protein abundance in comparison to control. Numbers display the average abundance of a certain protein for each condition. One representative blot of three independently repeated experiments is shown in the figure. Beta-actin served as a protein loading control due to its constitutive expression. B) One-way ANOVA statistical analysis was performed. Significant changes are indicated by * symbol: *** $P < 0.001$; ** $P < 0.01$; * $P < 0.05$.

11 DISCUSSION

11.1 THE TRANSMEMBRANE PROTEIN 109 (TMEM109)

Protein transport to the ER prominently is carried out by the SRP-dependent pathway. Due to the engagement of the SP or the TMH with the SRP molecule, the nascent precursor protein is directed to the SR and then to the Sec61 translocon (Figure 5A) (Blobel and Sabatini, 1971). Since the discovery of the SRP-dependent ER protein transport, novel pathways and accessory proteins have been described for conducting various proteins to the ER (Kutay *et al.*, 1993; Kutay *et al.*, 1995; Aviram *et al.*, 2016; Shao *et al.*, 2011; Brambillasca *et al.*, 2006; Shurtleff *et al.*, 2018; Anghel *et al.*, 2017; Meacock *et al.*, 2002).

Previous research identified the SRP-independent (SND) protein transport pathway in yeast cells (Aviram *et al.*, 2016). The SND pathway appears to conduct proteins bearing a transmembrane domain located downstream of the N-terminus to the ER; in yeast cells. This protein transport pathway has been scarcely characterized in human cells so far; one component of the pathway is known as the transmembrane protein 208 (TMEM208), also known as hSnd2 (Haßdenteufel *et al.*, 2017).

This study aimed to determine the role of the transmembrane protein 109 (TMEM109) regarding protein targeting to the endoplasmic reticulum (ER). TMEM109 appeared as a putative hSnd3 protein. It showed interaction with the hSnd2, determined by mass-spectrometric analysis of the eluate fraction from the co-immunoprecipitation reaction (Haßdenteufel *et al.*, 2017). Additionally, TMEM109 showed simultaneously reduced abundance when hSnd2 was silenced, based on mass-spectrometry results (Figure 6). Both these clues furthered the interest in addressing the potential contribution of TMEM109 as a novel component and targeting factor of the mammalian SND pathway.

The transmembrane protein 109 is a 23kDa three-transmembrane domain protein found in the ER membrane (Yamazaki *et al.*, 2010; Yamashita *et al.*, 2013; Venturi *et al.*, 2011). It is also known as mitsugumin23 (MG23), based on the Japanese terminology.

Previous research revealed that TMEM109 could promote cell survival of human kidney embryonic cells against ultraviolet C (UVC) radiation-induced damage (Yamashita *et al.*, 2013). However, thymocytes isolated from mice lacking the TMEM109 showed less radiosensitivity after γ-irradiation (Yamazaki *et al.*, 2010). Transfection of human embryonic kidney cells with a plasmid that encodes for *TMEM109* did not enhance cell survival in response to DNA damage induced by etoposide. Similarly, when TMEM109 was more abundant, it failed to promote cell survival in response to ER stress and unfolded protein response induced by tunicamycin or thapsigargin (Yamazaki *et al.*, 2010). This suggests that TMEM109 can protect cells specifically from UVC-induced cell death. The N-terminal

end of the protein can possibly interact with other ER chaperone proteins, which assumingly results in the inhibition of cell death induced by UVC (Yamashita *et al.*, 2013).

TMEM109 has also been described as a cation channel within the ER membrane (Takeshima *et al.*, 2015; Reilly-O'Donnell *et al.*, 2017; Venturi *et al.*, 2011). It conducts calcium and potassium ions. It has also been proposed that it can homo-oligomerize, which might be an essential feature for conducting ions (Venturi *et al.*, 2011). Reportedly, it forms an oligomer of two to six monomers; this was determined by chemical crosslinking experiments (Venturi *et al.*, 2011).

TMEM109 is widely expressed in various types of cells and highly expressed in lung tissue cells and reproductive organs, such as ovarian and prostate tissue cells. Immune cells are also expressing it in high amounts. (https://www.ncbi.nlm.nih.gov/gene, last accessed on 13 March 2022; http://biogps.org, last accessed on 13 March 2022). Some tissues that show strong *TMEM109* expression are secretory, providing a hint for the idea of the TMEM109 protein being involved in protein secretion.

The known SND pathway components, the human hSnd2 and the yeast Snd2, showed a conserved topology. Both the human and the yeast counterparts have four transmembrane domains, bearing cytosolic N-and C-terminus (Haßdenteufel *et al.*, 2017).

Comparing TMEM109 to the other ER-resident yeast SND pathway component, one can conclude that they do not have topology conservation (Figure 50). The yeast Snd3 is a one-transmembrane domain protein localized in the ER membrane and the mitochondrion membrane (Aviram *et al.*, 2016). It presumably has a cytosolic N-terminus, and its C-terminus is exoplasmic (type II single-pass transmembrane protein). However, taking advantage of the recent development of Alphafold for *in silico* structural predictions, yeast Snd3 harbors three or four TMHs (https://alphafold.ebi.ac.uk/entry/P38264, last accessed on 04 March 2022). TMEM109 is, as described before, a three-transmembrane domain protein carrying an N-terminal signal peptide. Both TMEM109 and Snd3 have a molecular weight of 21 kDa. In the case of the TMEM109, 21 kDa molecular weight is reached only after the cleavage of the N-terminal signal peptide. Snd3 has a phosphoserine residue as a post-translational modification site (https://www.uniprot.org/uniprot/P38264, last accessed on 13 March 2022).

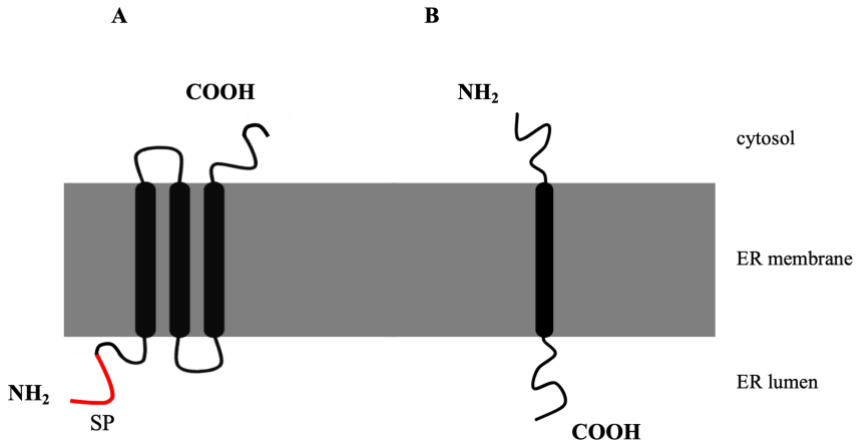

Figure 50. Topology of the A) human TMEM109 and B) yeast Snd3

The figure shows the predicted membrane topology of the putative hSnd3 protein, TMEM109 (A), and the yeast Snd3 protein (B). For details, see the text above.

Amino acid sequence alignment identified 14 % identity between the human TMEM109 and yeast Snd3, showing low sequence homology (Figure 51). 37 amino acids were found in identical positions and 54 amino acids in similar positions. However, this does not necessarily rule out that TMEM109 is the mammalian counterpart of the Snd3. In the evolutionarily conserved TRC pathway, the mammalian Caml also showed low sequence homology with its yeast equivalent, the Get2 (Yamamoto and Sakisaka, 2012; Borgese, 2020). The human SRα subunit also displayed low sequence homology with its yeast counterpart. ~28 % identity was found between the human and the yeast equivalent of SRα (https://www.uniprot.org/align/A20220425F248CABF64506F29A91F8037F07B67D101D673A, last accessed on 13 March 2022), (Ogg *et al.*, 1992). The mammalian SRβ subunit also showed low sequence similarity to the yeast homolog; ~20 % identity was found in their amino acid sequence (https://www.uniprot.org/align/A202204256320BA52A5CE8FCD097CB85A53697A3501D4EA, last accessed on 13 March 2022). However, an earlier analysis described a significant degree of similarity between the human and the yeast SRβ subunit (Ogg *et al.*, 1998).

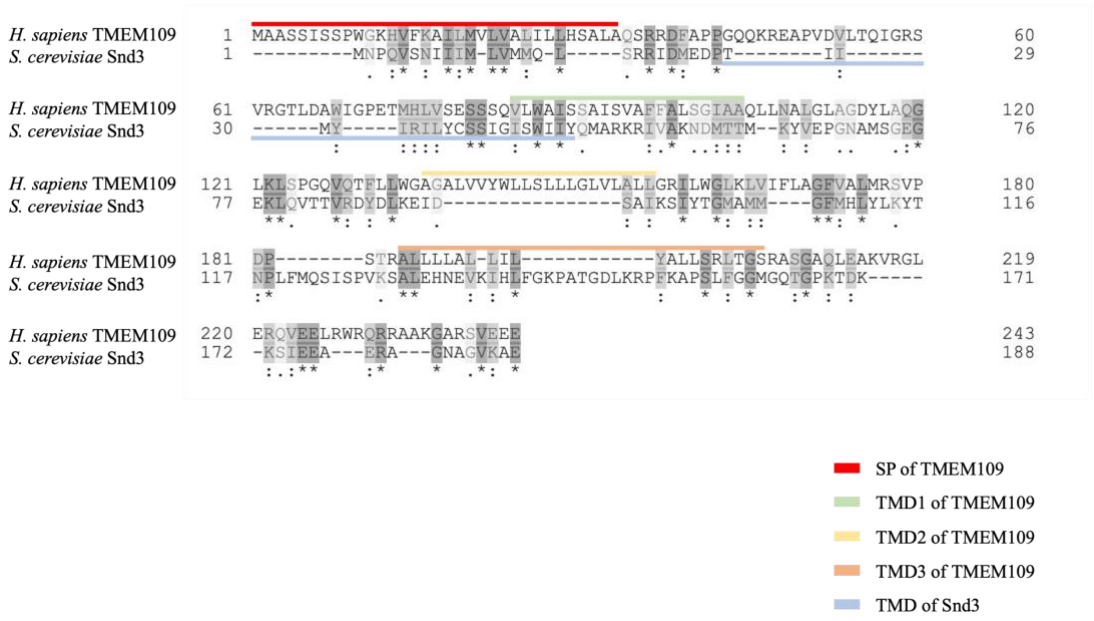

Figure 51. Amino acid sequence alignment of human TMEM109 and yeast Snd3

Results of amino acid sequence alignment of the putative human hSnd3 protein, TMEM109, and the yeast Snd3. For alignment, the https://www.uniprot.org/align/ webpage was used, last accessed on 13 March 2022. For details, see the text above.
" * " means that the match is a single, fully conserved residue; " : " means unable to find a match, amino acids with similar chemical properties; " . " means unable to find a match, amino acids with different chemical properties.

11.2 TMEM109 AND hSND2 INTERACTION; TMEM109 HOMO-OLIGOMERIZATION

To elucidate the potential interaction between the TMEM109 and hSnd2, a luminescence protein-protein interaction assay was performed, and it confirmed the interaction between the two proteins (Figure 19). Based on the luminescence protein-protein interaction assay, the C-terminal end of the TMEM109 did not prove to be an essential interaction site with hSnd2, determined by the C-terminal truncation of TMEM109 (Figure 19). Although, the endogenous TMEM109 was still present that could be capable of oligomerization with the truncated TMEM109. Through this interaction, the Large and the Small BiT could come into proximity and display efficient interaction between TMEM109 and hSnd2. It is also possible that the interaction site is not cytosolic but rather ER luminal, and the C-terminal truncation of TMEM109 does not disturb the interaction with the hSnd2.

TMEM109 homo-oligomerization was also tested by this luminescence protein-protein interaction assay. C-terminal truncation of TMEM109 did not disrupt the homo-oligomerization feature. One can conclude that amino acids that are responsible for homo-oligomerization are upstream of the C-terminal end of the TMEM109. Also, the wild-type TMEM109 could still oligomerize with the truncated version of it and display interaction, just like it is also possible in the case of TMEM109-hSnd2 interaction. To test this, it would be beneficial to use the TMEM109 knockout cell line (generated as described in Paragraph 9.19) for protein-protein interaction assays. So that by expressing the C-terminally truncated TMEM109 that carries the NanoBiT tag, one could obtain a result that would possibly not be biased by the presence of the endogenous, wild type TMEM109 that could potentially homo-oligomerize with the truncated version.

Additional possible interacting amino acids of TMEM109 and hSnd2 were determined by a series of peptide spot arrays *in vitro,* as well as the amino acids that are possibly responsible for the homo-oligomerization of the TMEM109. These unpublished results generated by Karsten Mayr and Professor Dr. Martin Jung are described in the following paragraphs.

11.3 SPOT PEPTIDE ARRAY

11.3.1 TMEM109 AND hSND2 INTERACTION

To reveal the interacting amino acids on TMEM109 and hSnd2 and the homo-oligomerization capability of TMEM109, spot peptide array was performed by Karsten Mayr and Professor Dr. Martin Jung as written in Paragraph 9.25. The primary sequence of the TMEM109 or hSnd2 was synthesized as short stretches of 15 amino acids onto a cellulose membrane covering the full-length protein. In the subsequent spot, the peptide was shifted by three amino acids compared to the previous spot (e.g. spot1: MAASSISSPWGKHVF, spot2: SSISSPWGKHVFKAI).

Based on these peptide array results, the N- and the C-terminal end of the hSnd2 (Figure 52) can be a potential interaction site with the solubilized TMEM109 from the dog pancreas microsomes. The identified interacting amino acids are in the cytosolic N-terminal end of the hSnd2. While the amino acids in spots I 11-18 and I 22-26 encode for the first TMD, partially and the first ER luminal domain, the second TMD, and partially the second cytosolic domain of the hSnd2. (For better understanding, see the predicted membrane topology of the two proteins in Figure 16 and its description.) Amino acids in the II 20-24 position partially translate the fourth TMD and the cytosolic C-terminal end of the hSnd2.
The peptide array experiment displayed interaction between the hSnd2 and the TMEM109 C-terminal end after the 208th amino acid (Figure 53). The N-terminal ER luminal end of the TMEM109 also showed interaction with hSnd2 in the first 40 amino acids (spots I 1-2 and I 5-9, Figure 53). However, these peptides cover the SP of the TMEM109 protein, which is cleaved off after ER transport and processing. Possible interacting amino acids were identified between the 46th and the 63rd amino acids (spot I 16-17, Figure 53), which are also N-terminally located amino acids in the ER luminal domain of the TMEM109.
Taken together, the cytosolic C-terminal end of the TMEM109 might interact with the cytosolic N-terminal end of the hSnd2. However, the C-terminal truncation of the TMEM109 did not disrupt the interaction with the hSnd2, as discussed previously (Figure 19). This could be verified by using the TMEM109 knockout cells for luminescence protein-protein interaction assay to avoid the possible wild-type TMEM109 oligomerization with the truncated version. Also, N-terminal hSnd2 truncation would be worthwhile for testing the disruption of the interaction between the two proteins.
However, it is also likely that certain amino acids in the first ER luminal domain ($Y_{46}SAS_{49}$) of the hSnd2 interact with the N-terminal ER luminal domain (K_{46}REAPVDVLTQIGRSVRG_{63}) of the TMEM109.

A

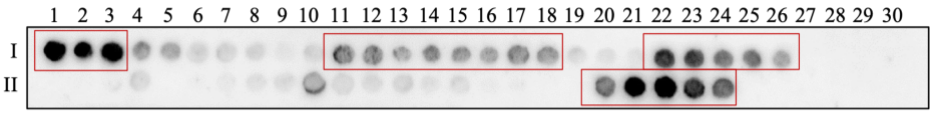

B

position	sequence	position	sequence
I 1	MAPKGKVGTRGKKQI	II 1	DLNMEQGMAEHLKDV
I 2	KGKVGTRGKKQIFEE	II 2	MEQGMAEHLKDVILL
I 3	VGTRGKKQIFEENRE	II 3	GMAEHLKDVILLTAI
I 4	RGKKQIFEENRETLK	II 4	EHLKDVILLTAIVQV
I 5	KQIFEENRETLKFYL	II 5	KDVILLTAIVQVLSC
I 6	FEENRETLKFYLRII	II 6	ILLTAIVQVLSCFSL
I 7	NRETLKFYLRIILGA	II 7	TAIVQVLSCFSLYVW
I 8	TLKFYLRIILGANAI	II 8	VQVLSCFSLYVWSFW
I 9	FYLRIILGANAIYCL	II 9	LSCFSLYVWSFWLLA
I 10	RIILGANAIYCLVTL	II 10	FSLYVWSFWLLAPGR
I 11	LGANAIYCLVTLVFF	II 11	YVWSFWLLAPGRALY
I 12	NAIYCLVTLVFFYSS	II 12	SFWLLAPGRALYLLW
I 13	YCLVTLVFFYSSASF	II 13	LLAPGRALYLLWVNV
I 14	VTLVFFYSSASFWAW	II 14	PGRALYLLWVNVLGP
I 15	VFFYSSASFWAWLAL	II 15	ALYLLWVNVLGPWFT
I 16	YSSASFWAWLALGFS	II 16	LLWVNVLGPWFTADS
I 17	ASFWAWLALGFSLAV	II 17	VNVLGPWFTADSGTP
I 18	WAWLALGFSLAVYGA	II 18	LGPWFTADSGTPAPE
I 19	LALGFSLAVYGASYH	II 19	WFTADSGTPAPEHNE
I 20	GFSLAVYGASYHSMS	II 20	ADSGTPAPEHNEKRQ
I 21	LAVYGASYHSMSSMA	II 21	GTPAPEHNEKRQRRQ
I 22	YGASYHSMSSMARAA	II 22	APEHNEKRQRRQERR
I 23	SYHSMSSMARAAFSE	II 23	HNEKRQRRQERRQMK
I 24	SMSSMARAAFSEDGA	II 24	EKRQRRQERRQMKRL
I 25	SMARAAFSEDGALMD	II 25	-
I 26	RAAFSEDGALMDGGM	II 26	-
I 27	FSEDGALMDGGMDLN	II 27	-
I 28	DGALMDGGMDLNMEQ	II 28	-
I 29	LMDGGMDLNMEQGMA	II 29	-
I 30	GGMDLNMEQGMAEHL	II 30	-

Figure 52. hSnd2 peptide spot incubation with RM extract and TMEM109 antibody, detecting the possible interaction sites of hSnd2 and TMEM109 by peptide array technique

Peptide fragments of A) hSnd2 were synthesized on a cellulose membrane. After blocking the membrane in BSA, RM extract was added. After washing steps and TMEM109 antibody incubation followed by peroxidase-labeled secondary antibody incubation, the chemiluminescence signal was scanned. One representative scan is shown here out of three independent repeats. The spots were highlighted where the signal showed high intensity; those are possible interaction sites. See the exact amino acid sequence of each spot in panel B.

Unpublished data generated by Karsten Mayr and Professor Dr. Martin Jung. Data analysis was carried out by me.

A

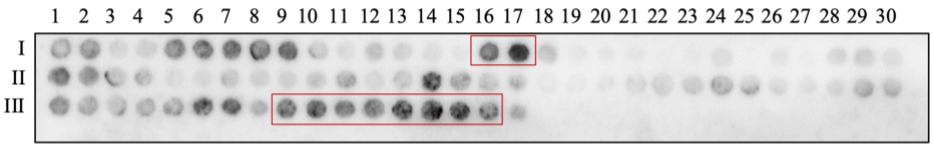

B

position	sequence	position	sequence	position	sequence
I 1	MAASSISSPWGKHVF	II 1	AISVAFFALSGIAAQ	III 1	DPSTRALLLLALLIL
I 2	SSISSPWGKHVFKAI	II 2	VAFFALSGIAAQLLN	III 2	TRALLLLALLILYAL
I 3	SSPWGKHVFKAILMV	II 3	FALSGIAAQLLNALG	III 3	LLLLALLILYALLSR
I 4	WGKHVFKAILMVLVA	II 4	SGIAAQLLNALGLAG	III 4	LALLILYALLSRLTG
I 5	HVFKAILMVLVALIL	II 5	AAQLLNALGLAGDYL	III 5	LILYALLSRLTGSRA
I 6	KAILMVLVALILLHS	II 6	LLNALGLAGDYLAQG	III 6	YALLSRLTGSRASGA
I 7	LMVLVALILLHSALA	II 7	ALGLAGDYLAQGLKL	III 7	LSRLTGSRASGAQLE
I 8	LVALILLHSALAQSR	II 8	LAGDYLAQGLKLSPG	III 8	LTGSRASGAQLEAKV
I 9	LILLHSALAQSRRDF	II 9	DYLAQGLKLSPGQVQ	III 9	SRASGAQLEAKVRGL
I 10	LHSALAQSRRDFAPP	II 10	AQGLKLSPGQVQTFL	III 10	SGAQLEAKVRGLERQ
I 11	ALAQSRRDFAPPGQQ	II 11	LKLSPGQVQTFLLWG	III 11	QLEAKVRGLERQVEE
I 12	QSRRDFAPPGQQKRE	II 12	SPGQVQTFLLWGAGA	III 12	AKVRGLERQVEELRW
I 13	RDFAPPGQQKREAPV	II 13	QVQTFLLWGAGALVV	III 13	RGLERQVEELRWRQR
I 14	APPGQQKREAPVDVL	II 14	TFLLWGAGALVVYWL	III 14	ERQVEELRWRQRRAA
I 15	GQQKREAPVDVLTQI	II 15	LWGAGALVVYWLLSL	III 15	VEELRWRQRRAAKGA
I 16	KREAPVDVLTQIGRS	II 16	AGALVVYWLLSLLLG	III 16	LRWRQRRAAKGARSV
I 17	APVDVLTQIGRSVRG	II 17	LVVYWLLSLLLGLVL	III 17	RQRRAAKGARSVEEE
I 18	DVLTQIGRSVRGTLD	II 18	YWLLSLLLGLVLALL	III 18	-
I 19	TQIGRSVRGTLDAWI	II 19	LSLLLGLVLALLGRI	III 19	-
I 20	GRSVRGTLDAWIGPE	II 20	LLGLVLALLGRILWG	III 20	-
I 21	VRGTLDAWIGPETMH	II 21	LVLALLGRILWGLKL	III 21	-
I 22	TLDAWIGPETMHLVS	II 22	ALLGRILWGLKLVIF	III 22	-
I 23	AWIGPETMHLVSESS	II 23	GRILWGLKLVIFLAG	III 23	-
I 24	GPETMHLVSESSSQV	II 24	LWGLKLVIFLAGFVA	III 24	-
I 25	TMHLVSESSSQVLWA	II 25	LKLVIFLAGFVALMR	III 25	-
I 26	LVSESSSQVLWAISS	II 26	VIFLAGFVALMRSVP	III 26	-
I 27	ESSSQVLWAISSAIS	II 27	LAGFVALMRSVPDPS	III 27	-
I 28	SQVLWAISSAISVAF	II 28	FVALMRSVPDPSTRA	III 28	-
I 29	LWAISSAISVAFFAL	II 29	LMRSVPDPSTRALLL	III 29	-
I 30	ISSAISVAFFALSGI	II 30	SVPDPSTRALLLLAL	III 30	-

Figure 53. TMEM109 peptide spot incubation with RM extract and hSnd2 antibody, detecting the possible interaction sites of TMEM109 and hSnd2 by peptide array technique

Peptide fragments of A) TMEM109 were synthesized on cellulose membranes. After blocking the membrane in BSA, RM extract was added. After washing steps and hSnd2 antibody incubation followed by peroxidase-labeled secondary antibody incubation, the chemiluminescence signal was scanned. One representative scan is shown here out of three independent repeats. The spots were highlighted where the signal showed high intensity; those are possible interaction sites. See the exact amino acid sequence of each spot in panel B.

Unpublished data generated by Karsten Mayr and Professor Dr. Martin Jung. Data analysis was carried out by me.

11.3.2 THE HOMO-OLIGOMERIZATION CAPABILITY OF TMEM109

Figure 54 displays the homo-oligomerization ability of TMEM109, indicated by the highlighted area. Where the signal shows enhanced intensity suggests the interaction between TMEM109 and TMEM109. The amino acid sequence of the possibly interacting amino acids is the following: FAPPGQQKREAPVDV. These amino acids also partially cover the possible interaction site with hSnd2 (Figure 53). The very intense chemiluminescence signal at the C-terminus is likely due to the antibody recognition site. This amino acid stretch was used to generate the polyclonal TMEM109 antibody. This experiment independently verifies the strong interaction of the TMEM109 antibody with the C-terminus that it was designed to recognize.

A

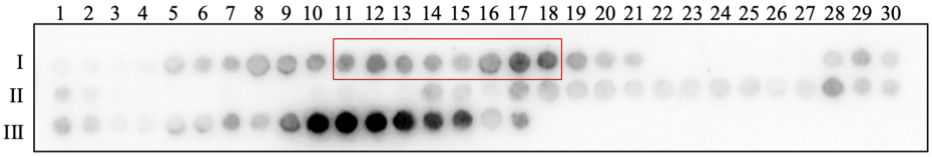

B

position	sequence	position	sequence	position	sequence
I 1	MAASSISSPWGKHVF	II 1	AISVAFFALSGIAAQ	III 1	DPSTRALLLLALLIL
I 2	SSISSPWGKHVFKAI	II 2	VAFFALSGIAAQLLN	III 2	TRALLLLALLILYAL
I 3	SSPWGKHVFKAILMV	II 3	FALSGIAAQLLNALG	III 3	LLLLALLILYALLSR
I 4	WGKHVFKAILMVLVA	II 4	SGIAAQLLNALGLAG	III 4	LALLILYALLSRLTG
I 5	HVFKAILMVLVALIL	II 5	AAQLLNALGLAGDYL	III 5	LILYALLSRLTGSRA
I 6	KAILMVLVALILLHS	II 6	LLNALGLAGDYLAQG	III 6	YALLSRLTGSRASGA
I 7	LMVLVALILLHSALA	II 7	ALGLAGDYLAQGLKL	III 7	LSRLTGSRASGAQLE
I 8	LVALILLHSALAQSR	II 8	LAGDYLAQGLKLSPG	III 8	LTGSRASGAQLEAKV
I 9	LILLHSALAQSRRDF	II 9	DYLAQGLKLSPGQVQ	III 9	SRASGAQLEAKVRGL
I 10	LHSALAQSRRDFAPP	II 10	AQGLKLSPGQVQTFL	III 10	SGAQLEAKVRGLERQ
I 11	ALAQSRRDFAPPGQQ	II 11	LKLSPGQVQTFLLWG	III 11	QLEAKVRGLERQVEE
I 12	QSRRDFAPPGQQKRE	II 12	SPGQVQTFLLWGAGA	III 12	AKVRGLERQVEELRW
I 13	RDFAPPGQQKREAPV	II 13	QVQTFLLWGAGALVV	III 13	RGLERQVEELRWRQR
I 14	APPGQQKREAPVDVL	II 14	TFLLWGAGALVVYWL	III 14	ERQVEELRWRQRRAA
I 15	GQQKREAPVDVLTQI	II 15	LWGAGALVVYWLLSL	III 15	VEELRWRQRRAAKGA
I 16	KREAPVDVLTQIGRS	II 16	AGALVVYWLLSLLLG	III 16	LRWRQRRAAKGARSV
I 17	APVDVLTQIGRSVRG	II 17	LVVYWLLSLLLGLVL	III 17	RQRRAAKGARSVEEE
I 18	DVLTQIGRSVRGTLD	II 18	YWLLSLLLGLVLALL	III 18	-
I 19	TQIGRSVRGTLDAWI	II 19	LSLLLGLVLALLGRI	III 19	-
I 20	GRSVRGTLDAWIGPE	II 20	LLGLVLALLGRILWG	III 20	-
I 21	VRGTLDAWIGPETMH	II 21	LVLALLGRILWGLKL	III 21	-
I 22	TLDAWIGPETMHLVS	II 22	ALLGRILWGLKLVIF	III 22	-
I 23	AWIGPETMHLVSESS	II 23	GRILWGLKLVIFLAG	III 23	-
I 24	GPETMHLVSESSSQV	II 24	LWGLKLVIFLAGFVA	III 24	-
I 25	TMHLVSESSSQVLWA	II 25	LKLVIFLAGFVALMR	III 25	-
I 26	LVSESSSQVLWAISS	II 26	VIFLAGFVALMRSVP	III 26	-
I 27	ESSSQVLWAISSAIS	II 27	LAGFVALMRSVPDPS	III 27	-
I 28	SQVLWAISSAISVAF	II 28	FVALMRSVPDPSTRA	III 28	-
I 29	LWAISSAISVAFFAL	II 29	LMRSVPDPSTRALLL	III 29	-
I 30	ISSAISVAFFALSGI	II 30	SVPDPSTRALLLLAL	III 30	-

Figure 54. The homo-oligomerization capability of the TMEM109

A) Peptide spots of the TMEM109 were synthesized on a cellulose membrane. After blocking the membrane in BSA, RM extract was added. After washing steps and TMEM109 antibody incubation followed by peroxidase-labeled secondary antibody incubation, the chemiluminescence signal was scanned. One representative scan is shown here out of three independent repeats. The highlighted area indicates signal enhancement and possible interacting amino acids. See the exact amino acid sequence of each spot in panel B.

Unpublished data generated by Karsten Mayr and Professor Dr. Martin Jung. Data analysis was carried out by me.

11.3.3 MUTATION ANALYSIS IN THE DOMAIN THAT IS RESPONSIBLE FOR HOMO-OLIGOMERIZATION

Substituting the amino acids in the F_{39}APPGQQKR$_{47}$EAPVDV$_{53}$ region in the TMEM109 amino acid sequence revealed that the lysine at the 46th amino acid position (Lys 46) and arginine at the 47th position (Arg 47) could be essential for its homo-oligomerization. Arg 47 mutation to alanine (Ala) did disrupt the interaction of TMEM109 with TMEM109 (Figure 55A). When both Lys 46 and Arg 47 were substituted with Ala, it had the same effect similar to when the Arg was mutated alone to Ala (Figure 55B).

A

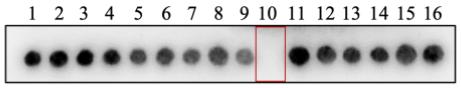

B

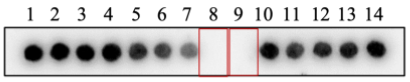

C

position	sequence	position	sequence
A 1	FAPPGQQKREAPVDV	B 1	FAPPGQQKREAPVDV
A 2	AAPPGQQKREAPVDV	B 2	AAPPGQQKREAPVDV
A 3	FAPPGQQKREAPVDV	B 3	FAAAGQQKREAPVDV
A 4	FAAPGQQKREAPVDV	B 4	FAPAAQQKREAPVDV
A 5	FAPAGQQKREAPVDV	B 5	FAPPAAQKREAPVDV
A 6	FAPPAQQKREAPVDV	B 6	FAPPGAAKREAPVDV
A 7	FAPPGAQKREAPVDV	B 7	FAPPGQAAREAPVDV
A 8	FAPPGQAKREAPVDV	B 8	FAPPGQQAAEAPVDV
A 9	FAPPGQQAREAPVDV	B 9	FAPPGQQKAAAPVDV
A 10	FAPPGQQKAEAPVDV	B 10	FAPPGQQKRAAPVDV
A 11	FAPPGQQKRAAPVDV	B 11	FAPPGQQKREAAVDV
A 12	FAPPGQQKREAPVDV	B 12	FAPPGQQKREAAADV
A 13	FAPPGQQKREAAVDV	B 13	FAPPGQQKREAPAAV
A 14	FAPPGQQKREAPADV	B 14	FAPPGQQKREAAVAA
A 15	FAPPGQQKREAPVAV		
A 16	FAPPGQQKREAPVDA		

Figure 55. Mutation analysis in the amino acid sequence of TMEM109 to test the effect of disrupting the homo-oligomerization

FAPPGQQKREAPVDV, the 39th-53rd amino acid sequence of the TMEM109 containing various point mutations synthesized on cellulose membrane by automated peptide synthesizer. Spot A10 shows Arg 47 substitution by Ala, spot B8 depicts Lys 46 and Arg 47 substitution by Ala, and B9 displays Arg 47 substitution by Ala. After blocking the membrane in BSA, RM extract was added. After washing steps and TMEM109 antibody incubation followed by peroxidase-labeled secondary antibody incubation, the chemiluminescence signal was scanned. The highlighted area indicates the loss of interaction of TMEM109 with TMEM109 in response to the mutation. See the exact amino acid sequence of each spot in panel C. One representative scan is shown here out of three independent repeats.

Unpublished data generated by Karsten Mayr and Professor Dr. Martin Jung. Data analysis was carried out by me.

Similar to alanine substitution, when the Arg 47 was mutated to glutamic acid (Glu), a negatively charged amino acid, it disrupted TMEM109 homo-oligomerization (Figure 56).

A

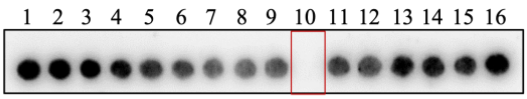

B

position	sequence
1	FAPPGQQKREAPVDV
2	EAPPGQQKREAPVDV
3	FEPPGQQKREAPVDV
4	FAEPGQQKREAPVDV
5	FAPEGQQKREAPVDV
6	FAPPEQQKREAPVDV
7	FAPPGEQKREAPVDV
8	FAPPGQEKREAPVDV
9	FAPPGQQEREAPVDV
10	FAPPGQQKEEAPVDV
11	FAPPGQQKREAPVDV
12	FAPPGQQKREEPVDV
13	FAPPGQQKREAEVDV
14	FAPPGQQKREAPEDV
15	FAPPGQQKREAPVEV
16	FAPPGQQKREAPVDE

Figure 56. Mutation analysis in the amino acid sequence of TMEM109 to test the effect of disrupting the homo-oligomerization feature

FAPPGQQKREAPVDV, the 39th-53rd amino acid sequence of the TMEM109 containing various point mutations synthesized on cellulose membrane by automated peptide synthesizer. Spot 10 is Arg 47 substitution by Glu. After blocking the membrane in BSA, RM extract was added. After washing steps and TMEM109 antibody incubation followed by peroxidase-labeled secondary antibody incubation, the chemiluminescence signal was scanned. The highlighted area indicates the loss of interaction of TMEM109 with TMEM109 in response to the mutation. See the exact amino acid sequence of each spot in panel B. One representative scan is shown here out of three independent repeats.

Unpublished data generated by Karsten Mayr and Professor Dr. Martin Jung. Data analysis was carried out by me.

When Arg 47 was mutated to Lys, the interaction was disrupted between the TMEM109 homo-oligomers (Figure 57A). However, when Lys 46 was mutated to Arg, it did not affect the interaction (Figure 57B).

Based on these experiments, one can conclude that positively charged amino acids, namely Lys 46 and Arg 47, in the TMEM109 sequence are crucial for the homo-oligomerization feature. And it seems that Arg 47 is more important than Lys 46, due to the fact that even when it was mutated to Lys, a positively charged amino acid as well, the interaction was disrupted, but when the Arg 47 was present again, it rescued the interaction (Figure 57A).

A

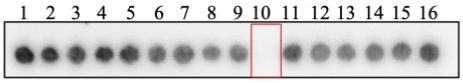

B

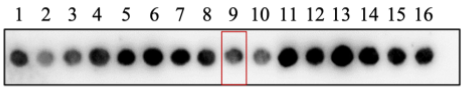

C

position	sequence	position	sequence
A 1	FAPPGQQKREAPVDV	B 1	FAPPGQQKREAPVDV
A 2	KAPPGQQKREAPVDV	B 2	RAPPGQQKREAPVDV
A 3	FKPPGQQKREAPVDV	B 3	FRPPGQQKREAPVDV
A 4	FAKPGQQKREAPVDV	B 4	FARPGQQKREAPVDV
A 5	FAPKGQQKREAPVDV	B 5	FAPRGQQKREAPVDV
A 6	FAPPKQQKREAPVDV	B 6	FAPPRQQKREAPVDV
A 7	FAPPGKQKREAPVDV	B 7	FAPPGRQKREAPVDV
A 8	FAPPGQKKREAPVDV	B 8	FAPPGQRKREAPVDV
A 9	FAPPGQQKREAPVDV	B 9	FAPPGQQRREAPVDV
A 10	FAPPGQQKKEAPVDV	B 10	FAPPGQQKREAPVDV
A 11	FAPPGQQKRKAPVDV	B 11	FAPPGQQKRRAPVDV
A 12	FAPPGQQKREKPVDV	B 12	FAPPGQQKRERPVDV
A 13	FAPPGQQKREAKVDV	B 13	FAPPGQQKREARVDV
A 14	FAPPGQQKREAPKDV	B 14	FAPPGQQKREAPRDV
A 15	FAPPGQQKREAPVKV	B 15	FAPPGQQKREAPVRV
A 16	FAPPGQQKREAPVDK	B 16	FAPPGQQKREAPVDR

Figure 57. Mutation analysis in the amino acid sequence of TMEM109 to test the effect of disrupting the homo-oligomerization feature

FAPPGQQKREAPVDV, the 39th-53rd amino acid sequence of the TMEM109 containing various point mutations synthesized on cellulose membrane by automated peptide synthesizer. A) A10 spot Arg 47 substitution by Lys B) B9 spot Lys 46 substitution by Arg. After blocking the membrane in BSA, RM extract was added. After washing steps and TMEM109 antibody incubation followed by peroxidase-labeled secondary antibody incubation, the chemiluminescence signal was scanned. The highlighted area indicates A) the loss of interaction of TMEM109 with TMEM109 or B) no effect on the interaction in response to the mutation. See the exact amino acid sequence of each spot in panel C.

Unpublished data generated by Karsten Mayr and Professor Dr. Martin Jung. Data analysis was carried out by me.

11.4 TMEM109 IS NOT AN SND SUBSTRATE

As TMEM109 showed reduced abundance after hSnd2 silencing (Figure 6), it was tested by *in vitro* transcription and translation assay (Paragraph 9.26) to determine whether it could be a substrate for the SND pathway. TMEM109 has an N-terminal signal peptide that is cleaved off in the ER lumen after its transport resulting in a smaller molecular weight (Figure 58). After hSnd2 silencing, the transport efficiency was not reduced, suggesting that TMEM109 is not an SND substrate. In contrast, the improved transport efficiency for TMEM109 upon hSnd2 depletion speaks in favor of TMEM109 representing a classic SRP-dependent substrate like preprolactin or invariant chain. Like TMEM109 shown here, preprolactin and invariant chain frequently demonstrated improved transport upon knockdown of the SND pathway (Figure 34, Figure 37).

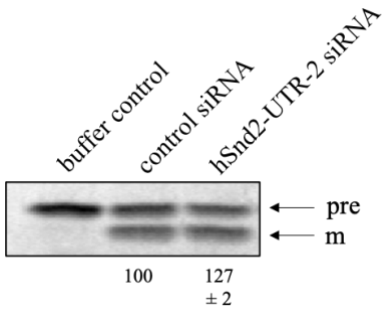

Figure 58. *In vitro* transcription and translation assay of TMEM109

Changes in *in vitro* transport efficiency of TMEM109 in response to hSnd2 silencing (20 nM, UTR-2 siRNA). After 96 hours of siRNA silencing, cells were harvested, and *in vitro* transcription and translation assay was performed. After SDS-PAGE, radioactive signals were captured on phosphor plates and scanned. KHM buffer control served as cell-free so that ER membrane-free condition. Numbers indicate the relative transport efficiency in comparison to control. One representative autoradiograph is shown out of two independently repeated experiments. Pre means premature polypeptide, and m means mature protein.

Unpublished data generated by Monika Lerner.

11.5 THE EFFECT OF TMEM109 KNOCKDOWN

To test the influence of the TMEM109 on protein targeting to the ER, Western blot and *in vitro* translation assays were performed after siRNA-mediated silencing of *TMEM109*. The siRNAs target different sequences on the 3' untranslated region on the TMEM109 mRNA. Different siRNA concentrations and silencing durations were tested. These Western blot results addressed that 25 nM siRNA concentration efficiently depleted TMEM109 (Figure 20). A longer silencing duration than 48 hours resulted in an increased silencing efficiency. RNA sequencing also confirmed the reduced expression of *TMEM109* after siRNA treatment (Figure 26). On the mRNA level, both 48 and 72 hours of silencing led to an almost complete *TMEM109* mRNA depletion, determined by real-time quantitative PCR (Figure 21).

However, a prolonged silencing time course caused decreased cell viability (Figure 22). Real-time cell analysis also confirmed that treating the cells with the four different siRNAs against the *TMEM109* reduced the cell viability and slowed down the cell proliferation rate substantially (Figure 23). However, when the culture medium was used up, the scarcity of the nutrients resulted in the decline of viability even in the control cells. Nevertheless, the TMEM109 knockdown cells displayed a declined cell proliferation compared to the control. This indicates that TMEM109 could be important for cells to be viable. Conversely, a *TMEM109* knockout HeLa cell line was generated (Paragraph 9.19), which indicates that losing TMEM109 is compatible with life in the case of HeLa cells. *TMEM109* knockout cells showed comparable cell viability to the wild type. In an independent study, a *TMEM109* knockout mouse was generated and also displayed compatibility with life at the organismal level (Yamazaki *et al.*, 2010).

TMEM109 has been described as a potential prognostic marker in endometrial cancer (Kunitomi *et al.*, 2020). Laminin subunit gamma 1 (LAMC1) has been linked to the malignant transformation of various tissues (fallopian tube cancer, hepatocellular carcinoma, meningeal tumor, endometrial cancer). Amongst other genes, *TMEM109* was found to be expressed differentially in endometrial cancer cells when *LAMC1* was depleted. It showed a simultaneously decreased mRNA level upon *LAMC1* knockdown. These differentially expressed genes could serve as prognostic markers in endometrial cancer (Kunitomi *et al.*, 2020). Another study has also elucidated that TMEMs can play a significant role as prognostic markers in several malignant tissue transformations. The various TMEMs have been described as tumor suppressors or oncogenes in different types of cancerous diseases. They can inhibit or even drive different cellular signaling pathways to limit/inhibit or promote the tumorigenesis (Schmit and Michiels, 2018). For example, *TMEM88* is highly expressed and can act as a tumor suppressor in lung and breast cancer cells (Ge *et al.*, 2018); while *TMEM45B* has been described as an oncogene, promoting lung cancer and gastric cancer progression (Shen *et al.*, 2018; Hu *et al.*, 2016).

11.6 IMMUNOCYTOCHEMISTRY

Fluorescence microscopic analysis was carried out to observe the ER localization of TMEM109 and hSnd2 and the effect of the silencing on the ER structure. Images were taken after TMEM109 and hSnd2 silencing compared to control conditions (Figure 59). The efficiency of the siRNA-mediated silencing can also be confirmed based on these immunofluorescence images. The intensity of the fluorescence signal is decreased by the TMEM109-UTR-1 siRNA and the hSnd2-UTR-2 siRNA treatment compared to the control samples. At the used magnification (20x), no significant changes in the ER structure were observed. Although, it could be informative to test the ER structure at a higher magnification or the use of an additional ER-specific dye.

Knocking down hSnd2 resulted in a lower signal abundance of TMEM109, which aligns with the previous result of hSnd2 silencing simultaneously reducing TMEM109 abundance (Figure 6).

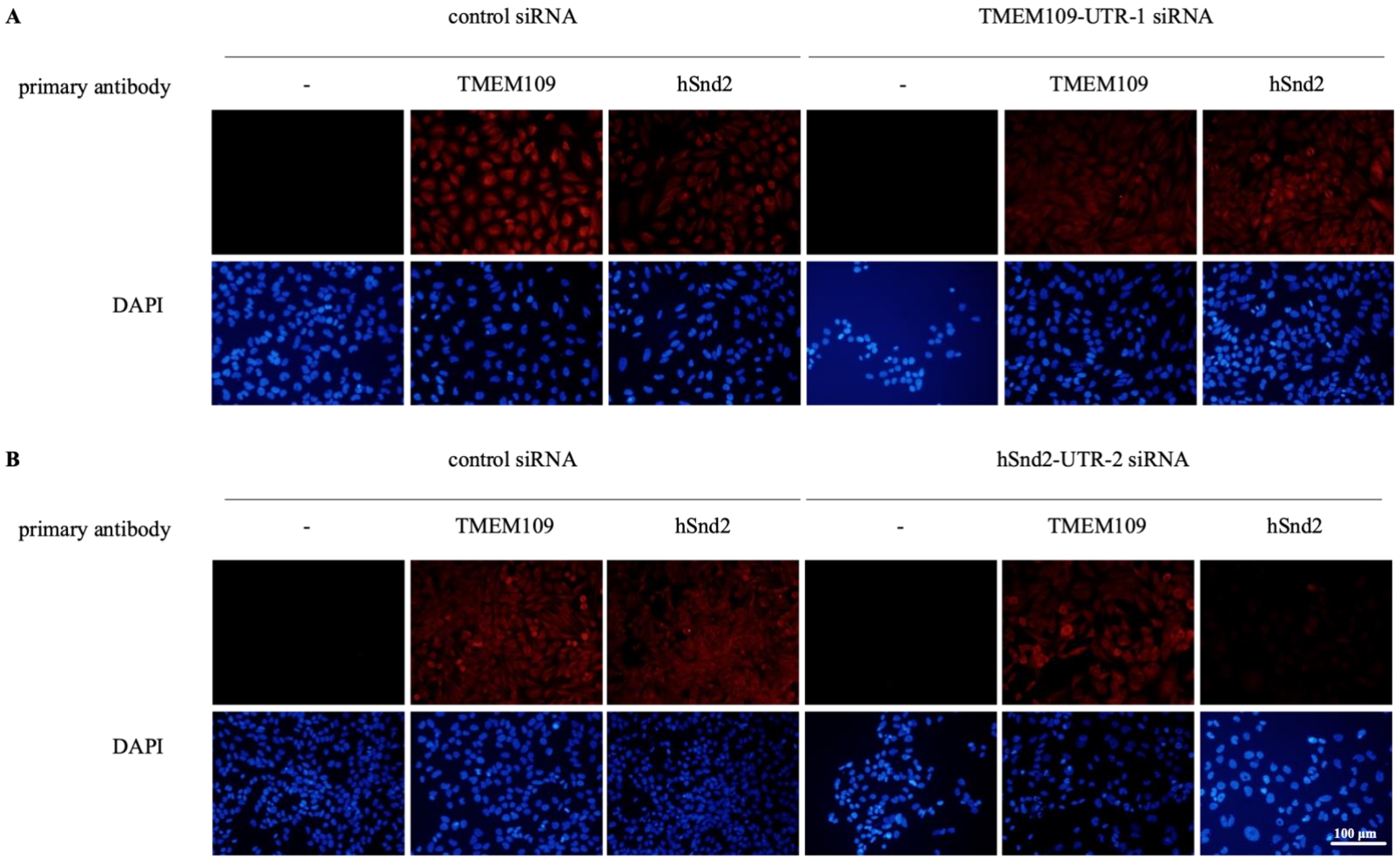

Figure 59. Immunofluorescence staining of TMEM109 and hSnd2

After 65 hours of TMEM109 (A) and hSnd2 (B) silencing at 20 nM final siRNA concentration, cells were fixed and incubated with primary antibodies against the TMEM109 or hSnd2. After fluorescently labeled secondary antibody and DAPI nucleic acid dye incubation, the samples were laser-excited, and images were captured by fluorescence microscope. The red color indicates the TMEM109 or the hSnd2. The blue color represents the cell nuclei. Unpublished data generated by Monika Lerner.

11.7 The effect of TMEM109 knockdown or knockout on protein transport efficiency to the ER

As previously addressed, an efficient silencing method was established for silencing *TMEM109*. The four siRNAs depicted differences regarding the protein abundance of different targeting receptors and the ER transport efficiency of specific substrates, and TMEM109-UTR-1 and TMEM109-UTR-4 were chosen for downstream experiments because they represented similar results to when hSnd2 was silenced (Haßdenteufel *et al.*, 2017). The differential biological effect of the different siRNA treatments can come from the fact that unpredicted off-target effects can occur (Aronin, 2006). Any off-target effect is unknown for the used siRNAs provided by the company; however, unintended sequence complementarity can occur and result in an off-target effect (Aronin, 2006).

TMEM109 knockdown caused enhanced protein level regarding the Sec61α subunit and both subunits of the SRP receptor (SR) in the case of TMEM109-UTR-1 and 4 siRNA treatment (Figure 31). This compensatory enhanced abundance of both SR subunits and the Sec61α subunit correlates to the results previously observed when hSnd2 was knocked down (Haßdenteufel *et al.*, 2017). The enhancement of the *SRPRB* and *SEC61A1* was also observed on the mRNA level (Figure 21) and on the gene expression level after TMEM109-UTR-1 siRNA treatment (Figure 28).

The protein abundance of the hSnd2 depicted no significant change in response to TMEM109-UTR-1 siRNA and resulted in a significant decrease with UTR-4 siRNA treatment (Figure 31). The mRNA level of the *HSND2* was found to increase after *TMEM109* silencing (Figure 21); in RNA sequencing results, it was only enlisted with the TMEM109-UTR-3 siRNA, displaying a decreased gene expression (data is not shown here).

As already mentioned earlier, the depletion of hSnd2 caused the lower abundance of TMEM109 (Figure 6). One could expect that TMEM109 silencing might induce a lower abundance of hSnd2. However, this correlation was previously described; for example, in the case of WRB and Caml, the silencing of one of the partner proteins similarly affected the abundance of the other (Colombo *et al.*, 2016). Nevertheless, WRB and Caml are subunits of the TRC40 receptor. At the same time, TMEM109 and hSnd2 are possibly just elements of the SND pathway, so their abundance could not be so strictly influenced by the other. Just like in the case of the SRP-dependent pathway, Sec61α silencing resulted in an elevated SRα protein level (Haßdenteufel *et al.*, 2017; Haßdenteufel *et al.*, 2018). However, SRα knockdown slightly lowered the Sec61α abundance (O'Keefe *et al.*, 2021).

The detected changes in the mRNA level in not all cases correlated well to the protein abundance. However, mRNA levels do not necessarily always correlate to protein levels. The ratio of mRNA and protein can be various for different genes.

Accordingly to the elevated level of the SR, *in vitro* translation assay depicted increased ER transport efficiency of the SRP-dependent substrates, such as preprolactin and invariant chain (Figure 35). Sec61β, a tail-anchored protein, did not show a significant dependence on TMEM109 silencing (Figure 35). However, in an other study, Sec61β showed reduced transport efficiency when hSnd2 was depleted (Casson *et al.*, 2017). Cytochrome b5, which is only partially dependent on the TRC pathway, displayed reduced transport efficiency with UTR-1 and 4 siRNA treatment. However, the ER transport of the prestatherin, a short secretory protein, was improved with TMEM109 silencing; it could be due to the elevated abundance of the SR subunits and Sec61α as prestatherin has a cleavable SP. Prestatherin can be efficiently targeted by SRP, as well as post-translationally by the TRC pathway and it was desired to test whether it could be a substrate for the SND pathway. It showed a post-translational transport deficiency when hSnd2 was knocked down (Haßdenteufel *et al.*, 2018). Nonetheless, *in vitro* protein transport assays described in this work were carried out in co-translational mode. So post-translational *in vitro* transport of prestatherin would address the answer for that.

11.7.1 TMEM109 COMPLEMENTATION ASSAY

To address whether TMEM109 complementation can rescue the transport defect of cytochrome b5 after siRNA-mediated silencing of TMEM109, cells were transfected with a plasmid encoding for *TMEM109*. It induced the increased protein abundance of the SR subunits and Sec61α to descend back to normal or nearly normal levels (Figure 36). The increase in the transport efficiency of SRP-dependent substrates, the preprolactin, the invariant chain, and the partially SRP-dependent prestatherin was declined when TMEM109 was re-expressed (Figure 37). The transport efficiency of Sec61β was not influenced by the changes in the TMEM109 level. As well as, the transport efficiency of cytochrome b5 remained the same even when TMEM109 was complemented (Figure 37). This indicates that cytochrome b5 is not a solely SND-dependent substrate and is known to be able to use other transport pathways to get to the ER, such as the TRC pathway and unassisted membrane insertion (Borgese *et al.*, 2019; Brambillasca *et al.*, 2006). TMEM109 re-expression did not rescue the abundance of the Caml; however, the TMEM109 silencing itself caused a more pronounced decrease in its abundance (Figure 36) than previously (Figure 31).

Nevertheless, a mock sample has not been tested whether the transfection reagent itself could cause any change in the protein level of specific substrates. Moreover, the efficiency of TMEM109 re-expression exceeded the abundance that was detected in the control cells. Based on that, a very high level of TMEM109 does not necessarily contribute to the better transport efficiency of potential SND clients. Potentially, the abnormally high TMEM109 abundance could disrupt the complex interaction of the targeting pathways or affect its homo-oligomerization.

11.7.2 Simultaneous silencing of TMEM109 and WRB (TRC and SND pathway depletion)

As cytochrome b5 could depend on the TRC pathway in its ER transport, it was tested whether its transport efficiency could be aggravated when the SND and TRC pathway are simultaneously silenced. For that WRB and TMEM109 were concurrently depleted. The silencing of the two did not worsen the transport efficiency of cytochrome b5 (Figure 39), corroborating the fact for alternative ER transport pathways for cytochrome b5. In a previous study, the transport efficiency of cytochrome b5 displayed a more significant defect when hSnd2 and WRB were simultaneously silenced compared to control or single depletions (Haßdenteufel *et al.*, 2017).

Nonetheless, both TMEM109 and hSnd2 silencing resulted in reduced cytochrome b5 transport efficiency indicating the overlapping client spectrum between the TRC and the SND pathway. Single WRB depletion induced the elevated level of TMEM109 (Figure 38), suggesting a compensatory mechanism for having fewer TRC receptors in the ER membrane.

It would be informative to test the effect of cytochrome b5 transport efficiency when both TMEM109 and hSnd2 are depleted. Moreover, the depletion of SR subunits or Sec61α alongside the hSnd2/TMEM109 or WRB could also be tested, as cytochrome b5 could access the ER via the SRP-dependent pathway (Casson *et al.*, 2017).

11.7.3 The effect of knocking out TMEM109

A *TMEM109* knockout cell line was generated using the CRISPR-Cas9 system (Paragraph 9.19). DNA sequencing confirmed the single nucleotide insertion mutation in the *TMEM109* gene (Figure 15). With Western blot analysis, the loss of the TMEM109 protein was also verified (Figure 40B, C). However, the antibody designed against the TMEM109 recognizes the C-terminal end of the protein, which is not translated as a result of the insertion mutation downstream of the N-terminal end. It is also possible that the truncated protein product was still present in the cells.

Nevertheless, a truncated protein is likely to be recognized and labeled by ubiquitination and eliminated by the proteasome within the cells. Moreover, the mRNA level of *TMEM109* was detected in a significantly lower amount. Even though a single nucleotide insertion in the *TMEM109* DNA occurred, depending on where the RT-qPCR primers and probes recognize the *TMEM109* mRNA, a portion of the mRNA could still be detected.

TMEM109 knockout cells showed similar results to when TMEM109 was knocked down regarding the SR receptor subunits and Sec61α. However, a higher level of enhancement was observed in the case of the TMEM109 knockout sample regarding the SR subunits. In contrast to TMEM109 depleted samples, Caml was more abundant in the knockout sample (Figure 40B, C). This phenomenon is likely a compensatory mechanism, and the cells tried to compensate for the loss of the TMEM109 by enhancing the level of other targeting receptors.

Accordingly to the elevated SR abundance, the SRP-dependent substrate (preprolactin, invariant chain) transport was significantly improved (Figure 41). Cytochrome b5 transport showed slightly better transport efficiency; however, when TMEM109 was knocked down, it showed the opposite with UTR-1 and -4 siRNA treatment (Figure 34, Figure 35). This could be due to the fact that the TRC pathway receptor, the Caml, showed the associated higher abundance with TMEM109 knockout. It is known that cytochrome b5 can be transported to the ER by the TRC pathway; and maybe it can use the SND pathway for getting to the ER, possibly only under certain circumstances. Also, the cells might be well adjusted to the absence of the TMEM109 protein finding alternative pathways for cytochrome b5 transport as described in a previous paragraph; it cannot only depend on the TRC pathway.

It would be beneficial to test the substrate specificity of the SND pathway by using a substrate that better suits the model protein used in the assay when the pathway was identified in yeast cells (Aviram *et al.*, 2016). Using a model protein that has central TMD would be advantageous for this, as well as to test additional substrates that have been identified as potential SND substrates and described in more detail in Paragraph 11.10.

Western blot analysis of these possible substrates in the TMEM109 knockout cell line could also reveal if there is any difference in their abundance in comparison to the wild type.

11.8 TMEM109 AS A CALCIUM CHANNEL IN THE ENDOPLASMIC RETICULUM

TMEM109 has been described as a calcium channel in the ER membrane (Venturi *et al.*, 2011; Takeshima *et al.*, 2015). The ion selectivity of TMEM109 has been tested by patch-clamp technique, and the channel proved to be K^+ and Ca^{2+} selective. This was tested in microsomes derived from rabbit muscle SR vesicles (Venturi *et al.*, 2011). Cation conducting properties of TMEM109 could be due to the fact that it is capable of homo-oligomerization. Based on the luminescence protein-protein interaction assay, the C-terminal end of TMEM109 did not prove to be essential for homo-oligomerization (Figure 54). Based on spot peptide array results, presumably, the N-terminal Lys 46 or the Arg 47 localized in the ER lumen could be necessary for the homo-oligomerization of TMEM109 (Figure 54, Figure 55, Figure 56, Figure 57).

Live-cell calcium imaging confirmed the contribution of the TMEM109 to calcium homeostasis. TMEM109 silencing induced the significantly reduced overall calcium content after 72 hours of TMEM109 silencing with both TMEM109-UTR-1 and 4 siRNA treatment and in the case of UTR-4 siRNA treatment for 48 hours of silencing (Figure 43). 96 hours of hSnd2 silencing with hSnd2-UTR-3 siRNA caused a significant reduction in the calcium content (Figure 44). This could be due to the fact that hSnd2 silencing resulted in reduced TMEM109 abundance (Figure 6).

The ER-specific calcium leak unmasked by thapsigargin was decreased upon TMEM109 depletion (UTR-1 or 4 siRNA treatment after 60 and 72 hours of silencing (Figure 45)). Furthermore, hSnd2 silencing by UTR-3 siRNA induced significantly reduced ER calcium leakage (Figure 46). That is possibly, as written before, the effect of hSnd2 silencing that reduced the TMEM109 abundance.

Whether the lower calcium content is a direct or indirect effect of TMEM109 silencing requires further research. Western blot analysis of known ER calcium leak or release channels or plasma membrane calcium channels that maintain cellular calcium homeostasis could uncover the answer for that.

RNA sequencing results showed that in the case of TMEM109-UTR-1 siRNA treatment, it significantly lowered *ATP2A2* (encoding for SERCA2) and enhanced *SEC61A1* and *ATP2B4* (encoding for PMCA) expression (Figure 28A). This could also contribute to the lower ER and depleted cytosolic calcium content. In the case of hSnd2 silencing, reduced *SEC61A1* and *TMEM109* expression could result in a decreased ER-specific calcium leak. However, the *ATP2A2* displayed an increased expression (Figure 28B). As previously described, Western blot analysis of plasma membrane and ER membrane calcium channels and receptors would address the exact relation of TMEM109 to cellular calcium homeostasis.

TMEM109 knockout did not significantly affect the overall calcium content in the cells (Figure 47A). Contradictory to the results obtained after TMEM109 depletion, the knockout of TMEM109 significantly increased the ER calcium leak (Figure 47B). This phenomenon can be because the complete loss of TMEM109 might initiate a higher abundance of specific ER leak channels, e.g. Sec61α (Figure 40B, C). It is also possible that the cells adapted well to the loss of TMEM109 and

counterbalanced the cellular calcium homeostasis. However, the basal calcium level is comparable in TMEM109 knockdown and knockout cells; there is a discrepancy regarding the control cells for TMEM109 knockdown and knockout samples in respect of the ER-specific calcium leak (thapsigargin treatments) and the cellular calcium content (ionomycin treatments) excluding the basal calcium level (specified as Δ ratios). The control for the knockdown cells might contain a fundamentally higher organellar calcium content.

RNA sequencing of transcripts after *TMEM109* knockout could reveal the alterations compared to the TMEM109 depleted samples. Western blot analysis could unveil the underlying compensatory mechanisms in the level of proteins that are involved in the calcium homeostasis when TMEM109 is completely lacking in cells.

11.9 THE ACTIVATION OF THE SND PATHWAY

When a specific substrate with a proper targeting signal emerges, it activates the assigned pathway (Tirincsi *et al.*, 2021). In the case of the SND pathway, this signal possibly is a TMH downstream of the N-terminus of a nascent polypeptide chain (Aviram *et al.*, 2016). However, it can also be possible that it serves as a backup pathway and can complement the known ER targeting pathways for substrates with N-terminal, central, or C-terminal TMH; or is activated in response to disturbed cellular homeostasis. What underlying or additional factors could influence the activation of the SND pathway so far is not known.

hSnd2 has been found as a regulator of ER stress. Its overexpression negatively regulated the LC3-II level; LC3-II is known to be essential for autophagosome formation. Contradictory knockdown of hSnd2 promoted LC3-II accumulation. The overexpression of hSnd2 upon dithiothreitol-mediated ER stress, induced the accumulation of the autophagic substrate and downregulated the abundance of CHOP, a proapoptotic transcription factor (Zhao *et al.*, 2013). Nevertheless, the authors did not indicate how the dithiothreitol-induced ER stress affected the hSnd2 abundance. However, in this study, it was observed that the chemically induced ER stress by thapsigargin and tunicamycin increased the level of the hSnd2 (Figure 49). Nonetheless, it was not tested how thapsigargin and tunicamycin regulate the autophagosome formation or the LC3-II protein level.

It has been shown that there is an interaction between the Sec61 translocon and the Ire1α (Plumb *et al.*, 2015). This interaction could enhance the fidelity and efficiency of Ire1α on substrate mRNA cleavage during ER stress. A critical target of Ire1α is the *XBP1* mRNA. The translating *XBP1* mRNA could be efficiently targeted to the Sec61 bound Ire1α by SRP, probably due to translational stalling to allow efficient SRP interaction. This facilitates the cleavage of the *XBP1* mRNA by Ire1α (Plumb *et al.*, 2015). This work showed that ER stress and consequent UPR induction by thapsigargin and tunicamycin resulted in an increased abundance of the targeting receptors, such as SR and hSnd2 (Figure 49). The role of the SR in UPR is elucidated in the previous sentences. Since hSnd2 also shows interaction with the Sec61 translocon (Haßdenteufel *et al.*, 2017), there might be additional factors that influence Ire1α and *XBP1* mRNA interaction.

It is also possible that the SND pathway is activated under non-physiological conditions in cells. It might contribute to overcoming ER stress in cells on some level since hSnd2 also showed enhanced abundance upon chemically-induced ER stress (Figure 49). Contrariwise, TMEM109 did not show significantly increased abundance; only thapsigargin treatment caused its higher abundance (Figure 49). This cannot rule out that TMEM109 is part of the ER protein targeting. It would be interesting to see whether ER stress induction could cause a shift in the transport efficiency of putative SND pathway substrates when SND pathway components are knocked down or knocked out.

It also has been shown that hSnd2 has an oxygen-dependent prolyl hydroxylation motif, similar to HIF1α (Lei *et al.*, 2020). HIF1α is a critical component in sensing low oxygen concentrations within cells and initiates the transcription of specific mRNAs. The synthesis of these particular proteins helps the cells cope with low levels of oxygen. It had also been described in the same study that the *HSND2* promoter has HIF1α transcription factor binding sites.

Sequence analysis of the promoter region of the *TMEM109* gene was carried out. Figure 60A depicts multiple HIF1α transcription factor binding sites. Based on that, it is possible that the SND pathway is hypoxia-regulated and is becoming more prevalent or activated when oxygen is deprived. For example, chromatin immunoprecipitation combined with high throughput screening (ChIP-seq) would reveal experimentally proven HIF1α transcription factor binding sites in the *TMEM109* promoter region. Additionally, Western blot assays and ER transport efficiency determined by *in vitro* translation experiments after hypoxia induction would address whether the activation and activity of the SND pathway could be hypoxia dependent. However, it is worthwhile to note that TMEM109 has been shown to be upregulated in endometrial cancer (Kunitomi *et al.*, 2020) and in various types of cancerous diseases (https://v15.proteinatlas.org/ENSG00000110108-TMEM109/cancer). Generally speaking, a tumor microenvironment is hypoxic (Petrova *et al.*, 2018; Pouysségur *et al.*, 2006), which could relate to the findings that TMEM109 is upregulated in different tumors.

A

TSS… (+80) 5'-GTCGCA**CGTG**AAGG-3'….(+235) 5'- GCCCAG**CGTG**CGAA-3'…(+380) 5'- CCCGGG**CGTG**GGGA-3'…

(+1195) 5'- CTAGTC**CGTG**GCAC-3'…(+3577) 5'- TGCAGC**CGTG**ACCT-3'…

B

Figure 60. Putative HIF1α transcription factor binding sites in the *TMEM109* promoter gene sequence

Putative HIF1α transcription factor binding sites were found downstream from the transcription start site (TSS) in the promoter region of the *TMEM109* gene (A). In panel B, the sequence logo displays the HIF1α transcription factor binding sites, featuring that CGTG bases are critical for efficient binding.

11.10 SUBSTRATE SPECIFICITY OF THE SND PATHWAY

No *bona fide* substrate has been identified for the SND pathway so far in human cells. When hSnd2 was described as part of the human SND pathway, it was found that it could complement the TRC pathway and could aid the ER transport of single-pass transmembrane proteins with less hydrophobic C-terminal targeting signals (Haßdenteufel *et al.*, 2017). This work also observed an overlap regarding the substrate specificity between the TRC and the SND pathway. The model protein, cytochrome b5, with a TMH lower than average hydrophobicity, demonstrated reduced ER transport efficiency when TMEM109 and TMEM109 plus WRB were knocked down (Figure 39).

Recent findings indicate that hSnd2 can aid the ER targeting of glycophosphatidylinositol (GPI) anchored proteins (GPI-APs) (Yang *et al.*, 2021). The C-terminal GPI attachment signal sequence (GPIAS) is essential for ER targeting since it is known that GPI-APs are dependent on the TRC pathway. However, it has been found that the N-terminal SP on GPI-APs also has a role in ER targeting by the hSnd2. It was also described that the cell surface expression of GPI-APs with lower than average hydrophobicity was reduced when hSnd2 was knocked out. However, it remains unclear whether the GPI-APs are targeted to the ER co- or post-translationally (Yang *et al.*, 2021).

These GPI-APs with reduced hydrophobicity, CD55, CD59, and CD109, were found in the mRNA sequencing database obtained from the experiment described in Paragraph 9.11. They showed reduced expression after *TMEM109* and *HSND2* silencing (results are not displayed). Contradictory, the CD55 showed enhanced expression after *HSND2* depletion (results are not displayed). Nevertheless, based on these results, it would be beneficial to test these substrates' *in vitro* ER transport efficiency after TMEM109 and hSnd2 depletion.

In another study based on genome-wide CRISPR screening, it has been elucidated that TRPC6, a multipass transmembrane protein with a "late" first TMH, requires hSnd2 over EMC for an efficient expression (Talbot *et al.*, 2019). They identified that other multi-spanning membrane proteins (KCNN4, a six-transmembrane domain protein, and SLC12A4, a five-transmembrane domain protein) also need hSnd2 for their topogenesis; however, single-span membrane proteins were not affected. Although mass spectrometry results after co-immunoprecipitation assay identified an interaction between Snd2 and EMC proteins (Aviram *et al.*, 2016), neither EMC nor hSnd2 loss affected the abundance of the other (Talbot *et al.*, 2019), suggesting they do not work together.

The topology of TMEM109 is similar to the EMC3, the WRB/Get1insertases, and the TMCO1 translocon complex (Paragraph 7.9). These proteins are involved in membrane protein biogenesis. TMCO1 is not only part of the translocon complex and aids membrane protein biogenesis, but it also has a role in calcium homeostasis. Findings in this work confirm that TMEM109 also has a dual role, such as TMCO1, which is involved in protein biogenesis and calcium homeostasis. Based on that, it is also possible that TMEM109 is just another auxiliary factor of the translocon.

A common feature of these studies is that substrates with less hydrophobic TMD appear dependent on hSnd2, thus, on the SND pathway. However, more research would address the exact nature of the SND-specific substrates. For example, the amino acid substitution of model proteins to initiate lower hydrophobicity in their TMH could reveal the changes in their *in vitro* ER transport efficiency.

It is also imaginable that a soluble component in human cells guides the SND substrate to the membrane-bound components of the pathway, similar to the yeast counterpart, where Snd1 is a ribosome-associated protein (Aviram *et al.*, 2016). In yeast cells, it has also been described that it is likely that the Snd2 and Snd3 hand off the protein to the translocon for ER delivery (Aviram *et al.*, 2016). Alphafold structural predictions *in silico* identified a hydrophilic vestibule in the structure of the yeast Snd2 and Snd3 (Liaci and Förster, 2021), which could be reminiscent of the hydrophilic substrate-binding pocket of the TMD of the WRB/Caml insertase. So far, it is not known whether the hSnd2 and hSnd3 use the Sec61 translocon for substrate insertion into the ER or if they have insertase activity.

11.11 CONCLUDING REMARKS

Protein targeting to the ER is a complex process. It involves many receptors and soluble proteins to deliver specific protein clients to the endoplasmic reticulum. The choice of targeting is greatly influenced by the hydrophobicity of the targeting signal and the location of this targeting peptide within a protein's primary structure. The concentration of certain soluble proteins and the abundance of the targeting receptors could also play an essential role in optimal targeting.

In the past decades, novel modes of ER transport and auxiliary factors have been described that help and extend the functionality of the translocon to insert specific substrates. It is also possible that the targeting pathways complement each other to reach the translocation to its maximum extent.

Both hSnd2 and TMEM109 depletion resulted in a similar outcome in human cells; they resulted in compensatory SR elevation so that improved SRP-dependent substrate ER transport was observed. Depleting both hSnd2 and TMEM109 caused the significantly reduced transport efficiency of a less hydrophobic C-terminal tail-anchored protein. Furthermore, results in this work confirmed crosstalk between the TRC and the SND pathway. There is also a physical interaction between hSnd2 and TMEM109. Based on these results, it is likely that TMEM109 is part of the SND pathway; however, it is also possible that it is just an additional factor for the translocon. Nonetheless, no *bona fide* SND substrate has been described in human cells. It is also imaginable that the SND pathway serves as a backup protein transport pathway. It is also probable that it is activated under nonphysiological conditions.

The picture that features protein conduction to the endoplasmic reticulum is broader than it was believed decades ago. Getting a panoramic view of protein targeting to the endoplasmic reticulum is an interesting and challenging scientific project, and future studies will address it.

12 APPENDIX

12.1 RNA SEQUENCING AFTER TMEM109 SILENCING

Table 7. Up-regulation or down-regulation of specific genes after 60 hours of *TMEM109* silencing in comparison to control siRNA treatment (Paragraph 10.5)

siRNA treatment	Genes annotated to	Category of GO	Significant regulation	Number of genes affected
TMEM109-UTR-1	rRNA metabolic process	BP	up-regulation	83
TMEM109-UTR-1	regulation of symbiosis, encompassing mutualism through parasitism	BP	up-regulation	69
TMEM109-UTR-1	regulation of viral process	BP	up-regulation	66
TMEM109-UTR-1	transcription coactivator activity	MF	up-regulation	95
TMEM109-UTR-1	promoter-specific chromatin binding	MF	up-regulation	22
TMEM109-UTR-1	histone binding	MF	up-regulation	87
TMEM109-UTR-1	ciliary basal body	CC	up-regulation	48
TMEM109-UTR-1	nucleolar part	CC	up-regulation	59
TMEM109-UTR-1	transcription factor complex	CC	up-regulation	94
TMEM109-UTR-1	liposaccharide metabolic process	BP	down-regulation	40
TMEM109-UTR-1	positive regulation of cell motility	BP	down-regulation	130
TMEM109-UTR-1	response to endoplasmic reticulum stress	BP	down-regulation	85
TMEM109-UTR-1	transferase activity, transferring hexosyl groups	MF	down-regulation	60
TMEM109-UTR-1	virus receptor activity	MF	down-regulation	26
TMEM109-UTR-1	hijacked molecular function	MF	down-regulation	26
TMEM109-UTR-1	membrane raft	CC	down-regulation	81
TMEM109-UTR-1	membrane microdomain	CC	down-regulation	81
TMEM109-UTR-1	membrane region	CC	down-regulation	83
TMEM109-UTR-3	entry into host cell	BP	up-regulation	51
TMEM109-UTR-3	entry into cell of other organism involved in symbiotic interaction	BP	up-regulation	51

TMEM109-UTR-3	protein targeting to ER	BP	up-regulation	49
TMEM109-UTR-3	phosphatase binding	MF	up-regulation	66
TMEM109-UTR-3	structural constituent of ribosome	MF	up-regulation	60
TMEM109-UTR-3	ATPase regulator activity	MF	up-regulation	21
TMEM109-UTR-3	endoplasmic reticulum lumen	CC	up-regulation	93
TMEM109-UTR-3	Golgi-associated vesicle	CC	up-regulation	62
TMEM109-UTR-3	cytosolic ribosome	CC	up-regulation	44
TMEM109-UTR-3	monosaccharide metabolic process	BP	down-regulation	78
TMEM109-UTR-3	generation of precursor metabolites and energy	BP	down-regulation	131
TMEM109-UTR-3	autophagy	BP	down-regulation	127
TMEM109-UTR-3	cofactor binding	MF	down-regulation	117
TMEM109-UTR-3	protein kinase C activity	MF	down-regulation	10
TMEM109-UTR-3	glucocorticoid receptor binding	MF	down-regulation	10
TMEM109-UTR-3	mitochondrial matrix	CC	down-regulation	124
TMEM109-UTR-3	ubiquitin ligase complex	CC	down-regulation	78
TMEM109-UTR-3	organelle membrane contact site	CC	down-regulation	11
TMEM109-UTR-4	positive regulation of cell adhesion	BP	up-regulation	80
TMEM109-UTR-4	antigen processing and presentation of exogenous peptide antigen via MHC class I, TAP-dependent	BP	up-regulation	26
TMEM109-UTR-4	regulation of mRNA metabolic process	BP	up-regulation	73
TMEM109-UTR-4	cell-cell adhesion mediator activity	MF	up-regulation	18
TMEM109-UTR-4	actin filament binding	MF	up-regulation	44
TMEM109-UTR-4	integrin binding	MF	up-regulation	31
TMEM109-UTR-4	cytoplasmic vesicle lumen	CC	up-regulation	65
TMEM109-UTR-4	secretory granule lumen	CC	up-regulation	61
TMEM109-UTR-4	mitochondrial inner membrane	CC	up-regulation	94
TMEM109-UTR-4	No significant down-regulation for any genes.			

Numbers of genes from RNA sequencing results affected by TMEM109 silencing by the different siRNAs. Genes that are up- or downregulated are annotated to molecular functions (MF), biological processes (BP), and cellular components (CC).

12.2 COOMASSIE GEL STAINING

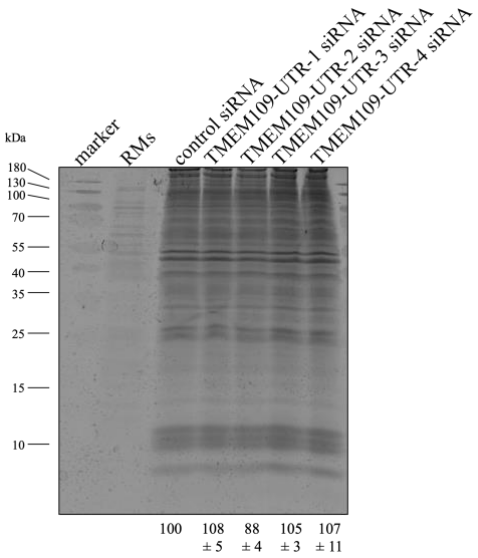

Figure 61. Coomassie gel staining after TMEM109 silencing (supplementary material to the results in Paragraph 10.6)

After 60 hours of TMEM109 siRNA-mediated silencing, samples were harvested and prepared for Western blot and *in vitro* translation analysis. 10 µl of the Western blot samples were loaded into 10 % SDS polyacrylamide gel and stained with Coomassie dye after SDS-PAGE (see Paragraph 9.13). Numbers indicate the total percentage of protein content in comparison to control; one representative gel is shown here out of three independently repeated experiments.

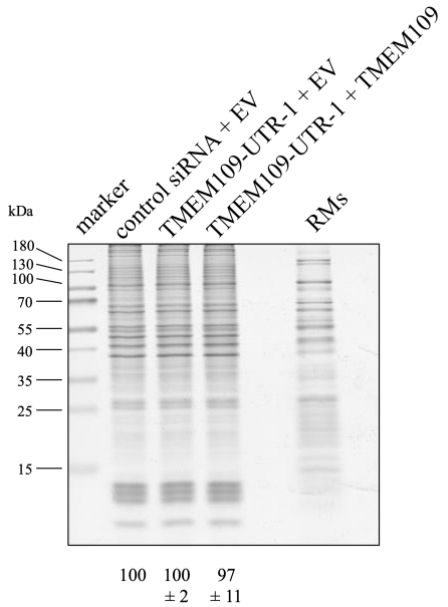

Figure 62. Coomassie gel staining for TMEM109 complementation assay (supplementary material to the results in Paragraph 10.7)

After 40 hours of TMEM109 siRNA-mediated silencing, an empty vector and TMEM109 expression plasmid were added, and samples were harvested and prepared for Western blot and *in vitro* translation analysis. 10 µl of the Western blot samples were loaded into 10 % SDS polyacrylamide gel and stained with Coomassie dye after SDS-PAGE (see Paragraph 9.13). Numbers indicate the total percentage of protein content in comparison to control; one representative gel is shown here out of three independently repeated experiments.

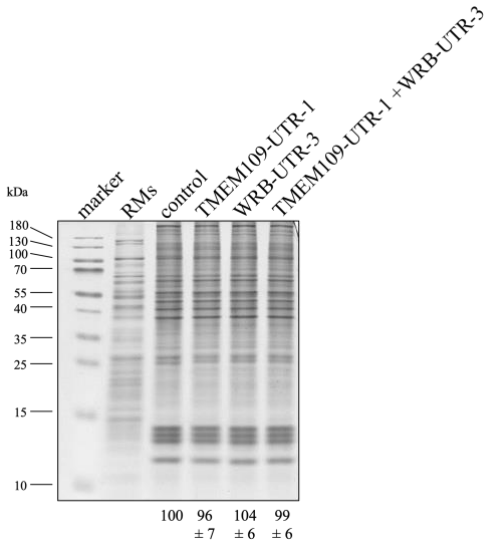

Figure 63. Coomassie gel staining for TMEM109 and WRB simultaneous silencing (supplementary material to the results in Paragraph 10.8)

After TMEM109 and WRB silencing and simultaneous silencing of the two, cells were harvested and prepared for Western blot and *in vitro* translation analysis after 72 hours. Samples were loaded into 10 % SDS polyacrylamide gel and stained with coomassie dye (see Paragraph 9.13). Numbers indicate the total percentage of protein content in comparison to control; one representative gel is shown here out of four independently repeated experiments.

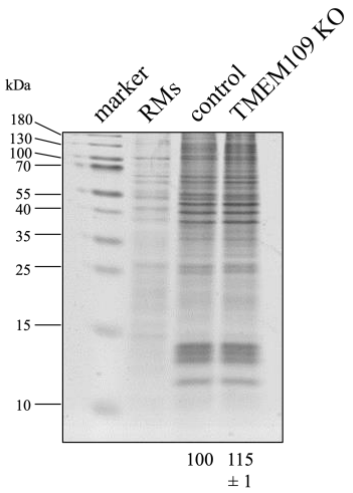

Figure 64. Coomassie gel staining for TMEM109 knockout (supplementary material to the results in Paragraph 10.9)

TMEM109 knockout and control cells were harvested and prepared for Western blot and *in vitro* translation analysis. 10 µl of the Western blot samples were loaded into 10 % SDS polyacrylamide gel and stained with Coomassie dye after SDS-PAGE (see Paragraph 9.13). Numbers indicate the total percentage of protein content in comparison to control; one representative gel is shown here out of three independently repeated experiments.

12.3 CALCIUM IMAGING AFTER HSND2 SILENCING

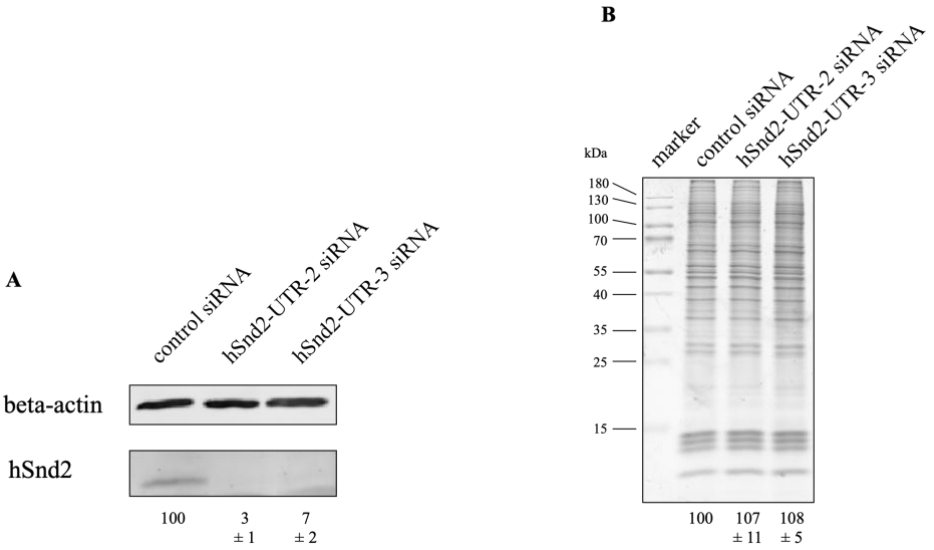

Figure 65. The efficiency of hSnd2 silencing after 96 hours (supplementary material to the results in Paragraph 10.11)

Samples were prepared for calcium imaging, as described in Paragraph 9.20. The remaining cells in the culture dish were harvested for Western blot analysis (see 9.12). A) Numbers indicate the relative protein abundance in comparison to control. One representative blot is shown here out of a minimum of three repeated experiments.
B) 10 µl of the Western blot samples were loaded into 10 % SDS polyacrylamide gel and stained with Coomassie dye after SDS-PAGE (see Paragraph 9.13). Numbers indicate the total percentage of protein content in comparison to control; one representative gel is shown here out of three repeated experiments.

13 REFERENCES

Abeele Vanden, F., Bidaux, G., Gordienko, D., Beck, B., Panchin, Y. V., Baranova, A. V., Ivanov, D. V., Skryma, R., Prevarskaya, N. (2006) Functional implications of calcium permeability of the channel formed by pannexin 1. *Journal of Cell Biology*. 174(4): 535–546.

Akopian, D., Shen, K., Zhang, X., Shan, S.O. (2013) Signal Recognition Particle: An Essential Protein-Targeting Machine. *Annual Review of Biochemistry*. 82(1): 693–721.

Alberts, B., Johnson, A., Lewis, J., Morgan, D., Raff, M., Roberts, K., Walter, P. (2015) *Molecular Biology of the Cell*. 6th ed. Garland Science Pub., 431–433.

Alvira, S., Corey, R.A., Collinson, I., Römisch, K. (2021) Membrane protein biogenesis by the EMC. *The EMBO Journal*. 40(2): 2020–2022.

Anghel, S.A., McGilvray, P.T., Hegde, R.S., Keenan, R.J. (2017) Identification of Oxa1 Homologs Operating in the Eukaryotic Endoplasmic Reticulum. *Cell Reports*. 21(13): 3708–3716.

Arnold, A., Horst, S.A., Gardella, T.J., Baba, H., Levine, M.A., Kronenberg, H.M. (1990) Mutation of the signal peptide-encoding region of the preproparathyroid hormone gene in familial isolated hypoparathyroidism. *Journal of Clinical Investigation*. 86(4): 1084–1087.

Aronin, N. (2006) Target selectivity in mRNA silencing. *Gene Therapy*. 13(6): 509–516.

Asseck, L.Y., Mehlhorn, D.G., Monroy, J.R., Ricardi, M.M., Breuninger, H., Wallmeroth, N., Berendzen, K.W., Nowrousian, M., Xing, S., Schwappach, B., Bayer, M., Grefen, C. (2021) Endoplasmic reticulum membrane receptors of the GET pathway are conserved throughout eukaryotes. *Proceedings of the National Academy of Sciences of the United States of America*. 118(1): 1–9.

Ast, T., Cohen, G., Schuldiner, M. (2013) A network of cytosolic factors targets SRP-independent proteins to the endoplasmic reticulum. *Cell*. 152(5): 1134–1145.

Avendaño-Monsalve, M.C., Ponce-Rojas, J.C., Funes, S. (2020) From cytosol to mitochondria: The beginning of a protein journey. *Biological Chemistry*. 401(6–7): 645–661.

Aviram, N., Ast, T., Costa, E.A., Arakel, E.C., Chuartzman, S.G., Jan, C.H., Haßdenteufel, S., Dudek, J., Jung, M., Schorr, S., Zimmermann, R., Schwappach, B., Weissman, J.S., Schuldiner, M. (2016) The SND proteins constitute an alternative targeting route to the endoplasmic reticulum. *Nature*. 540(7631): 134–138.

Bai, L., You, Q., Feng, X., Kovach, A., Li, H. (2020) Structure of the ER membrane complex, a transmembrane-domain insertase. *Nature*. 584(7821): 475–478.

Ben-Shem, A., Jenner, L., Yusupova, G., Yusupov, M. (2010) Crystal Structure of the Eukaryotic Ribosome. *Science*. 330(6008): 1203–1209.

Berbey, C., Weiss, N., Legrand, C., Allard, B. (2009) Transient Receptor Potential Canonical Type 1 (TRPC1) Operates as a Sarcoplasmic Reticulum Calcium Leak Channel in Skeletal Muscle. *Journal of Biological Chemistry*. 284(52): 36387–36394.

Berg, B. van den, Clemons, W.M., Collinson, I., Modis, Y., Hartmann, E., Harrison, S.C., Rapoport, T.A. (2004) X-ray structure of a protein-conducting channel. *Nature*. 427(6969): 36–44.

Berridge, M.J., Lipp, P., Bootman, M.D. (2000) The versatility and universality of calcium signalling. *Nature Reviews*. 1: 11–21.

Birgisdottir, Å.B., Lamark, T., Johansen, T. (2013) The LIR motif – crucial for selective autophagy. *Journal of Cell Science*. 126(15): 3237–3247.

Blobel, G., Sabatini, D.D. (1971) Ribosome-Membrane Interaction in Eukaryotic Cells. *Biomembranes*. 2: 193–195.

Borgese, N. (2020) Searching for remote homologs of CAML among eukaryotes. *Traffic*. 21(10): 647–658.

Borgese, N., Colombo, S., Pedrazzini, E. (2003) The tale of tail-anchored proteins: Coming from the cytosol and looking for a membrane. *Journal of Cell Biology*. 161(6): 1013–1019.

Borgese, N., Coy-Vergara, J., Colombo, S.F., Schwappach, B. (2019) The Ways of Tails: the GET Pathway and more. *Protein Journal*. 38(3): 289–305.

Bostina, M., Mohsin, B., Kühlbrandt, W., Collinson, I. (2005) Atomic model of the E. coli membrane-bound protein translocation complex SecYEG. *Journal of Molecular Biology*. 352(5): 1035–1043.

Brambillasca, S., Yabal, M., Makarow, M., Borgese, N. (2006) Unassisted translocation of large polypeptide domains across phospholipid bilayers. *Journal of Cell Biology*. 175(5): 767–777.

Brambillasca, S., Yabal, M., Soffientini, P., Stefanovic, S., Makarow, M., Hegde, R.S., Borgese, N. (2005) Transmembrane topogenesis of a tail-anchored protein is modulated by membrane lipid composition. *EMBO Journal*. 24(14): 2533–2542.

Bremser, M., Nickel, W., Schweikert, M., Ravazzola, M., Amherdt, M., Hughes, C.A., Söllner, T.H., Rothman, J.E., Wieland, F.T. (1999) Coupling of Coat Assembly and Vesicle Budding to Packaging of Putative Cargo Receptors. *Cell*. 96(4): 495–506.

Breyton, C., Haase, W., Rapoport, T.A., Kuhlbrandt, W., Collinson, I. (2002) Three-dimensional structure of the bacterial protein-translocation complex SecYEG. *Nature*. 418(6898): 662–665.

Burnette, W.N. (1981) "Western Blotting": Electrophoretic transfer of proteins from sodium dodecyl sulfate-polyacrylamide gels to unmodified nitrocellulose and radiographic detection with antibody and radioiodinated protein A. *Analytical Biochemistry*. 112(2): 195–203.

Casson, J., McKenna, M., Haßdenteufel, S., Aviram, N., Zimmerman, R., High, S. (2017) Multiple pathways facilitate the biogenesis of mammalian tail-anchored proteins. *Journal of Cell Science*. 130(22): 3851–3861.

Chami, M., Prandini, A., Campanella, M., Pinton, P., Szabadkai, G., Reed, J.C., Rizzuto, R. (2004) Bcl-2 and Bax Exert Opposing Effects on Ca2+ Signaling, Which Do Not Depend on Their Putative Pore-forming Region. *Journal of Biological Chemistry*. 279(52): 54581–54589.

Chen, Y. (2004) SPD--a web-based secreted protein database. *Nucleic Acids Research*. 33(1093): D169–D173.

Chio, U.S., Cho, H., Shan, S. (2017) Mechanisms of Tail-Anchored Membrane Protein Targeting and Insertion. *Annual Review of Cell and Developmental Biology*. 33(1): 417–438.

Chitwood, P.J., Hegde, R.S. (2020) An intramembrane chaperone complex facilitates membrane protein biogenesis. *Nature*. 584(7822): 630–634.

Clapham, D.E. (2007) Calcium Signaling. *Cell*. 131(6): 1047–1058.

Colombo, S.F., Cardani, S., Maroli, A., Vitiello, A., Soffientini, P., Crespi, A., Bram, R.F., Benfante, R., Borgese, N. (2016) Tail-anchored Protein Insertion in Mammals. *Journal of Biological Chemistry*. 291(29): 15292–15306.

Crick, F. (1970) Central Dogma of Molecular Biology. *Nature*. 227(5258): 561–563.

Culver, J.A., Mariappan, M. (2020) Membrane Protein Biogenesis: PAT Complex Pats Membrane Proteins into Shape. *Current Biology*. 30(22): R1387–R1389.

Davydova, E., Shimazu, T., Schuhmacher, M.K., Jakobsson, M.E., Willemen, H.L.D.M., Liu, T., Moen, A., Ho, A.Y.Y., Małecki, J., Schroer, L., Pinto, R., Suzuki, T., Grønsberg, I.A., Sohtome, Y., Akakabe, M., Weirich, S., Kikuchi, M., Olsen, J. V., Dohmae, N., Umehara, T., Sodeoka, M., Siino, V., McDonough, M.A., Eijkelkamp, N., Schofield, C.J., Jeltsch, A., Shinkai, Y., Falnes, P.Ø. (2021) The methyltransferase METTL9 mediates pervasive 1-methylhistidine modification in mammalian proteomes. *Nature Communications*. 12(1): 891.

Denzer, A.J., Nabholz, C.E., Spiess, M. (1995) Transmembrane orientation of signal-anchor proteins is affected by the folding state but not the size of the N-terminal domain. *The EMBO journal*. 14(24): 6311–6317.

Devaraneni, P.K., Conti, B., Matsumura, Y., Yang, Z., Johnson, A.E., Skach, W.R. (2011) Stepwise Insertion and Inversion of a Type II Signal Anchor Sequence in the Ribosome-Sec61 Translocon Complex. *Cell*. 146(1): 134–147.

Dixon, A.S., Schwinn, M.K., Hall, M.P., Zimmerman, K., Otto, P., Lubben, T.H., Butler, B.L., Binkowski, B.F., MacHleidt, T., Kirkland, T.A., Wood, M.G., Eggers, C.T., Encell, L.P., Wood, K. V. (2016) NanoLuc Complementation Reporter Optimized for Accurate Measurement of Protein Interactions in Cells. *ACS Chemical Biology*. 11(2): 400–408.

Donnell, J.P.O., Phillips, B.P., Yagita, Y., Juszkiewicz, S., Wagner, A., Malinverni, D., Keenan, R.J., Miller, E.A., Hegde, R.S. (2020) The architecture of EMC reveals a path for membrane protein insertion. 9(57887): 1–30.

Dowhan, W., Bogdanov, M. (2009) Lipid-Dependent Membrane Protein Topogenesis. *Annual Review of Biochemistry*. 78(1): 515–540.

Dremina, E.S., Sharov, V.S., Kumar, K., Zaidi, A., Michaelis, E.K., Schöneich, C. (2004) Anti-apoptotic protein Bcl-2 interacts with and destabilizes the sarcoplasmic/endoplasmic reticulum Ca2+-ATPase (SERCA). *Biochemical Journal*. 383(2): 361–370.

Duc, K.D., Batra, S.S., Bhattacharya, N., Cate, J.H.D., Song, Y.S. (2019) Differences in the path to exit the ribosome across the three domains of life. *Nucleic Acids Research*. 47(8): 4198–4210.

Erdmann, F., Schäuble, N., Lang, S., Jung, M., Honigmann, A., Ahmad, M., Dudek, J., Benedix, J., Harsman, A., Kopp, A., Helms, V., Cavalié, A., Wagner, R., Zimmermann, R. (2011) Interaction of calmodulin with Sec61alpha limits Ca2+ leakage from the endoplasmic reticulum. *EMBO Journal*. 30(1): 17–31.

Fagerberg, L., Jonasson, K., Von Heijne, G., Uhlén, M., Berglund, L. (2010) Prediction of the human membrane proteome. *Proteomics*. 10(6): 1141–1149.

Farkas, Á., De Laurentiis, E.I., Schwappach, B. (2019) The natural history of Get3-like chaperones. *Traffic*. 20(5): 311–324.

Favaloro, V., Spasic, M., Schwappach, B., Dobberstein, B. (2008) Distinct targeting pathways for the membrane insertion of tail-anchored (TA) proteins. *Journal of Cell Science*. 121(11): 1832–1840.

Favaloro, V., Vilardi, F., Schlecht, R., Mayer, M.P., Dobberstein, B. (2010) Asna1/TRC40-mediated membrane insertion of tail-anchored proteins. *Journal of Cell Science*. 123(9): 1522–1530.

Fedyukina, D. V., Cavagnero, S. (2011) Protein Folding at the Exit Tunnel. *Annual Review of Biophysics*. 40(1): 337–359.

Fu, Y.H.H., Chandrasekar, S., Lee, J.H., Shan, S.O. (2019) A molecular recognition feature mediates ribosome-induced SRP-receptor assembly during protein targeting. *Journal of Cell Biology*. 218(10): 3307–3319.

Fuller, C.W., Middendorf, L.R., Benner, S.A., Church, G.M., Harris, T., Huang, X., Jovanovich, S.B., Nelson, J.R., Schloss, J.A., Schwartz, D.C., Vezenov, D. V. (2009) The challenges of sequencing by synthesis. *Nature Biotechnology*. 27(11): 1013–1023.

Fumagalli, F., Noack, J., Bergmann, T.J., Cebollero, E., Pisoni, G.B., Fasana, E., Fregno, I., Galli, C., Loi, M., Soldà, T., D'Antuono, R., Raimondi, A., Jung, M., Melnyk, A., Schorr, S., Schreiber, A., Simonelli, L., Varani, L., Wilson-Zbinden, C., Zerbe, O., Hofmann, K., Peter, M., Quadroni, M., Zimmermann, R., Molinari, M. (2016) Translocon component Sec62 acts in endoplasmic reticulum turnover during stress recovery. *Nature Cell Biology*. 18(11): 1173–1184.

Gamerdinger, M., Kobayashi, K., Wallisch, A., Kreft, S.G., Sailer, C., Schlömer, R., Sachs, N., Jomaa, A., Stengel, F., Ban, N., Deuerling, E. (2019) Early Scanning of Nascent Polypeptides inside the Ribosomal Tunnel by NAC. *Molecular Cell*. 75(5): 996-1006.e8.

Ge, Y., Wang, C., Hu, F., Pan, L., Min, J., Niu, K., Zhang, L., Li, J., Xu, T. (2018) New advances of TMEM88 in cancer initiation and progression, with special emphasis on Wnt signaling pathway. *Journal of Cellular Physiology*. 233(1): 79–87.

Gemmer, M., Förster, F. (2020) A clearer picture of the ER translocon complex. *Journal of Cell Science*.

133(3): jcs231340.

Gray, M.W. (2013) Organelles. *Brenner's Encyclopedia of Genetics: Second Edition*. 17(2): 181–183.

Guha, P., Kaptan, E., Gade, P., Kalvakolanu, D. V., Ahmed, H. (2017) Tunicamycin induced endoplasmic reticulum stress promotes apoptosis of prostate cancer cells by activating mTORC1. *Oncotarget*. 8(40): 68191–68207.

Guna, A., Volkmar, N., Christianson, J.C., Hegde, R.S. (2018) The ER membrane protein complex is a transmembrane domain insertase. *Science*. 359(6374): 470–473.

Guth, S., Völzing, C., Müller, A., Jung, M., Zimmermann, R. (2004) Protein transport into canine pancreatic microsomes. *European Journal of Biochemistry*. 271(15): 3200–3207.

Halic, M., Beckmann, R. (2005) The signal recognition particle and its interactions during protein targeting. *Current Opinion in Structural Biology*. 15(1): 116–125.

Hamman, B.D., Hendershot, L.M., Johnson, A.E. (1998) BiP Maintains the Permeability Barrier of the ER Membrane by Sealing the Lumenal End of the Translocon Pore before and Early in Translocation. *Cell*. 92(6): 747–758.

Hann, B.C., Walter, P. (1991) The signal recognition particle in S. cerevisiae. *Cell*. 67(1): 131–144.

Harada, Y., Ohkawa, Y., Kizuka, Y., Taniguchi, N. (2019) Oligosaccharyltransferase: A gatekeeper of health and tumor progression. *International Journal of Molecular Sciences*. 20(23): 1–14.

Hasan, S., Platta, H.W., Erdmann, R. (2013) Import of proteins into the peroxisomal matrix. *Frontiers in Physiology*. 4(261): 1–12.

Haßdenteufel, S., Johnson, N., Paton, A.W., Paton, J.C., High, S., Zimmermann, R. (2018) Chaperone-Mediated Sec61 Channel Gating during ER Import of Small Precursor Proteins Overcomes Sec61 Inhibitor-Reinforced Energy Barrier. *Cell Reports*. 23(5): 1373–1386.

Haßdenteufel, S., Sicking, M., Schorr, S., Aviram, N., Fecher-Trost, C., Schuldiner, M., Jung, M., Zimmermann, R., Lang, S. (2017) hSnd2 protein represents an alternative targeting factor to the endoplasmic reticulum in human cells. *FEBS Letters*. 591(20): 3211–3224.

Hegde, R.S., Keenan, R.J. (2011) Tail-anchored membrane protein insertion into the endoplasmic reticulum. *Nature Reviews Molecular Cell Biology*. 12(12): 787–798.

Hegde, R.S., Keenan, R.J. (2021) The mechanisms of integral membrane protein biogenesis. *Nature Reviews Molecular Cell Biology*. 23(2): 107–124.

Hoth, M., Penner, R. (1992) Depletion of intracellular calcium stores activates a calcium current in mast cells. *Nature*. 355(6358): 353–356.

Hsieh, H.-H., Lee, J.H., Chandrasekar, S., Shan, S. (2020) A ribosome-associated chaperone enables substrate triage in a cotranslational protein targeting complex. *Nature Communications*. 11(1): 5840.

Hu, R., Hu, F., Xie, X., Wang, L., Li, G., Qiao, T., Wang, M., Xiao, H. (2016) TMEM45B, up-regulated in human lung cancer, enhances tumorigenicity of lung cancer cells. *Tumor Biology*. 37(9): 12181–12191.

Illumina Inc. (2017) Illumina sequencing introduction. *Illumina sequencing introduction*. Pub No. 77, 1–15.

Ismail, N., Crawshaw, S.G., High, S. (2006) Active and passive displacement of transmembrane domians both occur during opsin biogenesis at the Sec61 translocon. *Journal of Cell Science*. 119(13): 2826–2836.

Itskanov, S., Kuo, K.M., Gumbart, J.C., Park, E. (2021) Stepwise gating of the Sec61 protein-conducting channel by Sec63 and Sec62. *Nature Structural and Molecular Biology*. 28(2): 162–172.

Jackson, R.J., Hellen, C.U.T., Pestova, T. V. (2010) The mechanism of eukaryotic translation initiation and principles of its regulation. *Nature Reviews Molecular Cell Biology*. 11(2): 113–127.

Janda, C.Y., Li, J., Oubridge, C., Hernández, H., Robinson, C. V., Nagai, K. (2010) Recognition of a signal peptide by the signal recognition particle. *Nature*. 465(7297): 507–510.

Janoschke, M., Zimmermann, M., Brunauer, A., Humbel, R., Junne, T., Spiess, M. (2021) Efficient integration of transmembrane domains depends on the folding properties of the upstream sequences. *Proceedings of the National Academy of Sciences of the United States of America*. 118(33): 1–10.

Johnson, N., Vilardi, F., Lang, S., Leznicki, P., Zimmermann, R., High, S. (2012) TRC40 can deliver short secretory proteins to the Sec61 translocon. *Journal of Cell Science*. 125(18): 4414–4414.

Jonikas, M.C., Collins, S.R., Denic, V., Oh, E., Quan, E.M., Schmid, V., Weibezahn, J., Schwappach, B., Walter, P., Weissman, J.S., Schuldiner, M. (2009) Comprehensive characterization of genes required for protein folding in the endoplasmic reticulum. *Science*. 323(5922): 1693–1697.

Kamiya, T., Hara, H., Adachi, T. (2013) Effect of endoplasmic reticulum (ER) stress inducer thapsigargin on the expression of extracellular-superoxide dismutase in mouse 3T3-L1 adipocytes. *Journal of Clinical Biochemistry and Nutrition*. 52(2): 101–105.

Ke, N., Wang, X., Xu, X., Abassi, Y.A. (2011) The xCELLigence system for real-time and label-free monitoring of cell viability. *Methods in molecular biology (Clifton, N.J.)*. 740: 33–43.

Killian, J.A. (1998) Hydrophobic mismatch between proteins and lipids in membranes. *Biochimica et Biophysica Acta (BBA) - Reviews on Biomembranes*. 1376(3): 401–416.

Klein, M.-C., Zimmermann, K., Schorr, S., Landini, M., Klemens, P.A.W., Altensell, J., Jung, M., Krause, E., Nguyen, D., Helms, V., Rettig, J., Fecher-Trost, C., Cavalié, A., Hoth, M., Bogeski, I., Neuhaus, H.E., Zimmermann, R., Lang, S., Haferkamp, I. (2018) AXER is an ATP/ADP exchanger in the membrane of the endoplasmic reticulum. *Nature Communications*. 9(1): 3489.

Kosolapov, A., Deutsch, C. (2009) Tertiary interactions within the ribosomal exit tunnel. *Nature Structural and Molecular Biology*. 16(4): 405–411.

Kriegler, T., Kiburg, G., Hessa, T. (2020) Translocon-Associated Protein Complex (TRAP) is Crucial

for Co-Translational Translocation of Pre-Proinsulin. *Journal of Molecular Biology*. 432(24): 166694.

Kunitomi, H., Kobayashi, Y., Wu, R.-C., Takeda, T., Tominaga, E., Banno, K., Aoki, D. (2020) LAMC1 is a prognostic factor and a potential therapeutic target in endometrial cancer. *Journal of Gynecologic Oncology*. 31(2): 1–11.

Kutay, U., Ahnert-Hilger, G., Hartmann, E., Wiedenmann, B., Rapoport, T.A. (1995) Transport route for synaptobrevin via a novel pathway of insertion into the endoplasmic reticulum membrane. *EMBO Journal*. 14(2): 217–223.

Kutay, U., Hartmann, E., Rapoport, T. (1993) A class of membrane proteins with a C-terminal anchor. *Trends in Cell Biology*. 3(3): 72–75.

Lakkaraju, A.K.K., Thankappan, R., Mary, C., Garrison, J.L., Taunton, J., Strub, K. (2012) Efficient secretion of small proteins in mammalian cells relies on Sec62-dependent posttranslational translocation R. S. Hegde, ed. *Molecular Biology of the Cell*. 23(14): 2712–2722.

Landry, J.J.M., Pyl, P.T., Rausch, T., Zichner, T., Tekkedil, M.M., Stütz, A.M., Jauch, A., Aiyar, R.S., Pau, G., Delhomme, N., Gagneur, J., Korbel, J.O., Huber, W., Steinmetz, L.M. (2013) The Genomic and Transcriptomic Landscape of a HeLa Cell Line. *G3 Genes|Genomes|Genetics*. 3(8): 1213–1224.

Lang, S., Benedix, J., Fedeles, S. V., Schorr, S., Schirra, C., Schäuble, N., Jalal, C., Greiner, M., Haßdenteufel, S., Tatzelt, J., Kreutzer, B., Edelmann, L., Krause, E., Rettig, J., Somlo, S., Zimmermann, R., Dudek, J. (2012) Different effects of Sec61α, Sec62 and Sec63 depletion on transport of polypeptides into the endoplasmic reticulum of mammalian cells. *Journal of Cell Science*. 125(8): 1958–1969.

Lang, S., Erdmann, F., Jung, M., Wagner, R., Cavalié, A., Zimmermann, R. (2011) Sec61 complexes form ubiquitous ER Ca(2+) leak channels. *Channels*. 5(4): 228–235.

Lang, S., Pfeffer, S., Lee, P.-H., Cavalié, A., Helms, V., Förster, F., Zimmermann, R. (2017) An Update on Sec61 Channel Functions, Mechanisms, and Related Diseases. *Frontiers in Physiology*. 8(887): 1–22.

Lee, J.H., Chandrasekar, S., Chung, S.Y., Fu, Y.H.H., Liu, D., Weiss, S., Shan, S.O. (2018) Sequential activation of human signal recognition particle by the ribosome and signal sequence drives efficient protein targeting. *Proceedings of the National Academy of Sciences of the United States of America*. 115(24): E5487–E5496.

Lee, J.W., Ko, J., Ju, C., Eltzschig, H.K. (2019) Hypoxia signaling in human diseases and therapeutic targets. *Experimental and Molecular Medicine*. 51(6): 1–13.

Lei, P., Xiao, Y., Li, P., Xie, P., Wang, H., Huang, S., Song, P., Zhao, Y. (2020) hSnd2/TMEM208 is an HIF-1α-targeted gene and contains a WH2 motif. *Acta Biochimica et Biophysica Sinica*. 52(3): 328–331.

Lemos, F.O., Bultynck, G., Parys, J.B. (2021) A comprehensive overview of the complex world of the endo- and sarcoplasmic reticulum Ca2+-leak channels. *Biochimica et Biophysica Acta (BBA) - Molecular Cell Research*. 1868(7): 119020.

Leznicki, P., High, S. (2020) SGTA associates with nascent membrane protein precursors. *EMBO*

reports. 21(5): e48835.

Liaci, A.M., Förster, F. (2021) Take Me Home, Protein Roads: Structural Insights into Signal Peptide Interactions during ER Translocation. *International Journal of Molecular Sciences*. 22(21): 11871.

Liaci, A.M., Steigenberger, B., Telles de Souza, P.C., Tamara, S., Gröllers-Mulderij, M., Ogrissek, P., Marrink, S.J., Scheltema, R.A., Förster, F. (2021) Structure of the human signal peptidase complex reveals the determinants for signal peptide cleavage. *Molecular Cell*. 81(19): 3934-3948.e11.

Liao, S., Lin, J., Do, H., Johnson, A.E. (1997) Both lumenal and cytosolic gating of aqueous ER translocon pore are regulated from inside the ribosome during membrane protein integration. *Cell*. 90(1): 31–41.

Lin, J.H., Walter, P., Yen, T.S.B. (2008) Endoplasmic reticulum stress in disease pathogenesis. *Annual Review of Pathology: Mechanisms of Disease*. 3: 399–425.

Lindner, P., Christensen, S.B., Nissen, P., Møller, J.V., Engedal, N. (2020) Cell death induced by the ER stressor thapsigargin involves death receptor 5, a non-autophagic function of MAP1LC3B, and distinct contributions from unfolded protein response components. *Cell Communication and Signaling*. 18(1): 1–23.

Ling, M.-L., Risman, S.S., Klement, J.F., McGraw, N., McAllister, W.T. (1989) Abortive initiation by bacteriophage T3 and T7 RNA polymerases under conditions of limiting substrate. *Nucleic Acids Research*. 17(4): 1605–1618.

Linxweiler, M., Schick, B., Zimmermann, R. (2017) Let's talk about secs: Sec61, sec62 and sec63 in signal transduction, oncology and personalized medicine. *Signal Transduction and Targeted Therapy*. 2(17002): 1–10.

Liu, H., Naismith, J.H. (2008) An efficient one-step site-directed deletion, insertion, single and multiple-site plasmid mutagenesis protocol. *BMC Biotechnology*. 8(1): 91.

Losfeld, M.E., Ng, B.G., Kircher, M., Buckingham, K.J., Turner, E.H., Eroshkin, A., Smith, J.D., Shendure, J., Nickerson, D.A., Bamshad, M.J., Freeze, H.H. (2014) A new congenital disorder of glycosylation caused by a mutation in SSR4, the signal sequence receptor 4 protein of the TRAP complex. *Human Molecular Genetics*. 23(6): 1602–1605.

Loveland, A.B., Demo, G., Korostelev, A.A. (2020) Cryo-EM of elongating ribosome with EF-Tu•GTP elucidates tRNA proofreading. *Nature*. 584(7822): 640–645.

Lu, J., Deutsch, C. (2008) Electrostatics in the Ribosomal Tunnel Modulate Chain Elongation Rates. *Journal of Molecular Biology*. 384(1): 73–86.

Lu, J., Deutsch, C. (2005) Folding zones inside the ribosomal exit tunnel. *Nature Structural and Molecular Biology*. 12(12): 1123–1129.

Lu, J., Kobertz, W.R., Deutsch, C. (2007) Mapping the Electrostatic Potential within the Ribosomal Exit Tunnel. *Journal of Molecular Biology*. 371(5): 1378–1391.

Martoglio, B., Dobberstein, B. (1998) Signal sequences: More than just greasy peptides. *Trends in Cell*

Biology. 8(10): 410–415.

Mateja, A., Paduch, M., Chang, H.-Y., Szydlowska, A., Kossiakoff, A.A., Hegde, R.S., Keenan, R.J. (2015) Structure of the Get3 targeting factor in complex with its membrane protein cargo. *Science*. 347(6226): 1152–1155.

McDowell, M.A., Heimes, M., Fiorentino, F., Mehmood, S., Farkas, Á., Coy-Vergara, J., Wu, D., Bolla, J.R., Schmid, V., Heinze, R., Wild, K., Flemming, D., Pfeffer, S., Schwappach, B., Robinson, C. V., Sinning, I. (2020) Structural Basis of Tail-Anchored Membrane Protein Biogenesis by the GET Insertase Complex. *Molecular Cell*. 80(1): 72-86.e7.

McGilvray, P.T., Anghel, S.A., Sundaram, A., Zhong, F., Trnka, M.J., Fuller, J.R., Hu, H., Burlingame, A.L., Keenan, R.J. (2020) An ER translocon for multi-pass membrane protein biogenesis. *eLife*. 9(56889): 1–43.

Meacock, S.L., Lecomte, F.J.L., Crawshaw, S.G., High, S. (2002) Different Transmembrane Domains Associate with Distinct Endoplasmic Reticulum Components during Membrane Integration of a Polytopic Protein R. Gilmore, ed. *Molecular Biology of the Cell*. 13(12): 4114–4129.

Mekahli, D., Bultynck, G., Parys, J.B., de Smedt, H., Missiaen, L. (2011) Endoplasmic-reticulum calcium depletion and disease. *Cold Spring Harbor Perspectives in Biology*. 3(6): 1–30.

Misselwitz, B., Staeck, O., Rapoport, T.A. (1998) J Proteins Catalytically Activate Hsp70 Molecules to Trap a Wide Range of Peptide Sequences. *Molecular Cell*. 2(5): 593–603.

Mukhopadhyay, R., Ho, Y.-S., Swiatek, P.J., Rosen, B.P., Bhattacharjee, H. (2006) Targeted disruption of the mouse Asna1 gene results in embryonic lethality. *FEBS Letters*. 580(16): 3889–3894.

Nagai, K., Oubridge, C., Kuglstatter, A., Menichelli, E., Isel, C., Jovine, L. (2003) Structure, function and evolution of the signal recognition particle. *EMBO Journal*. 22(14): 3479–3485.

Neuhoff, V., Stamm, R., Eibl, H. (1985) Clear background and highly sensitive protein staining with Coomassie Blue dyes in polyacrylamide gels: A systematic analysis. *Electrophoresis*. 6(9): 427–448.

Ng, B.G., Raymond, K., Kircher, M., Buckingham, K.J., Wood, T., Shendure, J., Nickerson, D.A., Bamshad, M.J., Wong, J.T.S., Monteiro, F.P., Graham, B.H., Jackson, S., Sparkes, R., Scheuerle, A.E., Cathey, S., Kok, F., Gibson, J.B., Freeze, H.H. (2015) Expanding the Molecular and Clinical Phenotype of SSR4-CDG. *Human Mutation*. 36(11): 1048–1051.

O'Brien, E.P., Hsu, S.T.D., Christodoulou, J., Vendruscolo, M., Dobson, C.M. (2010) Transient tertiary structure formation within the ribosome exit port. *Journal of the American Chemical Society*. 132(47): 16928–16937.

O'Donnell, J.P., Phillips, B.P., Yagita, Y., Juszkiewicz, S., Wagner, A., Malinverni, D., Keenan, R.J., Miller, E.A., Hegde, R.S. (2020) The architecture of EMC reveals a path for membrane protein insertion V. Dötsch, ed. *eLife*. 9: e57887.

O'Keefe, S., Pool, M.R., High, S. (2021) Membrane protein biogenesis at the ER: the highways and byways. *FEBS Journal*, 1–28.

O'Keefe, S., Zong, G., Duah, K.B., Andrews, L.E., Shi, W.Q., High, S. (2021) An alternative pathway for membrane protein biogenesis at the endoplasmic reticulum. *Communications Biology*. 4(1): 828.

Ogg, S.C., Barz, W.P., Walter, P. (1998) A Functional GTPase Domain, but not its Transmembrane Domain, is Required for Function of the SRP Receptor β-subunit. *Journal of Cell Biology*. 142(2): 341–354.

Ogg, S.C., Poritz, M.A., Walter, P. (1992) Signal recognition particle receptor is important for cell growth and protein secretion in Saccharomyces cerevisiae. *Molecular Biology of the Cell*. 3(8): 895–911.

Orzáez, M., Pérez-Payá, E., Mingarro, I. (2000) Influence of the C-terminus of the glycophorin A transmembrane fragment on the dimerization process. *Protein Science*. 9(6): 1246–1253.

Paetzel, M., Karla, A., Strynadka, N.C.J., Dalbey, R.E. (2002) Signal Peptidases. *Chemical Reviews*. 102(12): 4549–4580.

Palade, G. (1975) Intracellular Aspects of the Process of Protein Synthesis. *Science*. 189(4200): 347–358.

Palade, G.E., Siekevitz, P. (1956) Liver microsomes; an integrated morphological and biochemical study. *The Journal of biophysical and biochemical cytology*. 2(2): 171–200.

Petrova, V., Annicchiarico-Petruzzelli, M., Melino, G., Amelio, I. (2018) The hypoxic tumour microenvironment. *Oncogenesis*. 7(1): 10.

Pfeffer, S., Dudek, J., Schaffer, M., Ng, B.G., Albert, S., Plitzko, J.M., Baumeister, W., Zimmermann, R., Freeze, H.H., Engel, B.D., Förster, F. (2017) Dissecting the molecular organization of the translocon-associated protein complex. *Nature Communications*. 8(14516): 1–9.

Phillips, M.J., Voeltz, G.K. (2016) Structure and function of ER membrane contact sites with other organelles. *Nature Reviews Molecular Cell Biology*. 17(2): 69–82.

Phoomak, C., Cui, W., Hayman, T.J., Yu, S.H., Zhao, P., Wells, L., Steet, R., Contessa, J.N. (2021) The translocon-associated protein (TRAP) complex regulates quality control of N-linked glycosylation during ER stress. *Science Advances*. 7(3): 6364.

Pinton, P., Rizzuto, R. (2006) Bcl-2 and Ca2+ homeostasis in the endoplasmic reticulum. *Cell Death & Differentiation*. 13(8): 1409–1418.

Plumb, R., Zhang, Z.-R., Appathurai, S., Mariappan, M. (2015) A functional link between the co-translational protein translocation pathway and the UPR. *eLife*. 4: 1–18.

Pouysségur, J., Dayan, F., Mazure, N.M. (2006) Hypoxia signalling in cancer and approaches to enforce tumour regression. *Nature*. 441(7092): 437–443.

Ran, F.A., Hsu, P.D., Wright, J., Agarwala, V., Scott, D.A., Zhang, F. (2013) Genome engineering using the CRISPR-Cas9 system. *Nature protocols*. 8(11): 2281–2308.

Rapoport, T.A. (2007) Protein translocation across the eukaryotic endoplasmic reticulum and bacterial

plasma membranes. *Nature*. 450(7170): 663–669.

Reilly-O'Donnell, B., Robertson, G.B., Karumbi, A., McIntyre, C., Bal, W., Nishi, M., Takeshima, H., Stewart, A.J., Pitt, S.J. (2017) Dysregulated Zn2 homeostasis impairs cardiac type-2 ryanodine receptor and mitsugumin 23 functions, leading to sarcoplasmic reticulum Ca2 leakage. *Journal of Biological Chemistry*. 292(32): 13361–13373.

Renart, J., Reiser, J., Stark, G.R. (1979) Transfer of proteins from gels to diazobenzyloxymethyl-paper and detection with antisera: a method for studying antibody specificity and antigen structure. *Proceedings of the National Academy of Sciences*. 76(7): 3116–3120.

Rizzuto, R., De Stefani, D., Raffaello, A., Mammucari, C. (2012) Mitochondria as sensors and regulators of calcium signalling. *Nature Reviews Molecular Cell Biology*. 13(9): 566–578.

Roe, M.., Lemasters, J.., Herman, B. (1990) Assessment of Fura-2 for measurements of cytosolic free calcium. *Cell Calcium*. 11(2–3): 63–73.

Ruiz-Canada, C., Kelleher, D.J., Gilmore, R. (2009) Cotranslational and Posttranslational N-Glycosylation of Polypeptides by Distinct Mammalian OST Isoforms. *Cell*. 136(2): 272–283.

Sabatini, D.D. (2014) Subcellular fractionation of rough microsomes. *Cold Spring Harbor Protocols*. 2014(9): 932–934.

Sato, M., Hresko, R., Mueckler, M. (1998) Testing the Charge Difference Hypothesis for the Assembly of a Eucaryotic Multispanning Membrane Protein. *Journal of Biological Chemistry*. 273(39): 25203–25208.

Schäuble, N., Lang, S., Jung, M., Cappel, S., Schorr, S., Ulucan, O., Linxweiler, J., Dudek, J., Blum, R., Helms, V., Paton, A.W., Paton, J.C., Cavalie, A., Zimmermann, R. (2012) BiP-mediated closing of the Sec61 channel limits Ca2+ leakage from the ER. *EMBO Journal*. 31(15): 3282–3296.

Schjoldager, K.T., Narimatsu, Y., Joshi, H.J., Clausen, H. (2020) Global view of human protein glycosylation pathways and functions. *Nature Reviews Molecular Cell Biology*. 21(12): 729–749.

Schmit, K., Michiels, C. (2018) TMEM Proteins in Cancer: A Review. *Frontiers in Pharmacology*. 9(1345): 1–13.

Schoebel, S., Mi, W., Stein, A., Ovchinnikov, S., Pavlovicz, R., DImaio, F., Baker, D., Chambers, M.G., Su, H., Li, D., Rapoport, T.A., Liao, M. (2017) Cryo-EM structure of the protein-conducting ERAD channel Hrd1 in complex with Hrd3. *Nature*. 548(7667): 352–355.

Schorr, S., Nguyen, D., Haßdenteufel, S., Nagaraj, N., Cavalié, A., Greiner, M., Weissgerber, P., Loi, M., Paton, A.W., Paton, J.C., Molinari, M., Förster, F., Dudek, J., Lang, S., Helms, V., Zimmermann, R. (2020) Identification of signal peptide features for substrate specificity in human Sec62/Sec63-dependent ER protein import. *The FEBS Journal*. 287(21): 4612–4640.

Schuchman, E.H., Suchi, M., Takahashi, T., Sandhoff, K., Desnick, R.J. (1991) Human acid sphingomyelinase. Isolation, nucleotide sequence and expression of the full-length and alternatively spliced cDNAs. *The Journal of biological chemistry*. 266(13): 8531–9.

Schuller, A.P., Green, R. (2018) Roadblocks and resolutions in eukaryotic translation. *Nature Reviews Molecular Cell Biology*. 19(8): 526–541.

Schwarz, D.S., Blower, M.D. (2016) The endoplasmic reticulum: Structure, function and response to cellular signaling. *Cellular and Molecular Life Sciences*. 73(1): 79–94.

Semenza, G.L. (2012) Hypoxia-inducible factors in physiology and medicine. *Cell*. 148(3): 399–408.

Shao, S., Hegde, Ramanujan S. (2011) A Calmodulin-Dependent Translocation Pathway for Small Secretory Proteins. *Cell*. 147(7): 1576–1588.

Shao, S., Hegde, Ramanujan S (2011) Membrane Protein Insertion at the Endoplasmic Reticulum. *Annual Review of Cell and Developmental Biology*. 27(1): 25–56.

Shen, K., Yu, W., Yu, Y., Liu, X., Cui, X. (2018) Knockdown of TMEM45B inhibits cell proliferation and invasion in gastric cancer. *Biomedicine & Pharmacotherapy*. 104(1016): 576–581.

Shurtleff, M.J., Itzhak, D.N., Hussmann, J.A., Schirle Oakdale, N.T., Costa, E.A., Jonikas, M., Weibezahn, J., Popova, K.D., Jan, C.H., Sinitcyn, P., Vembar, S.S., Hernandez, H., Cox, J., Burlingame, A.L., Brodsky, J., Frost, A., Borner, G.H.H., Weissman, J.S. (2018) The ER membrane protein complex interacts cotranslationally to enable biogenesis of multipass membrane proteins. *eLife*. 7: e37018.

Sicking, M., Jung, M., Lang, S. (2021) Lights, Camera, Interaction: Studying Protein–Protein Interactions of the ER Protein Translocase in Living Cells. *International Journal of Molecular Sciences*. 22(19): 10358.

Simpson, P.J., Schwappach, B., Dohlman, H.G., Isaacson, R.L. (2010) Structures of Get3, Get4, and Get5 Provide New Models for TA Membrane Protein Targeting. *Structure*. 18(8): 897–902.

Sitron, C.S., Brandman, O. (2020) Detection and Degradation of Stalled Nascent Chains via Ribosome-Associated Quality Control. *Annual Review of Biochemistry*. 89(1): 417–442.

Skach, W.R. (2007) The expanding role of the ER translocon in membrane protein folding. *The Journal of Cell Biology*. 179(7): 1333–1335.

Sparr, E., Ash, W.L., Nazarov, P. V., Rijkers, D.T.S., Hemminga, M.A., Tieleman, D.P., Killian, J.A. (2005) Self-association of Transmembrane α-Helices in Model Membranes. *Journal of Biological Chemistry*. 280(47): 39324–39331.

Stefanovic, S., Hegde, R.S. (2007) Identification of a Targeting Factor for Posttranslational Membrane Protein Insertion into the ER. *Cell*. 128(6): 1147–1159.

Takeshima, H., Venturi, E., Sitsapesan, R. (2015) New and notable ion-channels in the sarcoplasmic/endoplasmic reticulum: do they support the process of intracellular Ca2+ release? *The Journal of Physiology*. 593(15): 3241–3251.

Talbot, B.E., Vandorpe, D.H., Stotter, B.R., Alper, S.L., Schlondorff, J.S. (2019) Transmembrane insertases and N-glycosylation critically determine synthesis, trafficking, and activity of the nonselective cation channel TRPC6. *Journal of Biological Chemistry*. 294(34): 12655–12669.

Tamborero, S., Vilar, M., Martínez-Gil, L., Johnson, A.E., Mingarro, I. (2011) Membrane Insertion and Topology of the Translocating Chain-Associating Membrane Protein (TRAM). *Journal of Molecular Biology*. 406(4): 571–582.

Thomson, S.M., Pulido, P., Jarvis, R.P. (2020) Protein import into chloroplasts and its regulation by the ubiquitin-proteasome system. *Biochemical Society Transactions*. 48(1): 71–82.

Tirincsi, A., Sicking, M., Hadzibeganovic, D., Haßdenteufel, S., Lang, S. (2021) The Molecular Biodiversity of Protein Targeting and Protein Transport Related to the Endoplasmic Reticulum. *International Journal of Molecular Sciences*. 23(1): 143.

Towbin, H., Staehelin, T., Gordon, J. (1979) Electrophoretic transfer of proteins from polyacrylamide gels to nitrocellulose sheets: procedure and some applications. *Proceedings of the National Academy of Sciences*. 76(9): 4350–4354.

Tsai, B., Ye, Y., Rapoport, T.A. (2002) Retro-translocation of proteins from the endoplasmic reticulum into the cytosol. *Nat Rev Mol Cell Biol*. 3(4): 246–255.

Tsai, C.J., Sauna, Z.E., Kimchi-Sarfaty, C., Ambudkar, S. V., Gottesman, M.M., Nussinov, R. (2008) Synonymous Mutations and Ribosome Stalling Can Lead to Altered Folding Pathways and Distinct Minima. *Journal of Molecular Biology*. 383(2): 281–291.

Tyedmers, J., Lerner, M., Bies, C., Dudek, J., Skowronek, M.H., Haas, I.G., Heim, N., Nastainczyk, W., Volkmer, J., Zimmermann, R. (2000) Homologs of the yeast Sec complex subunits Sec62p and Sec63p are abundant proteins in dog pancreas microsomes. *Proceedings of the National Academy of Sciences*. 97(13): 7214–7219.

Valm, A.M., Cohen, S., Legant, W.R., Melunis, J., Hershberg, U., Wait, E., Cohen, A.R., Davidson, M.W., Betzig, E., Lippincott-Schwartz, J. (2017) Applying systems-level spectral imaging and analysis to reveal the organelle interactome. *Nature*. 546(7656): 162–167.

Venkatachalam, K., Montell, C. (2007) TRP Channels. *Annual Review of Biochemistry*. 76(1): 387–417.

Venters, B.J., Pugh, B.F. (2009) How eukaryotic genes are transcribed regulation of eukaroytic gene transcription B. J. Venters and B. F. Pugh. *Critical Reviews in Biochemistry and Molecular Biology*. 44(2–3): 117–141.

Venturi, E., Mio, K., Nishi, M., Ogura, T., Moriya, T., Pitt, S.J., Okuda, K., Kakizawa, S., Sitsapesan, R., Sato, C., Takeshima, H. (2011) Mitsugumin 23 Forms a Massive Bowl-Shaped Assembly and Cation-Conducting Channel. *Biochemistry*. 50(13): 2623–2632.

Vishnu, N., Jadoon Khan, M., Karsten, F., Groschner, L.N., Waldeck-Weiermair, M., Rost, R., Hallström, S., Imamura, H., Graier, W.F., Malli, R. (2014) ATP increases within the lumen of the endoplasmic reticulum upon intracellular Ca2+ release. *Molecular Biology of the Cell*. 25(3): 368–379.

Voeltz, G.K., Rolls, M.M., Rapoport, T.A. (2002) Structural organization of the endoplasmic reticulum. *EMBO Reports*. 3(10): 944–950.

Voigt, S., Jungnickel, B., Hartmann, E., Rapoport, T.A. (1996) Signal sequence-dependent function of the TRAM protein during early phases of protein transport across the endoplasmic reticulum membrane.

The Journal of Cell Biology. 134(1): 25–35.

Voorhees, R.M., Fernández, I.S., Scheres, S.H.W., Hegde, R.S. (2014) Structure of the Mammalian Ribosome-Sec61 Complex to 3.4 Å Resolution. *Cell*. 157(7): 1632–1643.

Voorhees, R.M., Hegde, R.S. (2016) Structure of the Sec61 channel opened by a signal sequence. *Science*. 351(6268): 88–91.

Wakasugi, K., Slike, B.M., Hood, J., Otani, A., Ewalt, K.L., Friedlander, M., Cheresh, D.A., Schimmel, P. (2002) A human aminoacyl-tRNA synthetase as a regulator of angiogenesis. *Proceedings of the National Academy of Sciences*. 99(1): 173–177.

Walter, P., Ibrahimi, I., Blobel, G. (1981) Translocation of proteins across the endoplasmic reticulum. I. Signal recognition protein (SRP) binds to in-vitro-assembled polysomes synthesizing secretory protein. *Journal of Cell Biology*. 91(2): 545–550.

Wang, F., Chan, C., Weir, N.R., Denic, V. (2014) The Get1/2 transmembrane complex is an endoplasmic-reticulum membrane protein insertase. *Nature*. 512(7515): 441–444.

Wang, Q.-C., Zheng, Qiaoxia, Tan, H., Zhang, B., Li, X., Yang, Y., Yu, J., Liu, Y., Chai, H., Wang, X., Sun, Z., Wang, J.-Q., Zhu, S., Wang, F., Yang, M., Guo, C., Wang, H., Zheng, Qingyin, Li, Y., Chen, Q., Zhou, A., Tang, T.-S. (2016) TMCO1 Is an ER Ca 2+ Load-Activated Ca 2+ Channel. *Cell*. 165(6): 1454–1466.

Weng, T., Steinchen, W., Beatrix, B., Berninghausen, O., Becker, T., Bange, G., Cheng, J., Beckmann, R. (2020) Architecture of the active post-translational Sec translocon. *The EMBO Journal*. 40(3): 1–12.

Wild, K., Juaire, K.D., Soni, K., Shanmuganathan, V., Hendricks, A., Segnitz, B., Beckmann, R., Sinning, I. (2019) Reconstitution of the human SRP system and quantitative and systematic analysis of its ribosome interactions. *Nucleic Acids Research*. 47(6): 3184–3196.

Wilson, D.N., Beckmann, R. (2011) The ribosomal tunnel as a functional environment for nascent polypeptide folding and translational stalling. *Current Opinion in Structural Biology*. 21(2): 274–282.

Woolhead, C.A., McCormick, P.J., Johnson, A.E. (2004) Nascent membrane and secretory proteins differ in FRET-detected folding far inside the ribosome and in their exposure to ribosomal proteins. *Cell*. 116(5): 725–736.

Wruck, F., Tian, P., Kudva, R., Best, R.B., von Heijne, G., Tans, S.J., Katranidis, A. (2021) The ribosome modulates folding inside the ribosomal exit tunnel. *Communications Biology*. 4(1): 1–8.

Wu, J., Chen, S., Liu, H., Zhang, Z., Ni, Z., Chen, J., Yang, Z., Nie, Y., Fan, D. (2018) Tunicamycin specifically aggravates ER stress and overcomes chemoresistance in multidrug-resistant gastric cancer cells by inhibiting N-glycosylation. *Journal of Experimental and Clinical Cancer Research*. 37(1): 1–12.

Wu, X., Siggel, M., Ovchinnikov, S., Mi, W., Svetlov, V., Nudler, E., Liao, M., Hummer, G., Rapoport, T.A. (2020) Structural basis of ER-associated protein degradation mediated by the Hrd1 ubiquitin ligase complex. *Science*. 368(6489): 1–13.

Xing, S., Mehlhorn, D.G., Wallmeroth, N., Asseck, L.Y., Kar, R., Voss, A., Denninger, P., Schmidt, V.A.F., Schwarzländer, M., Stierhof, Y.D., Grossmann, G., Grefen, C. (2017) Loss of GET pathway orthologs in Arabidopsis thaliana causes root hair growth defects and affects SNARE abundance. *Proceedings of the National Academy of Sciences of the United States of America*. 114(8): E1544–E1553.

Yamamoto, Y., Sakisaka, T. (2012) Molecular Machinery for Insertion of Tail-Anchored Membrane Proteins into the Endoplasmic Reticulum Membrane in Mammalian Cells. *Molecular Cell*. 48(3): 387–397.

Yamashita, A., Taniwaki, T., Kaikoi, Y., Yamazaki, T. (2013) Protective role of the endoplasmic reticulum protein mitsugumin23 against ultraviolet C-induced cell death. *FEBS Letters*. 587(9): 1299–1303.

Yamazaki, T., Sasaki, N., Nishi, M., Takeshima, H. (2010) Facilitation of DNA damage-induced apoptosis by endoplasmic reticulum protein mitsugumin23. *Biochemical and Biophysical Research Communications*. 392(2): 196–200.

Yang, J., Hirata, T., Liu, Y., Guo, X., Gao, X., Kinoshita, T., Fujita, M. (2021) Human SND2 mediates ER targeting of GPI-anchored proteins with low hydrophobic GPI attachment signals S. Sonnino, ed. *FEBS Letters*. 595(11): 1542–1558.

Yuan, J.P., Zeng, W., Huang, G.N., Worley, P.F., Muallem, S. (2007) STIM1 heteromultimerizes TRPC channels to determine their function as store-operated channels. *Nature Cell Biology*. 9(6): 636–645.

Yusupova, G., Yusupov, M. (2017) Crystal structure of eukaryotic ribosome and its complexes with inhibitors. *Philosophical Transactions of the Royal Society B: Biological Sciences*. 372(1716): 20160184.

Zhang, Y., Berndt, U., Gölz, H., Tais, A., Oellerer, S., Wölfle, T., Fitzke, E., Rospert, S. (2012) NAC functions as a modulator of SRP during the early steps of protein targeting to the endoplasmic reticulum J. L. Brodsky, ed. *Molecular Biology of the Cell*. 23(16): 3027–3040.

Zhang, Y., De Laurentiis, E., Bohnsack, K.E., Wahlig, M., Ranjan, N., Gruseck, S., Hackert, P., Wölfle, T., Rodnina, M. V., Schwappach, B., Rospert, S. (2021) Ribosome-bound Get4/5 facilitates the capture of tail-anchored proteins by Sgt2 in yeast. *Nature Communications*. 12(1): 1–17.

Zhao, Y., Hu, J., Miao, G., Qu, L., Wang, Z., Li, G., Lv, P., Ma, D., Chen, Y. (2013) Transmembrane Protein 208: A Novel ER-Localized Protein That Regulates Autophagy and ER Stress. *PLoS ONE*. 8(5): e64228.

Zheng, S., Zhou, L., Ma, G., Zhang, T., Liu, Jindou, Li, J., Nguyen, N.T., Zhang, X., Li, W., Nwokonko, R., Zhou, Y., Zhao, F., Liu, Jingguo, Huang, Y., Gill, D.L., Wang, Y. (2018) Calcium store refilling and STIM activation in STIM- and Orai-deficient cell lines. *European Journal of Physiology*. 470(10): 1555–1567.

Zimmermann, R., Eyrisch, S., Ahmad, M., Helms, V. (2011) Protein translocation across the ER membrane. *Biochimica et Biophysica Acta*. 1808(3): 912–924.

14 PUBLICATIONS

PUBLICATIONS THAT WERE PUBLISHED DURING THE DOCTORAL STUDIES

Andrea Tirincsi*, Sarah O'Keefe*, Duy Nguyen*, Mark Sicking, Johanna Dudek, Friedrich Förster, Martin Jung, Drazena Hadzibeganovic, Volkhard Helms, Stephen High, Richard Zimmermann and Sven Lang (2022) Proteomics identifies substrates and a novel component in hSnd2-dependent ER protein targeting. *bioRxiv-Preprint*

* These authors contributed equally to this work.

Mark Sicking, Martina Živná, Pratiti Bhadra, Veronika Barešová, **Andrea Tirincsi**, Drazena Hadzibeganovic, Kateřina Hodaňová, Petr Vyleťal, Jana Sovová, Ivana Jedličkova, Martin Jung, Thomas Bell, Volkhard Helms, Anthony Bleyer, Stanislav Kmoch, Adolfo Cavalié and Sven Lang (2022) Phenylbutyrate rescues the transport defect of the Sec61α mutations V67G and T185A for renin. *Life Science Alliance* 5(4): e202101150.

Andrea Tirincsi, Mark Sicking, Drazena Hadzibeganovic, Sarah Haßdenteufel and Sven Lang (2021) The Molecular Biodiversity of Protein Targeting and Protein Transport Related to the Endoplasmic Reticulum. *International Journal of Molecular Sciences*. 23(1): 143.

15 ACKNOWLEDGMENTS

I would like to express my sincere gratitude to my supervisor Dr. Sven Lang, who gave me the opportunity to complete my Ph.D. study at the Saarland University. All achievements in this study would not have been possible without his support and scientific advice.

I am grateful for all the scientific recommendations from Professor Dr. Richard Zimmermann that elevated the quality of this work.

I would also like to express my deepest appreciation to the Homburger Forschungsförderungsprogramm (HOMFOR) research foundation for all their financial contribution to this project.

Individually, I would like to thank Professor Dr. Martin Jung and Sabine Pelvay for the generation of the antibodies. I would also like to express my appreciation to Karsten Mayr and Professor Dr. Martin Jung for performing the peptide array experiments.

I also would like to thank Monika Lerner for generating the immunofluorescence images and for all her help with any laboratory practical skills.

I also would like to express my gratitude to Professor Dr. Adolfo Cavalié for allowing the use of the calcium imaging facility.

In addition, a thank you to Dr. Alex von der Malsburg for his advice and help with the CRISPR-Cas9 system, and PD Dr. Elmar Krause for his help with the fluorescence-activated cell sorting.

Last but not least, I would like to thank all my group members for all their support and contribution to this Ph.D. project: Dr. Mark Sicking, Dražena Hadžibeganović, Petra Endlein, and Gamar Musayeva.